

ABSTRACT

Title of Dissertation: PHYSICAL PROPERTIES OF COMETARY NUCLEI

Yanga Rolando Fernández, Doctor of Philosophy, 1999

Dissertation directed by: Professor Michael F. A'Hearn
 Department of Astronomy

I present results on the physical and thermal properties of six cometary nuclei. This is a significant increase in the number of nuclei for which physical information is available. I have used imaging of the thermal continuum at mid-infrared and radio wavelengths and of the scattered solar continuum at optical wavelengths to study the effective radius, reflectivity, rotation state, and temperature of these objects. Traditionally the nucleus has been difficult to observe owing to an obscuring coma or extreme faintness. I have taken advantage of new mid-infrared array detectors to observe more comets than were possible before; I have also co-developed a technique to separate the coma and nucleus from a comet image. I developed a simple model of the thermal behavior of a cometary nucleus to help interpret the thermal flux measurements; the model is an extension to the Standard Thermal Model for asteroids. We have enough nuclei now to see the first demarcations of the “cometary” region on an albedo-diameter plot; I make a comparison of the cometary nuclei with outer Solar System small bodies and near-Earth asteroids. All of the cometary nuclei studied in this thesis are dark, with geometric albedos below 8%, and have

effective diameters of around 3 to 8 km, except for comet Hale-Bopp C/1995 O1, which is in the next order of magnitude higher. I give an extensive discussion of the nuclear characteristics of comets Hale-Bopp and 2P/Encke, the two comets for which I have large datasets.

PHYSICAL PROPERTIES OF COMETARY NUCLEI

by

Yanga Rolando Fernández

Dissertation submitted to the Faculty of the Graduate School of the
University of Maryland, College Park, in partial fulfillment
of the requirements for the degree of
Doctor of Philosophy
1999

Advisory Committee:

Professor Michael F. A'Hearn, Chair
Doctor Alan P. Boss
Professor Paul D. Feldman
Doctor Lucy A. McFadden
Professor Virginia Trimble
Professor Richard J. Walker

©Copyright by

Yanga Rolando Fernández

1999

PREFACE

Sections of this thesis have already been published in scientific, peer-reviewed journals and conference proceedings. A discussion of comet Hyakutake appeared in *Planetary and Space Science* in 1997 (volume 45, pages 735-739). A treatment of comet Encke is currently under review by *Icarus*. An overview of comets Tempel-Tuttle, Wild2, and Utsunomiya will appear in the upcoming book *Cometary Nuclei in Space and Time* (edited by M. F. A'Hearn and published by the Astronomical Society of the Pacific), which is based on the IAU colloquium held in Nanjing, China, in May of 1998. A paper on comet Hale-Bopp appeared in *Icarus* in July 1999 (volume 140, pages 205-220). A discussion of the image-processing technique that I call the “coma-fitting method” appears in a paper first-authored by my co-investigator Dr. C. M. Lisse, published in *Icarus* in July 1999 (volume 140, pages 189-204).

DEDICATION

To the two constants of my Universe, Mom and Dad.

ACKNOWLEDGEMENTS

This thesis is formally credited to one person, but it is not completed without the assistance of many other people, of course. Mike A'Hearn has guided me through the bulk of my graduate career and to him I owe many thanks, not only for mentoring me through the scientific aspects of my apprenticeship, but through the sociological and political ones as well. The first scientific talk I heard him give was at the Donn Symposium in Charlottesville, VA, in November of 1995. Until then I had been waffling about deciding on a concentration for my thesis, but after hearing him speak about his database paper, and seeing his enthusiasm about these new breakthroughs that finally revealed themselves after studying seven dozen (!) comets, I really started to understand some of the excitement and allure of studying these buggers. So thank you so much, Mike, for all your help.

Casey Lisse has been my other close collaborator in this scientific journey. I am grateful for his quick mind, infinite patience with my questions, and wacky humor. And of course who can forget the Red Pen? I will always look fondly back on these very scientifically productive years with him.

I also owe a deep debt of thanks to Dennis Wellnitz, who is such an expert on things mechanical and electronic. The smashing success of the Hale-Bopp occultation adventure – in a trash-dump in upstate Utah – would not have happened

without his expertise and quick thinking at the critical moments. Yet again, I think how fortunate I am to have entered Mike's Comet Group just when all these terrific people were there to help me out.

I am very grateful to Lucy McFadden for allowing me to start work on an asteroid project in 1994 and finally allowing me to realize that I really did like planetary science much more than studying clusters of galaxies! And she has continued to be a great teacher through my graduate career. Thanks Lucy!

Lastly (on the scientific front) I have to thank both NASA and NSF for their consistent financial support throughout these last years; the telescope allocation committees and staffs of IRTF, KPNO, CTIO, ESO, VLA, Lowell Observatory, and MKO, for their helpful service and positive attitude; Mike Ressler, Bill Hoffmann, and Ulli Käufl, for granting us permission to play with their instruments. Without all of these people, I would not have been so successful in gaining the necessary data to complete this thesis. Among other things I've learned: you can have oodles of fun with only 60% oxygen in your lungs; form-fitting foam is a godsend; there's nothing like jicama and asparagus salad to help you figure out how to drive a stick-shift.

Now planetary science has been good to me: if I had not been studying comets I would not have been able to travel all over the world and experience more of our planet than I had imagined. It makes you realize how much of Earth's culture and nature is still left to explore. Twenty-eight trips in grad school, and I have only scratched the surface, from strolling along Victoria Harbor among the bright lights of Hong Kong, to bathing in a giant waterfall in Waipi'o Valley on the Big Island, to being the highest human for miles around at the tip of Mt. Lassen, to watching the

rainbows appear and reappear on a misty summer's day in Stockholm. (I could go on for a while.) Unfortunately now I have no choice but to submit to this wanderlust I've picked up and spend the rest of my life traveling the nooks and crannies of our planet.

One repercussion of all this scampering around has been to instill in me a great sense of appreciation for how lucky I am. Though the physical distance between me and that subsistence farmer in central Chile, that family selling trinkets in Nogales, and those poor homeless blokes near Constitution Avenue may be small, what an incredibly fortunate person I am to be able to go to my warm house, my well-supplied grocery, my steadily paying job. We are all just a few small but critical events away from any of these predicaments.

And now, for the other important people of my time here: Thanks to Arunav, Kartik, and Laura. I wouldn't have been able to finish this tome without all of their support and understanding through this crabby and grumpy time, especially near the end. Mes amis, your friendships mean more to me than you imagine. The mid to late 1990s would have been quite a bit more difficult to slog through without you all. Let's all find enough inner peace and gumption to make the XXIst century better than the XXth. AK: Thank you for keeping my head on straight. KS: Thank you for keeping me honest. LW: Thank you for giving me self-confidence.

Continuing with the important people: thanks Don for (among other things) bringing ice cream and going sledding, thanks Leslie for (among other things) playing racquetball and finding my bike, thanks Amy for (among other things) going to see offbeat movies with me, thanks Doug for (among other things) making me stay loyal

to the Padres, thanks Steve for (among other things) having practical knowledge in a institute full of geeks, thanks Pete for (among other things) endlessly quoting “The Simpsons,” thanks Alison for (among other things) endlessly quoting “Star Wars.”

Where would we be without the department staff shielding us from the three-toed sloth that is the university administration? To John T., Mary Ann, and Maggie, thanks for your protection. Where would I be if I hadn’t babysat the PDS machine during S-L 9 impact week? To Anne: thanks for that job 5 years ago and for your humor in the meantime.

Where would I be if I were not able to go to Giant at 3 o’clock in the morning and buy Pop-Tarts? What a country.

Finally, thanks to:

- ...Carl Sagan for writing *Cosmos*;
- ...Halley’s Comet, for being visible right when I was so impressionable – may

I see you again when I’m ninety;

- ...Voyager 2, for sending back very cool pictures of Uranus and Neptune.

TABLE OF CONTENTS

List of Tables	xi
List of Figures	xii
1 Cometary Nuclei: Their History and Importance	1
1.1 A Brief Rundown	1
1.2 The Role in the Solar System	9
1.3 Motivation	15
1.4 A Description of Chapters	18
2 Data Acquisition and Processing	19
2.1 Obtaining Optical Data	19
2.2 Obtaining Infrared Data	20
2.3 Obtaining Radio Data	24
2.4 The Ideal Dataset	26
2.5 Processing the Data: Coma Removal	27
3 Data Interpretation	32
3.1 Philosophy of Thermal Modeling	32
3.2 The Energy of a Nucleus	36
3.3 The Augmented Thermal Model	40
3.4 Rotation of the Nucleus	42

4 The Nucleus of Comet Hale-Bopp	46
4.1 Background	46
4.2 Occultation Measurements	46
4.3 Thermal Emission and Scattered Light Imaging	91
4.4 Summary of Hale-Bopp Results	115
5 The Nucleus of Comet Encke	117
5.1 Background	117
5.2 Observations and Reduction	118
5.3 Analysis	119
5.4 Discussion	129
5.5 Previous Work	151
5.6 Summary of Encke Results	155
6 The Nucleus of Comet Hyakutake C/1996 B2	158
6.1 Background	158
6.2 Thermal Measurements	160
6.3 Optical Measurements	168
6.4 Summary of Hyakutake Results	174
7 The Nucleus of Comet Tempel-Tuttle	177
7.1 Background	177
7.2 Thermal Measurements	177
7.3 Optical Measurements	180
7.4 Summary of Tempel-Tuttle Results	184
8 The Nuclei of Comets Wild 2 and Utsunomiya	186

8.1 Background	186
8.2 Utsunomiya	187
8.3 P/Wild 2	189
8.4 Summary of This Chapter	191
9 Conclusions and The Future	193
9.1 Comets and Their Disguised Relations	193
9.2 Comparing Radii and Albedos of “Cometary Nuclei”	209
9.3 Albedo and Orbital Parameters	211
9.4 A Motivator for the Future	212
9.5 Future Data Rates	216
References	219

LIST OF TABLES

4.1	Characteristics of Comet Hale-Bopp Occultation	50
4.2	Observations of Occultation by Comet Hale-Bopp	51
4.3	Parameters of the Model of Nuclear and Comatic Structure	68
4.4	Constraints on Parameters to Occultation Model	76
4.5	Observations of Comet Hale-Bopp	93
5.1	Observations of Comet Encke	120
5.2	Flux of Comet Encke	121
5.3	Estimated “Nuclear” or “ m_2 ” Magnitudes for Encke’s Nucleus	139
9.1	Sizes and Albedos of “Cometary Nuclei”	200

LIST OF FIGURES

1.1	Current “Canonical” Cometary Nucleus	8
1.2	Main Belt Asteroids Radius Distribution Function	17
2.1	Schematic of Mid-Infrared Observing	23
3.1	Schematic of Temperature Map for Slow- and Fast-Rotators	35
4.1	Locations of Observers for Occultation by Hale-Bopp	54
4.2	Comparison of Occulter (Cometary) and Occultee (Stellar) Spectra	57
4.3	Light Curve of Occultation by Hale-Bopp: Team 5	60
4.4	Light Curve of Occultation by Hale-Bopp: Team 6	64
4.5	Schematic of Occultation and Light Curve	66
4.6	(a-d) Example Model Fits to Occultation Light Curve	72
4.6	(e-h) Example Model Fits to Occultation Light Curve	74
4.7	Pre-Occultation Image of Comet and Star	84
4.8	Coma-Fitting Method Applied to Optical Image of Hale-Bopp	97
4.9	Coma-Fitting Method Applied to Optical Image of Hale-Bopp	98
4.10	Coma-Fitting Method Applied to Optical Image of Hale-Bopp	99
4.11	Coma-Fitting Method Applied to Optical Image of Hale-Bopp	100
4.12	Coma-Fitting Method Applied to Mid-Infrared Image of Hale-Bopp	101
4.13	Rotation Sequence of Comet Hale-Bopp	103

LIST OF FIGURES – *cont'd*

4.14	CLEAN Contour Map of Comet Hale-Bopp Microwave Continuum	107
4.15	Radio Continuum Spectrum, Hale-Bopp Nucleus, Mar 1997	109
4.16	Temperature Map of Hale-Bopp, 26 Mar 1997	112
5.1	Comet Encke at 10 Microns (a) and 7200 Angstroms (b)	124
5.2	Radial Profiles of Comet Encke in Mid-IR (a) and Optical (b)	126
5.3	Light Curve of Comet Encke Phased by 15.2 hr	128
5.4	String-Length Method Determination of Encke's Rotation Period	130
5.5	Optical Phase Behavior of Comet Encke's Nucleus	137
5.6	ISOPHOT Spectrophotometry of Encke Dust Coma Plus Nucleus	150
5.7	χ^2 Plots of Encke Dust Temperature and Nucleus Size	152
6.1	Comet Hyakutake in a 40°-wide Field of View	159
6.2	CLEAN Contour Map of C/1996 B2	163
6.3	Size and Temperature of C/1996 B2 Nucleus	167
6.4	Coma-Fitting Method Applied to Optical Image of Hyakutake	171
6.5	Rotation Sequence of Comet Hyakutake	173
6.6	Photometry Light Curve of Comet Hyakutake's Photocenter	175
7.1	Mid-Infrared Images of Comet Tempel-Tuttle	179
7.2	Mid-Infrared Spectrophotometry of Comet Tempel-Tuttle's Nucleus	181

LIST OF FIGURES – *cont'd*

7.3	Coma-Fitting Method Applied to Optical Image of Tempel-Tuttle	183
7.4	Optical Phase Behavior of Comet Tempel-Tuttle's Nucleus	185
8.1	Mid-Infrared Images of Comets Utsunomiya and Wild 2	188
8.2	Coma-Fitting Method Applied to Comet Utsunomiya	190
8.3	Coma-Fitting Method Applied to Comet P/Wild 2	192
9.1	Size and Albedo of Cometary Nuclei and Comet-Like Asteroids	194
9.2	Albedo-Orbit Connection of Cometary Nuclei and Comet-Like Asteroids: Perihelion	213
9.3	Albedo-Orbit Connection of Cometary Nuclei and Comet-Like Asteroids: Tisserand Invariant	215
9.4	Current Size Distribution of Known Cometary Nuclei and Comet-Like Asteroids	217

Chapter 1

Cometary Nuclei:

Their History and Importance

1.1 A Brief Rundown

Most studies of the comet phenomenon focus on the coma and tail of the object, usually the most obvious parts that one sees. However this thesis presents a study of the nuclei of several comets, which are in general much harder to observe. While much work has been done to understand the nuclei indirectly by studying the gas and dust around them, I have tried to directly probe their physical and thermal properties. It is only in the last two decades that this has been observationally and computationally possible; the recorded history of the study of comets extends back a few millenia but for the vast majority of that time the very existence of a cohesive body in the middle of the coma, never mind its properties, was not known.

Though Seneca seems to have had the correct idea in the 1st century A.D., for much of history a comet seen in the sky by the ancients was not even recognized as an astronomical phenomenon until the 16th century, when Tycho Brahe set an upper limit on the comet's parallax that put it far from Earth; previously comets were believed to be atmospheric phenomena. The comets' basic place in the planetary system – moving on parabolae or on ellipses typically crossing the orbits of several major planets – was of course noted by Halley using Newton's then-new universal gravitation idea, through his accurate timing and astrometric prediction of the 1758 return of the comet now bearing his name. Aside from, most notably, work by Bessel, investigations into the physical nature of comets – as opposed to just orbital or astrometric studies – began in earnest only in the late 19th century, with detailed studies of morphology and apparent luminosity, and the advent of photography and then spectroscopy.

The study of a comet's nucleus specifically was fraught with uncertainty. As Bobrovnikoff (1931) wrote in reference to comet 1P/Halley's appearance around 1910, “[t]he term nucleus has no precise significance. Sometimes the nucleus was perfectly star-like without any measurable diameter. Sometimes it looked like a small planetary disc. Sometimes there was nothing that could be interpreted as a nucleus. It is questionable whether most observations of the diameter of the nucleus refer to the real nucleus.” A paper by Vorontsov-Velyaminov (1946) gives no less

than seven separate operational definitions of the nucleus. The rampant confusion of nuclear nomenclature is indicative of the lack of understanding of exactly what is at the heart of a comet. That is not to say that we are fully enlightened now, but in hindsight we can see fundamental misconceptions.

The dominant model for the comet's nucleus for about a full century, from the mid-1800s to the mid-1900s, was the sandbank model, whose tenets were most recently championed by Lyttleton (1953, 1963). The main motivations for postulating the nucleus as an unbound agglomeration of meteoritic solids and not a monolithic model were (a) a cometary coma contracts as the comet approaches the Sun, (b) meteor streams are coincident with cometary orbits, (c) nuclei tend to fluctuate in apparent size and brightness, sometimes even disappearing, and (d) comets are often as much as an arcminute away from predicted ephemeris positions, even for well determined orbits. The obvious choice to make, at least back then, was to assume that there is no one central body in the photocenter of the comet, but rather just a cloud of dust grains, and that what one observes as the nucleus is just the place where the optical depth or the concentration of particles is higher. The complicated patterns that emerge in the near-nuclear coma of some of the more active comets made it attractive to assume that there is just an amorphous cloud of dust grains deep inside the coma. For example, the head of comet 1P/Halley during its apparition in 1910 (Bobrovnikoff 1931) showed many centers of brightness with tendrils and sheets of coma pointing in multiple directions. The mass of the comet would be spread out over much of the coma, not just in the photocenter, but all of the particles in the comet are on independent orbits of all more or less the same period – there is no gravitational binding but also they are not tidally disrupted as they pass close to a planet or the Sun.

The literature is full of measurements of the size of the “nucleus” that range from a few tens to a few thousand kilometers (e.g., Chambers 1909, p. 222; Vorentsov-Velyaminov 1946; Lyttleton 1953, pp. 45-46). Frequently observers would measure the angular size of whatever resolved disk was at the center of the comet, if any. A few published reports give values within the same order of magnitude of the modern values, i.e., a few kilometers, but the majority are similar to the case, e.g., of a specific comet mentioned by Richter (1963) with a diameter lower limit that is 10 times bigger than the currently accepted value. Of course there was also the problem of a then-totally unknown albedo and then-undetermined phase effect that complicated matters. The observation of comets transiting the solar disk (Finlay and Elkin 1882, Bobrovnikoff 1931) placed upper limits on the diameter of roughly 50 to 100 km, but in the context of the sandbank model this was taken to confirm the idea that there were several smaller bodies at the heart of the comet rather than one single body producing the coma and tail phenomena.

This then was the heart of the problem for the sandbank model: the actual diameters of cometary nuclei – and here I do mean the central monolithic body – are much smaller than was commonly thought a century ago. As I will show in later chapters, most comets seem to be on the order of just a few kilometers in radius. This is not to say that comets do not have multiple sources for the dust and gas we see, for of course there are a couple dozen cometary nuclei that have been known to split into pieces, some for not obvious reasons (Sekanina 1982, 1997). However,

usually the pieces evaporate away (or cease activity) in short order so that at any given moment a comet's nucleus is usually just a singular object with a radius on the order of 1 to 10 km. This should not belittle the work of the 19th and early 20th centuries; I merely point out that in hindsight many conclusions were based on incorrect precepts. Indeed, the main problematical situation in observing cometary nuclei still remains: when the comet is close by, the nucleus is shrouded in the coma, but when it is far away and the coma is not so strong, the nucleus is faint and difficult to measure. The recent journals contain many estimates of the size of cometary nuclei, but the error bars are usually large, and if they are not, then many times they probably should be!

The late 1940s and early 1950s saw the publication of significant papers on several cometary phenomena: the nucleus (Whipple 1950), the plasma tails (Biermann 1951), the reservoir of long-period comets (Oort 1950), and the source of the Jupiterfamily comets (Edgeworth 1949, Kuiper 1951). For my immediate purposes here, Whipple's work is the most significant. The nucleus is a single body, a "conglomerate of ices... combined in a conglomerate with meteoric materials," to use the original wording, with ices subliming off due to insolation. Quantitative studies of the sheer magnitude of gas mass in cometary comae and tails at the time indicated that a huge reservoir of ice was needed in the comet – far more than could be supplied by the grains in a sandbank even if the grains did adsorb volatiles on their passage through space. The ejection of material would, over time, leave an insulating mantle on the nucleus' surface and also measurably push the nucleus in a reaction force. This latter point made Whipple's model superior to the sandbank model in that both acceleration and deceleration could be explained by the sense of rotation of the central body. The sandbank model used solar radiation pressure and collisions within the bank to explain acceleration but not deceleration. The idea of a single body for the nucleus was not totally new in 1950; e.g., Wurm (1939) mentions it in the context of the formation of the gas coma.

Whipple was the first to make an extensive analysis of the rotation states of many cometary nuclei; he (1982) has given a summary and historical and contextual review. However his method for determining rotation periods, based on the timing of features moving through the coma, appears frequently to give misleading results. Whipple himself states that his method either gives exactly the right answer or something totally specious. The photoelectric measurement of the brightness of a comet's photocenter as a function of time was first done only in 1976. The determination of a cometary rotation state is a difficult problem – a good review of the pitfalls is given by Belton (1991) – and it has not been done satisfactorily even for the nucleus of comet 1P/Halley, a comet visited by several spacecraft! I will elaborate on the methodology of rotation period determination later.

In the mid- to late-1980s a series of ground-based experiments were performed that gave us size and reflectivity information on cometary nuclei for the first time. Much of my work elaborates on the same principle, i.e., combining the information from the thermal radiation and reflected light of a nucleus. The advent of sensitive germanium-gallium bolometers to detect 10 to 20 μm radiation made this method possible. I will describe the method fully in Chapter 3. The work gave our first indication that cometary nuclei are some of the blackest objects in the solar system,

with geometric albedos of just a few percent. Previously the consensus was to assume a much higher value, something comparable to the icy satellites of the outer Solar System.

The study of cometary nuclei received a boost in 1986 with the data taken by the flotilla of spacecraft that flew by comet 1P/Halley, most especially by *Giotto*. For the first time ever a resolved image of a nucleus was produced, and I show a representation in Fig. 1.1 (taken from a review article by Keller [1990]), which is the combination of several high-resolution images. The flybys confirmed many of our basic suspicions: Halley’s nucleus is a cohesive body and not a sandbank, its visual geometric albedo is very low (a few percent), it is approximately prolate and elongated by about 2:1, there are regions on the surface that are more active than their neighbors are; these regions produce jets similar to what is seen in the ground-based images; an active region is active apparently only on the sunlit side, not on the night side; but a good fraction of the gas and dust does not come from these active regions. While the study of Comet 1P/Halley revolutionized cometary science, it of course left many questions still unanswered. Most obviously, it would be wise to obtain similarly detailed close-up data of other nuclei. Fortunately this will probably happen in the next decade; there are several spacecraft missions with cometary targets scheduled to fly in the coming years and we hope not all of them will suffer from the budget axe or system failure. The near future will bring exciting scientific knowledge to us about these denizens of our Solar System.

This short history should make it clear how difficult observations of the nucleus can be. In general, if the comet is close to Earth, it is also close enough to the Sun to be outgassing, and the light from the gas and dust coma competes with and often swamps the light from the nucleus. On the other hand, if the comet is far from the Sun, where it is not outgassing and we have an easier view of the nucleus, the comet is also far from Earth, and the nucleus is difficult to observe due to its faintness. Furthermore once the comet is several AU away it becomes extremely difficult to tell the difference between a little bit of comatic flux and no comatic flux, since there is no set distance known *a priori* at which one can declare the comatic activity negligible. . This “Catch-22” problem exists in both the infrared and optical regimes. In the radio, there is some hope because there are not enough grains in the coma to produce enough radiation to compete with the nucleus. However at these wavelengths the PSF – “beam” in this case – is so large as to make spatial differentiation of the coma and nucleus very difficult – it is even harder to tell how much flux is comatic and how much is nuclear. Interferometric observations can be used to improve the spatial resolution, as I will show in Chapter 4, but then one needs a large nucleus since the wavelengths are so far down on the Rayleigh-Jeans side of the Planck function. The fact that our knowledge of cometary nuclei was almost non-existent all the way up into the mid-1980s dramatically indicates the difficulties in approaching the study of these objects.

1.2 The Role in the Solar System

1.2.1 Origins

In the mid-18th century, Kant speculated that the non-astrological and non-

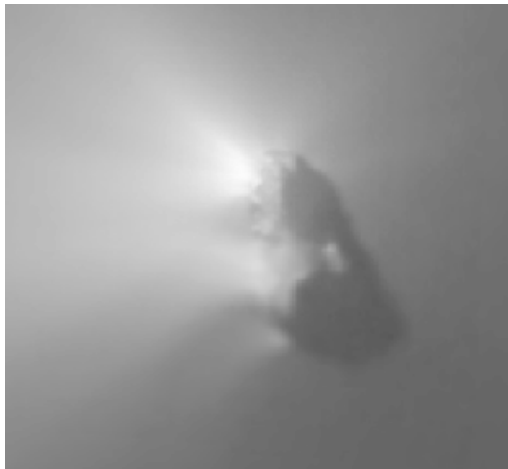


Figure 1.1: Current “canonical” cometary nucleus. This is a processed image of the nucleus of comet 1P/Halley, taken by the *Giotto* spacecraft in March 1986 (Keller 1990). This image represents our current view of the “typical” cometary nucleus.

anthropic reason for the comets' existence was tied to the origin of the Solar System. To this day, among the largest unanswered questions in comet science are: "What exactly was the role of the comets in the Solar System's formation?" and "How is the currently-observed group of comets related to the original population?" The comets are some of the best probes we have for studying Solar System origins, since they are some of the least processed observable objects.

The story apparently begins before the Solar System was born. Recent studies of the bright comets Hyakutake and Hale-Bopp have indicated an interstellar origin for the ices, based on the isotopic ratios (Meier *et al.* 1998a, 1998b) and unusual hydrocarbon abundances (Mumma *et al.* 1996). The ices were in the solar nebula as the gas giants were forming, and the comets are remnants from the accretion process that created the gas giants. There is much debate about the exact method of gas giant formation – gravitational stability (Boss 1998) or core accretion (Pollack *et al.* 1996) – but low-speed collisions of grains undoubtedly played some role in the agglomeration of the cometesimals. The existence of the ice implies that the comets we see today formed in the 5 AU range and beyond, since closer to the Sun they would not have retained the volatile component.

Currently there are four major ideas for the structure of the nucleus as a result of the formation process. Whipple's (1950) icy conglomerate model is the original. Variations on that idea have been created by Donn (1990), who created a fractalized, fluffy aggregate; by Weissman (1986), who created a primordial "rubble pile" of a cometesimal collection with low tensile strength; and by Gombosi and Houppis (1986), who postulated a collection of closely-packed boulders held together with "icy glue." This is by no means exhaustive, and extensive reviews of the models of the bulk structure of cometary nuclei have been written by, e.g., Donn (1991). The main variations among the models are: the density of packing of the cometesimals from which they formed, and the makeup of the ice-rock matrix of which they are made. There are apparently testable predictions for the models, based on how they suffer collisions and the physics and hydrodynamics of the gas and dust ejection. Work on split comets (Sekanina 1982, 1997) seems to indicate a very low tensile strength for the bodies, but in general differentiating between the models may have to wait until we have many very close observations of several nuclei by spacecraft. Notable among the future missions is *Deep Impact*, which will fire a missile at a comet and simulate a meteorite impact, and thus allow us to observe crater formation on the surface.

The current domicile of a comet within the Solar System depends strongly on its birthplace 4.5 Gyr ago. According to numerical simulations, comets born near Jupiter and Saturn predominantly found themselves either crashing into the Sun or being ejected from the Solar System entirely, due to the strong gravitational influence of the two largest gas giants. A small percentage collided with the terrestrial planets; i.e., Jupiter and Saturn provided the impetus for some of the heavy bombardment suffered by Earth in its early history. It should be noted that even today it is thought that a typical short-period comet – with a 6-year period and aphelion passing less than 1 AU from Jupiter's orbit – can expect to survive less than a million years before being strongly perturbed into the Sun, out of the Solar System, or into a near-Earth asteroid-like orbit (Wetherill 1991).

Then there are the comets born near Uranus and Neptune. The lower mass of these gas giants (compared to Jupiter and Saturn) prohibited them from completely ejecting the comets into interstellar space. However, they were apparently very good at populating the Oort Cloud (Weissman 1991). Once a comet had been flung outward by Uranus or Neptune, it would spend several thousand years barely held by the Sun's gravity and subject to significant perturbations by passing stars, giant molecular clouds, and the Galactic tides. One net effect was to raise the perihelia and aphelia distances of these comets and, hence, keep them out of the inner Solar System (Weissman 1991); the residents of the Oort Cloud live between about 5×10^3 AU and 1×10^5 AU from the Sun. However the perturbative sources also tend to destroy the Oort Cloud over time, sending the comets into interstellar space. The existence of an Inner Oort Cloud has been invoked to resupply the outer cloud, since apparently few outer cloud members could survive 4.5 Gyr at the edge of the Sun's gravity. Duncan *et al.* (1987) have done numerical calculations to show that an inner cloud would be populated by ejected members of the Uranus-Neptune region and could help to preserve the outer cloud's population.

Lastly I will mention the Kuiper Belt, originally filled with comets that were born beyond Neptune. With no large planet to shepherd them, the planetesimals remained planetesimals. Many of the Kuiper Belt objects discovered in the past seven years reside in a resonance with Neptune – as Pluto does – that keep them safely orbiting over Gyr timescales. However, Fernández (1980; no relation) was one of the first to numerically explore the idea that the short-period comets originally came from this region, and recently Levison and Duncan (1997) have performed extensive numerical calculations to model the currently observed orbital spread of Jupiter family comets by integrating the orbits of particles in the Kuiper Belt.

1.2.2 Classification

I will give here a brief description of the relation between cometary dynamics and nomenclature. Historically, a comet has either a “short-period” (SP) or a “long-period” (LP), the dividing line being at 200 years. An LP comet can either be new or old in the “Oort sense” depending on whether or not it is passing for the first time through the inner Solar System. An SP comet can either be a member of the Jupiter family (JF) or Halley family (HF). JF comets originally come from the Kuiper belt; HF ones came from the Oort Cloud. Both JF and HF comets have been perturbed by the gas giants into orbits that keep them mostly in the inner Solar System. The usual distinguishing characteristics between JF SP and HF SP comets are the inclination and period. In my opinion one can make a case for the existence of an Encke family of SP comets (EF), for comets in orbits similar to the majority of near-Earth asteroids (NEAs). Levison (1996) has come up with a similar categorization, but currently this family is populated by only 2 known members. Recent observations have found comets residing in the Main Asteroid Belt (Marsden 1996b, Lien 1998), but these objects represent exceptional cases and are probably caused by colliding asteroids rather than independent outgassing, so it is likely that this is not a separate dynamical class of comets.

With the publication of a paper by A'Hearn *et al.* (1995) detailing molecular gas species abundances in seven dozen comets, we may have entered the era of com-

etary taxonomy based on compositional differences instead of just dynamics. Such categorizations are just starting to be found and understood, but continuing surveys of cometary comae and improved remote sensing techniques may allow us to obtain more accurate determinations of the compositional differences from comet to comet.

1.2.3 Evolution

The cometary nuclei have not been quiet since their formation. Numerical considerations indicate that comets from anywhere – from both the Oort Cloud and Kuiper Belt – have undergone some collisional events in the intervening eons (Stern 1988, Stern 1995, Farinella and Davis 1996); an important question is how many? The observed size and rotation distribution that we measure from the population of nuclei that has managed to penetrate the inner Solar System will likely not be the same as the original distribution with which the nuclei were born. However we would be able to tell if the nuclei are as collisionally relaxed as the main belt asteroids are or if they have not quite reached that stage yet.

There are other effects that have altered the comets, even those that were in the deep freeze of the Oort Cloud. Cosmic rays have bombarded the nuclei and affected the top layer of cometary material, although presumably this is blown off on the first passage of a comet near the Sun. Passing stars and nearby supernovae briefly warm the nuclei from their usual 3-K temperature, and hence motivate some chemical reactions in the ice. Some calculations (Stern and Shull 1988) indicate that at least once during the previous 4.5 Gyr have the Oort Cloud nuclei warmed up to 45 K due to passing stellar or supernova radiation, which could initiate sublimation of the more volatile icy components and induce some otherwise-inert chemical reactions.

The short-period comet population of course is more evolved than their long-period, new (in the Oort sense) counterparts. The aging process is thought to manifest itself, among other ways, in the chemical differentiation of the topmost layers of the nucleus and the creation and thickening of a mantle (Meech 1991). The physical destruction of the comet also contributes: e.g., via splitting or the blowing off of relatively large fractions of the comet's mass during outbursts. These phenomena could affect any observed size distribution and would tend to smear out the small end of the distribution. However, currently there is a much more worrisome problem to overcome, namely the small number of objects about which we have a detailed physical understanding. Also, the evolution of cometary nuclei is a mostly theoretical pursuit at the moment because we have not been able to observe the decay of a nucleus through multiple passages. The most obvious candidate for such a study – Encke's comet – has selfishly guarded its nuclear secrets until recently (see Chapter 5) and we will have to wait a few more years before the effect can be observed on that object. There may be some indication that small comets simply do not exist in great numbers in the inner Solar System (Rickman 2000) and that nuclei disintegrate rapidly once they get below some threshold size. However the observational bias is strong and until we are more confident of sampling most of the short-period comets we should hold off on any conclusions. Future comet-detection searches or asteroid-searches adapted for comets could help improve the statistics by at least removing the sky coverage bias that currently prevents us from discovering many long period objects.

1.3 Motivation

We need detailed studies of more than just a few cometary nuclei if we are ever to place the nuclei in the correct context of Solar System formation and evolution. Our current knowledge of the nuclei is rather limited, so learning basic physical characteristics such as size, shape, reflectivity, rotation state, and thermal behavior represents a major step. Spacecraft will be busy during the next few years studying a few nuclei in detail, but I hope that we can more rapidly build up a reliable database of information with ground-based observations.

As an indicator of how important thermal studies of nuclei are, as opposed to just using optical data, I show the cumulative size distribution function of the Main Belt asteroids in Fig. 1.2. I have used the database of Bowell (located on the World Wide Web at <http://asteroid.lowell.edu>) to create this graph. One can estimate a radius based on just the optical magnitude by assuming a geometric albedo, in this case 4%, for the asterisks in the graph – and for these 51,517 main-belt asteroids that gives roughly a $R^{-2.5}$ size distribution. I have considered only the high end of the distribution where the sampling is at least reasonably complete. However, if one looks at the actual radii of the objects, measured via the thermal radiation for about 2100 main-belt asteroids with the *IRAS* satellite, one gets a much different distribution of $R^{-3.5}$ in the more complete end. This effect does not depend on the value of the assumed albedo since changing it would merely slide the position of the asterisks left or right. Moreover, the slope is shallower for the better-sampled optical case, whereas if this albedo effect were a manifestation of our incomplete knowledge of the main-belt one would expect a steeper slope since there would be more smaller asteroids known. I do not want to argue the actual value of these slopes; my point is simply that they are very different, and that a similar pitfall could very well occur for the cometary nuclei. Optical data alone cannot necessarily guarantee the validity of size distribution information.

The fruition of such an endeavour is guaranteed, as evidenced by the previously-unknown conclusions from the work of A'Hearn *et al.* (1995). I make no claims that an understanding of the Solar System origins can be teased out of my study of a half-dozen objects, but the revolution in infrared astronomy currently happening will make it technically and observationally feasible to continue studying the small bodies of the Solar System and eventually reach the “holy grail” of comet science, answers to such questions as: How do comets fit into the birth and evolution of the Solar System? How many times have they collided with each other? What accounts for the differences in the reflectivity, the dust-to-gas ratios, the active regions, and the emitted grains? Is there any correlation with dynamical age? How do the comets contribute to the interplanetary medium and the dust population of the Solar System? How does their appearance reflect the alterations they have suffered? Does their composition reflect an interstellar origin for the volatiles?

1.4 A Description of Chapters

I will first describe the methods used to study the nuclei, and then individually discuss each nucleus. Specifically: in Chapter 2 I will discuss my reduction methods for this study. Chapter 3 will have a description of my interpretation methods; this

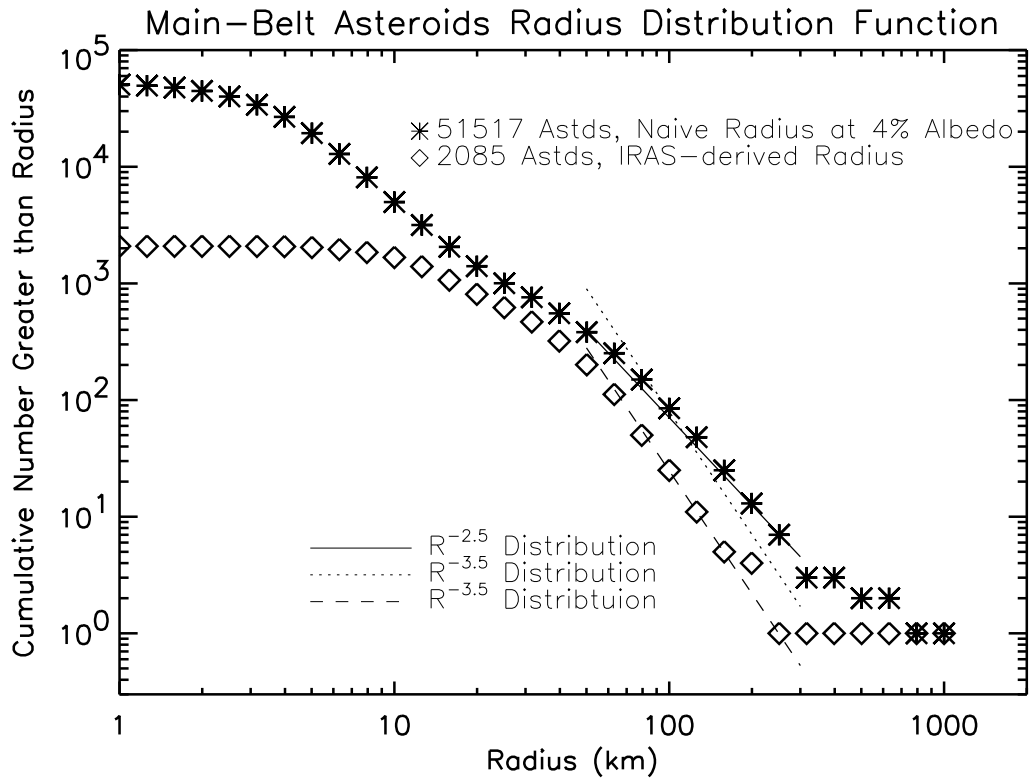


Figure 1.2: Main Belt asteroids’ radius distribution function. The asterisks represent the distribution using an assumed albedo, and so give a “naive” radius when combined with the known absolute visual magnitude. The diamonds represent the *IRAS*-derived radii, and so they have the albedo ambiguity removed. Note that the slopes of the two distributions in the large particle, well-sampled end are quite different.

chapter will explain how I have taken advantage of the new generation of sensitive mid-infrared detector arrays to overcome the problems of nucleus observation that I mentioned in Section 1.1. In Chapters 4 through 7, I will discuss the nuclei of comets Hale-Bopp, Encke, Hyakutake, and Tempel-Tuttle, respectively. I will add some information about two other comets (with smaller datasets) in Chapter 8. Finally in Chapter 9 I will combine the results of the previous chapters and make comparisons with other objects of the Solar System, and try to place these results within the framework of Solar System formation and evolution.

Chapter 2

Data Acquisition and Reduction

The vast majority of the data for this thesis are in the form of continuum imaging. That is true for all wavelength regimes, optical, infrared, and radio. The remaining small fraction of data consists of mid-infrared photometry (with no spatial resolution).

2.1 Obtaining Optical Data

In the optical, a charge-coupled device (CCD) was used in combination with either broadband or narrowband filters. For most comets, in order to get a sufficient signal-to-noise ratio in a short amount of time, the ~ 1000 Å filters were necessary. We typically used the Cousins R and I filters. Bessel (1990) discusses the spectral responses of these filters; Bessel (1979) and Zombeck (1990, p.100) discuss the photometric zero points.

For the bright comets, Hyakutake and Hale-Bopp, narrowband (~ 50 Å) “comet filters” could be employed. The narrow widths can isolate portions of the spectrum that are relatively gas-free, to just sample the scattered solar continuum. There are currently two sets of narrowband filters in existence, one from the International Halley Watch (A’Hearn 1991, Osborn *et al.* 1990), the other recently developed specifically for Hale-Bopp, with improvements in the wavelength ranges to remove contamination to the continuum filters by unwanted gaseous emission (Farnham *et al.* 1999). Fortunately, it turns out that most of the strong gas emission occurs in the bluer end of the optical spectrum, making R and I bands fairly free of gas emission lines.

The basic procedure for obtaining calibration data for the CCD is as follows. Images of the blank twilight sky (or, if not possible, of a blank space inside the telescope’s dome) were used to remove pixel-to-pixel variations in the CCD response, i.e., to “flatten” it with a “flat field.” Sets of zero-exposure frames were taken, at least twice during a night, to measure the bias count level of the CCD. All CCDs used in this study had a low enough dark current to make it unnecessary to perform that calibration procedure. To measure the photometry and account for the extinction of the atmosphere, standard stars were observed during the night at various zenith distances.

I note that some of the optical imaging has come via the *Hubble Space Telescope*. The Space Telescope Science Institute of course has a detailed set of calibration and reduction procedures that they incorporate into the *HST* data, so the scientist frequently obtains science-quality images with very little further processing

necessary. The only processing I personally have done to *HST* data that I use in this dissertation is to remove cosmic ray-affected bad pixels.

2.2 Obtaining Infrared Data

Of the infrared data I have used for this dissertation, all sets measure the thermal emission from the comets, and reside in what is loosely called the “mid-infrared” wavelength regime, from about 5 to $25\mu\text{m}$. Thus my use of the word “infrared” or “IR” should be taken to refer to this wavelength range. Strictly speaking the “infrared” part of the electromagnetic spectrum includes 1 to $4\mu\text{m}$ flux that in comets is usually dominated by scattered sunlight. For my purposes it is important to be only measuring the thermal emission, not the scattered, in the infrared.

Recent advances in infrared detector technology have made it possible to create array detectors, thus bringing high-spatial resolution imaging to these wavelengths. This is a critical aspect to this dissertation, as will be seen, since it allows us to separate the comatic and nuclear contributions to the flux.

At this wavelength range, room temperature objects near the detector (e.g., the telescope, the sky itself) provide the vast majority of the counts; the astronomical source is usually only a small 0.001% or 0.01% excess on top of all that terrestrial flux. Thus “chopping” and “nodding” are employed to remove all of that. The former involves the secondary mirror of the telescope oscillating back and forth, usually 2 to 5 times per second, so that the detector sees alternately the field of view with the comet and a field of view some distance away – I often used a “throw” (offset) of 30 to 60 arcseconds. The difference of the two fields leaves the comet, although the subtraction is not perfect because the sky’s apparent brightness is not necessarily the same in the two frames. To correct this one nods the telescope off the source by some distance – again, I used 30 to 60 arcseconds – and does the same procedure as before with chopping and subtracting. If the nod is not too far then the difference of the two difference frames will remove all of the focus problems and sky variations and retain just the comet. In summary, one obtains four frames, first one on the source, then one off the source after chopping the secondary, then another one off the source after nodding the telescope, and finally yet another one off the source after chopping the secondary with the telescope still at the nodded position. The workable image is: (first minus second) minus (third minus fourth), that is, the result of a double difference. A caveat here is that for the bright comets the nod and chop frames cannot be so close to the comet’s photocenter that one accidentally incorporates coma in the three off-source positions, since then some of the coma signal would be subtracted off! A schematic of this chopping-and-nodding idea is shown in Fig. 2.1.

In practice one obtains several “first” and several “second” frames, combining them via the average or the median, to get a more accurate “first” and “second” frame. Then the nod occurs, and the same thing happens for the “third” and “fourth” frames. This is done since nodding takes several seconds but chopping is relatively quick, at a rate of a few hertz. To clarify my nomenclature, an “image” of a comet is built up from averaging or medianing several “frames” together from the 4 positions, and then taking the double difference. Commonly we used 5 to 10 frames at each of the four positions before creating an image.

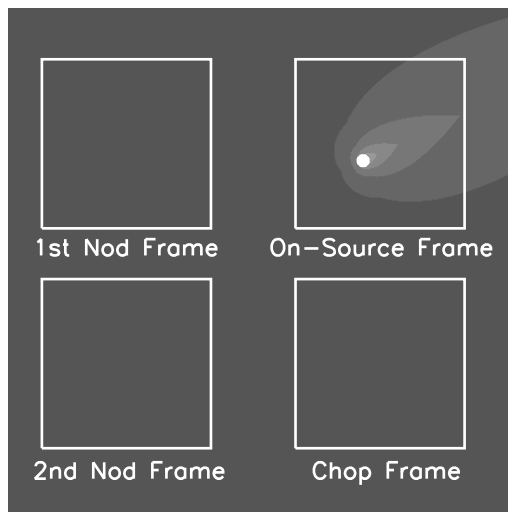


Figure 2.1: Schematic of Mid-Infrared Observing. Here is the basic idea for the ideal method of observing in the mid-IR. One uses four frames and their double difference to actually get an image of the comet. Note that the three off-source frames do not cover any of the comet's coma.

To account for atmospheric absorption and obtain a photometric calibration one observes standard stars. At this wavelength range the behavior of the atmosphere is not necessarily as straightforward as in the optical, so to be safe it is wise to pay attention to the humidity and see if the magnitudes of the standard stars as a function of airmass are not following a straight line.

The flattening of the array can be done by a variety of methods. One method is to observe a star multiple times at various locations on the array, calculate the relative photometry, and then interpolate for the rest of the array. One drawback is just that – the uncertainty in interpolation. Moreover you *a priori* have to know that the pixel-to-pixel variations in the array are smooth enough to be well sampled by this shotgun technique. Another subtlety is that one must be sure to observe the star over a large enough region on the array to include all of the observations of the comet; i.e., it is difficult to extrapolate the flat field, so any images of the comet near the edge of the array have much larger errors associated with their flux.

An alternate method is to stare at a blank sky and then at the inside of the telescope dome, and take the difference of the two images. The sky is a fairly uniform emitter but when looking at the “blank sky” one is really seeing the contribution from the hot telescope as well (not just atmospheric emission) and indeed that can dominate the signal. The telescope’s dome on the other hand is brighter than the telescope and swamps the detector; that is, in a sense one sees more flux in the mid-infrared with the dome shutter closed than when it is open! Subtracting the “blank sky” image from the dome image effectively takes away the telescope’s contribution, and the observer is left with a flat field for the IR array. Of course one does this multiple times, say ten times, to build up good statistics.

2.3 Obtaining Radio Data

In this wavelength regime again I have only looked at a small fraction of the full part of the electromagnetic spectrum classified as the “radio” part. My radio data covers the X band, i.e, a wavelength of 3.55 cm, and has a bandwidth of 100 MHz. This wavelength was chosen mainly for two reasons: (a) I desired to detect as little of the coma as possible and the longer the wavelength the fewer dust grains there are, and (b) the sensitivity of the centimeter-wave receivers is near its maximum.

Only comets Hyakutake and Hale-Bopp were observed at this wavelength, both at NRAO’s interferometer, Very Large Array (VLA). At least 26 of the available 27 telescopes were used at all times. The observations were all done almost totally automatically. A VLA user typically writes an observing program (with a syntax applicable to the telescope control computer) and submits it; the observatory does the rest and the user later picks up the data via Internet or magnetic recording material. For the Hyakutake observations, a colleague was dispatched to oversee the experiment; during Hale-Bopp’s apparition, everything was done remotely.

For flux calibration one observes a calibration source – in this case, a quasar near the comet – at the beginning and end of each observing day, or “track,” in the parlance of the radio astronomer. Since these were interferometric observations, it is necessary to monitor the phase stability of the telescopes; this is done by observing a bright (~ 1 Jy) source near ($\sim 10^\circ$) the target roughly every 45 minutes or so.

The reduction uses the Astronomical Image Processing System (AIPS) software package specifically designed for this interferometric data. The procedure is outlined in *The AIPS Cookbook* (National Radio Astronomy Observatory 1997). The basic idea is to flag the bad visibility data points, compare with the flux calibrator, then do the inverse fourier transform to obtain an image. Deconvolution can then be employed using the CLEAN algorithm (Högbom 1974), although in this case there was not much difference since in one case the comet was not detected, and in the other case the comet was a point source.

2.4 The Ideal Dataset

It is worthwhile to clearly spell out exactly how the ideal observing campaign would proceed for the study of the nucleus. Of course reality often prevents one from performing this, but here are my observational goals during an experiment.

Two observing runs would be scheduled simultaneously, one at an optical telescope and one at an IR telescope. Obviously colleagues' assistance is vital. Each run would last at least four nights. This length of time and the simultaneity allows us to follow the rotational variations in the comet's brightness in both wavelength regimes. At both telescopes we would obtain continuum images at two or three wavelengths, cycling through them continuously. We would use another filter every so often to have better spectrophotometric wavelength coverage. The images would contain coma, and we would see the coma out to several PSF FWHMs away from the photocenter. Of course the data would be photometric since we are after absolute brightnesses.

We choose the targets that are observed during our telescope time by two methods. First, we find which short-period comets are within roughly 1 AU of Earth; of course we try to choose a time for the observing run when we would maximize the number of possible targets. It was our experience that the typical comet that is farther than about 1 AU from Earth is exceedingly difficult to observe, so much so that one cannot usually even find the comet on the instrument monitor. Hale-Bopp of course was an exception to this.

The second criterion for choosing targets is more up to random chance. Occasionally a long-period comet that was discovered after the telescope's proposal deadline will be visible in the infrared sky at the time of the scheduled run. This is usually the only way to observe long-period comets: by fortuitous accident. Hale-Bopp again was a notable exception. If a long-period comet is available, and all else is equal, that new comet will take observational precedence during the run over the short-period objects.

2.5 Processing the Data: Coma Removal

A cometary image usually includes flux from the coma. To understand the nucleus requires accounting for this contribution and deleting it. For this thesis, this was a severe problem for comets Hyakutake and Hale-Bopp, and a less severe but still appreciable problem for the other comets. One way to deal with the coma is to model its shape in the skirt and extrapolate back to the photocenter to calculate its contribution in those few central pixels, since that is where the nucleus is. We

dubbed this method the “coma-fitting method.” Dr. C. M. Lisse and I codeveloped the computer program that uses it, although we are not the first: Lamy and Toth (1995), Lamy *et al.* (1998a), and Jorda *et al.* (1999) have done similar experiments, although they have concentrated on *HST* optical and low spatial resolution *ISO* IR data.

To use the coma-fitting method, the PSF is required. It is desirable to have as high a signal-to-noise PSF as possible, so usually a bright flux standard star is used. Not only should the total integrated signal-to-noise be high, but in each pixel near the center as well. It is best also if the PSF’s wings are apparent. Naturally of course the PSF should be well-sampled spatially, since that will make it easier to find the location of the point-source nucleus within in the image. Unfortunately high spatial resolution and high signal-to-noise per pixel are competing desires, but usually one has no choice about the spatial resolution, since it just depends on the instrument and telescope that is being used. It is also desirable to image the star close to the time at which the comet image was obtained, so that effects that change the seeing – like thermal flexure of the instrument, temperature changes of the telescope, and evolving sky conditions – are not significant.

In addition, the cometary image itself should be of high signal-to-noise, again per pixel, not just integrated. Modeling the coma’s shape is easier if there is decent signal in many pixels away from the photocenter. (I define “decent” and “many” below.) However this only holds up to a point, because at a high cometocentric distance a coma’s surface brightness is less likely to be correlated with its behavior close to the nucleus. This distance is different from comet-to-comet, so there is no set rule about how far the coma should be imaged. The dust grains in the coma could be fading, or they could be feeling significant radiation pressure before they reach the edge of the image’s field of view, making it much more difficult to model their behavior. Related to this, it is always preferable to obtain images with flux that mostly comes from the comet’s continuum. If the flux is heavily contaminated by emission from the gas species in the coma, it again hugely complicates the effort to model the coma’s structure since the shape of the gas coma is a much more complicated function.

A rule of thumb that has been employed at the telescope is that one should try to see the coma out to at least a few and probably several FWHMs. This guarantees that there is no flux from the nucleus being spread into the part of the coma that is being modeled, and of course with more coma available it is more modelable. Frequently, however, nature does not follow the rules of thumb and the images that are acquired at the telescope show just a hint of coma. As said above, strong coma was detected in Hale-Bopp and Hyakutake at both optical and mid-infrared wavelengths, while a fairly weak coma existed for Encke and Tempel-Tuttle, even in the optical. Moreover, there is no clearly detectable coma at all in the mid-infrared images of the other comets.

The actual procedure for modeling the coma’s shape is straightforward. Assuming the coma is strongly present, first a location for the nucleus within or near the brightest pixel is assumed and the image is “unwrapped” about this point, that is, mapped onto the r - θ plane. This is done using a cubic convolution interpolation method. Then a certain number of azimuths – usually 360 – are chosen and the

surface brightness of the coma in each azimuth is fit according to $(A/\rho^n) * \text{PSF}$, i.e., the convolution of a power law with the PSF, and A and n are obtained. This is where it is critical that at each azimuth the coma behaves like a single power law, and not, say, the sum of two power laws. Each azimuth can have a different power law, but each must be characterizable by a single A and n . Presently our computer code finds the value of A and n by trial and error, since it is not so easy to analytically derive the best-fit values when there is a convolution integral involved. The fitted region extends from a cometocentric distance 1 or 2 FWHMs away from the photocenter out until the signal-to-noise is too small to be useful. If there are obvious kinks in the surface brightness profile at the azimuth, the fitting region is shortened to not include that.

There is a subtlety here in the way the surface brightness is fit. The PSF is usually not azimuthally symmetric, so it cannot be unwrapped to get a radial profile. That would make the convolution easy, since it would basically only require a convolution in one dimension, r , the radial dimension, but it is rare that the PSF actually is circular. Instead it is necessary to make a separate model coma image from the trial values of A and n : we assume for the moment that every azimuth in the coma has those values of A and n that are currently being tried, and we make a coma map out of those parameters in the x - y plane, convolve that with the PSF, unwrap this image, and then see how well it fits to what the coma actually looks like.

Strictly speaking, this is not the correct way, since adjacent azimuths contribute to each other upon convolution, and our method does not account for this. To do this rigorously would require fitting hundreds of parameters simultaneously by trial-and-error, a computationally intensive prospect. Hence, this simplification was introduced. It does not create a significant error as long as the fitting is done far enough away from the photocenter so that the surface brightness is not changing rapidly, i.e., at least 1 FWHM away from the photocenter.

Once A and n are found for every azimuth, that is all one needs to recreate an image of the comet's coma. The model coma is subtracted from the image and the residual is compared to the PSF. The only slight complication is the pixelization of the photocenter, since in those pixels one must do an integral of an expression in polar coordinates over a Cartesian area.

The whole process is iterated several times by assuming the nucleus' location in a grid of locations within and near the brightest pixel of the image. Of all these trials, the residual that is most like the PSF and leaves as little flux as possible in the skirt is chosen to be the correct one, and that location is declared to be where the nucleus is. One can then move on to the photometry.

I will make a final note concerning images of comets that only possess a weak dust coma, i.e., a coma that does not extend more than a few pixels away from the photocenter. In this case the same algorithm described above is used except there is no fitting of the exponent n to each azimuth. The lack of data simply just does not justify such an extensive parametrization. Instead I let $n = 1$ for all azimuths and fit a value for A that is applicable for every azimuth. As will be seen in later chapters, this approximation works well for the low signal images.

Chapter 3

Data Interpretation

In this chapter I will discuss the interpretation methods that are common to most of the data used in this thesis. Descriptions of specialized analyses – e.g., of a technique that is applicable to only one of the comets – will be discussed in the relevant comet-specific chapters.

3.1 Philosophy of Thermal Modeling

The energy available to a cometary nucleus comes from the Sun. Internal heating by e.g. radioactive decay is not an important factor owing to the small size of the object. The insolation absorbed by a surface element of the nucleus either is reradiated, is passed along to adjacent elements, or helps to sublimate ice. Currently the numerical value of important factors that heavily influence the nucleus' thermal behavior are unknown, though we hope to achieve some understanding with the cornucopia of spacecraft visits in the coming decade. Detailed models of a cometary nucleus make estimates of such quantities as the thermal conductivity, the porosity, the heat capacity, the surface roughness, the shape, the effective radius, the composition, the structure of the ice/rock matrix, the emissivity, and the rotation state to try to match the observed flux. Only rarely are any of these quantities actually known for a given nucleus *a priori*; the modeler must simplify the situation to make the problem tractable.

The advent of more sensitive IR instrumentation has led to the acquisition of better datasets, and I have attempted to apply some thermal modeling that goes beyond the standard simple methods to some of the datasets in this study. There are models created by others that are more complex, but in my opinion the direct application of a very complicated model to a real nucleus about which we know very little detail may not really help one understand the basic properties of the nucleus any better than a relatively simple model can.

Previous work on understanding the thermal behavior of nuclei has mostly exploited the two popular thermal models for asteroids: the “standard” thermal model (STM), also known as the slow-rotator model (SRM); and the rapid-rotator model (RRM), also known as the isothermal latitude model (ILM) and the fast-rotator model (FRM). As the names imply, the STM assumes the asteroid is rotating slowly compared to the timescale for the thermal wave to penetrate one thermal skin depth into the nucleus, and the RRM assumes it is rotating much faster than that.

For example, for objects 1 AU from the Sun, a “slow” rotator would have a rotation period of roughly 15 hours, whereas a “fast” rotator would spin in roughly 4 hours. Both models assume the object is spherical. The temperature map of a sphere that follows the STM looks like a bull’s-eye centered on the subsolar point, the hottest point on the object, with the temperature decreasing as the local solar zenith angle increases. The night side is at absolute zero. For an object following the RRM, the temperature at any point only depends on the distance from the subsolar point’s latitude, not the longitude. (This is the origin of the “isothermal latitude” name.) I have displayed in Fig. 3.1 a schematic, based on a similar figure made by Lebofsky and Spencer (1989; their Fig. 4), showing typical temperature maps for the two models.

The STM uses a measured flux and assumes values for the bolometric IR emissivity, the optical geometric albedo, the IR phase function, the optical phase integral, and the roughness of the surface (embodied in a factor diminishing or enhancing the overall observed flux). With these quantities, one finds the effective radius. The RRM uses the measured flux and requires values for the bolometric IR emissivity, the optical geometric albedo, the optical phase integral, and the rotation axis direction to find the effective radius. As an aside, if one assumes a pole orientation pointing toward the Sun, then the RRM and the STM yield the same temperature map.

For this asteroidal model to be applicable to a cometary nucleus, one has to be sure that (a) the nucleus is a slow-rotator; (b) it is not very active, or rather, not much of the solar input energy is going to sublimating gas instead of heating up the rock; and (c) the coma is not providing a secondary source of energy via backwarming, which is only a problem for very active comets like Hale-Bopp. It is not really necessary that the cometary nucleus be spherical, which is advantageous since many are not (Meech 1999), but the output of the STM is then the effective radius, not the radius itself. There is a complication with this, since the radiometric effective radius does not have to be the same as the geometric effective radius: suppose the nucleus were cigar shaped with the long axis pointing toward the Sun. An observer would measure a relatively small thermal flux and derive a small effective radius, since most of the cigar would not be significantly warmed by the Sun. Fortunately, observing the thermal flux over the course of a rotation period, and if possible at several points in the orbit, can assuage most fears about this pathological case skewing the radiometrically-derived size. The uncertainties from other aspects of the model – e.g., the infrared phase effect, and the beaming effect, described below – usually make the uncertainty in the resulting radius estimate large enough so that it engulfs some of this systematic error anyway. Moreover the uncertainty from extracting the nuclear signal from a coma-laden image increases the error estimate.

3.2 The Energy of a Nucleus

The STM and RRM model mark the extremes; many objects lie in between. For cometary nuclei, historically the STM has been used because it has been assumed that the thermal inertia, Γ , of nuclei are small; i.e., the nuclei are slow-rotators. The value of Γ is known only for the Moon and a few other satellites, and Spencer *et al.* (1989) point out that the value for an asteroid (or cometary nucleus) could

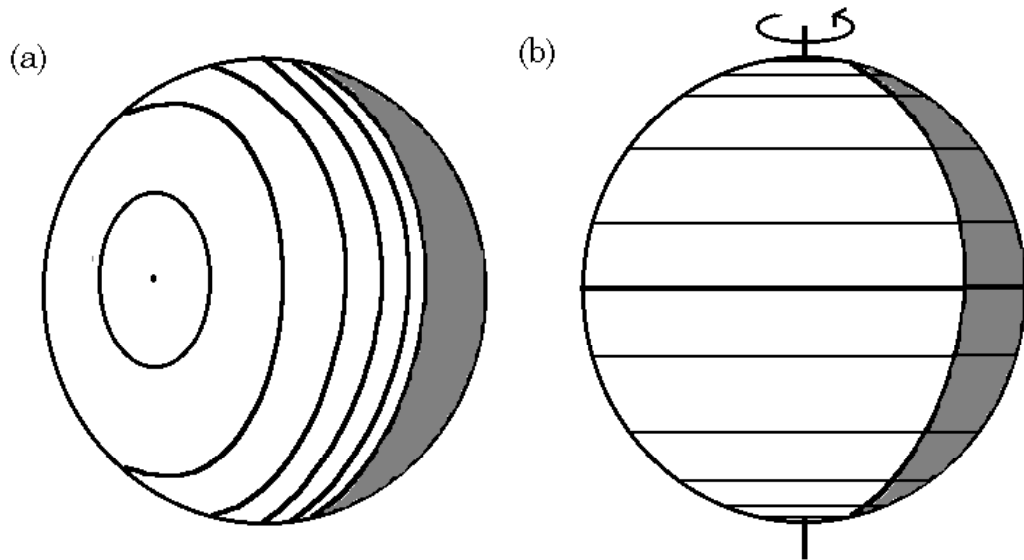


Figure 3.1: Schematic of contour temperature map for (a) slow- and (b) fast-rotators. For each spherical object, the gray-shaded area is unlit by the Sun. In (a), the subsolar point and location of highest temperature is at the dot left-of-center; the temperature decreases toward the terminator in every direction. In (b), I have assumed that the rotation axis is perpendicular to the object's orbit plane, so the subsolar latitude is at the equator. The temperature is a maximum there and falls off toward the poles. Note that the contours extend beyond the terminator. This figure is based on Figure 4 of Lebofsky and Spencer (1989).

be lower since most of these objects are farther from the Sun so the heat capacity could be lower at the cooler temperatures. Moreover at the lower temperatures the radiative heat transport that is so important in the lunar regolith – and which boosts the effective conductivity – is not necessary. On the other hand the thermal inertia could be higher since the small bodies of the Solar System presumably have less regolith – they simply cannot gravitationally retain it – and the bare rock is a more effective conductor. Harris *et al.* (1998) have claimed that thermal IR data on some NEAs, incorporating some of modeling done by Spencer (1990), seem to indicate a higher thermal inertia than previously supposed.

I have made an attempt to handle the intermediate case between the STM and RRM with a model that is one or two steps farther in complexity. Further augmentation beyond what I describe here should wait until more elaborate datasets have been collected. As it is I will only apply the model to the Hale-Bopp data, since certain important physical properties of the other comets in this thesis – most notably the spin axis direction – are unknown. First I will describe the basic STM, and then the enhancements that I have supplied. A good discussion of the STM is given by Lebofsky and Spencer (1989).

The energy balance on a facet on the nucleus is:

$$\text{Energy Absorbed} = \text{Energy Emitted}, \quad (3.1)$$

where for a facet at some latitude $\pi/2 - \theta$ and longitude ϕ on a spherical nucleus the l.h.s. is

$$\text{Energy Absorbed} = \int \frac{F_{\odot}(\lambda)}{4\pi r^2} (1 - A(\theta, \phi, \lambda)) R^2 \cos z(\theta, \phi) d \cos \theta d \phi d \lambda, \quad (3.2)$$

and the r.h.s. is

$$\text{Energy Emitted} = \int B(\lambda, T(\theta, \phi)) \epsilon(\theta, \phi, \lambda) R^2 d \cos \theta d \phi d \lambda, \quad (3.3)$$

where F_{\odot} is the solar specific luminosity; r is the comet's heliocentric distance; A is the Bond albedo and is equal to pq , the product of the geometric albedo and the phase integral; R is the nucleus' radius; z is the zenith angle of the Sun as seen from the facet; B is the Planck function; ϵ is the emissivity, which is near unity; and T is the temperature. Since the STM was designed for asteroids, usually A and ϵ are taken to be independent of position, although currently there is no indication of any large albedo spots on cometary nuclei either. In addition, it is assumed that A is independent of wavelength in the optical, where most of the Sun's energy is, and ϵ is independent of wavelength in the mid-IR, where most of its thermal output is. This simplifies the equations to

$$\frac{L_{\odot}}{4\pi r^2} \pi R^2 (1 - A) \cos z(\theta, \phi) = \epsilon R^2 \sigma T^4(\theta, \phi), \quad (3.4)$$

where L_{\odot} is the solar luminosity and σ is the Stefan-Boltzmann constant. The result is a temperature that depends on the one-fourth power of the local solar zenith angle, with no dependence on R ; only T_{SS} , the subsolar point's temperature,

is needed to describe the temperature map. By plugging in the temperature map into Eq. 3.3 accounting for the observing geometry, one can find the value of R satisfying what the observer measures with the photometry.

There are two added features to the STM that complicate this picture. First, there is an arbitrary constant multiplied to the r.h.s. (Eq 3.3), η , a beaming factor, to account for the fact that the asteroid is actually not a perfect sphere, but has surface roughness. For example, if at the subsolar point on the asteroid there were a crater, the thermal flux coming out of the asteroid would be higher since the surface of the asteroid in the crater would be hotter (from backwarming by the walls). The value of η seems to be approximately unity, with a known range for a few asteroids and satellites of 0.7 to 1.2 (Spencer *et al.* 1989, Harris 1998). The problem is η is not known *a priori*, so there is some ambiguity akin to the albedo problem with optical data. However it is much less significant since the possible range of η only covers about a factor of 2, and moreover with flux measurements at multiple mid-IR wavelengths it is in principle possible to constrain the value (Harris *et al.* 1998).

The other added feature to the STM is the phase effect. Since we hardly ever observe an object at phase angle α of zero, and often α is $\geq 40^\circ$ when observing nearby comets and NEAs, one needs to know the phase behaviour. One popular model is to have the phase effect in magnitudes proportional to α itself (Matson 1972, Lebofsky *et al.* 1986). The known range for the proportionality constant is 0.005 to 0.017 mag/degree. Another method is to just integrate the amount of light one sees on the Earth-facing hemisphere. This is akin to using a $\frac{1}{2}(1 + \cos \alpha)$ phase law in the optical regime, except that in the mid-IR each differential of area on the surface is weighted by T^4 . There is some evidence (Harris 1998) that this latter method describes the phase behavior of asteroids better than the older method, at least for the large asteroids.

The optical data enter the analysis for the determination of the albedo A in Eq 3.4, since the optical flux from a spherical object is proportional to pR^2 . The phase integral, q , connecting A and p , is roughly known from the optical phase behavior, which has been studied quite a bit more than its IR counterpart. The result is that the problem essentially becomes a system of two equations with two unknowns, R and p . This is the basic method behind the work of Campins *et al.* (1987), Millis *et al.* (1988), and A'Hearn *et al.* (1989) when they made the first ground-based measurements of nuclear albedos in the mid-1980s.

3.3 The Augmented Thermal Model

For the augmentation of the model, I have used two basic equations: the conservation of energy equation, and the one-dimensional heat transport equation, the simple parabolic partial differential equation. Energy conservation is treated with the input being insolation and the outputs being reradiation, volatile vaporization, and conduction into the subsurface layers. I have not attempted to treat lateral heat transport.

Energy conservations dictates

$$\frac{L_\odot}{4\pi r^2}(1 - A) = \sigma \int \int T^4(\theta, \phi) \epsilon d \cos \theta d\phi + \kappa \frac{dT}{dz} + L(T) \frac{dM}{dt}, \quad (3.6)$$

where κ is the thermal conductivity, $L(T)$ is the latent heat of vaporization, and dM/dt is the gas mass loss rate. Except for comets such as Hyakutake, which had an extremely active nucleus, the contribution of the third term in that equation will usually be only on the few percent level. For this reason, I have simplified the model by having the gas emanate uniformly over the nucleus' surface.

The heat equation is

$$\frac{\partial T}{\partial t} = \frac{\kappa}{\rho c} \frac{\partial^2 T}{\partial z^2}, \quad (3.7)$$

where ρ is the bulk density and c is the heat capacity. The simultaneous solution of these equations is the basis of my augmented thermal model. The solution is a temperature map from which the expected flux is calculated for a given radius size. The continuum between STM and RRM is sampled simply by altering the thermal inertia $\Gamma = \sqrt{\kappa\rho c}$.

Spencer *et al.* (1989) have done much work on the thermophysical behavior between the STM and the RRM. They formulated the constant Θ , the thermophysical parameter, to indicate when the STM, the RRM, or something in between is applicable, defined as

$$\Theta = \sqrt{\kappa\rho c\omega}/(\epsilon\sigma T_{SS}^3), \quad (3.8)$$

where ω is just 2π divided by the rotation period. It is basically a comparison of the rotation time scale and the timescale for the thermal wave to penetrate one skin depth, where the skin depth l is given by

$$l = \frac{2}{\omega} \frac{\kappa}{\rho c}. \quad (3.9)$$

If $\Theta \ll 1$, then STM is applicable, whereas if $\Theta \gg 1$, the RRM is the one to use. For example, if a cometary nucleus at 1 AU from the Sun has a lunar thermal inertia ($50 \text{ J K}^{-1} \text{ m}^{-2} \text{ s}^{-1/2}$), and spins on its axis in 10 hours, then $\Theta = 0.2$ (since the subsolar point will have $T_{SS} = 390 \text{ K}$). This places it in the slow-rotator regime, but since 0.2 is of the same order as unity, we would not expect the STM to perfectly describe the object's thermal behavior.

Another aspect of my augmented model is the ability to handle ellipsoidal nuclei. This introduces yet more parameters into the model, since not only are the axial ratios of the nucleus required, but also the rotation state, since the flux observed at Earth will now depend on the sub-earth latitude and longitude. Note that the usual observations of nuclei that measure the varying cross section reveal only the projected axial ratio, not the actual ones, unless the data can be combined with measurements at other points in the comet's orbit. I will show an example of this in Chapter 5. Brown (1985) has studied the effects of ellipticity on the output of the STM, and shown that slight asphericity does not make much difference in the use of the STM, but – as with the cigar-shaped nucleus example that I previously mentioned – serious systematic problems can exist if the objects are significantly elongated.

Since the augmented model explicitly calculates the temperature at several layers within the nucleus, the model is able to handle my radio data, which the STM is

unable to do. Our microwave observations do not sample the surface temperature, but rather the temperature several “skin depths” below the surface. The subsurface layer that is sampled could be a few wavelengths deep (for relatively rocky material) or a few tens of wavelengths deep (for icier material) (de Pater *et al.* 1985). Regardless of the exact depth, it is clear that the microwave data show a lower temperature than at the surface. Here we see a case where the uncertain nuclear porosity, composition, and conductivity have a very direct effect on the interpretation of data.

3.4 Rotation of the Nucleus

The rotation of cometary nuclei has been studied for the past few decades, as mentioned in Chapter 1. However for only a handful of nuclei are there arguably well-determined rotation periods. A thorough review has been written by Belton (1991), and Meech (1999) has added more information from the 1990s. It is likely that some cometary nuclei are in complex rotation, complicating one’s derivation of the rotation state via observations, and it is telling that there is still uncertainty in the rotation state of 1P/Halley’s nucleus, one of the most deeply studied comets in all history. In this section I will give a brief description of the easy methods to determine a periodicity in the rotation state of the nucleus, but there is the caveat that it is not the only periodicity.

There are two main methods I employ for determining periodicity, one based on the morphology of the near-nuclear coma, the other based on the photometry of the comet’s photocenter. I did not use the zero-date method used by Whipple (1982) because the other two methods are more reliable, as Whipple himself has stated.

The first method, used for Comet Hyakutake and Hale-Bopp, requires taking images over a long enough time baseline to be able to match up when a particular feature in the dust coma – e.g., a jet or an envelope – returns to the same orientation. The time between these witnessed events is an integer multiple of the rotation period. There are pitfalls to this method: there is a basic assumption that an active area on the nucleus that produces the coma feature when it is first seen will stay active long enough for the observer to witness it later. Moreover, even if it does stay active, it may not be easy to tell when that particular feature is back in view: e.g., one could be fooled if there is another similar-looking jet in the coma. Implicit in the use of this method is that the comet itself does not change significantly during the observing interval. For example determining the periodicity could become problematical if, during the observing interval, the comet goes into outburst or splits.

The second method, which was also used on comet Hyakutake and on comet Encke, involves measuring the photometry over a long enough continuous time interval to watch the variation in brightness. In principle one could do this with the post-processed images, where the coma has been removed leaving just the light of the nucleus, but this has not been possible for any of the comets in this study. This method measures the variation due to the changing cross section of the nucleus plus whatever variation is due to the coma. Fortunately for the two comets it was not difficult to tell which component was both dominating the flux value and the variation. The data set for this method is a light curve, a time-series of the flux.

The extraction of a period from these data is a non-trivial problem. For the first method, at the most basic level one matches images by eye, although for good

temporal sampling cross-correlation methods may be possible. When employing the second method, common simple algorithms that are used in the cometary science community (as well as other fields of astronomy, e.g., variable star research) are described by Stellingwerf (1978) and Dworetsky (1983); these involve trial-and-error of many potential periods, minimizing the length of a string that connects the time series photometry in a phased light curve plot. An advantage is that the algorithm is perfectly able to deal with data sampled at a non-periodic rate, and also it is not beholden to any assumed shape of the light curve, sinusoidal or otherwise. A related method is to just take the Fourier transform – i.e., get a power spectrum – of the time-series, and find the most important frequency. Since the mathematical process of transforming can introduce extra noise into the data, this method works best when there are many points to the light curve.

One significant problem with the morphological and photometric methods is that an observer usually does not have perfect temporal coverage of the entire rotational phase. An observing night often just does not last long enough to watch a nucleus cycle through one complete rotation. Stringing observations together over several nights helps alleviate this problem, but it is hardly ever completely eradicated: there are usually aliases to the best choice of periodicity P that one finds for the particular observing run, aliases with values like $\frac{3}{2}P$ or $\frac{1}{2}P$, i.e., small whole-number ratios multiplying P . In general the longer the baseline over which one observes, the better one can constrain the period.

Chapter 4

The Nucleus of Comet Hale-Bopp

4.1 Background

Comet Hale-Bopp, discovered in July of 1995, likely was the most watched comet in all of history. A prodigious producer of dust and gas and a marginally advantageous orbital geometry combined to provide quite a show for several months in early 1997. However, all of that gas and dust made it exceedingly difficult to measure the nucleus; the continuum of the comet was dominated by the dust grains in the optical and mid-IR regimes. Two unusual techniques helped to partially sidestep this problem – the observation of an occultation of a star by the comet, and the measurement of the microwave continuum. The latter has been discussed briefly in Chapter 2. The former I will describe in detail here, with text heavily borrowed from a paper I wrote (Fernández *et al.* 1999).

4.2 Occultation Measurements

4.2.1 Introduction

Since the length scales of the nuclei and inner comae of comets are so small, stellar occultations hold great promise for probing these deep regions at the heart of the comet (see, e.g., Combes *et al.* [1983]). For a comet that is 1 AU away, the ~ 10 -km length scale subtends less than $0.02''$, or less than half the width of a pixel on the Planetary Camera of *HST*'s WFPC2. Unfortunately, there are only a few published reports of observed occultations by comets, and the reported chords have not come particularly close to the nuclei. The extinction of the star has been found to be a few percent at a distance of several hundred kilometers from the nucleus for comets of various activity levels and dust-to-gas ratios (e.g., Larson and A'Hearn 1984, and Lecacheux *et al.* 1984). One comet has been the target of an occultation observation with an impact parameter so small that the star was occulted by the nucleus itself, not just the coma: 95P/(2060) Chiron (Bus *et al.* 1996). Of course the very low activity, large nucleus, and regular orbit of this object mark this as a special case.

Though most previous data on cometary occultations were obtained at permanent observatories, with a sufficient number of portable telescope systems spaced across a territory over which an occultation is predicted to occur, as we have done

here, one can in principle obtain a size and shape estimate of the nucleus – independent of the albedo ambiguity found in optical photometry – and an estimate of the opacity structure of the coma to learn about the dynamics and scattering properties of the dust.

It is worthwhile to emphasize the differences between observing comet occultations and the much more common asteroid counterparts. While an asteroid is a point source, located near the center of brightness, and usually on a well-defined path (making the prediction uncertainty just a few shadow widths), a cometary nucleus is often swamped by coma emission of an uncertain morphology, making it hard to decide exactly where the nucleus is within the comet image’s brightest pixel. (This is especially true for Hale-Bopp, the dustiest comet on record.) Moreover, nongravitational forces push the comet away from the ephemeris position (although fortunately this is probably not a problem for Hale-Bopp). There are even potentially significant errors in the ephemeris itself, since it is usually derived from astrometry of the comet’s brightest spot, not the nucleus’ location. Lastly the typical comet nucleus is only a few kilometers wide. The result is to make observing cometary occultations more logistically difficult than observing their asteroid counterparts.

Here I report the observation of the dimming of star PPM 200723 due to its occultation by Comet Hale-Bopp (C/1995 O1). (The star is also known as SAO 141696, BD -04 4289, and GSC 5075-0004.) Barring a terrestrial explanation, the star’s light was completely or nearly completely blocked along part of one occultation chord, implying that a line of sight through an optically thick portion of the inner coma, or through the nucleus itself, was observed. On two other chords, no significant diminution of light was observed. If our interpretation is correct, this is the closest to the nucleus a typical comet has ever been sampled via a stellar occultation. I will give results from analyses of the data from this unique observation in the following sections.

4.2.2 Observations

The circumstances of the 5 October 1996 (UT) event are given in Table 4.1. The occultation path (uncertain to ± 60 s in time and ± 700 km in distance) passed through the western United States soon after sunset on 4 Oct. Six portable teams were arrayed across the region and one permanent facility was used; a map is shown in Fig. 4.1 with the location of the teams as crossed-squares. Table 4.2 lists the location, equipment, and data obtained by the seven teams. Each mobile team (1 through 6) had two members; I was part of Team 5. Originally the teams were to spread out from central Nevada northward to maximize the chance that at least one team would record a significant optical depth ($\geq 10\%$) through the coma; clouds covering Washington, Oregon, Idaho, and western Montana during the event dictated where each portable team positioned itself. Sufficient signal during the event was obtained only by Teams 5, 6, and 7: Team 5 recorded a feature that appears to be the event itself through passing cirrus clouds, while observing at the town dump of Snowville, Utah. Team 6 has at best a marginal light curve feature at the appropriate time, and Team 7 did not detect the event.

Table 4.1. Characteristics of Comet Hale-Bopp Occultation

• The Star, PPM 200723	
Magnitude ^{a,b}	$m_V=9.1$
MK Spectral Type ^b /Luminosity Class ^c	K0V
J2000 Right Ascension ^b	17 ^h 29 ^m 59 ^s .845
J2000 Declination ^b	-4°48'09".45.
• The Comet, C/1995 O1 (Hale-Bopp)	
Magnitude (in 24-arcsec wide circular aperture)	$m_R=8.5$
Heliocentric Distance	2.83 AU
Geocentric Distance	3.00 AU
Distance Scale at Comet	2.18 km \doteq 10 ⁻³ arcsec
Solar Elongation	71.0°
Phase	19.5°
Proper Motion and PA	8.41 arcsec/hr, 30.6°
Equivalent Linear Speed	5.11 km/s
• The Observing Locale ^d	
Time of mid-event	5 Oct 1996, 03:17:48 UT \pm 3 s
Speed of Nuclear Shadow	11.6 km/s
Elevation and Azimuth of Comet	25.8°, 235.8°

a Smithsonian Astrophysical Observatory 1966.

b Röser and Bastian 1991.

c Measured by Jeffrey Hall of Lowell Obs. (private communication).

d Specifically, location of Team 5 (see Table 4.2) at the time of event.

Table 4.2. Observations of Occultation by Comet Hale-Bopp

Team	Location		System [†]		Summary of Results
			CCD	PMT	
1.	44°39' N	112°05' W	✓		Heavy clouds during event
2.	43°19' N	114°41' W	✓		Heavy clouds during event
3.	43°05' N	116°19' W	✓		Heavy clouds during event
4.	42°30' N	114°47' W	✓		Heavy clouds during event
5.	41°57' N	112°44' W		✓	Thin clouds, but detection of event
6.	37°12' N	117°00' W		✓	Clear; marginal detection?
7.	35°06' N	111°32' W		✓	Clear, but not detection

[†] Teams 1 through 6 used Celestron C14 14-in (0.35-m) telescopes; Team 7 used the Lowell Observatory 31-in (0.8-m) NURO telescope. Teams with “CCD” used a charge-coupled device. Teams with “PMT” used a photomultiplier tube with effective wavelength near 4000 Å.

The three solid lines in Fig. 4.1 trace out two 100-km wide swaths which show the last pre-event prediction of the occultation track. The true track was only as wide as Hale-Bopp’s nucleus (with projection effects), and the swaths do *not* represent the systematic error in the determination of the track’s location, which were closer to ± 700 km (1σ). These swaths were used to aid in choosing locations for the portable teams.

The pre-event ephemeris (Solution 41 by D. K. Yeomans of Jet Propulsion Laboratory) predicted an occultation path shown by the long-dashed lines in Fig. 4.1. Astrometric corrections to this path, using images of the comet taken with the U. S. Naval Observatory Flagstaff Station (USNOFS) 1.5-m telescope, moved the predicted track to the short-dashed lines in Fig. 4.1. The coma-fitting technique that I describe in Chapter 3 was employed to find the source of the coma (i.e., the nucleus) within an image of the comet’s center of brightness, moving the track to the solid lines in Fig. 4.1. The corrections gave a net shift to the prediction of Yeomans’ ephemeris of about 9×10^2 km northwest. Our apparent detection of the nucleus occurred closer to the original prediction than the corrected one, indicating we had underestimated the prediction errors and that our corrections did not reduce the error, only delimit it. As we will show, with all the uncertainties of event prediction (as mentioned in Section 4.2.1), the detection of the occultation ~ 800 km away from the “best” guess is perfectly reasonable.

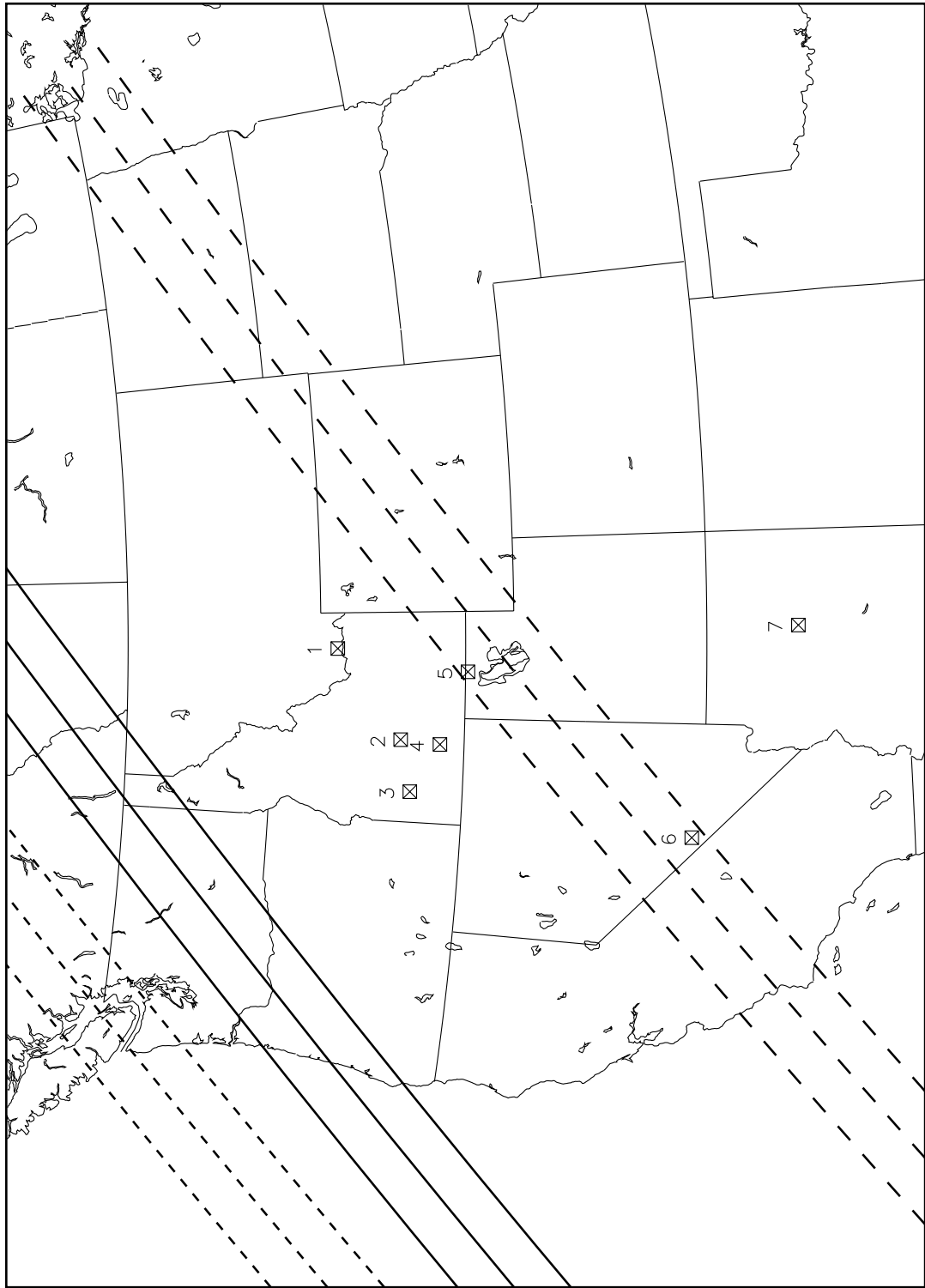
Weather and equipment problems prevented Team 5 from observing the comet and the star separately to determine their relative brightnesses in the photometer passband. Using the known spectral characteristics of both objects, combined with broad- and narrow-band imaging taken near the day of the event, we estimate the star to be 0.35 ± 0.02 times as bright as the sum of the comet, sky flux, and detector noise. The method is described here.

The bandpass of Team 5’s system is shown in Fig. 4.2; all that is needed is the ratio C of star flux to the sum of fluxes from comet, sky, and detector noise within this band and within the 1-arcmin wide aperture that was used. Starting with CCD observations of the comet and star taken with the USNOFS 1.5-m telescope on 2, 3, and 5 Oct 1996. We know the relative brightnesses (to $\pm 5\%$) in their passband, the spectral shape of which is also shown in Fig. 4.2 (Monet *et al.* 1992). To switch to Team 5’s band now requires knowing the spectra of the comet and the star.

Fig. 4.2 shows the spectrum of a typical K0V star (Kharitonov *et al.* 1988, Silva and Cornell 1992, Jacoby *et al.* 1984) and of the Sun (Neckel and Labs 1984, Labs *et al.* 1987). The comet’s spectrum is the same as the solar spectrum plus fluorescence emission lines and any reddening of the dust. Using CCD imaging taken on 12 Oct 1996 UT with the Lowell Observatory 1.1-m Hall telescope and narrow-band International Halley Watch filters (as described by Vanýsek [1984]), we found the dust to be at most only 0.03 ± 0.05 mag redder than the Sun. Moreover we found that CN and C₂ emission (the dominant species in Team 5’s spectral range) would contribute only about $6\% \pm 1\%$ of the flux. Hence the solar spectrum in Fig. 4.2 is actually a good representation of the comet’s spectrum. In Oct 1996 the comet had almost constant morphology and magnitude, so there is little error in using images taken 7 days after the occultation.

Thus we can calculate the relative star and comet brightnesses to within a few

Figure 4.1 (next page): Locations of observers for occultation by Hale-Bopp. Here is a map of the western United States showing the locations of the participating teams (crossed-squares) and the occultation track predictions. The long-dashed lines show the original ephemeris prediction; short-dashed lines show intermediate solution including astrometric corrections; solid lines show last prediction including corrections from deriving the nucleus' position within the comet's photocenter. The three lines mark out a 200-km wide swath, which was used for planning purposes; the nucleus' shadow is much narrower.



percent. The only caveat is that the systematic error may be higher if our star is not a typical K0V star. Our remaining task is to account for sky and detector noise contributions. The latter we measured to be negligible compared to that of the sky and the comet. From practice observations in conditions roughly as dark as for the observation of the occultation itself, we found the sky to be about $8\% \pm 2\%$ of the comet's brightness, thus the factor from the spectral analysis should be divided by 1.08 ± 0.02 . The combination of all information yields $C = 0.35 \pm 0.02$.

4.2.3 Data

The light curve from Team 5 is shown in Fig. 4.3. The data span about 34 minutes (top graph); the ~ 7 minutes centered on the time of deepest occultation (at 03:17:48 UT ± 3 s) are shown in the lower panel. The photometer integrations were 100 ms long, and the aperture was circular and one arcminute wide.

The light curve is characterized by (a) long (several minute), gradual changes in the count rate due to passing clouds (e.g., the general trend from 03:14:30 to 03:27:30); (b) precipitous drops in flux due to the comet and star (which were nearly superimposed) being near the edge of the aperture, immediately followed by even more rapid (few second) rises as the target is restored to the center of the field of view (e.g., at 03:26 and 03:27:45); (c) small drops in flux due to the comet and star moving a bit off-center in the aperture, followed by a quick restoration as the target is recentered (e.g., at 03:11:30, 03:16:30, 03:19:00, 03:20:00 and [importantly] at 03:17:35); and (d) the occultation event itself near 03:17:48. The distinct morphological differences between these four types give us confidence that we have observed the occultation event. The occultation caused a fairly symmetric valley in the light curve of about one minute in length, shorter than the time scale for the effects of passing clouds, but longer than the time scale for a drop and rise in flux due to the position of the target in the aperture.

Cases (b) and (c) above were caused by the telescope not exactly tracking at the proper motion rate of the comet. The times of these corrections are marked with arrows in Fig. 4.3. The correction at 03:17:35, the one before it, and the two after were all minor and belong to case (c). Since most of the comet's flux was in its coma, a slight offset of the target did not cause a significant decrease in flux; the more obvious manifestations of these corrections are the small noise spikes from the telescope drive's electrical interference.

The drop in count rate at the time of deepest occultation is about 25%, which is consistent with the star being totally blocked from view, since it was 0.35 times the brightness of the other contributors to the flux ($0.35/1.35 \approx 25\%$). Moreover it occurs close to the predicted time of 03:18:10 for the location of Team 5. The dip could not be due to a jet contrail since the light curve would resemble a profile through a uniform density gas cylinder, which would have a shallower slope through the middle of the event, unlike what has been recorded. While we cannot unambiguously rule out that an unusual cloud passed in front of the comet, the circumstantial evidence does imply an observation of the occultation.

There is a dip in the light curve at approximately 03:12:30 UT which may be interpreted as morphologically distinct from the effects of both clouds and tracking errors, and so could be construed to be the occultation event; it is the only other

Figure 4.2 (next page): Comparison of occulter (cometary) and occultee (stellar) spectra. The dashed lines give the bandpass of the observing system at the USNO 1.5-m telescope and of the C-14 and photometer system used by Team 5 for the occultation. A comparison of the spectra (solid lines) of a K0V star and a solar-type star, which in this case approximates the spectrum of the comet, was used to transform the relative brightnesses of the comet and star from the USNO system to the Team 5 system.

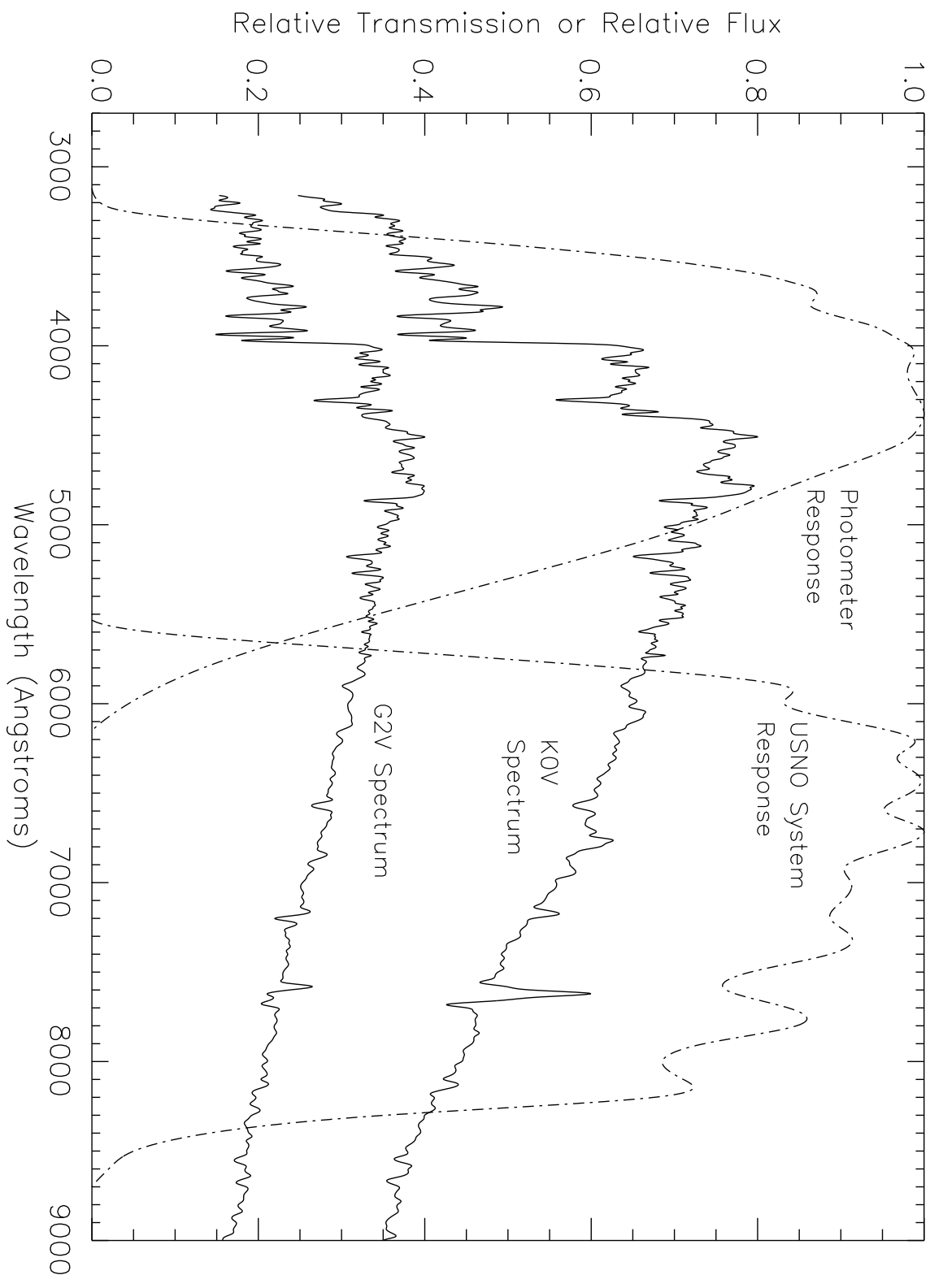
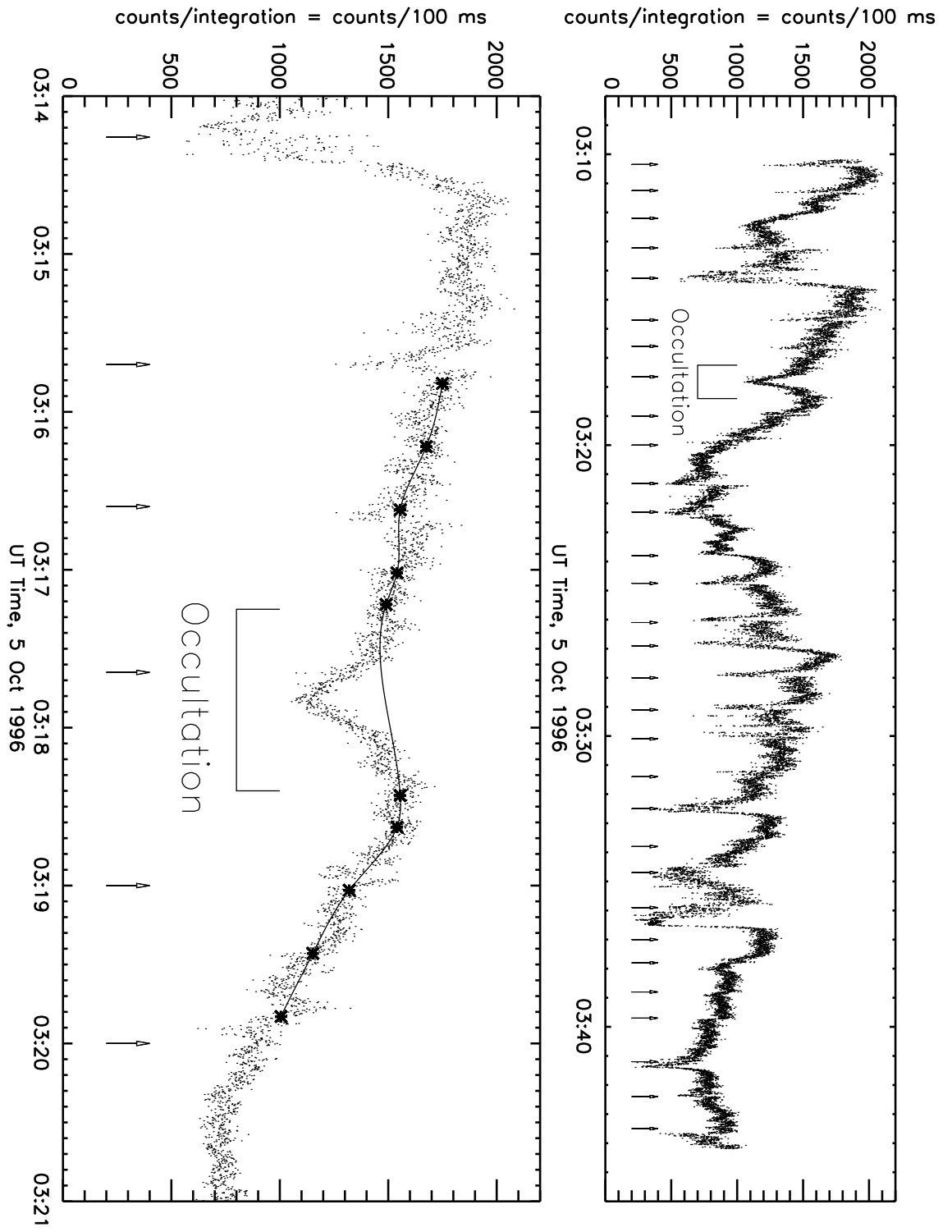


Figure 4.3 (next page): Light curve of occultation by Hale-Bopp, Team 5. This light curve shows the occultation event, a feature that is morphologically distinct from all others. The top plot covers all 34 minutes of the light curve; bottom plot shows 7 minutes centered on the occultation feature. The integration time for each data point was 100 ms. Arrows indicate tracking corrections; see text for details. The tracking correction near the center of the occultation was not significant. The asterisks indicate the locations where the large-scale effect of the cirrus clouds was sampled, and the thick line is a spline fit to those points. This fit was used by our model to grossly account for the non-photometric conditions.



feature in the light curve, aside from the one at 03:17:48 UT, that could have been caused by the occultation. An event this early would, however, imply a rather large error of thousands of kilometers. While it is possible to model the circumstances of the event (in the manner described in the next section) to reproduce the curve, the fits are less robust than those for the 03:17:48 feature. Accounting for the effects of extinction by the clouds makes the feature quite skew, which reduces the ability of our model to adequately fit it.

In sum, due to the unique shape of the feature at 03:17:48, our ability to model it well, its closeness to the predicted time, and its depth, we believe that it is likely due to the occultation event and not due to tracking errors or clouds.

The light curve recorded by Team 6 is shown in the top of Fig. 4.4, observed from a position 643 km farther along the shadow track from Team 5, and 170 km perpendicular to it. This light curve was obtained in a cloudless sky so all variations are due to tracking errors, gain changes, and manifestations of the occultation. At the time one would expect the comet's shadow to pass over Team 6 (based on Team 5's results; marked on the figure), there is a drop in flux of a few percent (lower panel of Fig. 4.4). That feature's shape is similar to other tracking error corrections in the light curve, so it is not clear if this is the occultation. However, it does allow us to limit the opacity of the coma 170 km from Team 5's chord at 8%.

4.2.4 Analysis

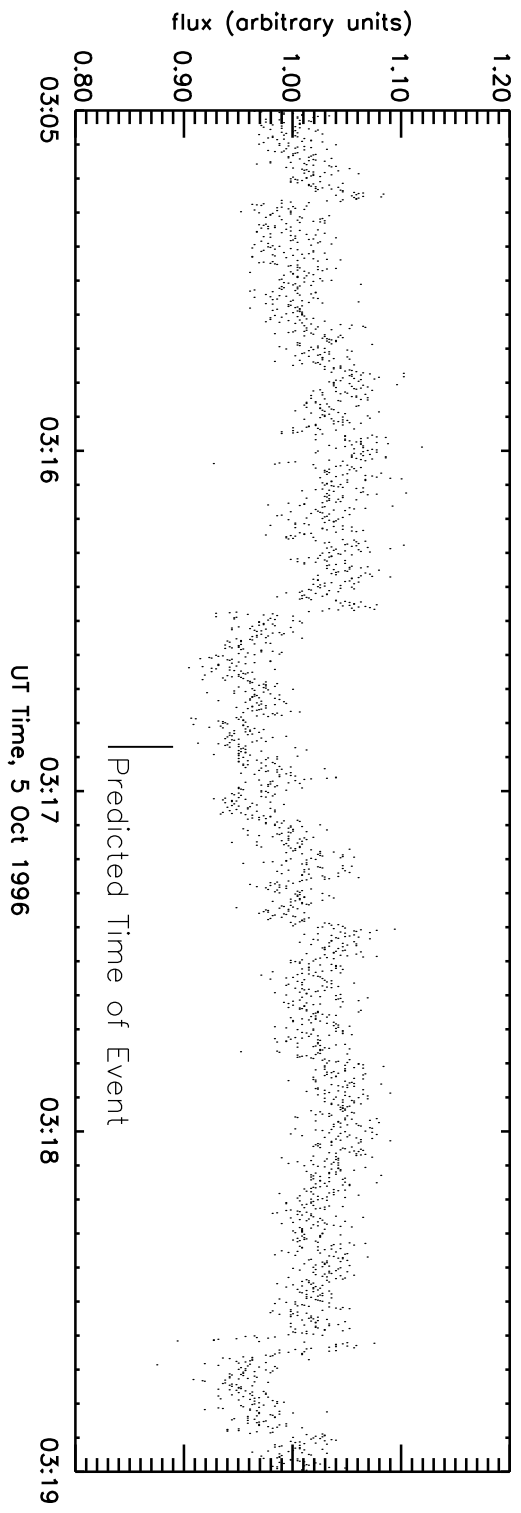
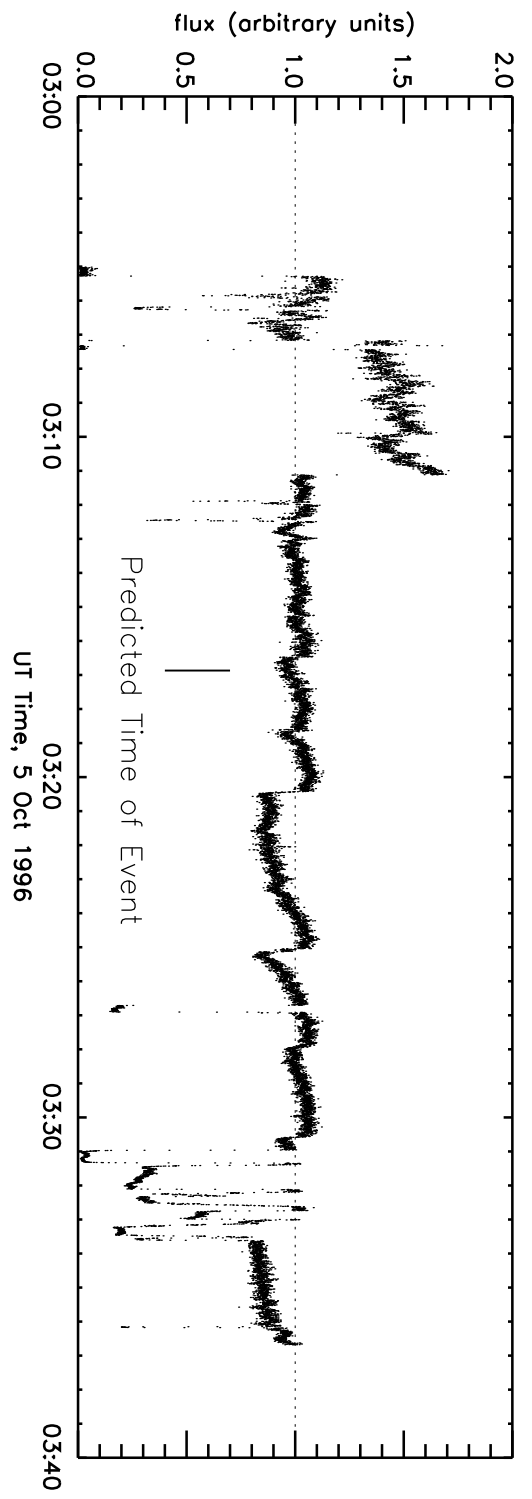
4.2.4.1 Model and Assumptions

Our model for the light curve assumes the optical depth, τ , is proportional to the inverse of the cometocentric distance, $1/\rho$, raised to a constant power n . (The steady-state, force-free, radially-flowing dust coma would have $n = 1$.) As the comet passes between Earth and the star, the attenuation of starlight will depend on time. A schematic of the scenario is given in Fig. 4.5. Ignoring clouds for the moment, we express each point in the light curve, $S(t)$, as a constant term (S_0 , the comet's flux plus sky flux and detector noise) plus a term representing the star's flux times the attenuation factor ($e^{-\tau(t)}$). Let $C = 0.35 \pm 0.02$ be the ratio of the star's unattenuated flux to S_0 . Then $S(t) = S_0(1 + Ce^{-\tau(t)})$. If the comet's nucleus itself passes between the star and Earth, the flux during that interval will just be S_0 . If the star disappears behind the nucleus at time t_i , and reappears at time t_o , then the light curve can be represented by

$$S(t) = \begin{cases} S_0(1 + Ce^{-\tau_i(t)}), & \text{if } t < t_i; \\ S_0, & \text{if } t_i < t < t_o; \text{ and} \\ S_0(1 + Ce^{-\tau_o(t)}), & \text{if } t > t_o. \end{cases} \quad (4.1)$$

Since we do not assume *a priori* that the two sides of the coma that are sampled by the inbound and outbound sections of the occultation are the same, we have a three-piece function. We can however remove the nuclear chord in the model simply

Figure 4.4 (next page): Light curve of occultation by Hale-Bopp, Team 6. This light curve has the expected time of the occultation marked, based on the time of deepest occultation recorded by Team 5. The Top panel shows the whole curve; lower panel shows a close-up of the most relevant section. Ordinate units are arbitrary. There is a slight dip in the count rate at the appropriate time, but it is not distinguishable from other, comparably-shaped features.



by setting $t_i = t_o$. The subscript i denotes a quantity related to the ingress; o , to the egress.

Evaluating τ as a function of time requires knowing ρ . The distance from the center of the nucleus at a given time t is just $\sqrt{b^2 + (v(t - t_m))^2}$, where b is the impact parameter, v is the speed of the comet across the sky, and t_m is the time of mid-occultation. Since the center of the (assumed spherical) nucleus does not have to be the coordinate origin for ρ , we include an extra term, l_0 , that describes the offset (parallel to the star's direction of motion) of the coordinate origin from the nuclear center. Thus, $\rho(t) = \sqrt{b^2 + (v(t - t_m) - l_0)^2}$ and the optical depth is given by

$$\tau_i(t) = \left(\frac{\kappa_i}{\sqrt{b^2 + (v(t - t_m) - l_{0i})^2}} \right)^{n_i}, \quad (4.2a)$$

$$\tau_o(t) = \left(\frac{\kappa_o}{\sqrt{b^2 + (v(t - t_m) - l_{0o})^2}} \right)^{n_o}, \quad (4.2b)$$

where κ is the length scale of the opacity. Since we allow the time t_m to be fit by the model, we have overparameterized the lateral shift in the coordinate origin; the best parameter to quote really is $\Sigma l_0 \equiv l_{0i} + l_{0o}$, i.e., the separation of the two coordinate origins. In later discussion we will mention the nuclear radius, R , which is just

$$R = \sqrt{b^2 + \left(\frac{1}{2}l_n\right)^2} \equiv \sqrt{b^2 + \left(\frac{1}{2}v(t_o - t_i)\right)^2}, \quad (4.3)$$

i.e., the square root of the quadrature-addition of the impact parameter and half the length of the chord through the nucleus. A listing of all quantities is given in Table 4.3.

Note that the impact parameter b was *not* used as a measure of the offset from the coordinate origin in the perpendicular direction. The coordinate origin always lies on the horizontal line in Fig. 4.5 that runs through the center of the nucleus. There is no evidence that our assumption is justified but it does make the modeling tractable and allowed us to constrain properties of the nucleus.

In addition to this theoretical model, we accounted for the large-scale extinction in the light curve due to clouds near the time of the event by multiplying our model by an empirical function. On Fig. 4.3, the asterisks in the light curve indicate where it was sampled to estimate the clouds' effect. The thick line is a spline fit through those points and represents the empirical function. We sampled the clouds' effect outside the region to which we applied our model. The observation site of Team 5 was dark and moonless, so the clouds would only cause extinction of the starlight, not increase the sky brightness.

We have made some assumptions to simplify the fitting. The spherical nucleus assumption immediately implies that $t_o - t_m = t_m - t_i$. Also note that our model coma (Fig. 4.5) is not perfectly circular; n and κ can be different between the two hemispheres, but within one hemisphere they cannot vary. We have not included in our fitting the data near the time of the tracking correction (2.8 seconds centered at 03:17:45.9 UT), and two brief noise spikes (0.5 seconds starting at 03:17:39.0 UT);

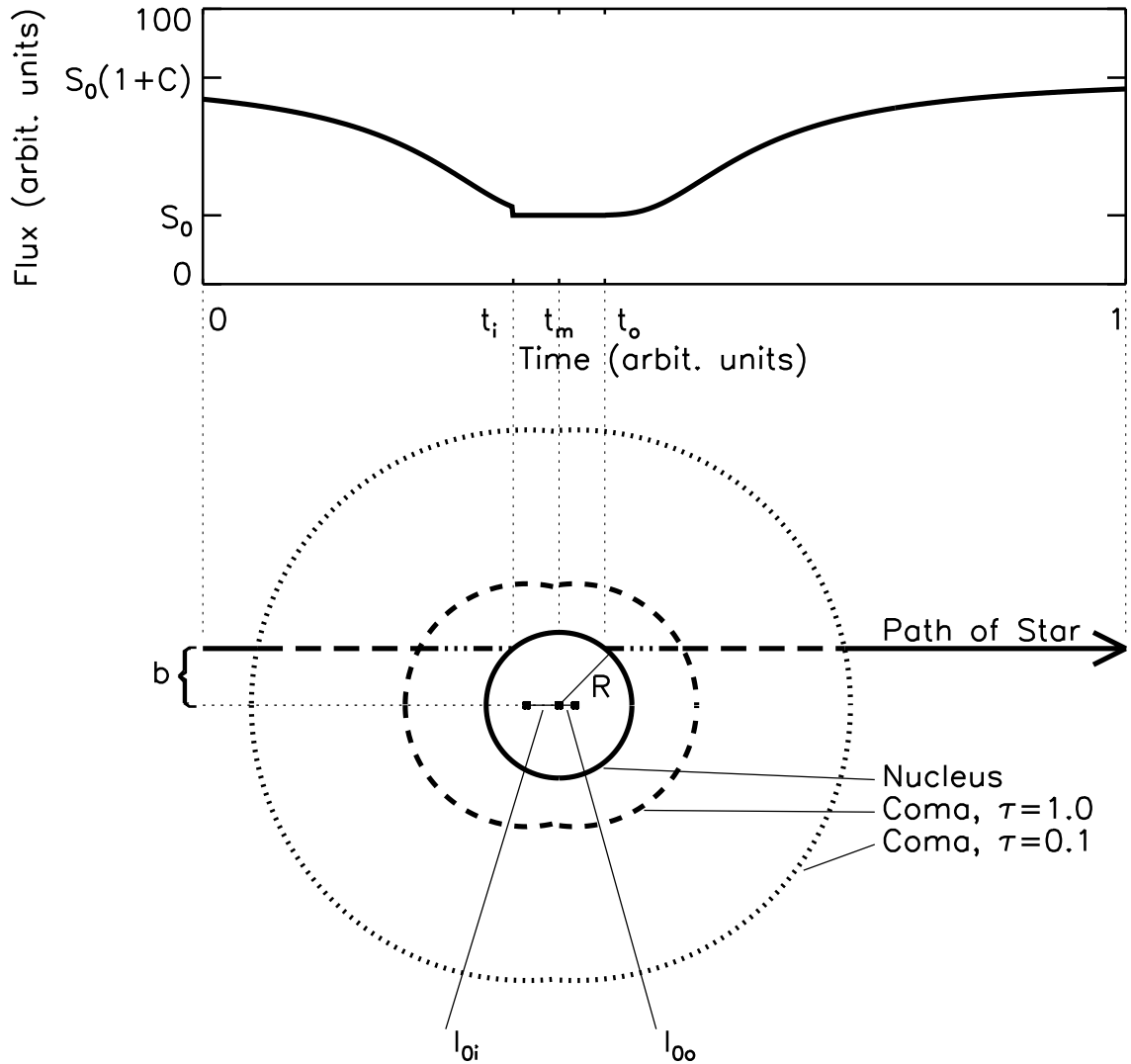


Figure 4.5: Schematic of occultation scenario and light curve. The top plot shows a generic light curve based on the star's passage behind the coma and nucleus of the comet. The arrow in the drawing indicates the star's motion. Times of the beginning and end of nuclear chord are marked (t_i and t_o , respectively), as is mid-occultation (t_m); note the abrupt jump in the flux at time t_i as the star passes behind the nucleus. The locations of a coma opacity of 0.1 and 1.0 are marked. All variables are defined in Table 4.3.

Table 4.3. Parameters of the Model of Nuclear and Comatic Structure

Symbol	Description
<i>Fit Variables</i>	
S_0	count rate from comet+sky+dark current
t_i & t_o	beginning and ending times of occultation by nucleus
t_m	time of mid-event
l_n	length of the nuclear chord of the occultation
b	impact parameter
n_i & n_o	exponent of the power-law profile of the opacity
κ_i & κ_o	length scale of the opacity
l_{0i} & l_{0o}	distance of cometocentric coordinate origin from center of nucleus
<i>Variables Derived from Fit</i>	
τ_i & τ_o	opacity
R	nuclear radius
<i>Known Constants</i>	
C	ratio of count rate from star to S_0 (0.35 ± 0.02)
v	speed of comet across sky (5.11 km/s)
<i>Subscripts</i>	
subscript i & o	variable pertains to ingress and egress of occultation

1.3 seconds starting at 03:17:52.8 UT; see Fig. 4.3). Lastly, we have assumed that the radius of the nucleus is no bigger than 50 km. Analysis of high-resolution mid-infrared, microwave, and optical imaging of the comet have constrained the nuclear size to be smaller than this value (Altenhoff *et al.* 1999, Weaver and Lamy 1999, and a later section of this Chapter), so our assumption allows for a large error in these works. In terms of our fitting, this means we will not consider models that require a combination of b and l_n such that $R \geq 50$ km.

Further assumptions were made about the physical environment of the coma. First, we assumed that n could be no larger than 2.4. Hydrodynamic models of the coma (Divine 1981) imply that a steepening of the dust density profile to the equivalent of ρ^{-3} (yielding a surface brightness (and opacity) proportional to ρ^{-2}) can occur within a few nuclear radii of the nucleus. Others (e.g., Gombosi *et al.* [1983, 1985], Marconi and Mendis [1983, 1984]) have also used dusty-hydrodynamic models to calculate dust velocities and/or number densities as a function of cometocentric distance, and their results do show some steepening of the dust profile within a few nuclear radii of the surface. From these works we conjecture that the tenable limit to n in this phenomenon is ~ 2 to $2\frac{1}{2}$, though the higher values have less theoretical support. Again, we allow for a large error in these previous works. Our second assumption is that l_0 can not be so large as to extend off the near edge of the nucleus itself. In other words, we did not allow the case where $\rho = 0$ (and the divergence of the opacity) could be encountered by the star.

4.2.4.2 Results of Model Fitting

Since there are so many data points, in this case the χ^2 statistic is useful only as a coarse indicator of “good” and “bad” fits; e.g., a fit that goes through all of the points but is too shallow to cover the light curve’s minimum could have a reduced χ^2 (χ_R^2) of just 1.15, which would still be beyond the 99% confidence level for the 620-odd degrees of freedom. The best way to ascribe a “good” fit is by eye, with χ^2 being a rough guide. There are three morphological characteristics that must be satisfied for a fit to be considered “good”: a) it must be sufficiently deep to cover the valley at 03:17:48 UT (determined by κ , n , b , and to some extent by $t_o - t_i$); b) it must follow the shape of the valley’s walls (from 03:17:33 to 03:17:45 and from 03:17:53 to 03:18:03 UT; determined by κ , n , and l_0); and c) it must lie on the median value of the wings (from 03:17:15 to 03:17:33 and from 03:18:03 to 03:18:22 UT; determined by κ and n). We say “median” because we do not attempt to fit the small jumps in flux that occur in the wings; these may be due to clouds or to real opacity features in the comet’s coma. A given model was detuned with the various parameters until the fit could no longer be considered marginally “good.”

The results of the fitting are summarized in Table 4.4. We have explored parameter space using $b = 0, 6.5, 11, 22, 26, 33, 39,$ and 45 km (and higher values, but it turned out that they never sufficiently fit the light curve), and $n = 0.8, 1.0, 1.2, 1.4, 1.6, 1.8, 2.0,$ and 2.4 . Entries in the table give values or ranges for the quantities κ_i , κ_o , and l_n that yield “good” or marginally “good” fits as defined above. (In the “Comments” column, the presence or absence of “m” indicates a marginally good or good fit.) All fits listed in the table have $0.96 \leq \chi_R^2 \leq 1.05$, with most around 0.97, 0.98, or 0.99. With only one chord through the comet showing unambiguous

extinction, the valid parameter space offered by our model is large. Moreover, the unfortunate location of the tracking correction so close to the valley of the light curve, thus removing those data points, allows an even wider valid space.

Figure 4.6 displays representative fits to our light curve. It is not meant to be as exhaustive as Table 4.4 is, but graphically shows the large variation in parameter values that still allows adequate fitting. The first four plots have forced $\Sigma l_0 = 0$, the last four allow it to vary. The value of b is written within each plot. The abrupt jumps in the flux predicted by some models are due to the star passing behind the nucleus; note the jump at time t_i in the schematic light curve of Fig. 4.5. Special note should be taken of one model in Fig. 4.6a using $n_i = n_o = 1.0$; it cannot fit the curve. Also, Fig. 4.6d shows a model with $b = 39$ km; such a high impact parameter allows only a marginal fit to the curve. The value of χ_R^2 is 1.0 in all but the one obviously incorrect model, where it is 1.2.

We mention some other notable results from the modeling:

- Our modeled constraints on b limit the nucleus' radius R (via Eq. 4.3) to ≤ 48 km. Restricting ourselves to the best (not marginal) fits and to $n \leq 2.0$, then $R \leq 30$ km.

- For completeness we modeled the case where $b = 0$ and $l_n = 0$, even though clearly this is an unphysical scenario. Fortunately, it was never the case that the light curve was significantly better fit with $l_n = 0$ than with $l_n > 0$.

- The distance from the coordinate origin to the $\tau = 1$ point in the coma is given by κ . For some models in Table 4.4 $R > \kappa$, so the maximum coma opacity is less than unity. (The fit to the light curve for these models requires the nuclear chord to pass through the bad-data gaps.) On the other hand with a small R the maximum opacity can be as high as 2. Note that the noise in the light curve prevents us from confidently distinguishing between $\tau = 2$ and $\tau > 2$ (or $\tau = \infty$).

- For clarity we have not put in the allowable ranges of κ for each model in Table 4.4. Typically changing κ by ± 3 km still yields a good or marginally good fit.

- The acceptable fits to the light curve require n to be at least 1.0, though the fits are slightly better as n increases. Further, if $n \leq 1.2$ in one hemisphere, then $n \geq 2.0$ in the other. This steepness to the coma is opposite the sense found in *Giotto* images of comet Halley's inner coma, where $n < 1$ as $\rho \rightarrow R$ due to localized sources of dust on the surface (Thomas and Keller 1990, Reitsema *et al.* 1989). We postulate that the steepness in Hale-Bopp's coma is due to azimuthal structure (where we have assumed none) and/or to the passage of the star's path through the acceleration region of the dust. Clearly our model is simplistic, but the lack of data does not justify using a more complex formulation.

- One power law can satisfy the constraints of the light curves measured by both Team 5 and Team 6 if, in general, $n \geq 1.6$. A letter "c" in the "Comments" column of Table 4.4 indicate which models are consistent with both curves. Furthermore, if we force the coma to be consistent, it would then be impossible for the nuclear shadow to have passed between the two teams. I.e., if Teams 5 and 6 were on opposite sides of the nucleus, the parameters describing the two sides of the coma sampled by the two teams would have to be different, which is beyond the scope of our modeling. An alternate explanation is that the coma merely does not have the spherical or hemispherical symmetry that is assumed.

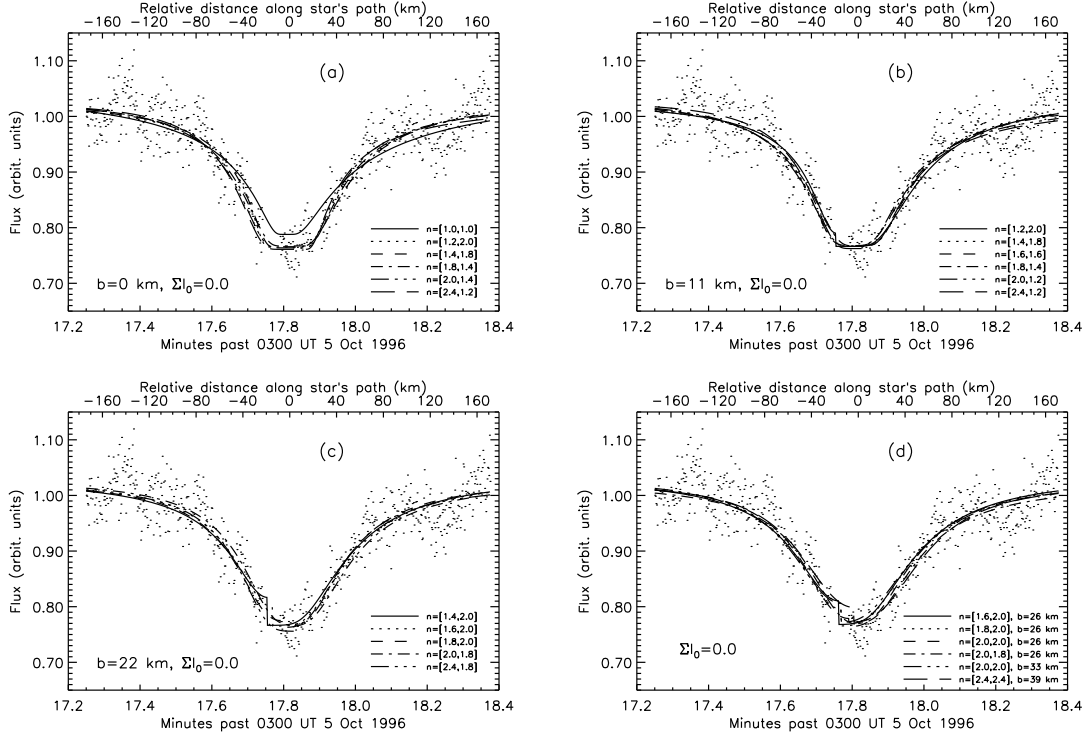


Figure 4.6a-d: Example model fits to occultation light curve. Shown here are example “good” model fits using various combinations of parameters, overlaid on the Team 5 light curve. This is not an exhaustive portrayal of the entire valid parameter space, but only demonstrates how well the curve can be fit. All models presented here assume there was no nuclear chord. Each plot has the impact parameter b written within its borders. The first 4 plots assume $\Sigma l_0 \equiv l_{0i} + l_{0o} = 0.0$. Each plot shows 5 or 6 models with varying n_i and n_o (written as $n = [n_i, n_o]$). Plot (a) shows clearly that $n_i = n_o = 1.0$ does not fit the curve; plot (d) shows an example of an impact parameter higher than ~ 35 km that marginally fits the curve. The blank section near 17.7 minutes past 0300 UT, caused by a tracking correction, allows for great latitude in the kind of models that can fit the data.

- For most models, we find $-10 \text{ km} \leq \Sigma l_0 \leq 15 \text{ km}$, though for $b > 30 \text{ km}$, the range is only a few kilometers. Moreover, having the coordinate origin of both hemispheres on the ingress side of the nucleus is slightly favored (by a $\leq 2\%$ decrease in χ_R^2). Note that in comet Halley, the origin was found to be near the center of the nucleus (Thomas and Keller 1987).

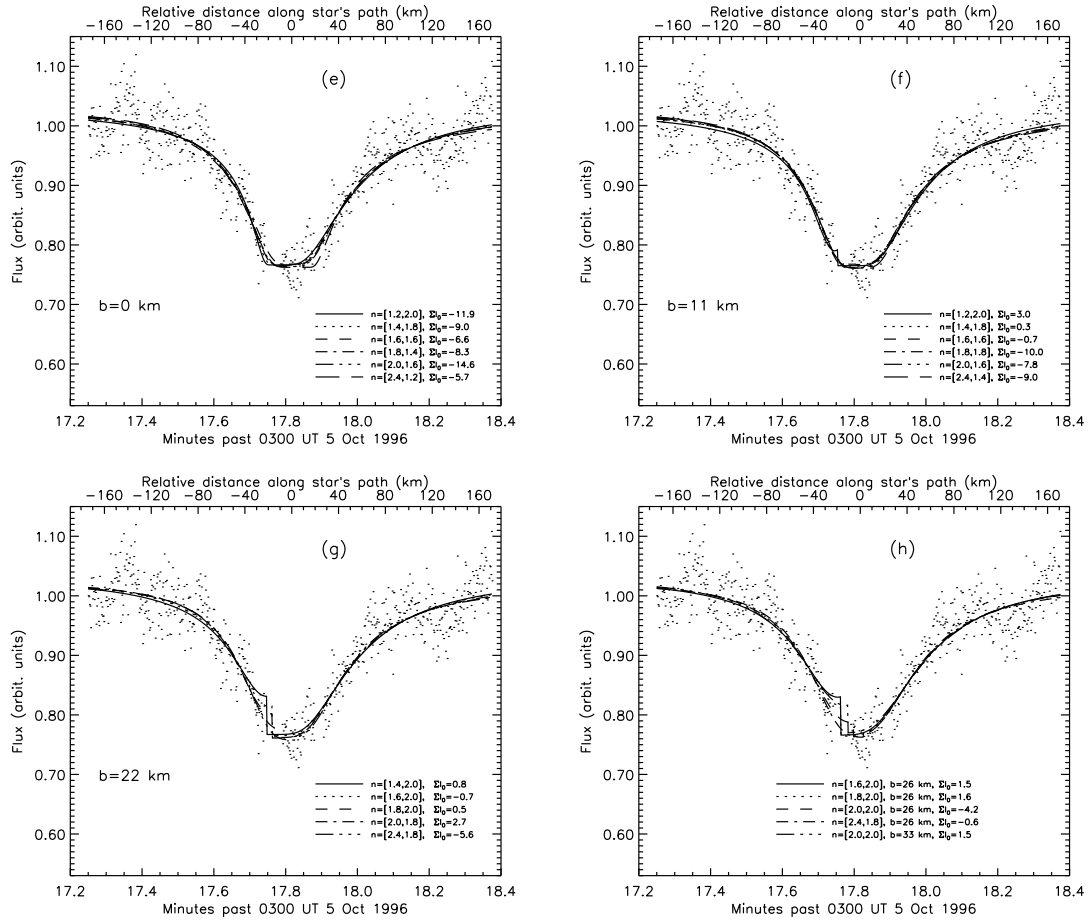


Figure 4.6e-h: Example model fits to occultation light curve. Here is the same scenario as for 6a-d, except the 4 plots allow $\Sigma l_0 \neq 0.0$, and each model mentions the value used.

Table 4.4 Constraints on Parameters to Occultation Model

b (km)	n_i	n_o	κ_i (km) ^a	κ_o (km) ^a	$\rho(\tau = 0.1)$ _{b}	$\overline{1 - e^{-\tau}}$ _{c}	l_n range (km) ^d	R range (km) ^e	Comm. _{f}
0	1.0	1.8	21	64	[157,188]	0.40	0-26	0-13	m
0	1.0	2.0	19	66	[155,190]	0.39	0-22	0-11	
0	1.0	2.4	16	67	[153,174]	0.36	0-15	0-8	
0	1.2	1.8	25	61	[159,185]	0.41	0-24	0-12	m
0	1.2	2.0	23	60	[159,185]	0.38	0-24	0-12	
0	1.2	2.4	20	62	[135,159]	0.35	0-24	0-12	m, c
0	1.4	1.6	32	53	[166,179]	0.44	0-40	0-20	m
0	1.4	1.8	32	54	[162,179]	0.42	0-40	0-20	
0	1.4	2.0	28	55	[143,175]	0.38	0-36	0-18	c
0	1.6	1.2	45	40	[179,166]	0.48	0-52	0-26	m
0	1.6	1.4	43	44	[177,168]	0.47	0-56	0-28	
0	1.6	1.6	38	47	[158,172]	0.44	0-55	0-23	m
0	1.8	1.2	50	37	[179,161]	0.48	0-42	0-21	m
0	1.8	1.4	43	42	[154,168]	0.46	0-45	0-23	
0	1.8	1.6	42	42	[149,168]	0.43	0-54	0-27	m, c
0	2.0	1.0	54	30	[172,157]	0.49	0-30	0-15	m
0	2.0	1.2	52	34	[164,159]	0.48	0-34	0-17	c
0	2.0	1.4	45	39	[142,166]	0.45	0-48	0-24	c
0	2.0	1.6	44	39	[137,166]	0.43	0-48	0-24	m, c
0	2.4	1.0	55	27	[142,157]	0.48	0-25	0-13	m, c

Table 4.4 – *Continued*

b (km)	n_i	n_o	κ_i (km) ^a	κ_o (km) ^a	$\rho(\tau = 0.1)$ _{b}	$\overline{1 - e^{-\tau}}$ _{c}	l_n range (km) ^d	R range (km) ^e	Comm. _{f}
0	2.4	1.2	53	29	[140,157]	0.46	0-27	0-14	m, c
0	2.4	1.4	52	30	[135,154]	0.44	0-30	0-15	m, c
6.5	1.0	1.8	22	67	[155,190]	0.39	0-15	0-10	m
6.5	1.0	2.0	19	68	[153,192]	0.37	0-15	0-10	
6.5	1.2	1.6	26	60	[160,186]	0.40	0-28	0-15	m
6.5	1.2	1.8	26	61	[160,186]	0.39	0-25	0-14	
6.5	1.2	2.0	23	63	[155,188]	0.36	0-25	0-14	m
6.5	1.4	1.4	37	50	[170,175]	0.43	0-47	0-24	m
6.5	1.4	1.6	34	53	[168,177]	0.42	0-46	0-24	
6.5	1.4	1.8	32	55	[163,179]	0.39	0-41	0-22	
6.5	1.4	2.0	27	57	[137,181]	0.36	0-36	0-19	m, c
6.5	1.6	1.4	43	44	[177,168]	0.44	0-55	0-28	m
6.5	1.6	1.6	38	48	[161,172]	0.41	0-54	0-28	
6.5	1.6	1.8	35	50	[147,175]	0.39	0-46	0-24	m
6.5	1.8	1.0	56	33	[188,158]	0.49	0-33	0-18	m
6.5	1.8	1.2	52	35	[185,160]	0.41	0-35	0-19	
6.5	1.8	1.4	47	39	[167,163]	0.36	0-45	0-23	c
6.5	1.8	1.6	42	43	[150,168]	0.31	0-48	0-25	m, c
6.5	1.8	1.8	39	45	[139,159]	0.27	0-54	0-28	m, c
6.5	2.0	0.8	64	23	[196,149]	0.49	0-15	0-10	m

Table 4.4 – *Continued*

b (km)	n_i	n_o	κ_i (km) ^a	κ_o (km) ^a	$\rho(\tau = 0.1)$ _{b}	$\overline{1 - e^{-\tau}}$ _{c}	l_n range (km) ^d	R range (km) ^e	Comm. _{f}
6.5	2.0	1.0	60	26	[190,151]	0.45	0-18	0-11	
6.5	2.0	1.2	53	32	[168,158]	0.40	0-33	0-18	m, c
6.5	2.4	0.8	64	20	[166,148]	0.47	0-15	0-10	m
6.5	2.4	1.0	62	22	[162,149]	0.44	0-13	0-9	m, c
6.5	2.4	1.2	57	26	[148,153]	0.41	0-19	0-12	m, c
11	1.0	1.8	22	70	[153,192]	0.38	0-15	0-13	m
11	1.0	2.0	20	72	[151,194]	0.37	0-11	0-12	
11	1.2	1.8	25	64	[158,188]	0.38	0-23	0-16	m
11	1.2	2.0	23	65	[155,190]	0.36	0-17	0-14	c
11	1.4	1.6	34	55	[166,179]	0.36	0-35	0-21	m
11	1.4	1.8	31	57	[159,182]	0.38	0-30	0-19	c
11	1.4	2.0	28	59	[145,184]	0.35	0-27	0-17	m, c
11	1.6	1.4	41	45	[174,170]	0.42	0-52	0-28	
11	1.6	1.6	32	55	[136,182]	0.39	0-30	0-19	c
11	1.6	1.8	30	56	[124,184]	0.33	0-28	0-18	m, c
11	1.6	2.0	27	58	[112,182]	0.32	0-22	0-16	m, c
11	1.8	1.2	52	36	[186,160]	0.45	0-34	0-20	m
11	1.8	1.4	48	40	[171,164]	0.37	0-39	0-22	
11	1.8	1.6	43	44	[154,168]	0.40	0-48	0-26	m, c
11	2.0	1.2	53	34	[166,160]	0.44	0-33	0-20	c

Table 4.4 – *Continued*

b (km)	n_i	n_o	κ_i (km) ^a	κ_o (km) ^a	$\rho(\tau = 0.1)$ _{b}	$\overline{1 - e^{-\tau}}$ _{c}	l_n range (km) ^d	R range (km) ^e	Comm. _{f}
11	2.0	1.4	49	37	[156,162]	0.37	0-33	0-20	m, c
11	2.0	1.6	47	39	[147,164]	0.33	0-39	0-22	m, c
11	2.4	1.0	58	28	[152,155]	0.46	0-15	0-13	m, c
11	2.4	1.2	55	31	[142,158]	0.43	0-20	0-15	m, c
11	2.4	1.4	53	31	[138,158]	0.38	0-25	0-17	m, c
22	1.4	2.0	30	66	[157,189]	0.34	0-22	0-25	m, c
22	1.4	2.4	26	72	[134,187]	0.32	0-13	0-23	m, c
22	1.6	1.8	33	62	[141,187]	0.36	0-24	0-25	m, c
22	1.6	2.0	33	63	[138,187]	0.34	0-25	0-25	c
22	1.6	2.4	30	65	[126,168]	0.29	0-19	0-24	m, c
22	1.8	1.6	39	55	[138,180]	0.37	0-35	0-28	m, c
22	1.8	1.8	35	58	[124,185]	0.35	0-35	0-28	c
22	1.8	2.0	31	62	[113,189]	0.33	0-25	0-25	c
22	2.0	1.6	47	47	[149,170]	0.38	0-40	0-30	m, c
22	2.0	1.8	38	54	[121,180]	0.35	0-31	0-27	c
22	2.0	2.0	33	60	[105,187]	0.32	0-21	0-24	m, c
22	2.4	1.6	50	41	[131,165]	0.36	0-25	0-25	c
22	2.4	1.8	43	47	[112,169]	0.34	0-35	0-28	c
22	2.4	2.0	39	51	[102,159]	0.31	0-37	0-29	m, c
26	1.6	2.0	33	69	[139,192]	0.35	0-20	0-28	m, c

Table 4.4 – *Continued*

b (km)	n_i	n_o	κ_i (km) ^a	κ_o (km) ^a	$\rho(\tau = 0.1)$ _{b}	$\overline{1 - e^{-\tau}}$ _{c}	l_n range (km) ^d	R range (km) ^e	Comm. _{f}
26	1.6	2.4	30	72	[125,188]	0.32	0-12	0-27	m, c
26	1.8	1.8	40	60	[141,183]	0.36	0-35	0-31	m, c
26	1.8	2.0	34	65	[123,189]	0.33	0-23	0-28	c
26	1.8	2.4	30	70	[107,183]	0.31	0-11	0-27	m, c
26	2.0	1.8	40	59	[124,183]	0.33	0-29	0-30	m, c
26	2.0	2.0	36	62	[113,187]	0.33	0-24	0-29	c
26	2.0	2.4	31	68	[99,176]	0.30	0-15	0-27	m, c
26	2.4	1.8	45	50	[118,174]	0.34	0-45	0-34	c
26	2.4	2.0	42	53	[108,168]	0.32	0-40	0-33	c
26	2.4	2.4	32	65	[82,170]	0.29	0-15	0-27	m, c
33	2.0	2.0	42	65	[132,186]	0.33	0-27	0-36	m, c
33	2.0	2.4	37	70	[118,182]	0.30	0-17	0-34	m, c
33	2.4	2.0	48	56	[124,177]	0.31	10-30	33-36	c
33	2.4	2.4	38	68	[99,177]	0.30	0-15	0-34	c
39	2.4	2.4	50	63	[131,163]	0.28	10-30	39-42	m, c
45	2.4	2.4	59	64	[153,168]	0.28	15-38	46-48	m, c

Table 4.4 – *Notes*

^a Error from fitting is ± 3 km.

^b Cometocentric distance at which coma opacity is 0.1. Error from fitting is ± 20 km. Two values are given, one for each hemisphere.

^c Mean value of $1 - e^{-\tau}$ within 100 km of nuclear surface. Error from fitting is about 8%.

^d Range of lengths of nuclear chord that yields an adequate fit. Error from fitting is ± 4 km.

^e Range of possible nuclear radii based on the range of l_n and b .

^f Comments. Letters' meanings: m = marginally good fit. c = fit is consistent with opacity measured by Team 6.

4.2.5 Discussion

4.2.5.1 Nucleus

As mentioned, we assumed that the nucleus has $R \leq 50$ km, but our fitting further constrains this number, to 30 km, by making two reasonable assumptions. Only marginally good fits are found for models with R much bigger than this, up to 48 km, i.e., almost up to the assumed maximum. For models that yield $R > 48$ km (or even > 50 km, for that matter), the fits are not even marginally “good.”

Millimeter wave measurements by Altenhoff *et al.* (1999) and our centimeter wave measurements – as will be seen later in this Chapter – agree with this occultation-derived limit. However I emphasize that this occultation analysis assumes a spherical nucleus.

4.2.5.2 Astrometry

Our apparent detection of the occultation implies the nucleus was $(8.0 \pm 0.5) \times 10^2$ km on a perpendicular from the last prediction of the nuclear track. Mid-event occurred about 22 s before the predicted time for the location of Team 5, corresponding to 255 km along the track. Considering the errors involved with the prediction, this is not an unacceptably large offset, as we now explain.

Figure 4.7a shows an image of the comet and star taken one hour before the event (from the USNO Flagstaff Station 1.5-m telescope). Figure 4.7b, showing an expanded view of the central pixels of the comet, is marked with the middle of the brightest pixel (“M”), the location of the centroid of brightness (“C”), and the estimated position of the nucleus using our coma-fitting technique (“L”; ± 0.25 pixel). The pixel size for the images in Fig. 4.7 is 0.33 arcsec (7.2×10^2 km at the comet). Our astrometry of the comet’s offset from the ephemeris position (using 3 nights of USNO images, as mentioned in §II) was uncertain to 0.3 arcsec (6.5×10^2 km), i.e., almost one pixel. Combined with the uncertainty from the coma-fitting technique, this gives an $1\text{-}\sigma$ error of about 7×10^2 km. So it is quite reasonable to expect the nuclear shadow to have passed over a team several hundred kilometers from the predicted center line.

Our constraint on the location of the nucleus is reasonably consistent with 1998 calculations for the orbit of Hale-Bopp (Donald Yeomans, private communication). However, it should be noted that we are estimating the error with respect to the measured position of the comet from the astrometry, not from the ephemeris. Had we used a different ephemeris, say, one that was thought to be more accurate, the only difference would have been to change the offsets measured via the astrometry of the USNO images. We would have arrived at the same prediction and the same observing strategy. Hence, a post-facto ephemeris, which might be used to try to pin down exactly how far Team 5 was from the nucleus’ shadow, would not make much difference. In essence, our astrometry provided a truer prediction of the comet’s position than any ephemeris would have. Astrometric measurements from post-event imaging would have helped but these data were not taken.

4.2.5.3 Inner Coma: Albedo of Dust Grains

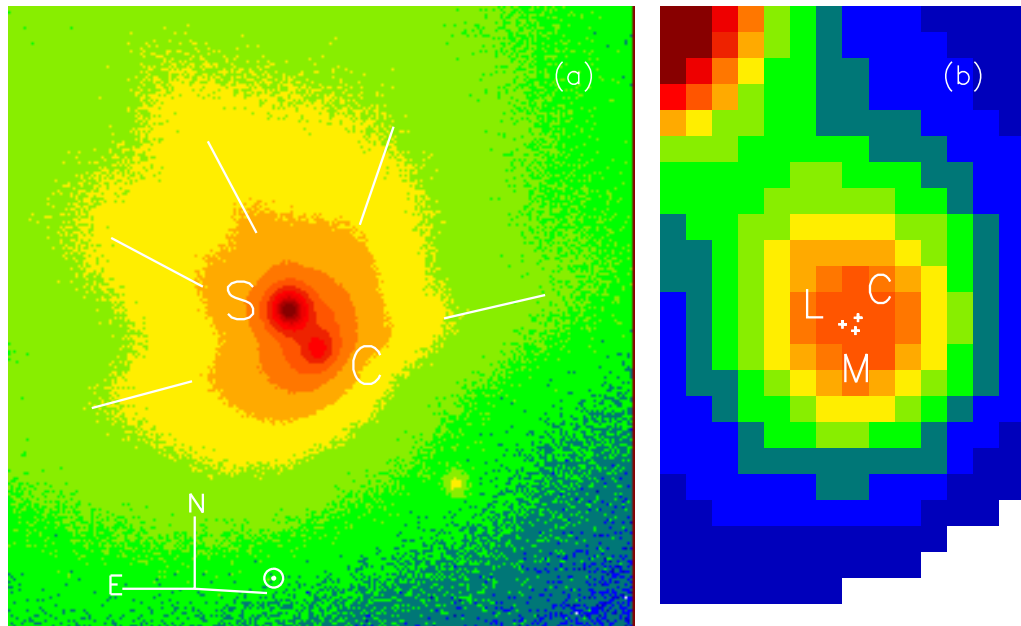


Figure 4.7: Pre-occultation image of comet and star. In (a), an image of both comet Hale-Bopp (“C”) and PPM 200723 (“S”) is shown, taken less than one hour before the occultation. The scale is 0.33 arcsec per pixel, corresponding to 720 km of linear distance at the comet; our entire occultation event marked in Fig. 4.3 covers about one-half of a pixel. Line segments indicate the most prominent jets in the comet’s coma, and show that on ingress the star was traveling along a jet’s edge. In (b), I show an expanded view of the central pixels of the comet. The middle of the brightest pixel “M”, centroid of brightness “C”, inferred position from coma-fitting technique of Lisse *et al.* (1999b) “L”.

Since we have measured the opacity of the coma, we can calculate the albedo of the dust in the inner coma by using measured values of $Af\rho_o$, a quantity introduced by A’Hearn *et al.* (1984) where A is the albedo, f is the filling factor, and ρ_o is the size at the comet of the aperture used. It is obtained via

$$Af\rho_o = \frac{F_{\text{comet}}}{F_{\odot}} \times \left(\frac{r}{1\text{AU}}\right)^2 \times \frac{4\Delta^2}{\rho_o}, \quad (4.4)$$

where r is the heliocentric distance of the comet, Δ is the geocentric distance, F_{\odot} is the solar flux at Earth, and F_{comet} is the comet’s flux measured in the aperture. The filling factor is the aperture-average of $1 - e^{-\tau(\rho)}$. Here the albedo is properly the value of the scattering function relative to a conservative, isotropic scatterer, as outlined by Hanner *et al.* (1981; and equal to $4\pi\sigma(\theta)/G$ in that work).

We analyzed *HST* WFPC2 images of the comet obtained twelve days before and twelve days after the occultation event (provided by H. A. Weaver of Johns Hopkins Univ.), and $Af\rho_o$ was measured down to a cometocentric distance of 400 km (about 0.2 arcsec). A steady-state, force-free, radially-flowing dust coma would have an aperture-independent value of $Af\rho_o$, but since Hale-Bopp’s coma was not like this, we extrapolated $Af\rho_o$ down to 100 km for comparison with our occultation results. Since the phase angle of the observations was only 19° , we removed the phase angle effect, $\phi(\alpha)$, by using

$$\phi(\alpha) = 10^{-0.4\alpha\beta}, \quad (4.5)$$

where β is the phase coefficient of 0.025 mag/degree (a value roughly consistent across several comets; Meech and Jewitt 1987), and α is the phase angle at the time of the observation. We estimate that $Af\rho_o/\phi(\alpha)$ was about 1.3 ± 0.3 km on 23 Sep 1996 and 1.9 ± 0.3 km on 17 Oct 1996. Time variability of the comet’s flux in the *HST* images leads to the large error estimates. Taking $Af\rho_o/\phi(\alpha) = 1.6 \pm 0.3$ km on 5 Oct 1996, $\rho_o = 100$ km, and the aperture-average of $1 - e^{-\tau}$ to be about 0.38 ± 0.05 , we find $A/\phi(\alpha)$ to be 0.04 ± 0.01 (formal error). This leads to an equivalent geometric albedo, p , of $\frac{1}{4}A/\phi(\alpha) = 0.01 \pm 0.002$. (I use the value of $\frac{1}{4}$ to follow the notation of Hanner *et al.* [1981].) This value is rather low (e.g., Divine *et al.* (1986) collate information from various workers to obtain an average p of 0.03 ± 0.01), and a possible explanation (similar to that given by Larson and A’Hearn [1984]) is that a photon is doubly-scattered by the dust in the inner coma. It is not unreasonable to expect such a scenario in the optically-thick portion of the coma. If every photon were doubly-scattered, $A/\phi(\alpha)$ would be the square root of the value given above: 0.21 ± 0.02 (formal error), and $p = 0.05 \pm 0.006$. That the calculated albedo is acceptable provides one self-consistent check that our model results – and specifically the high opacity of the coma – make sense.

4.2.5.4 Inner Coma: Plausibility of Findings

Our modeling implies that the column density of dust in the inner coma follows a power law of ρ with an index steeper than 1.4. This steepness is not evident in large-scale imaging of the comet. The path of the star’s ingress followed the edge of one of Hale-Bopp’s jets (short line segments in Fig. 4.7a) that had a surface brightness

proportional to $\rho^{-0.86}$; during egress, the path did not follow a jet, and the coma surface brightness was proportional to $\rho^{-1.26}$. However, one can fit just the wings of our occultation light curve (i.e., between 100 and 170 km from mid-occultation) and match the profiles from the large-scale imaging. It is only in the central region, within 100 km of the nucleus, where these profiles fail and the density of dust must be a steep function of ρ . Unfortunately the small scale of these properties of the coma are beyond the reach of other Earth-based observations – even *HST* Planetary Camera imaging would have covered a full 98 km per pixel.

It is possible that we observed the acceleration region of the dust, and that it may have extended ~ 100 km from the nucleus, steepening the dust profile. Gombosi *et al.* (1986), in their review of inner coma dynamics, state that their modeling shows dust still accelerating toward terminal velocity several nuclear radii away from the nucleus, albeit in a model coma with a lower dust-to-gas ratio (χ) and lower r than Hale-Bopp’s. A larger χ could extend the coma’s acceleration region, but the larger r (lower insolation, lower dust speed) may counter that effect.

A detailed dusty gas-dynamic model of Hale-Bopp’s coma is beyond the scope of this paper, but, using estimates of the dust speed v , we can show the steep opacity profile is roughly compatible with the models of Gombosi *et al.* (1986). We note that azimuthal variations in the dust density (not only the acceleration of the dust) can contribute to the measured shape of the dust profile, but a model of such variations would be difficult to constrain owing to a lack of data. Thus we show here only a gross justification of a steep opacity profile. The profile is proportional to $\rho^{-1.7\pm 0.3}$ or so, which makes $v \propto \rho^{0.7\pm 0.3}$ (since surface brightness is proportional to $(\rho v)^{-1}$). Let us take the nucleus’ radius to be 25 km; we cannot expect the ρ dependence of v to hold all the way to the surface, so we will estimate v at 5 kilometers above it, say $\rho = 30$ km. Assuming the dust is accelerated out to $\rho = 100$ km, v will be about $(100/30)^{0.7} = 2.3$ times smaller.

Now, the terminal velocity v_t of the dust grains at the time of the occultation was about 0.6 km/s. This is based on (a) v_t at perihelion ($r = 0.9$ AU) being about 1.0 km/s (Schleicher *et al.* 1998a), and (b) $v_t \propto r^{-0.41}$, which is a relation similar to that used for the speed of the gas in the coma (Biver *et al.* 1999). Therefore, at $\rho = 30$ km, $v \approx (0.6 \text{ km/s})/2.3 \approx 0.27$ km/s. Figure 12a of Gombosi *et al.* (1986) shows their model giving a 0.84-micron wide dust grain a speed of about 0.25 km/s at about 0.2 nuclear radii above the surface – equivalent in this case to $\rho \approx 30$ km. Since there are differences between Hale-Bopp’s environment and that used in the model of Gombosi *et al.* (1986), and further their calculated v does not strictly follow $\rho^{0.7}$, this match between v is somewhat coincidental, but it is clear that v is roughly comparable to model calculations.

We noted the high optical depth implied by our modeling. Canonically, comae must be optically thin so that sunlight can reach the nucleus to drive the sublimation of gas, leading to the production of the dust in a self-regulating manner. However, an optically thick inner coma could be a secondary source for energy, via scattering of sunlight and thermal reradiation, especially if the dust has been superheated, as seems to be the case for Hale-Bopp (Lisse *et al.* 1999a). This problem has been analyzed by others, who have found by various analytic and numerical simulation methods that the energy deposited to the nucleus is a weak function of comatic

optical depth, even up to $\tau \sim 2$; reradiation almost compensates (or, in some analyses, over-compensates) for the decrease in sunlight (see, e.g., Salo [1988], Hellmich [1981]).

An important check is whether a high τ makes sense. We argue that it does, as follows. $Af\rho_o/\phi(\alpha)$, derived above, is 1.6 ± 0.2 km at $\rho_o = 100$ km. At the time of the *Giotto* flyby of comet 1P/Halley, Schleicher *et al.* (1998b) report that Halley’s $Af\rho_o/\phi(\alpha) = 0.53$ km, and Keller *et al.* (1987) calculate from *Giotto* imaging that the peak opacity of the dust coma, a few kilometers above the surface of the nucleus, was about 0.3. So Hale-Bopp’s $Af\rho_o/\phi(\alpha)$ from §IVc was at least 3 times larger than Halley’s during the flyby. With the two comets’ dust grains having roughly the same albedo, it is clear that it would be not be difficult for Hale-Bopp to have had a peak τ around unity. Furthermore, it is likely that Hale-Bopp’s near nucleus $Af\rho_o/\phi(\alpha)$ was even higher, for the following reason. Our modeling shows the dust opacity profile to be proportional to $\rho_o^{-1.7 \pm 0.3}$ or so, making

$$Af\rho_o/\phi(\alpha) \propto \rho_o^{-0.7 \pm 0.3}. \quad (4.6)$$

This is not strictly true at the higher optical depths, since $f > 1$ is not allowed, but it does imply that $Af\rho_o/\phi(\alpha)$ is higher than the 1.6 km as one travels in from $\rho = 100$ km, so that it is probably more than three times larger than Halley’s when measured near the nucleus’ surface.

4.2.6 Summary of Occultation Results

We report constraints on the nuclear and comatic properties of Comet Hale-Bopp as implied by our observations of an occultation of a ninth-magnitude star. Except for the special case of Comet Chiron, this would be the first time such an event with so small an impact parameter has been observed. Our observations were marred by thin clouds and a lack of adequate corroborating data – only one chord through a sufficiently thick portion of the coma was apparently measured – but there are many pieces of circumstantial evidence to show that we indeed observed the occultation. Moreover, we know of no other observations of the comet that can refute our conclusions. Our data nearest the nucleus were collected about 800 km from the latest prediction, but this is not unreasonable since such a distance is comparable to the astrometric error in determining the nucleus’ location within a finitelypixelized image dominated by comatic flux.

By modeling the shape of our light curve with a simple coma and spherical nucleus model, and assuming that our observation recorded the occultation, we find the following:

- 1. Assuming the power-law opacity profile of the coma, with exponent n , is as shallow as or shallower than 2.4, the impact parameter b is ≤ 45 km, but the best fits occur when $b \leq 33$ km. Our occultation observation has sampled the near-nuclear inner coma, which has only rarely been observed before in any comet.
- 2. If $n \leq 2$, the nucleus is spherical, and the coordinate origin is constrained as depicted in Fig. 4.5, then the nuclear radius R must be smaller than about 30 km. Relaxing the constraints on n yields an upper limit of 48 km.
- 3. The inner coma of Hale-Bopp is probably optically thick, even at nearly 3 AU from the Sun. Regardless of the values for the other parameters, good fits to the

data can only be found if the opacity within the first few tens of km of the center (not the surface) of the nucleus was at least unity. For some applicable models R is bigger than this distance, in which case the maximum coma opacity is less than one, but never much less.

- 4. We find that the albedo ($A/\phi(\alpha)$) of the dust, while it is within 100 km of the nucleus' center, is 0.21 ± 0.02 (formal error). The equivalent geometric albedo p is 0.05 ± 0.005 (formal error). This assumes that all photons within this region are doubly-scattered. Without this caveat, the calculated albedo is lower than the "typical" value ($p = 0.01$, compared to 0.03 from Divine *et al.* [1986]).

- 5. The dust opacity profile is probably steeper than the canonical ρ^{-1} power law, being most likely proportional to ρ^{-n} with $n \geq 1.4$. Marginal fits can be found for $n = 1.0$ for one hemisphere. (The other hemisphere is, in that case, quite steep, $n \approx 2$.) This occurs possibly within 160 or 170 km of the nuclear center, but definitely within 100 km. This chord through the coma may have sampled the acceleration region of the dust, and/or azimuthal variations in the inner coma, so our model, which describes the coma's density as two hemispheres each having a single power-law function of cometocentric distance, would be too simplistic.

- 6. The steepness of the profile in the deepest coma does not match that of the jet structure seen in large-scale images, although the resolution of all ground-based imaging fails to directly sample the 100-kilometer scales we are measuring via the occultation. The characteristic n for the wings of the occultation light curve could follow the same value as for the large-scale images and the processes mentioned in Item 5 above may only be important within the first 100 km of the coma.

4.3 Thermal Emission and Scattered Light Imaging

4.3.1 Observations

Table 4.5 lists the non-occultation data taken on comet Hale-Bopp, in the optical, mid-IR, and radio regimes. Heliocentric distance (r), geocentric distance (Δ), and phase angle (ϕ) are given, along with our measurement of the flux from the nucleus of the comet. In all observations except for the microwave, where the comet appeared as a point source, processing using the coma-fitting method from Chapter 3 was required to separate the comatic from the nuclear flux. One notices that unfortunately the image processing was inconclusive for many of the datasets. The brightness of the nucleus is stated using either its Cousins R magnitude or its flux in Janskys. (One Jansky is 10^{-26} W/m²/sr/Hz.) Images from Apr 1997 (near perihelion) were too choked with coma to detect the nucleus; these data were used, however, to infer the nucleus' rotation period. The comet's coma during late November and December 1996, and July 1997 was not structured enough to allow an analysis with our method; these entries are italicized in the table.

4.3.2 Analysis

4.3.2.1 Infrared and Optical Data

We performed the coma-fitting analysis on our infrared and optical data sets, and we show some of the results in Figs. 4.8, 4.9, 4.10, 4.11 (optical), and 4.12

Table 4.5. Observations of Comet Hale-Bopp

No.	Date (UT)	System	Wavelength
1	23 Oct 1995	<i>HST</i> + WFPC2	6750 Å
2	20 May 1996	<i>HST</i> + WFPC2	6750 Å
3	22 Jun 1996	<i>HST</i> + WFPC2	6750 Å
4	17 Oct 1996	<i>HST</i> + WFPC2	6750 Å
5	31 Oct - 2 Nov 1996	ESO 3.6-m + TIMMI	11 μm
6	30 Nov - 3 Dec 1996	ESO 3.6-m + TIMMI	11 μm
7	21 - 24 Jan 1997	NASA/IRTF + MIRAC	11 μm
8	21 - 27 Mar 1997	VLA	3.55 cm
9	4 - 12 Apr 1997	NASA/IRTF + MIRAC	5-20 μm
10	15 - 21 Jul 1997	ESO 3.6-m + TIMMI	11 μm

Table 4.5 - Continued

No.	r (AU)	Δ (AU)	ϕ (deg)	Nuclear flux	CF? ^a	Rot? ^b
1	6.35	6.71	8.2	$R_C = 18.3 \pm 0.1$	Y	N
2	4.35	3.68	10.8	$R_C = 16.0 \pm 0.1$	Y	N
3	4.01	3.03	4.5	$R_C = 15.6 \pm 0.1$	Y	N
4	2.69	3.04	18.8	$R_C = 15.3 \pm 0.1$	Y	N
5	2.53-2.50	3.05	17.4-17.2	5.0 ± 0.5 Jy	Y	N
6	<i>2.16-2.12</i>	<i>2.93-2.91</i>	<i>13.9-13.7</i>	NA	N	N
7	<i>1.50-1.46</i>	<i>2.22-2.16</i>	<i>21.4-22.6</i>	NA	N	N
8	0.94-0.92	1.32	49.0-48.9	20 ± 3 μ Jy	NA ^c	N
9	0.92-0.93	1.38-1.47	46.6-42.5	NA	N	Y
10	<i>1.94-2.02</i>	<i>2.75-2.80</i>	<i>15.1-15.6</i>	NA	N	N

^a “CF” = “Coma fitting.” Are the data good enough to use the coma-fitting technique (Chapter 3)?

^b “Rot” = “Rotation.” Was the rotation period deriveable from the data?

^c Image is a point-source – no coma seen.

(infrared). Each figure shows the analysis of one typical image from each of the five observing runs where the analysis was applicable. The upper left panel in each figure shows the original image, the upper right shows the model, the lower left shows the residual, and the lower right compares the residual's profile with that of a PSF. All images have used logarithmic scaling. The residual plot in each figure follows the profile of the PSF reasonably well.

For the four optical datasets, we find a consistent value for the nuclear cross section even though the inner coma of Hale-Bopp is thought to be optically thick, as explained in Section 4.2. It is possible that all three 1996 measurements show actually the cross section of the optically-thick portion of the coma rather than of the nucleus. Optical images from Oct 1995 offer the best chance to detect the nucleus without much intervening near-nuclear coma. The interpretation of the optical and mid-IR measurements of the nucleus will be explained below.

Infrared images taken near perihelion were useful in constraining the rotation period of the nucleus. Indeed, it was the only portion of the datasets that indicated this, since photometric determinations of the rotation were impossible. Morphological changes in the coma during the period of (UT) 4 Apr to 12 Apr 1997 were analyzed and it was found that the repeatability of the structure had a mean periodicity of $P = 11.30 \pm 0.05$ hr ($1\text{-}\sigma$) over that time period. The sequence of images is shown in Fig. 4.13. The rotational phase is written in each image of the sequence. I have a nine-hour sequence of images from 4 Apr and a five-hour sequence from 5 Apr, which have been combined to produce the 39-image sequence; this is the “MIR-LIN” sequence labelled on the figure. The two days limited the possible periods to P and $2P$. Subsequent imaging on 12 Apr – the “MIRAC” image on the figure – was matched with the first two days to remove the period ambiguity. The caveats to attaching a rotation period of the nucleus to the variability of coma morphology have been explained in Chapter 3.

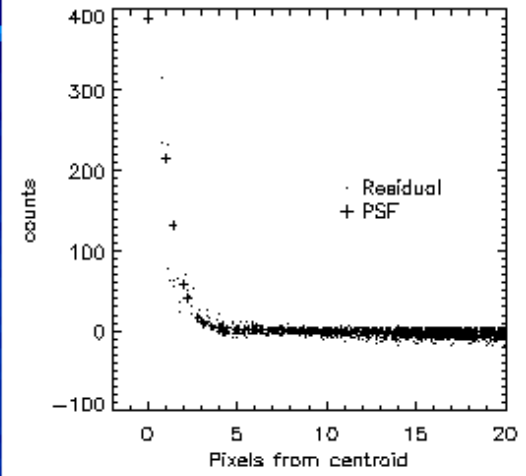
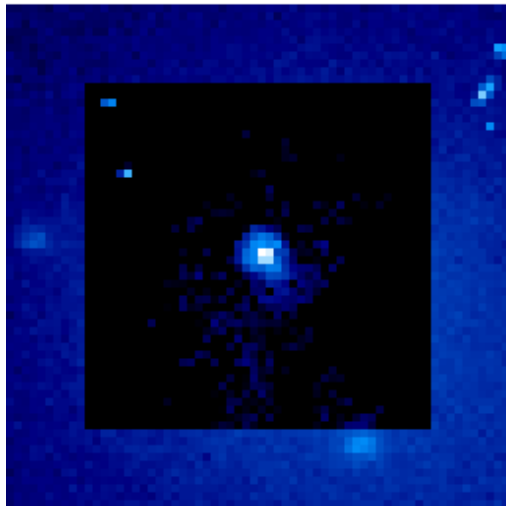
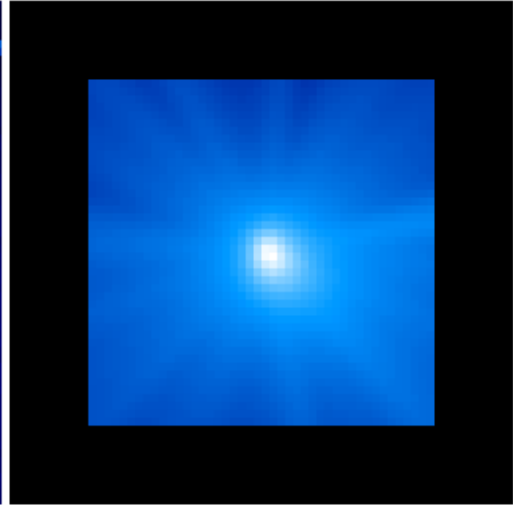
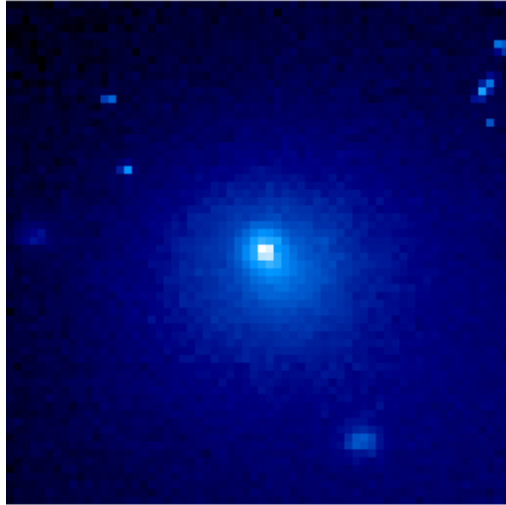
Figure 4.8 (next page): Coma-fitting method applied to optical image of Hale-Bopp. The extraction of the nucleus from *HST* WFPC2 image of the comet taken on 23 Oct 1995 is displayed. Upper left panel is the original image, upper right is the model created by the “coma-fitting method,” lower left is the residual, and lower right shows a plot comparing the profile of the residual and the PSF; the two match each other very well, indicating we have removed the skirt of the coma. The intensity scale in the 3 images is logarithmic.

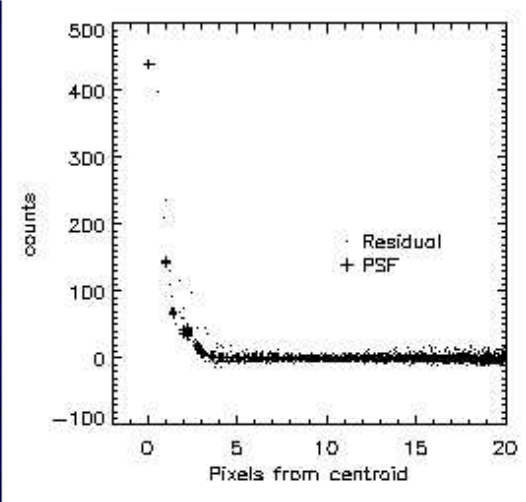
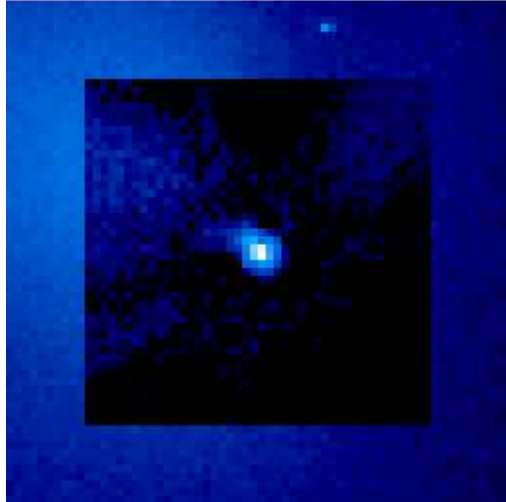
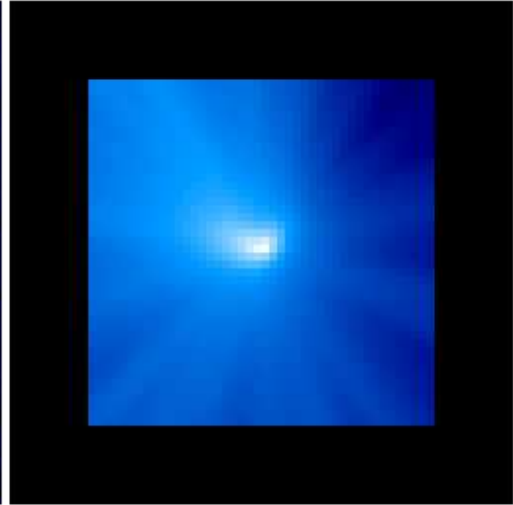
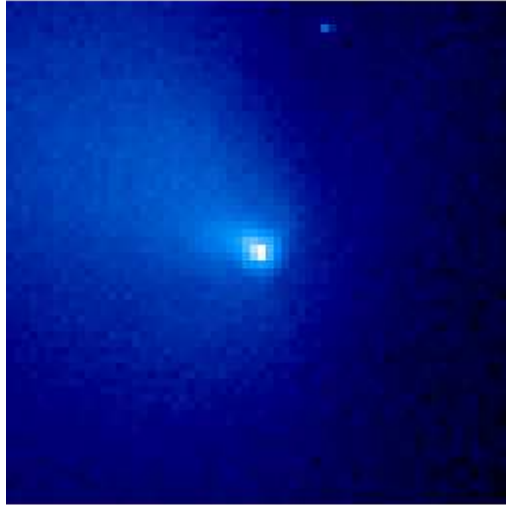
Figure 4.9 (page 98): Coma-fitting method applied to optical image of Hale-Bopp. Same as Fig. 4.8, except for 20 May 1996.

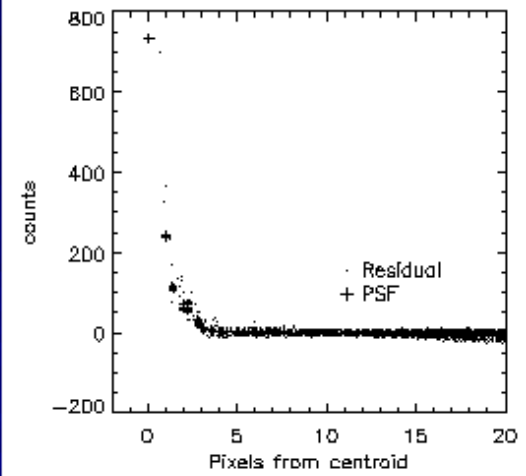
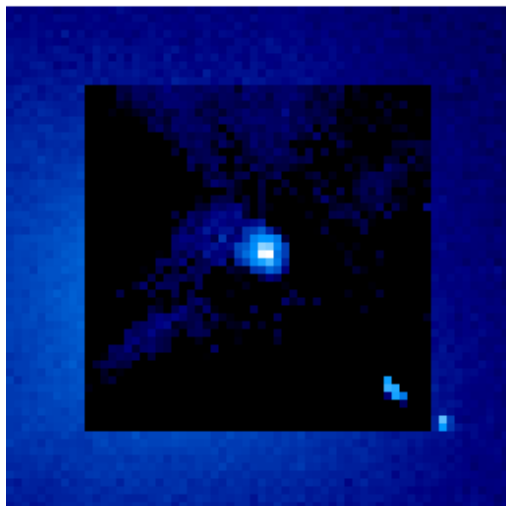
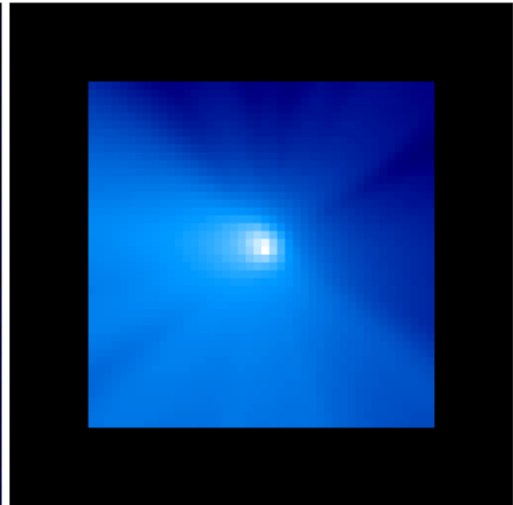
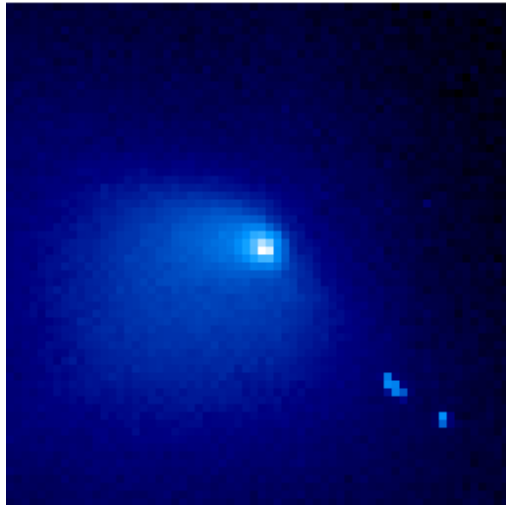
Figure 4.10 (page 99): Coma-fitting method applied to optical image of Hale-Bopp. Same as Fig. 4.8, except for 22 Jun 1996.

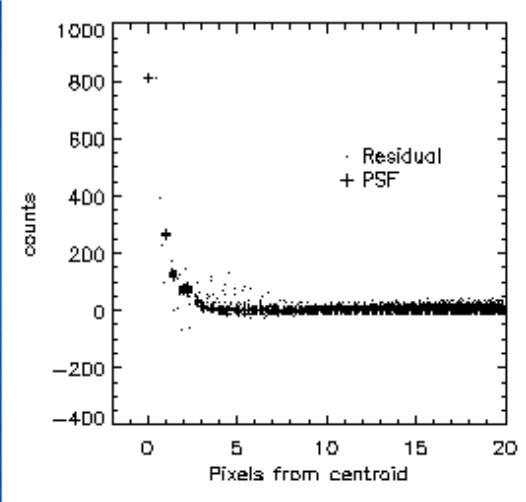
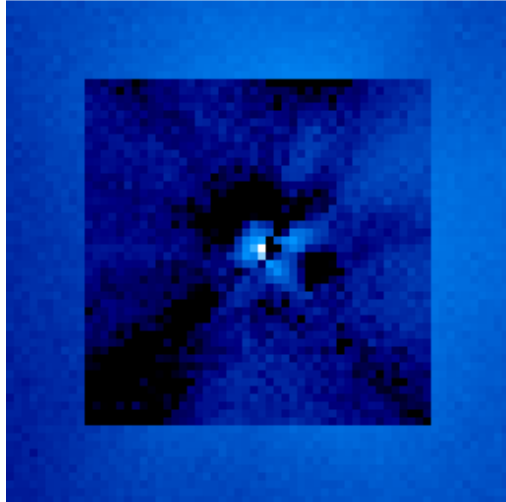
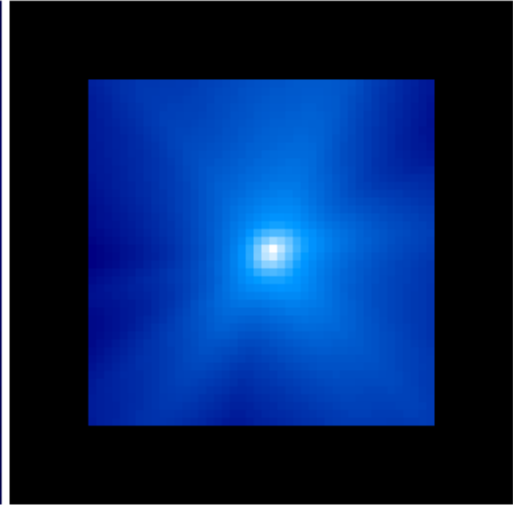
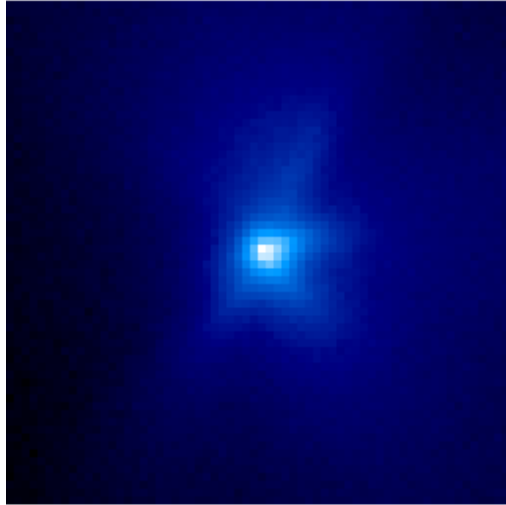
Figure 4.11 (page 100): Coma-fitting method applied to optical image of Hale-Bopp. Same as Fig. 4.8, except for 17 Oct 1996.

Figure 4.12 (page 101): Coma-fitting method applied to mid-infrared image of Hale-Bopp. Same as Fig. 4.8, except for 31 Oct 1996, and taken with ESO 3.6-m telescope and TIMMI mid-infrared camera.









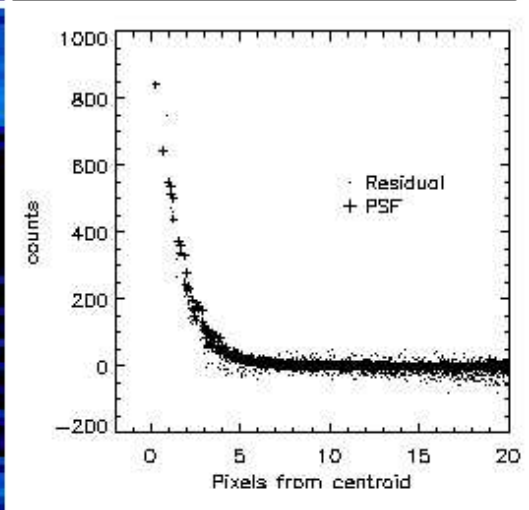
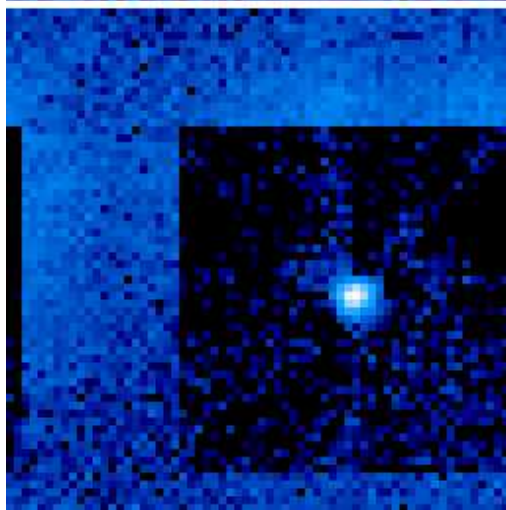
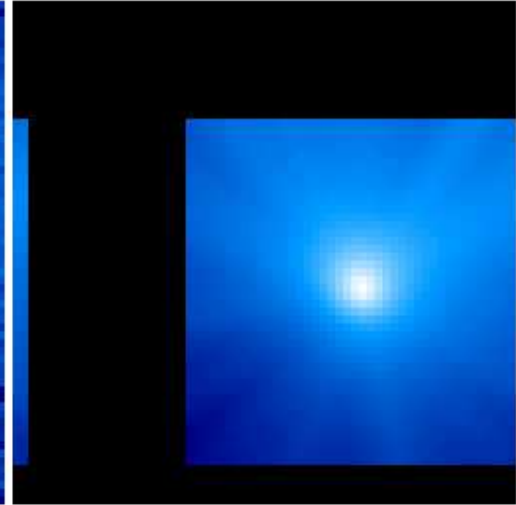
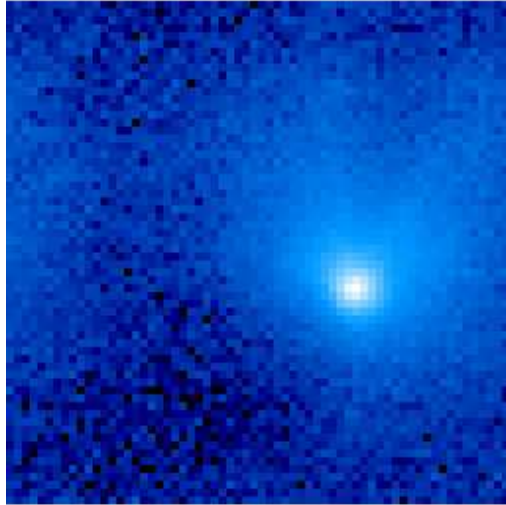
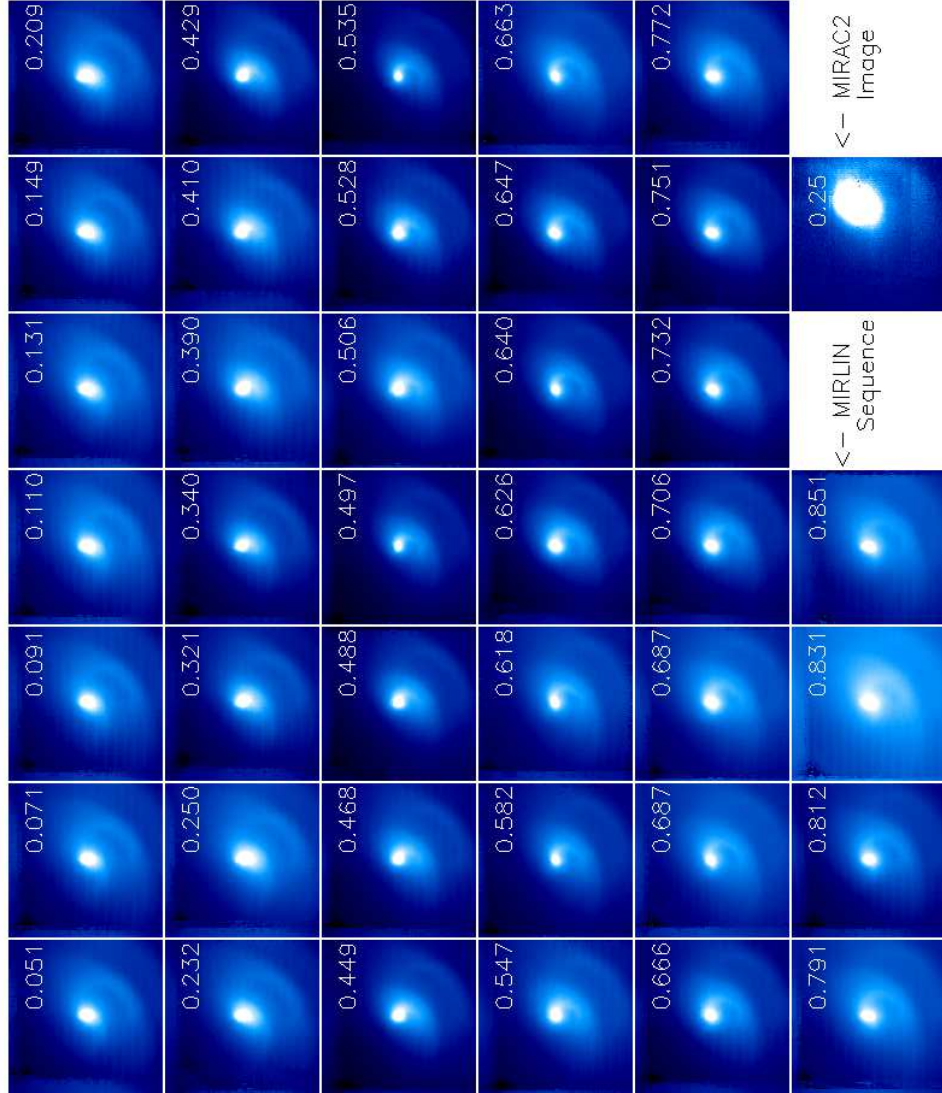


Figure 4.13 (next page): Rotation sequence of comet Hale-Bopp. Sequence of IRTF 10.3- μ images of the comet indicating its rotation period, taken during 4 to 12 Apr 1997. Two days of MIRLIN images were phased together to create the 39-image sequence. The rotational phase of the image is noted in white in each frame. About a week later, we obtained MIRAC images and were able to match the phase with the earlier sequence, as shown. The period is 11.3 ± 0.03 hr.

C/1995 O1 Hale-Bopp. Rotation Period, 4 – 12 Apr 1997. Fernandez et al. 1998
 NASA/IRTF: MIRLIN (4–5 Apr), MIRAC2 (12 Apr). P=11 h, 18 min \pm 3 min



4.3.2.2 Secondary Nuclei

We have examined the *HST* images for evidence of any secondary nuclei, as was suggested by Sekanina (1998b). We deconvolved the residual images left after our application of the coma-fitting method. We used the same point-spread function as Sekanina used, and also a theoretical one that we found to closely mimic the structure of observed stars. The two PSFs differ a bit in shape, but are not too dissimilar when pixelized to the WFPC2 PC resolution. We found no clear indication of a second nucleus; we were able to obtain satisfactory fits to our residual maps using just one point-source. A second point-source would of course improve our fits but not significantly. Moreover we do not find the need to introduce a secondary nucleus as strong (about one-fifth the brightness of the primary) as mentioned by Sekanina (1998b). Undoubtably this is due to the different methods used to model the emission from the coma; Sekanina uses an analytic function with just a few parameters to match the coma's brightness whereas we are fitting the structure at every azimuth for a total of a few hundred parameters. It is also possible that the secondary nuclei that Sekanina claims are actually jet features in the near-nuclear coma.

4.3.2.3 Microwave

We detected the thermal continuum from the comet's nucleus at the $7 - \sigma$ level after a 66-hr integration at VLA. The image is a point source, and the most important section of our CLEAN map is shown in Fig. 4.14. The detection at VLA of Hale-Bopp's thermal continuum was the first such detection by that observatory, after only upper-limits were found for five other comets (Snyder *et al.* 1983, de Pater *et al.* 1985, Schenewerk *et al.* 1986, Hoban and Baum 1987, and Chapter 6 of this thesis). It is arguably the first detection ever of the thermal continuum radiation from a cometary nucleus in the centimeter-regime; similar observations of comets West (C/1975 XX = 1976 XX = 1975n; Hobbs *et al.* 1977) and Kohoutek (C/1973 XX = 1973 XX = 1973f; Hobbs *et al.* 1975) imaged their comae, and single-dish observations of comet *IRAS-Araki-Alcock* (Altenhoff *et al.* 1983), while yielding fluxes consistent with a nucleus, had beam sizes that were large enough to arguably include flux from the coma, especially since a skirt of decimeter-sized grains was detected by the radar experiments of Goldstein *et al.* (1984) and Harmon *et al.* (1989). Our VLA measurements had a synthesized HPBW of only 1 arcsecond, and moreover a reduction of the data excluding the very long antenna baselines of VLA, which de-emphasizes any smooth underlying component to the emission (i.e., a coma), still yielded a point source. Hence, we conclude that thermal emission from centimeter-to-decimeter sized grains in Hale-Bopp's coma is negligible in comparison to the emission from the nucleus itself. At the very least, this is the first interferometric detection of the microwave continuum from a nucleus.

There have been other interferometric observations of the radio continuum, in the millimeter regime, and they too were taken near perihelion, so we can construct a radio spectrum of the Hale-Bopp nucleus, one of the first such spectra in existence. This is shown in Fig. 4.15. We used the fluxes reported by Altenhoff *et al.* (1999) using the IRAM Plateau de Bure interferometer, and Blake *et al.* (1999) using the

Owens Valley interferometer, and scaled them to account for the small differences in geocentric distance in the comet. The spectrum follows the λ^{-2} Rayleigh-Jeans law quite well; fitting the points to a line implies the emissivity could not have any more than a $\lambda^{-0.1}$ overall dependence. Alternatively, the deviation from the Rayleigh-Jeans law could be due to the different depths (and hence different temperatures) at which the millimeter-wave and centimeter-wave observations sample.

4.3.3 Discussion

4.3.3.1 Model of Microwave Emission

Use of the augmented thermal model I described in Chapter 3 is justified with comet Hale-Bopp, since we have an idea of the rotation state and photometry at multiple wavelengths. The extra trick however is that the microwave data does not sample the nucleus' surface but several (radiative) skin depths deep, and the flux that the augmented model predicts for the centimeter wavelengths depends on how steep the temperature gradient is within the nucleus. The wavelength is 3.55 cm; exactly how far down from the surface the continuum is emitted is a matter of some debate, it could be a few wavelengths – roughly one decimeter – if the material is mostly rock, or it could be significantly larger, roughly half a meter or more, if a substantial ice component is present (de Pater *et al.* 1985). Since the cometary ice is not expected to be found in patches around the surface but rather in a mixture with the rock, I will choose the former scenario to constrain the modeling.

Another matter that one must take into account is the effect of the coma on the total energy put into the nucleus. The contribution of direct sunlight is decreased due to the optically thick coma, but this is somewhat compensated by the thermal emission of the dust and, to a lesser extent, by the scattering of the visual-band sunlight off the dust grains. Salo (1988) has already made detailed calculations of the energy available to a nucleus surrounded by a coma of a given optical depth with grains of a given single-scattering albedo and Henyey-Greenstein asymmetry factor (Henyey and Greenstein 1941). I will use his results here. For small (1 micron and below) dust grains, of which Hale-Bopp was a prodigious producer (Lisse *et al.* 1999a, Williams *et al.* 1997), forward scattering is expected to be important, and Salo (1988) calculates that in that case the reradiative component to the total power onto the nucleus would be about 50 to 60% of the total power on a bare-nucleus. This is for opacities of unity and greater. In other words, in the limit of an infinitely thick coma, the nucleus would receive 50 to 60% of the energy it otherwise would without that coma. For the opacities of Hale-Bopp's coma, described in section 4.2, there would be the $e^{-\tau}$ -reduced direct sunlight component also, or 30 to 40% of the unextincted sunlight, to bring the total to about 80 to 90% of the original available energy. I do not want to overstate the accuracy of this calculation; other workers have done similar computational experiments and have found different answers depending on the model assumptions (e.g. Marconi and Mendis 1984, Hellmich 1981). However the consensus seems to have the nucleus losing little net available energy despite having a coma with $\tau \approx 1$.

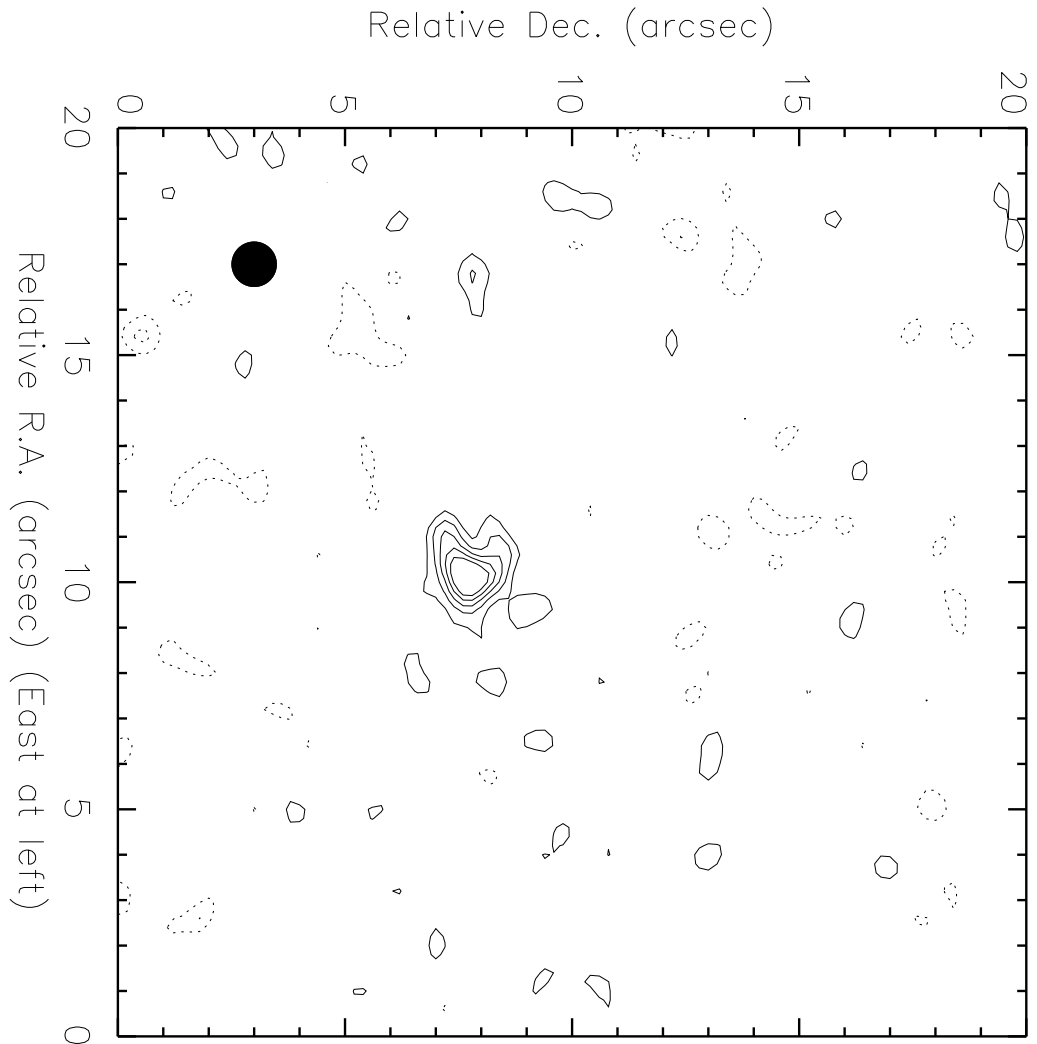


Figure 4.14: CLEAN contour map of comet Hale-Bopp microwave continuum. This is the image obtained with the VLA, between 20 and 27 March 1997, of the nucleus' microwave continuum. The CLEAN algorithm has been applied. Contours are -2 , 2 , 3 , 4 , 5 , and 6σ . The dark circle at lower left represents the synthesized beam HPBW, about 1 arcsec wide.

Thus, the augmented model was modified to allow an additional 50% of the solar flux on top of the extincted ($\sim e^{-1}$) direct contribution. The rotation period of 11.3 hr was used, and the comet's rotation axis was directed toward a cometocentric ecliptic longitude of 275° and latitude of -50° , a direction close to what has been derived by several groups (Licandro *et al.* 1999, Jorda *et al.* 1999). The shape of the nucleus is totally unknown, but due to its apparently large size it may be tempting to think of it as spherical. This is complete guesswork, since plenty of comparably-sized asteroids are elongated. To reduce the number of parameters I have arbitrarily set one axial ratio to 1.3 and the other to 1.0.

To model the microwave flux, I allowed the thermal inertia and effective radius to vary, leaving the opacity at unity. The problem was then to just find a combination of effective radius and emitting layer depth that produced the observed microwave flux. The trend is for the emitting layer to be deeper as both the effective radius and thermal inertia increase; a higher thermal inertia means there is less of a temperature gradient in the nucleus, and a higher effective radius simply means there is more surface area and the object is more luminous.

For a lunar-like thermal inertia, and an effective radius of 27 km, I find that my augmented model reproduces the observed flux if the microwave continuum were emitted from a layer 20 cm deep. This is toward the high end of the plausible depths – it is 6 wavelengths. For comparison, the thermal inertia for (3200) Phaethon (a likely dormant comet) is about 10 times the lunar value (Harris *et al.* 1998) and the emitting layer on Hale-Bopp would be about 120 cm deep, probably too far. However if the radius were in this case only about 19 km, then the emitting layer would be only 20 cm.

For a thermal inertia more like that of the Main Belt asteroids – roughly one-fifth the lunar value (Spencer *et al.* 1989) – the depth of the emitting layer is only 6 cm for a radius of 27 km, and so the radius can be very large, 50 km or more, if we allow the emitting layer to be as deep as 20 cm. Based on my occultation results, such a radius is too large since the impact parameter of that observation was so small, so one could conclude that Hale-Bopp's nucleus has lunar-like or Phaethon-like thermal inertia and the radius is in the 20 to 30 km range.

Figure 4.16a shows the temperature map derived from the augmented thermal model using the lunar-like thermal inertia. The axes are longitude and latitude. Since the nucleus is aspherical, the longitude and latitude system are based on the sphere that inscribes the ellipsoid; i.e., a sphere with a radius equal to the smallest semimajor axis of the ellipsoid. The undulations in the contours give some indication of where the elongation of the nucleus lies. Also note that near perihelion the currently accepted pole position pointed almost directly at the Sun, causing the almost STM-like contours. The flat temperature on the night side is due to the (isotropic) coma's contribution to the impinging power. Figure 4.16b shows the temperature map of the surface; the difference is about 150 K in just a few decimeters.

Of course near perihelion the nucleus' orientation with respect to the Sun was changing most rapidly. Depending on the inertia, this affects the model temperature map, especially since a large fraction of the Sun-facing hemisphere of the nucleus near perihelion is almost totally in darkness for most of Hale-Bopp's orbit. That

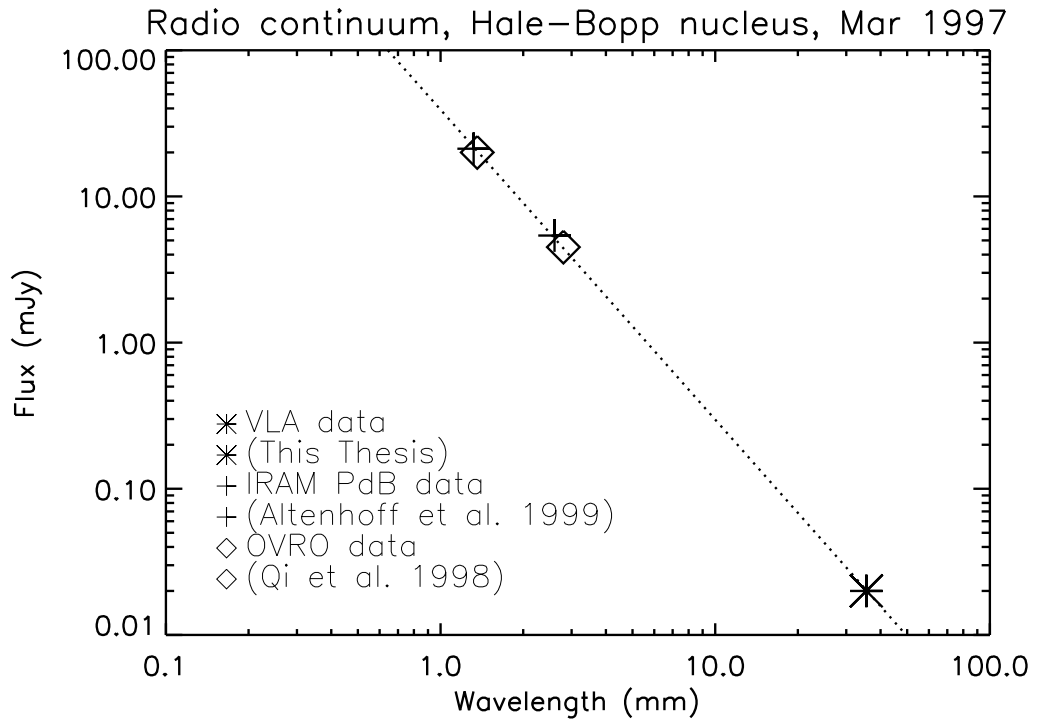


Figure 4.15: Radio continuum spectrum, Hale-Bopp nucleus. This broadband spectrum has been created by combining my VLA results with OVRO and IRAM PdB data. The points follow a Rayleigh-Jeans law quite well (dashed line). What little deviation there is could be due to wavelength dependence of the emissivity or the thermal gradient of the nucleus sampled by the different wavelengths.

hemisphere turns toward the Sun just a few months before perihelion and turns away again a few months after. For this reason, I ran my augmented thermal model over 50 to 60 rotations to remove any transient effects from the choice of initial conditions.

4.3.3.2 Model of Mid-IR Emission

The next step is to check the low conductivity and the effective radius with the infrared photometry from October/November 1996. Of course the coma's conditions are different but we will take the opacity to be approximately unity again. Unfortunately the model predicts about 2 Jy, less than half the 5 Jy we found from Fig. 4.12. In fact the radiation of thermal continuum from the dust would have to deliver about 200% of the energy received by a bare nucleus, not the 50% we have used, based on the work of Salo (1988). Under the formalism I have used here, the dust grains cannot be efficient enough to backwarm the nucleus surface to the requisite temperature. Now the grains of the coma were apparently indeed superheated (Williams *et al.* 1997, Lisse *et al.* 1999a), but this likely could not provide the extra energy needed since the emissivity of the grains is too low; these grains are smaller than the wavelength of the continuum emission spectrum's maximum.

Comet Hale-Bopp was about 3 AU from Earth at the time of these mid-IR observations, and so one pixel of the detector covered more than 700 km. Though it is a testament to the incredible infrared brightness of this comet, this pixel scale is much larger than the usual case, where we concentrate on comets that are less than 1 AU away. This means that the coma-to-nucleus brightness ratio within the central pixels is in general higher, since each of those pixels can pick up such a huge area of comatic flux. Thus, it is not completely surprising that the coma-fitting technique is unable to cleanly separate the coma and the nucleus. This "extra" point-source emission that the technique found in Fig. 4.12 may be related to the opacity of the coma near the nucleus.

4.3.3.3 Implications of Optical Measurements

The optical magnitudes of the nucleus in Table 4.5 can be used with above derived range of the radius to find the albedo. As stated, I will use the October 1995 value since that dataset is probably the least contaminated with an optically thick coma. Also note that the phase angle is small so there is little added error from the uncertain optical phase behavior. A caveat to this analysis is that different workers have derived different brightnesses for the embedded point source within these very same *HST* images (Weaver *et al.* 1997, Weaver and Lamy 1999, Sekanina 1999) using different, independent programs to account for the coma. This is almost certainly due to two factors: the pixel scale covers a large linear distance at the comet compared to the size of the nucleus, and the dust coma morphology in the inner coma is more complicated than what we naively see in the images. Small, subpixel features in the coma will adversely affect one's ability to photometrically extract the nucleus, especially when the comet is very active and nearly 3 AU away.

Yet another potential problem that adds to the error in the nuclear flux estimate is the unknown rotational context of the *HST* images, since we may be viewing different cross sections at different times.

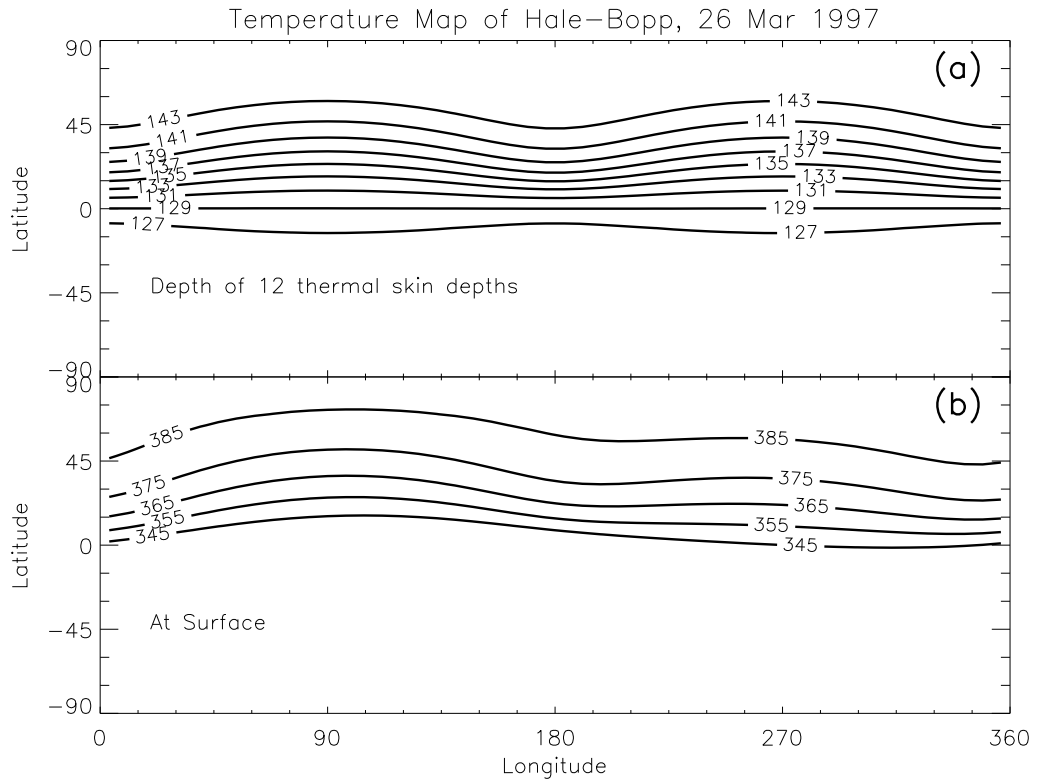


Figure 4.16: Temperature map of Hale-Bopp, 26 Mar 1997. This figure shows the temperature map of comet Hale-Bopp’s nucleus for Mar 26 1997, during the time of our VLA microwave observations. The map was created from my augmented thermal model. The top panel shows the temperature 12 skin depths into the nucleus; the bottom shows the surface temperature. The temperature drops by roughly 150 K in just a few decimeters.

For an effective radius of 25 ± 5 km, and an *HST* R_C magnitude of 18.3 ± 0.1 on 23 Oct 1995, the geometric albedo is $6\% \pm 2\%$. Including the relatively dimmer nucleus found by Weaver *et al.* (1997) and Weaver and Lamy (1999), and the relatively brighter nucleus found by Sekanina (1999), the geometric albedo is within $4.5\% \pm 3\%$.

4.4 Summary of Hale-Bopp Results

The combination of the occultation observations and the modeling of the thermal data provides the following conclusions about Hale-Bopp's nucleus:

- If the thermal inertia to Hale-Bopp's nucleus is lunar-like or Phaethon-like, and if the emitting layer sampled by the VLA observations is less than 20 cm, then the effective radius of Hale-Bopp's nucleus is 25 ± 5 km. In general, the higher the thermal inertia, the smaller the radius must be in the range given. This range is also consistent with the upper limit derived from the occultation results, which set a limit of 30 km on the radius.

- These inertias and radii cannot reproduce the 5 ± 0.5 Jy of flux that was measured at 11 microns in October and November 1996, so presumably the large geocentric distance prevented our coma-fitting method from reliably extracting the nucleus. This is because there were too many kilometers at the comet per pixel, and hence too much coma.

- The occultation modeling assumed a spherical nucleus, so if the real nucleus deviates from this, then it is conceivable that the effective radius is larger than 30 km but that the section sampled during the occultation has locally a smaller radius, or that the near-nuclear dust coma has an unusual morphology that would fool us into thinking that the nucleus' radius is smaller than it is. In that case, the thermal inertia could conceivably be lower than the lunar value. Moreover, then it is easier to reproduce the thermal IR measurement from later 1996, since with a larger radius the nucleus has a higher luminosity.

- The optical *HST* data have been analyzed by many people in an attempt to extract the nuclear flux. Based solely on my results, the geometric albedo is 0.06 ± 0.02 , but by including the efforts of others on the same dataset, the visual geometric albedo is 0.04 ± 0.035 .

- Using the morphological changes in the mid-IR data, I constrain the rotation rate to be $11.3 \text{ hr} \pm 0.05 \text{ hr}$. Strictly speaking, this is the average rate between 4 and 12 April 1997.

Lastly, I mention the very significant finding of an optically thick inner coma from the occultation observation. This was the first time a dust coma with such a high opacity had been found.

Chapter 5

The Nucleus of Comet Encke

5.1 Background

Comet 2P/Encke has been observed by mankind since 1786. Of the roughly 150 known periodic comets that have not been lost, only four others have an observational baseline as long. The comet was discovered independently four times, once each on four different apparitions, before J. F. Encke published an orbit connecting them all and successfully predicting the next apparition. The orbital period is 3.3 years, the shortest known, and so at first glance one would think that it would be the comet we know the most about. In some aspects this is true – e.g. Whipple and Sekanina (1979) and Sekanina (1988a,b) have a detailed model of the nucleus' rotation – but the comet furtively guarded the basic properties of its nucleus until the 1997 apparition, when it made its closest recorded passage to Earth ever. We set up a multiwavelength observing campaign to take advantage of this opportunity. I have described much of this experiment elsewhere (Fernández *et al.* 1999c) and reproduce much of the text.

5.2 Observations and Reduction

The three datasets used in this study are described in Table 5.1, along with heliocentric distances, geocentric distances, and phase angles. The measured fluxes are given in Table 5.2. Images from the European Southern Observatory (ESO) 3.6-m telescope were taken with the TIMMI instrument (Käufl *et al.* 1994) at wavelengths between 8 and 12 μm . The images have 64^2 pixels and cover $(21.8'')$ ². Each pixel width covered 65 to 87 km at the comet during the observing run. The plate scale was measured using the known relative positions of α Cen A and B (Perryman *et al.* 1997). The point-spread function’s (PSF) full width at half-maximum (FWHM) varied from 0.7 to 1.0 arcsec. Chopping of the secondary mirror northward and nodding of the telescope westward, with typical throws of 30 arcsec, were employed. An array flat field was created by measuring the relative photometry of a bright star at 23 different locations on the array and then interpolating a surface with a minimum of curvature. We observed the comet at three wavelengths but only at $\lambda = 10.7 \mu\text{m}$ was the comet bright enough to let us build a well-sampled time series of data. Absolute flux calibration was done using α Cen A and interpolating in wavelength information given by van der Bliek *et al.* (1996); its 10.7 μm magnitude is -1.56 ± 0.05 , and the zero point is at 35.7 Jy. Color corrections were at most a few percent. Relative flux calibration was done using SAO 243305 = HD 143796 = V362 Nor (Kazarovets *et al.* 1999), a star that was a short angular distance from the comet and thus useful for measuring the atmospheric effects and the comet’s light curve. Its optical variability is $\leq \pm 0.05$ mag with sporadic ~ 0.1 mag jumps every few years (Perryman 1997). There was no indication of variability in the mid-IR data that exceeded photometric uncertainty.

The *Infrared Space Observatory* (ISO) data, taken with the ISOPHOT instrument (Lemke *et al.* 1996), used a 180-arcsec wide circular aperture at wavelengths between 3.6 and 100 μm . The data were reduced using the “PIA” software version 7.1 (Gabriel *et al.* 1997). Corrections to the measured fluxes were made to account for the nonlinearities in the detector, the diffraction of light beyond the aperture, and the color of the flux standard vis-à-vis the comet; these corrections were at most 3%.

The *Hubble Space Telescope* (HST) images were taken with the CCD on the Space Telescope Imaging Spectrograph (STIS; Woodgate *et al.* 1998) as acquisition images for a separate spectroscopic program. A $\sim 5500 \text{ \AA}$ -wide red filter was used. We used the science-quality output of the pipeline processing of the data. Each pixel covers $(0.051'')$ ², or $(7.4 \text{ km})^2$ at the comet. The high proper motion of the comet ($\sim 0.2''$ per second) left all stars as trails; we estimate that the PSF FWHM = $0.1''$ based on archival HST images taken with the same instrument, detector, and filter within a few weeks of our observations.

5.3 Analysis

5.3.1 ESO Photometry

Figure 5.1a shows the median of 61 ESO TIMMI images of the comet, with a linear intensity scale. Each image was weighted by the total signal. The total

Table 5.1. Observations of Comet Encke

No.	Date (UT)	System	Wavelength (μm)
1	1.3 Jul 1997	<i>HST</i> + STIS	0.72
2	15.0 Jul 1997	<i>ISO</i> + ISOPHOT	3.6 - 100
3	15.0-21.1 Jul 1997	ESO 3.6-m + TIMMI	8.5 - 11.6

No.	r (AU)	Δ (AU)	α ($^\circ$)
1	0.942	0.200	106.2
2	1.164	0.264	50.3
3	1.164-1.257	0.264 - 0.351	50.3 - 40.3

Table 5.2. Flux of Comet Encke

Wavelength (μm)	Filter Name	Filter Width ^a (μm)	Aperture Radius ($''$)	Flux (Jy)
<i>ESO^b</i>				
8.5	“N1”	0.9	3	2.5 ± 0.7
10.7	“NN1”	1.2	3	3.1 ± 0.2
11.6	“SiC”	1.6	3	2.8 ± 0.7
<i>ISO</i>				
3.6	“P1_3p6_UM”	1.00	90	0.060 ± 0.018
4.8	“P1_4p8_UM”	1.53	90	0.53 ± 0.11
10.0	“P1_10_UM”	1.80	90	14.27 ± 2.8
12.8	“P1_12p8_UM”	2.40	90	24.97 ± 5.0
21.0	“P2_20_UM”	9.03	90	32.48 ± 6.5
23.8	“P2_25_UM”	9.12	90	32.69 ± 6.5
60.9	“P3_60_UM”	25.9	90	15.58 ± 4.7
102.4	“P3_100_UM”	39.5	90	3.91 ± 1.2
<i>HST</i>				
0.723	“28X50LP”	0.200	0.5	$(2.6 \pm 0.2) \times 10^{-4}$ ^c

Table 5.2 – Notes

^a Width at half-maximum efficiency for ESO (Käufel 1997) and *HST* (Space Telescope Science Institute 1998). For *ISO*, the width of the equivalent rectangular filter that has a height of the mean efficiency of the real filter (Klaas *et al.* 1994, Laureijs *et al.* 1998).

^b Fluxes refer to the comet's brightness at a geocentric distance of 0.32 AU and in the middle of the amplitude due to rotation.

^c Flux is valid for $\lambda = 0.64 \mu$, i.e., Cousins *R* band. We transformed the instrumental flux to this band. The equivalent magnitude is 17.7 ± 0.1 .

effective on-source integration time is 47.5 min. Figure 5.2a compares this median comet’s and α Cen A’s enclosed flux as a function of photocentric distance. The star is a proxy for the PSF, taken during the course of the 61 comet images. The graph shows that a higher fraction of the comet’s flux resides in the wings compared to the PSF, and hence the comet is an extended source, although the extent may be an artifact of imprecise adding of the images. The amount of coma in the image is calculated in Section 5.3.2.

Figure 5.3 shows our time series of the comet’s flux over four nights. The flux and $1\text{-}\sigma$ error bar of each point are calculated from three flux measurements spaced closely in time. The time axis is modulo 15.2 hr to show the periodicity in the data (explained in Section 5.4.1). The ordinate is heliocentric magnitude m_h at a wavelength of $10.7\ \mu\text{m}$, which is related to the observed apparent magnitude m by

$$m_h = m - 5 \log\left(\frac{\Delta}{1\text{AU}}\right), \quad (5.1)$$

where Δ is the geocentric distance. This accounts for the changes in brightness due to the rapidly varying Δ during the observing run. The $10.7\text{-}\mu\text{m}$ flux of the comet, referred to the geocentric distance on 1997 Jul 19.0 UT ($\Delta = 0.32\ \text{AU}$), and midway between the minimum and maximum flux of the rotational variation, was $3.1 \pm 0.2\ \text{Jy}$.

5.3.2 ISO Photometry

The high spatial resolution of the ESO image has resolved out most of the comatic flux, but it is clear from Table 5.2 that Comet Encke had a dust coma: the flux measured with *ISOPHOT* in the $\sim 11\ \mu\text{m}$ range is much higher than that measured with TIMMI. Using the aperture size ($\rho_{\text{ISO}} = 90''$) and flux, we can estimate the amount of coma in the ESO image (Fig. 5.1a), as follows. Let F_{ESO} be the flux measured from the comet via our ground-based imaging, $3.1 \pm 0.2\ \text{Jy}$. The aperture radius ρ_{ESO} is $3''$. Let F_{ISO} be the flux measured by *ISO* within its aperture. The wavelengths sampled by ESO and *ISO* do not exactly match but interpolating with a cubic spline we find that *ISO* saw $15 \pm 3\ \text{Jy}$ at $10.7\ \mu\text{m}$. The rotational phase at the time of the *ISO* observations falls near a time of mid-brightness in the nucleus’ rotation, though this is a small effect since the coma’s flux dominates.

The flux measured at ESO is valid for heliocentric distance $r = 1.22\ \text{AU}$, $\Delta = 0.32\ \text{AU}$, and phase angle $\alpha = 44^\circ$, while the flux measured by *ISO* is valid for $r = 1.164\ \text{AU}$, $\Delta = 0.263$, and $\alpha = 50.4^\circ$. To compare, we must correct for the geometry and apertures. First, we assume that the surface brightness of the coma is proportional to $1/\rho^n$, where ρ is the cometocentric distance, so that the comatic flux is proportional to $1/\Delta^n$, and that the flux within an aperture of radius of ρ_0 is proportional to ρ_0^{2-n} . A $12\text{-}\mu\text{m}$ ISOCAM image of the comet taken in early July 1997 (Reach *et al.* 1999) shows a coma with mean $n = 1.1$. Second, we assume that the comatic and nuclear fluxes are proportional to

$$\frac{1}{-1 + \exp\left(\frac{hc\sqrt{r}}{\lambda k T_0}\right)}, \quad (5.2)$$

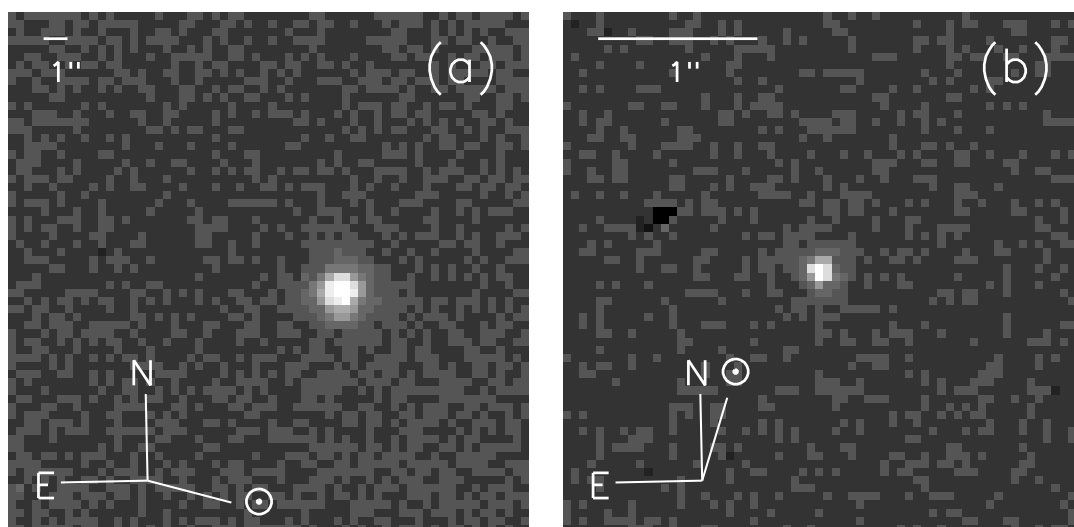


Figure 5.1: Comet Encke at 10 microns (a) and 7200 Angstroms (b). Here images of Comet 2P/Encke, with linear intensity scale, are displayed. Image (a) was taken with the TIMMI camera at ESO 3.6-m telescope on UT 18-19 Jul 1997, and image (b) was taken with the STIS instrument aboard *HST* on 1 Jul 1997. North, east, and the solar directions are marked. Pixel scales are $0.34''$ and $0.051''$, respectively. Wavelengths of observation are $10.7\mu\text{m}$ and 7200 \AA , respectively. The ESO image is the weighted median of 61 individual frames, and the total integration time was 47.5 minutes. The *HST* image exposure time was 5 s.

where h is Planck's constant, c is the speed of light, k is Boltzmann's constant, and T_0 is 278 K $\sqrt{\text{AU}}$ for the coma and 331 K $\sqrt{\text{AU}}$ for the nucleus. This is just the representation for a sphere's and a hemisphere's, respectively, temperature. Since the two r are not very far apart this gross approximation will suffice. Third, we assume that the nuclear flux is proportional to $1/\Delta^2$ and $10^{-0.4\beta\alpha}$, where β is 0.011 mag/degree (further discussed in Section 5.4.4). Fourth, we assume no phase dependence over the phase angles for the thermal emission of the dust.

With these assumptions we calculate that *ISO* would have seen a coma that was $G_C = 1.41$ times brighter than what ESO saw with the same aperture, and a nucleus that was $G_N = 1.54$ times brighter. The aperture correction is $A = 21.35$. Let F_C and F_N be the flux of the coma and nucleus, respectively, as seen by ESO: $F_{\text{ESO}} = F_C + F_N$. Then $F_{\text{ISO}} = F_C G_C A + F_N G_N$. Solving, we find $F_N = 2.74 \pm 0.24$ Jy, $F_C = 0.36 \pm 0.11$ Jy, and thus only twelve percent of the flux seen by ESO is due to coma.

5.3.3 HST Photometry

Due to guide-star acquisition problems, only two images of the comet were acquired with STIS. Figure 5.1b shows the higher signal-to-noise image of the two, with a linear intensity scale. The integration time is only five seconds, which prevents us from seeing much of the extended structure. In addition, the high spatial resolution has resolved out most of the coma, Figure 5.2b compares the comet's and PSF's enclosed flux as a function of photocentric distance. The graph shows that a higher fraction of the comet's flux resides in the wings compared to the PSF, so the comet is an extended source. Also plotted is the profile of a model comet, with a point source nucleus plus a PSF-convolved $1/\rho$ coma, that mimics the real comet. About 75% to 85% of the flux is due to the nucleus, so in our analysis below we have assumed that the nucleus' magnitude is $-2.5 \log(0.75) = 0.3$ mag fainter than the total magnitude. Fortunately the derivation of the absolute zero-phase magnitude (in Section 5.4.3) is insensitive to the exact *HST* magnitude within a few tenths.

5.4 Discussion

5.4.1 Periodicity of Flux.

We determined the aforementioned 15.2-hr periodicity in our ESO data using the string-length method outlined by Dworetzky (1983) mentioned in Chapter 3. The string length trials are shown in Fig. 5.4. Also marked in the figure are the possible periods quoted by Jewitt and Meech (1987; JM87 hereafter) and Luu and Jewitt (1990; LJ90 hereafter) using optical measurements near aphelion; there is good agreement among the three datasets. A 7.6-hr or 11.5-hr period gives a single-peaked light curve, but 15.2 ± 0.3 hr, 22.4 ± 0.8 hr, and the higher periods either imply two peaks or leave enough unsampled room in the phase plot to allow for a second peak and valley. One expects a double-peaked curve for a rotating nucleus as it shows different cross sections to the observer. The 15.2-hr period is the only one that gives temporal coverage of most of the rotational phase and shows two peaks.

The errors attached to the rotation periods are derived from a visual inspection of the phased light curve plot. Periods near the local minima in Fig. 5.4 are

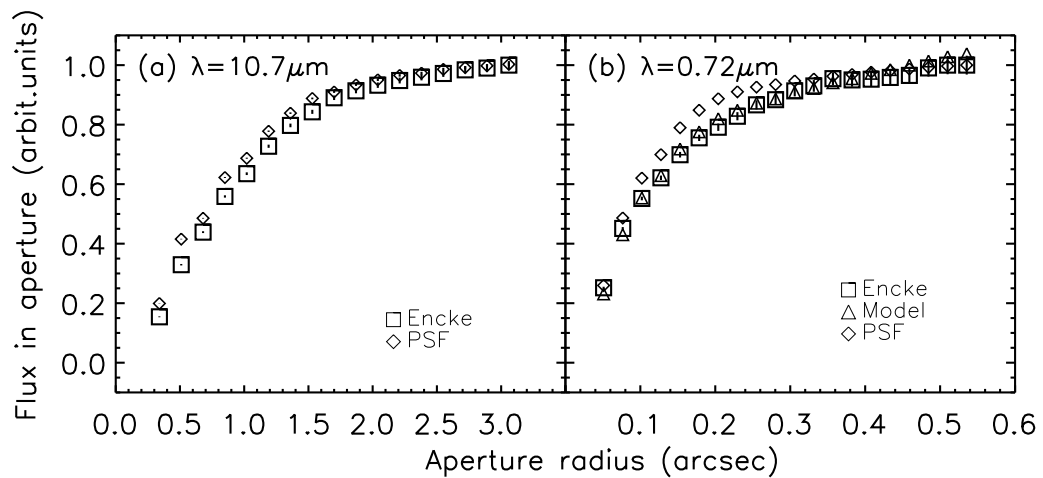


Figure 5.2: Radial profiles of Comet Encke in mid-IR (a) and optical (b). Here I compare the cumulative flux profiles of Comet Encke and the point-spread function. Squares are for the comet, diamonds are for the PSF, and triangles are for the model. (a) This is the profile from the TIMMI image in Fig. 5.1a. An image of α Cen A is used as a PSF proxy, and the profile is scaled to the right-most comet point. (b) This is a profile from the STIS image in Fig. 5.1b. A bright star imaged near in time with the same instrument setup is used as a PSF proxy, and the profile is scaled to the right-most comet point. The model is a point-source plus a PSF-convolved $1/\rho$ coma; the coma contributes 15% to 25% of the total flux.

acceptable only if the overlapping data in the phased light curve do not have widely disparate magnitudes. This defines the range of possible periods, and thus the errors are not normally distributed.

LJ90 remark that 15.08 ± 0.08 hr is “the most likely synodic period” of the nucleus’ rotation, so our measurement is consistent with this. The correction from our measured synodic period to the sidereal period is small, since the aspect angle of the comet as seen by Earth changed by only about 0.6° per rotation period between UT 16.0 Jul and UT 22.0 Jul 1997. At most the correction is $0.6^\circ/360^\circ = 0.2\%$, much smaller than the fractional error $0.3/15.2 = 2\%$.

5.4.2 Shape and Precession of the Nucleus.

By inspection of Fig. 5.3, the peak-to-peak amplitude (p.t.p.a.) is 0.7 ± 0.1 mag, though it may be higher since we have not sampled all turnover points. This p.t.p.a. is similar both to that found for other comets (Meech 1999) and to that measured for Encke by JM87 and LJ90 in the optical regime. This variability is likely due to the changing cross section and not the albedo. The emissivity would have to be near 0.5 or 0.75, much too low, to explain this mid-IR variability with albedo spots, since the mid-IR flux is proportional to the emissivity.

Assuming that the results of JM87 and LJ90 and our ESO results are all free of coma contamination, we can constrain the nucleus’ shape and rotation state. The four data points for this exercise are the different p.t.p.a.: JM87 measured the p.t.p.a. ≥ 0.8 mag on 23 Sep 1985, and ≥ 0.4 mag on 30 Oct 1986; LJ90 measured 0.62 ± 0.04 mag on 7 Sep 1988; and we measured ≥ 0.7 mag on 19 Jul 1997.

Sekanina (1988a) found a rotation axis direction that did not change much from 1924 to 1984, but this direction cannot account for the four p.t.p.a. – a drifting axis is required. We created a simple model where the angular momentum vector, initially at the location found by Sekanina (1988a), is pushed by a torque from the outgassing regions on the surface. The nucleus would be a triaxial ellipsoid in principal axis rotation about the shortest axis. To make the problem tractable we restricted this “precession” of the vector to a constant rate in a circle. The model thus has five parameters: the latitude and longitude of the precession axis, the period of the precession P_p , and the two axial ratios a/c and b/c of the nucleus (where c represents the short one). The p.t.p.a. δm is related to the shape by

$$\delta m = 1.25 \log \left(\frac{(a/c)^2 + \tan^2 l}{(b/c)^2 + \tan^2 l} \right), \quad (5.3)$$

where l is the sub-Earth latitude on the comet’s surface.

With no degrees of freedom, we could find which parameter values were possible but not their likelihood. We found that (a) any precession axis direction greater than 14° from the angular momentum vector was allowable, (b) P_p must be ≤ 81 years, (c) a/c must be ≥ 2.6 , and (d) $1.0 \leq b/c \leq 0.5 \times a/c - 0.3$. Furthermore the limit of P_p is smaller for smaller values of b/c . This short precession period and high elongation are necessary to reconcile the p.t.p.a. lower limits in 1985 and 1997 with the p.t.p.a. that was smaller in 1988.

Comparing with a review by Meech (1999), Encke’s long axial ratio is toward the high end of known values, with four nuclei having a ratio of 2 or larger. Only

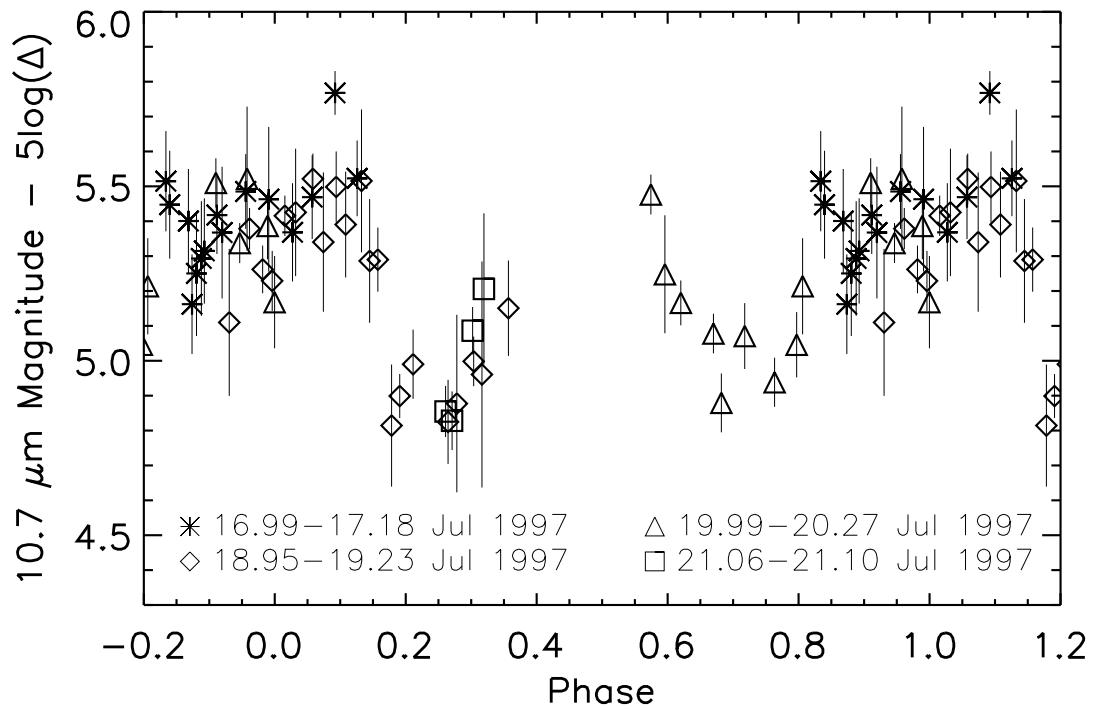


Figure 5.3: Light curve of Comet Encke phased by 15.2 hr. This is a four-day light curve of comet Encke, where the time coordinate is modulo 15.2 hr. The ordinate shows heliocentric magnitude in the 10.7- μm filter. The periodicity is derived from Fig. 5.4. Zero phase corresponds to 1997 Jul 19.0 UT.

29P/Schwassmann-Wachmann 1 has a ratio as large as 2.6. However many of these are projected ratios so it is unclear how Encke precisely compares to these other bodies. A recent study of comet 19P/Borrelly’s nucleus yielded a deprojected axial ratio of 2.4 (Lamy *et al.* 1998b).

According to Sekanina’s analysis (1988a,b), the comet’s angular momentum vector was precessing at a continuously decreasing rate (averaging $0.3^\circ/\text{yr}$) until around 1924, after which it was mostly constant up to 1984. A mass ejection event or the activation of new vents may have occurred in the mid-1980s to start the nucleus precessing again. Although Samarasinha and Belton (1995) showed that the nucleus’ ratio of precession to rotation period could evolve to a constant value, that assumes a consistent pattern of outgassing orbit after orbit, which may not be the case for Encke. Samarasinha and Belton (1995) and Samarasinha (1997) also mention that the nucleus will spin up and eventually orient itself with the pole pointing at the orbital longitude at which maximum outgassing occurs. (Usually this is just the Sun’s cometocentric longitude at the comet’s perihelion.) The uncertainties here are too great to address this; the *CONTOUR* visit in 2003 will hopefully help our understanding of Encke’s rotation state.

The contribution of the coma to the rotational modulation is important to consider. If coma was present in JM87’s and LJ90’s photometry but not rotationally modulated then the lower limits to the p.t.p.a. are even higher and the limits on P_p , a/c , and b/c would be more extreme. If however the coma was modulated by e.g. an active patch or small jet swinging in and out of view, then the comet’s light curve would show the addition of two oscillating curves – a two-peak curve from the nucleus and a one-peak curve from the coma – and the nuclear p.t.p.a. could be smaller than the total p.t.p.a. We argue here though that the comatic contribution to the amplitude is probably negligible. First, the bright aphelion outburst witnessed by Barker *et al.* (1981) showed no extended emission but completely obliterated any modulation of the flux over the course of the night. Hence we suppose that the coma’s flux in the outburst was not tied to its natal active area. Second, LJ90 show no difference between the amplitudes and shapes of their light curve’s two peaks, unlike what one would expect if there were a strong, singly-peaked, comainduced underlying curve.

Our own light curve (Fig. 5.3) may be asymmetric between the two peaks but the photometric uncertainties are too large to be sure. A lower 1997 p.t.p.a. than the one used above would slightly mitigate the axial ratio and precession period limits, but the optical data of JM87 and LJ90 are the more restrictive constraints.

5.4.3 Optical Phase Behavior.

We combined our *HST* nuclear magnitude with measurements from previous apparitions to estimate the phase behavior of the nucleus and derive the absolute magnitude $m(1, 1, 0)$. We used three phase laws: the linear law

$$m(1, 1, \alpha) = m(1, 1, 0) + \beta\alpha, \quad (5.4)$$

where β is a constant; the IAU-adopted (H, G) formalism for asteroids (Lumme *et*

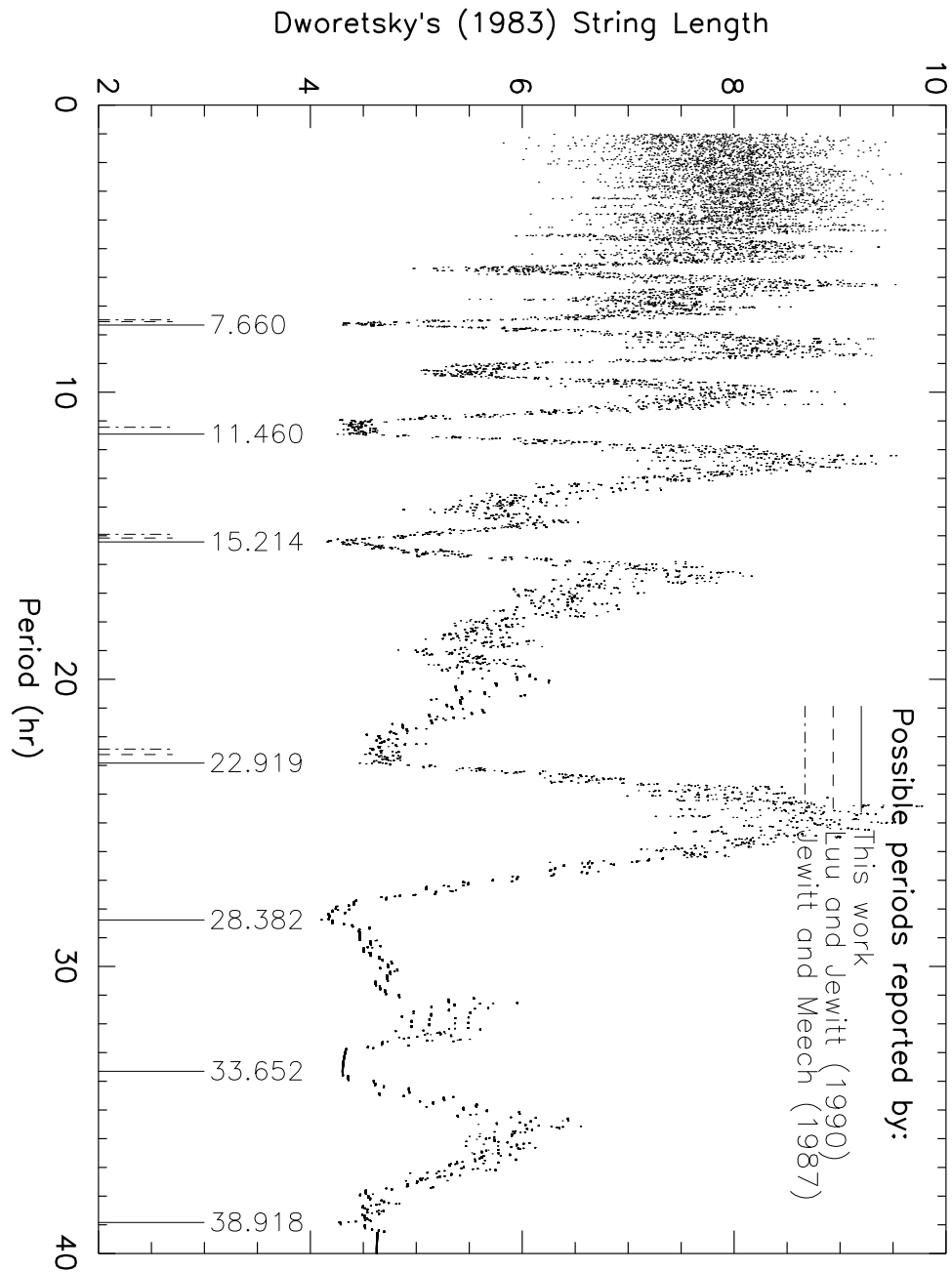


Figure 5.4: String-length method determination of Encke's rotation period. This is a diagram to find periodicity based on the method of Dworetsky (1983). Four days' worth of data were used to find the rotation period. Minima indicate the most likely rotation periods, but some are more favorable than others; text gives details. The dashed and dash-dotted lines indicate periods that have been postulated by LJ90 and JM87.

al. 1984, Swings 1985)

$$m(1, 1, \alpha) = H - 2.5 \log \left[(1 - G)e^{-3.33 \tan^{0.63}(\alpha/2)} + Ge^{-1.87 \tan^{1.22}(\alpha/2)} \right], \quad (5.5)$$

where $H = m(1, 1, 0)$; and the original Lumme-Bowell law (Lumme and Bowell 1981):

$$m(1, 1, \alpha) = m(1, 1, 0) - 2.5 \log F, \quad (5.6)$$

$$F \equiv (1 - Q)e^{-3.343 \tan^{0.632}(\alpha/2)} + (Q/\pi)(\sin \alpha + (\pi - \alpha) \cos \alpha),$$

where Q is the fraction of multiply-scattered light.

Figure 5.5 shows a plot of $m(1, 1, \alpha)$ for the Encke nucleus as measured by several observers; the data with notes are listed in Table 5.3. An observer had to report either the “nuclear” magnitude or the “ m_2 ” magnitude to have his/her datum included in this plot. The ordinate $m(1, 1, \alpha)$ is the observed magnitude minus the geometric factor $5 \log(r\Delta)$. Symbols indicate some information about each datum, written in the legend. The data from LJ90, JM87, Barker *et al.* (1981), Garradd (1997), Spinrad (as reported by LJ90), and us were taken with linear-response detectors; the other points are photographic. Our data and those of Garradd (1997) do not have much coma contamination despite being taken at low r . Of the historical data, only JM87, LJ90, and Barker *et al.* (1981) have information on the rotation of the nucleus, hence all the other points have an uncertainty of at least ± 0.4 mag, i.e., half the approximate p.t.p.a. Only Barker *et al.* (1981) and LJ90 were able to measure enough of the light curve to factor out the rotational modulation; in the former case there was no modulation detected. JM87 were twice able to find the turnover point at the bright end of the rotational variation, but not at the dim end, so we have used magnitudes for Fig. 5.5 that (we estimate) probably lie close to the average brightness and we have assigned sensible error bars. (Specifically, for one point we plotted a magnitude 0.6 mag fainter than their extremum, with errors of ± 0.2 mag; for the other point, we plotted a magnitude 0.4 mag fainter than their extremum, with errors of ± 0.3 mag.)

We assigned a photometric error of ± 0.5 mag to photographic data. This partially comes from the fact that Roemer and Lloyd (1966) photographed the comet only 14 minutes after van Biesbroeck (1962) did on 22 Oct 1960 and yet they differ in their magnitude estimates by 0.9 mag. Combined with the 0.4 mag of uncertainty due to rotation the total error is about 0.6 mag. We assigned an error of 0.1 mag to the data from linear-response detectors when no other estimate was available. Thus, the rotational uncertainty dominates, and the total uncertainty is about 0.4 mag.

We converted all data in Table 5.3 to Cousins R magnitude R_C , the band of our *HST* magnitude, before plotting in Fig. 5.5. To do this we assumed the following solar colors: (a) $B_J - R_J = 1.17$ (Allen 1973), (b) $B_J - m_{pg} = 0.11$ (Allen 1973), (c) $V_J - m_{pv} = 0.0$ (Allen 1973), (d) $V_J - R_J = 0.52$ (Allen 1973), (e) $R_J - R_C = -0.17$ (Ferne 1983), and (f) $R_{Mould} - R_C = -0.17$. For some points (noted in Table 5.3) we have assumed that the photographic data were taken on blue plates so that m_{pg} is the applicable quantity. (Roemer [1965] for example explicitly states that this is the case.)

Figure 5.5 (next page): Optical phase behavior of comet Encke's nucleus. By collecting historical data, I plot comet Encke's nuclear magnitude as a function of phase angle. Ordinate is in Cousins R magnitude, offset by $-5 \log(r\Delta)$ to account for differing observing geometries. A linear phase law, the Lumme-Bowell (Lumme and Bowell 1981) phase law, and the IAU-style asteroid phase law (Lumme *et al.* 1984, Swings 1985) are plotted. Despite the uncertain interpretation of some reported magnitudes, there is steep phase darkening, more drastic than that of other cometary nuclei and C type asteroids (shown).

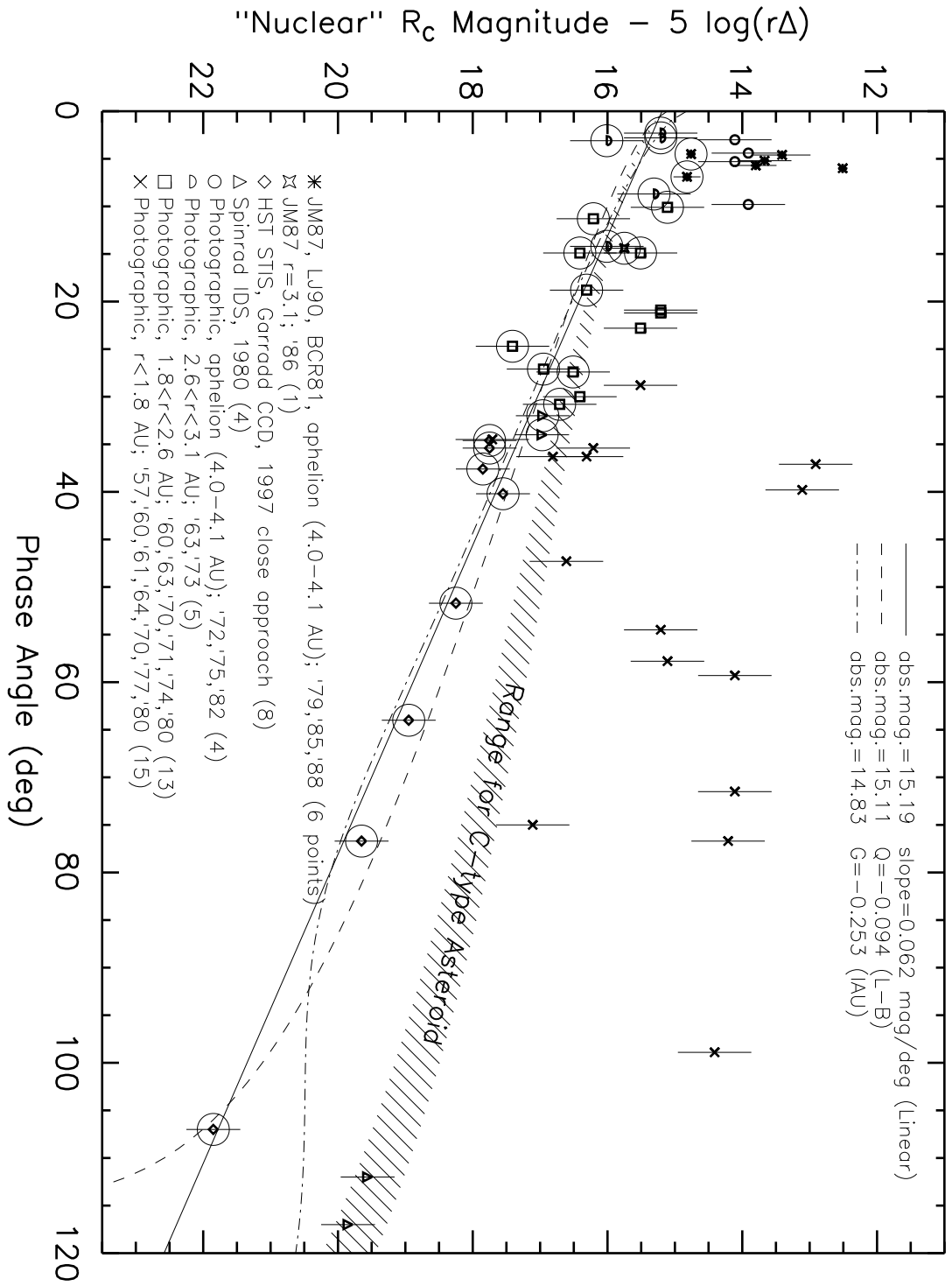


Table 5.3. Estimated “Nuclear” or “ m_2 ” Magnitudes for Encke’s Nucleus

Date	Medium ^a	Band ^b	Reported	α	r^c	Δ	Color	$m(1, 1, \alpha)$	Coma?	Wt.	Ref.
(UT)			Mag.	($^\circ$)	(AU)	(AU)	Crxn. ^d	e	f	g	k
30.5 Jul 1997	CCD	V_J	17.4	34.6	1.39	0.51	-0.35	17.8	F	2	1
28.5 Jul 1997	CCD	V_J	17.1	35.4	1.36	0.47	-0.35	17.7	F	2	1
24.5 Jul 1997	CCD	V_J	16.9	37.6	1.31	0.41	-0.35	17.9	F	2	1
21.4 Jul 1997	CCD	V_J	16.2	40.2	1.26	0.36	-0.35	17.6	F	1	1
14.4 Jul 1997	CCD	V_J	16.0	51.7	1.16	0.26	-0.35	18.3	F	2	1
10.5 Jul 1997	CCD	V_J	16.1	64.0	1.09	0.21	-0.35	19.7	F	2	1
7.4 Jul 1997	CCD	V_J	16.6	76.7	1.04	0.20	-0.35	20.0	F	2	1
1.3 Jul 1997	CCD	R_C	17.92	106	0.94	0.20	0.0	21.85 ^h	F	2	2
3-7 Sep 1988	CCD	R_M	19.8	4.2	3.83	2.85	+0.17	14.76	N	1	3
30 Oct-3 Nov 1986	CCD	R_M	20.0 ⁱ	14.8	3.15	2.46	+0.17	15.75	N	1	4
22-23 Sep 1985	CCD	R_M	20.2 ^j	6.8	4.06	3.15	+0.17	14.82	N	1	4
30 Jul 1982	Photo	m_{pg}^*	20.5	9.8	4.10	3.3	-0.89	13.9	?	0	5
5 Nov 1980	IDS	R_M	16.7	117	0.82	0.31	+0.17	19.9	Y	0	7

Table 5.3 – continued

Date (UT)	Medium ^a	Band ^b	Reported Mag.	α (°)	r^c (AU)	Δ (AU)	Color Crxn. ^d	$m(1, 1, \alpha)$ ^e	Coma? ^f	Wt. ^g	Ref. ^k
4 Nov 1980	IDS	R_M	16.5	112	0.84	0.31	+0.17	19.6	Y	0	7
8 Oct 1980	Photo	m_{pg}^*	16.5	47.3	1.26	0.49	-0.89	16.6	Y	0	6
7 Sep 1980	IDS	R_M	18.1	34	1.69	1.09	+0.17	17.0	Y	1	7
21 Aug 1980	IDS	R_M	19.0	32	1.90	1.47	+0.17	17.0	Y	1	7
13 Aug 1980	Photo	m_{pg}^*	20.0	30.8	1.80	1.65	-0.89	16.7	?	1	8
8.5 Aug 1980	Photo	m_{pg}^*	20	30.0	2.02	1.75	-0.89	16.4	?	0	9
26 Aug 1979	DAP	V_J	19.13	4.6	3.96	2.99	-0.35	13.21	N	0	10
24 Aug 1979	DAP	V_J	19.39	5.2	3.96	3.00	-0.35	13.67	N	0	10
22 Aug 1979	DAP	V_J	19.53	5.7	3.96	3.01	-0.35	13.80	N	0	10
21 Aug 1979	DAP	V_J	18.25	6.0	3.97	3.02	-0.35	12.51	N	0	10
14.3 Oct 1977	Photo	m_{pg}^*	15.1	39.8	1.17	1.56	-0.89	12.9	?	0	11
9.3 Oct 1977	Photo	m_{pg}^*	15.6	37.1	1.25	1.65	-0.89	13.1	?	0	11
12 Sep 1975	Photo	m_{pg}	20.2	4.4	4.02	3.05	-0.89	13.9	N	0	12

Table 5.3 – continued

Date (UT)	Medium ^a	Band ^b	Reported Mag.	α (°)	r^c (AU)	Δ (AU)	Color Crxn. ^d	$m(1, 1, \alpha)$ ^e	Coma? ^f	Wt. ^g	Ref. ^k
12 Sep 1974	Photo	m_{pg}	21.0	24.7	2.19	1.58	-0.89	17.4	?	2	13
25.0 Oct 1973	Photo	m_{pg}^*	20.25	14.2	2.63	1.80	-0.89	16.0	?	2	15
26 Sep 1973	Photo	m_{pg}	20.5	3.1	2.85	1.86	-0.89	16.0	N	2	14
13 Sep 1972	Photo	m_{pg}	20.5	3.0	4.09	3.11	-0.89	14.1	N	0	16
15 Aug 1972	Photo	m_{pg}	20.5	5.3	4.09	3.13	-0.89	14.1	N	0	16
29 May 1971	Photo	m_{pv}	20.5	27.1	2.22	1.95	-0.35	16.9	N	2	17
27 May 1971	Photo	m_{pg}	20.6	27.4	2.20	1.97	-0.89	16.5	N	1	17
28 Nov 1970	Photo	m_{pg}	16.5	75.0	1.00	0.43	-0.89	17.1	Y	0	18
26.4 Sep 1970	Photo	m_{pg}	18.4	18.8	1.87	0.95	-0.89	16.3	Y	2	18
7.1 Sep 1964	Photo	m_{pg}	18.6	34.5	1.75	1.26	-0.89	16.0	Y	0	19
30.2 Aug 1964	Photo	m_{pg}	19.0	36.3	1.65	1.08	-0.89	16.8	Y	0	19
16.1 Dec 1963	Photo	m_{pg}	20.3	22.8	2.50	2.46	-0.89	15.5	N	0	19
12.3 Oct 1963	Photo	m_{pg}	20.2	8.7	2.99	2.07	-0.89	15.3	N	1	19

Table 5.3 – continued

Date	Medium ^a	Band ^b	Reported	α	r^c	Δ	Color	$m(1, 1, \alpha)$	Coma?	Wt.	Ref.
(UT)			Mag.	($^\circ$)	(AU)	(AU)	Crxn. ^d	e	f	g	k
25.4 Sep 1963	Photo	m_{pg}	20.2	2.6	3.10	2.11	-0.89	15.2	N	1	19
24.3 Sep 1963	Photo	m_{pg}	20.2	2.5	3.11	2.11	-0.89	15.2	N	1	19
17.1 Jan 1961	Photo	m_{pg}	14.3	98.9	0.59	0.70	-0.89	14.4	Y	0	19
6.1 Jan 1961	Photo	m_{pg}	15.0	76.7	0.79	0.79	-0.89	14.2	Y	0	19
20.2 Dec 1960	Photo	m_{pg}	17.0	59.3	1.08	0.87	-0.89	14.1	Y	0	19
8.2 Nov 1960	Photo	m_{pg}	15.9	28.8	1.67	0.89	-0.89	15.5	N	0	19
22.1 Oct 1960	Photo	m_{pg}	17.6	14.9	1.87	0.94	-0.89	15.5	N	1	19
22.1 Oct 1960	Photo	m_{pg}	18.5	14.9	1.87	0.94	-0.89	16.4	F	2	21
17.3 Oct 1960	Photo	m_{pg}	18.5	11.3	1.93	0.97	-0.89	16.2	F	2	21
26.2 Sep 1960	Photo	m_{pg}	18.0	10.1	2.15	1.19	-0.89	15.1	N	1	19
19.3 Aug 1960	Photo	m_{pg}	19.5	20.9	2.51	1.87	-0.89	15.2	N	0	19
17.3 Aug 1960	Photo	m_{pg}	19.5	21.2	2.52	1.91	-0.89	15.2	N	0	19
19.4 Sep 1957	Photo	m_{pg}	15	71.5	0.80	0.91	-0.89	14.8	Y	0	20

Table 5.3 – continued

Date	Medium ^a	Band ^b	Reported	α	r^c	Δ	Color	$m(1, 1, \alpha)$	Coma?	Wt.	Ref.
(UT)			Mag.	(°)	(AU)	(AU)	Crxn. ^d	e	f	g	k
4.4 Sep 1957	Photo	m_{pg}	16	57.8	1.05	1.03	-0.89	14.9	Y	0	20
31.4 Aug 1957	Photo	m_{pg}	16.5	54.5	1.12	1.08	-0.89	15.2	Y	0	20
30.4 Jul 1957	Photo	m_{pg}	19.3	36.3	1.57	1.67	-0.89	16.3	Y	0	20
28.4 Jul 1957	Photo	m_{pg}	19.3	35.4	1.60	1.72	-0.89	16.2	Y	0	20

^a CCD = Charge-coupled device. Photo = photographic plates. IDS = image dissector scanner.

DAP = digital area photometer.

^b Asterisks indicate where the use of a blue-sensitive plate was assumed.

^c Aphelion: $r = 4.1$ AU; Perihelion: $r = 0.3$ AU.

^d Term to convert from reported magnitude to R_C band.

^e $m(1, 1, \alpha) = \text{Reported Mag.} - 5 \log(r\Delta) + \text{Color Crxn.}$

^f Indicates presence of an observed coma: Y = yes, F = yes but faint, N = no, ? = unknown.

^g Relative weight of the point used when fitting the phase law.

Table 5.3 – continued

^h Added 0.3 mag to account for coma.

ⁱ Magnitude is 0.4 mag fainter than authors' reported bright extremum.

^j Magnitude is 0.6 mag fainter than authors' reported bright extremum.

^k References: 1 = Garradd 1997. 2 = This work. 3 = LJ90. 4 = JM87. 5 = Gibson, reported by Marsden 1985b. 6 = Shao and Schwartz 1980. 7 = Spinrad 1985, private communication reported in JM87. 8 = Shao, reported by Marsden 1985a. 9 = Helin *et al.* 1980. 10 = Barker *et al.* 1981. 11 = Gilmore and Kilmartin 1978. 12 = Roemer, reported by Marsden and Roemer 1978b. 13 = Roemer, reported by Marsden and Roemer 1978a. 14 = Roemer, reported by Marsden 1974. 15 = Shao 1973. 16 = Roemer, reported by Marsden 1973. 17 = Roemer, reported by Marsden 1972. 18 = Roemer, reported by Marsden 1971. 19 = Roemer and Lloyd 1966. 20 = Roemer 1965. 21 = van Biesbroeck 1962.

Ideally all the points would tightly follow a curve, but clearly some choice has to be made about which data are worth fitting, since the coma contamination is obvious for some points, e.g. the ten photographic points at low r between $35^\circ < \alpha < 100^\circ$. For such points the observers likely measured the comet's central condensation (inner coma) rather than the nucleus itself. With other points the exact amount of contamination is unclear, it may be none or half a magnitude's worth. An indication of how much coma contamination there is might be determined by looking at the intrinsically faintest data at a given α , but in this case that is not so helpful because that usually turns out to be a photographic point and the error bars are too large. Hence, it is nontrivial to incorporate all the data into a fit to the phase law. Moreover the problem is most contentious at low phase angle, i.e., right at the location where we need the best data to determine the absolute magnitude. The data point due to LJ90 is very well determined (± 0.04 mag), and so normally would provide a very good constraint; however, if there were a tiny amount of coma contamination, that would compromise its usefulness in the fitting.

A further complication is that the plotted error bars are not normally distributed, so any fit statistic must be carefully interpreted. A sinusoidally-varying flux spends more time at the extrema than at the average value, so the measured value is likely to be far from the average brightness.

Our solution is to fit the phase laws through the selection of points marked in Table 5.3 and enclosed in circles in Fig. 5.5. We use all of the linear-detector data and the fainter photographic points. For a given point we assigned it double weight if it was an intrinsically fainter point relative to its immediate neighbors in phase angle. The results are provided in Fig. 5.5. The r.m.s. offset is about 0.4 mag for all three fits. The IAU law fails at the higher phase angle but the other two laws are adequate. Considering the uncertainties we take the absolute magnitude to be 15.2 ± 0.5 mag.

The slope of the phase law is quite steep at 0.06 mag/degree, making Encke's nucleus one of the most phase-darkened objects in the Solar System. It is possible that shape effects are anomalously depressing the brightness at high phase angle and fooling us, but the smooth, linear behavior of our *HST* point and the Garradd (1997) points argue against this. Cometary nuclei (Jewitt and Meech 1988, Chapter 7 of this thesis) and C-type asteroids (Lumme and Bowell 1981), to which the nuclei are commonly thought to be evolutionarily linked, typically have only about 0.04 mag/degree of phase effect, as drawn in Fig. 5.5. Further study of the phase behavior of near-Earth asteroids (NEAs) and cometary nuclei over a large range of α is clearly desirable.

The unphysical and negative value of Q , the fraction of multiply scattered light, and the steep slope both imply that the surface of Encke is very rough. Lumme and Bowell (1981) mention this phenomenon in reference to (944) Hidalgo, a cometary candidate also with $Q < 0$. Specifically, the depth-to-diameter ratio of features on the surface is apparently larger than for their average asteroid, and Q is actually close to zero. This makes sense since the reflectivity of the nucleus is so low, so very few measured photons would have been multiply scattered.

It is interesting to note that the aphelion data from 1972, 1975, 1979, and 1982 all apparently have significant coma, though none were spatially resolved by

the observers. The Barker *et al.* (1981) data prove that aphelion outbursts exist, and it is important to justify the inability to spatially resolve the coma, which we assume is mostly dust. Some measurements had fairly large seeing disks which could potentially hide the coma, but JM87 and LJ90, with $\sim 1''$ seeing, specifically used differing apertures to detect comatic flux, but did not find any. Thus, any existing dust would have to be slow-moving and/or have a surface brightness steeper than the usual dependence on cometocentric distance. We know that large (tens to thousands of microns) grains are emitted by Encke from *IRAS* trail and *ISO* tail and trail observations (Sykes and Walker 1992, Reach *et al.* 1999, Lisse *et al.* 2000), and such particles move slowly with respect to the nucleus since radiation pressure is inefficient. Thus, it is not unreasonable to expect that the outbursts originate as large dust grains traveling at ~ 1 m/s (i.e., just below escape velocity) and eventually falling back on to the surface. At aphelion the largest dust grain that can be lifted off the nucleus has a radius of just $130 \mu\text{m} \times \left(\frac{v_g}{10 \text{ m/s}}\right) \times (Z \times 10^{-16} \text{ s cm}^2)$, where v_g is the speed of the gas and Z is the vaporization rate, based on an equation given by Keller (1990).

5.4.4 Nucleus Size and Geometric Albedo.

Now we can apply the thermal model to the data. First, let us assume $\epsilon = 0.9$ and $T_{ss} = 360$ K (which will be justified below). If $\Gamma = 50 \text{ J K}^{-1} \text{ m}^{-2} \text{ s}^{-1/2}$, i.e. about the lunar value (Winter and Saari 1969), then $\Theta = 0.23$ (defined in Chapter 3) and Encke's nucleus is a moderately slow-rotator. Harris *et al.* (1998) estimate $\Gamma = 320 \text{ J K}^{-1} \text{ m}^{-2} \text{ s}^{-1/2}$ on the surface of (3200) Phaethon, which is presumably an extinct comet owing to its parentage of the Geminid meteor stream; if applicable to Encke's nucleus, $\Theta = 1.5$, placing it on the border between slow and fast rotator. Thus the STM will work reasonably well but not perfectly represent Encke's thermal behavior. Since the orientation of the nucleus' spin axis appears to have changed since the Sekanina (1988a) analysis, it would be difficult to constrain any of the other parameters in the augmented thermal model even though we have derived some information about the shape. Thus we will apply the STM and compare the results with the RRM to get some sense of the model-dependent error.

Some parameters of the STM were assumed to be as follows: infrared phase coefficient β_i , 0.005 to 0.017 mag/degree; emissivity ϵ , 0.9; optical phase integral q , 0.17, which can be derived from the phase analysis of a previous section; beaming parameter η , 0.7 to 1.2. For the RRM, we assume the limiting case of the rotation axis perpendicular to the Sun-Earth-Comet plane.

In Section 5.3.3 we found the nucleus' flux to be 2.74 ± 0.24 Jy; for this flux the STM provides us with an effective radius R_N of 2.40 ± 0.27 km and a subsolar temperature T_{SS} in mid-July 1997 of 365 ± 14 K. This justifies our use of 360 K in the Θ calculation above. The (1- σ) errors are derived from a Monte Carlo simulation letting $0.9 < \epsilon < 1.0$, $0.7 < \eta < 1.2$, and $0.005 < \beta_i < 0.017$, all uniformly distributed, and using the normally-distributed flux estimate. By similarly applying the simplified RRM, we find $R_N = 3.55 \pm 0.15$ km and $T_{SS} = 270 \pm 5$ K. These may be interpreted as the upper and lower limits, respectively, to these quantities since they would be physical only if we were grossly underestimating the thermal

inertia of cometary nuclei. It is clear however that if the thermal inertia is more Phaethon-like than Moon-like then R_N is probably a few tenths of a kilometer larger than that given by the STM.

From our discussion in Section 5.4.3 we estimate the optical cross section at zero phase angle to be equivalent to a magnitude of 15.2 ± 0.5 . The relation between the optical cross section and the comet's magnitude is

$$pR_N^2 = 2.238 \times 10^{16} \text{ km}^2 \times 10^{0.4(m_\odot - m(1,1,0))} \quad (5.8)$$

based on an equation given by Jewitt (1991), where p is the geometric R band albedo and m_\odot is the solar apparent R band magnitude of -27.10 . We calculate from this that $p = 0.047 \pm 0.023$.

5.4.5 Consistency with ISO Data.

Our broadband spectrophotometry obtained by *ISO* is shown in Fig. 5.6. The dust's contribution to these data is more fully discussed in a related paper by Lisse *et al.* (2000). Presently we will only show that our other results are consistent with this dataset.

Our simple model of the spectrum uses the sum of two component spectra, one for the dust and one for the nucleus. Reach *et al.* (1999) have shown that there is a significant population of large (radius $\gtrsim 100 \mu\text{m}$) grains in Encke's coma, so we have modeled the thermal emission of the dust in the 4.8 to 100 μm wavelength range as a greybody, with temperature as a free parameter and emissivity independent of wavelength. Such a null dependence can explain mid-IR observations of large dust grains from other comets (Lisse *et al.* 1998). We are unconcerned with the actual values of the dust's emissivity and optical depth; we scale our model to yield the best fit for particular values of the parameters. ISOPHOT's 3.6 μm flux has a significant scattered sunlight component in addition to the thermal emission and so is not used to constrain our model beyond being an upper limit to the thermal flux.

We modeled the spectrum of the nucleus using the STM, choosing η to be either 0.7, 0.95, or 1.2, β_i to be either 0.005 or 0.017 mag/degree, and ϵ to be 0.9. The parameter R_N could be any value. Thus our model has four important parameters: temperature of the dust T_D , R_N , η , β_i . An example model and the excellent fit to the spectrophotometry are shown in Fig. 5.6.

With this methodology, the results of the fitting can be displayed as a contour plot of the reduced χ^2 fit-statistic (χ_ν^2) as a function of T_D and R_N . The six plots in Fig. 5.7 show this, for each value of η and β_i . Owing to the low number of spectrum points vis-à-vis the model parameters, it is impossible to constrain the four parameters, but the ISOPHOT spectrum is consistent with our ground-based derivation of R_N (whose 1- σ boundaries are noted by the shaded rectangles) across the range of previously-found values for η and β_i . In particular, η cannot be constrained from Fig. 5.7 since the ESO constraint on R_N never strays far from $\chi_\nu^2 \approx 1$, even when $\eta = 0.7$. It is satisfying that the derived dust temperatures are sensible; an isothermal black body at Encke's distance from the Sun would have $T_D = 258$ K.

5.5 Previous Work

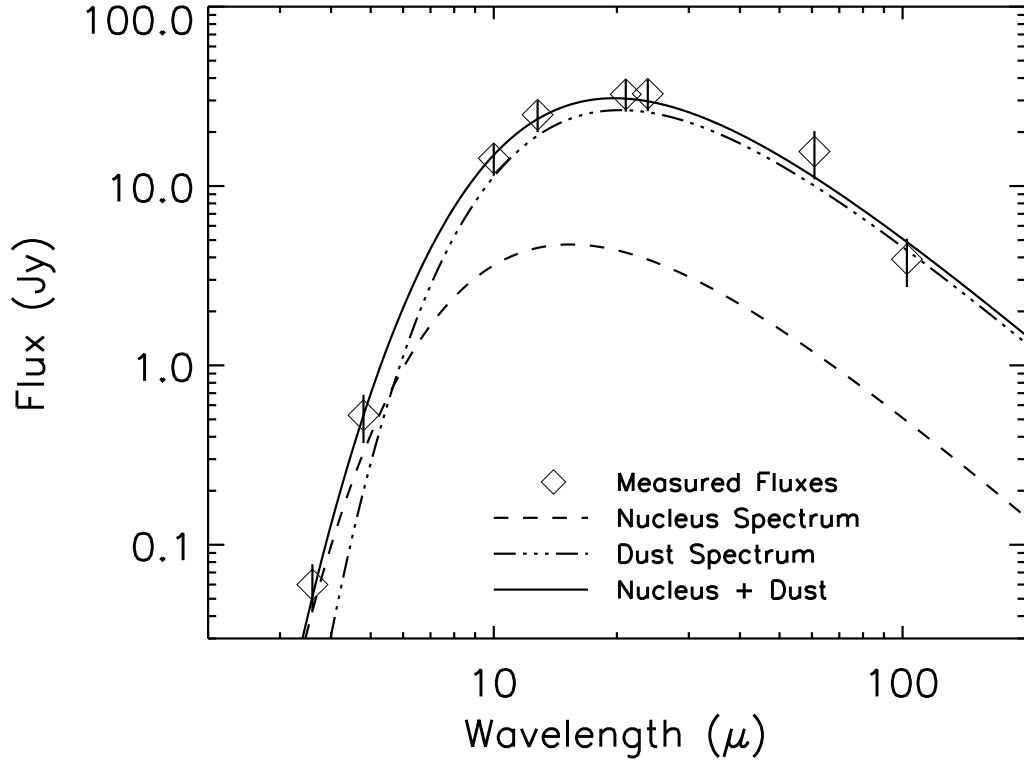


Figure 5.6: ISOPHOT spectrophotometry of Encke dust coma plus nucleus. The symbols show a broadband mid-infrared spectrum of the nucleus and dust of comet Encke, taken by ISOPHOT. Also plotted is a sample model (solid line) that fits the spectrum ($\chi^2_{\nu} = 0.64$ with 3 degrees of freedom, $R_N = 2.5$ km, $T_D = 250$ K, $\eta = 1.1$, $\beta_i = 0.01$ mag/degree). Dashed line is a model spectrum of the nucleus generated by the STM; dash-dotted line is a Planck spectrum of the dust.

Thermal infrared measurements in the past have been made by Ney (1974), Campins (1988), and Gehrz *et al.* (1989) to estimate the size of the nucleus. All used single-element bolometers, so no spatial information was obtained. The present study is an improvement because of our higher sensitivity and spatial resolution.

5.5.1 Ney (1974).

On 25 Apr 1974, Ney (1974) measured a flux of 11 ± 1 and 19 ± 2 Jy at wavelengths of 4.8 and 8.5 μm , respectively (converting from the reported magnitudes). His reported upper limit to Encke's R_N of 0.25 to 0.5 km is derived from an assumed correlation between nuclear size and comatic thermal infrared behavior, observations of Comet Bradfield (1974b = 1974 III = C/1974 C1), and an assumed value for the nuclear albedo that is now known to be too high. Instead, if we apply the STM to his Encke thermal fluxes, and use the assumptions we outlined in Section 5.4.4, we find an upper limit to the nuclear radius of approximately 7.5 km, which is above our calculated value.

5.5.2 Campins (1988).

Seven observations at 10.6 μm are reported during the 1984 apparition, two during the 1980 apparition, and the fluxes vary from 0.6 to 6.1 Jy. By using his intrinsically faintest data point, and applying the STM, he estimates an effective radius of ≤ 2.9 km at rotational minimum and ≤ 4.4 km at rotational maximum. These are the mid-IR measurements with formerly the least amount of coma contamination, but our calculated effective radius is smaller.

5.5.3 Gehrz *et al.* (1989).

Near and mid-IR measurements are reported on four dates during the 1974 apparition and two dates during the 1987 apparition, with fluxes ranging from 1 to 20 Jy. Using their intrinsically faintest data point, and assuming an isothermal nucleus (not the STM), they derive an upper limit to R_N of 5 km. Applying the STM to their reported fluxes gives an upper limit of 3 to 5 km, depending on the model's parameter values, which is above our calculated value.

5.5.4 Kamoun *et al.* (1982).

From the radar echoes at $\lambda = 12.6$ cm, these workers found a radar cross section of 1.1 ± 0.7 km² in the circular polarization sense orthogonal to that of the transmitted pulse. If Encke is like other comets where the radar's reflection is mostly specular (Harmon *et al.* 1989), then this is roughly the total radar cross section also. Further, using the bandwidth of the returned pulse, they found an effective radius R_N of $1.5^{+2.3}_{-1.0}$ km, although with more modern values of the rotation period (LJ90) and spin axis direction (Sekanina 1988a) R_N would be 4^{+6}_{-3} km. Our measurement of R_N is within this range.

With our effective radius in hand further rudimentary interpretation of the radar results are possible. The geometric albedo at $\lambda = 12.6$ cm, $p_{12.6}$, which is just

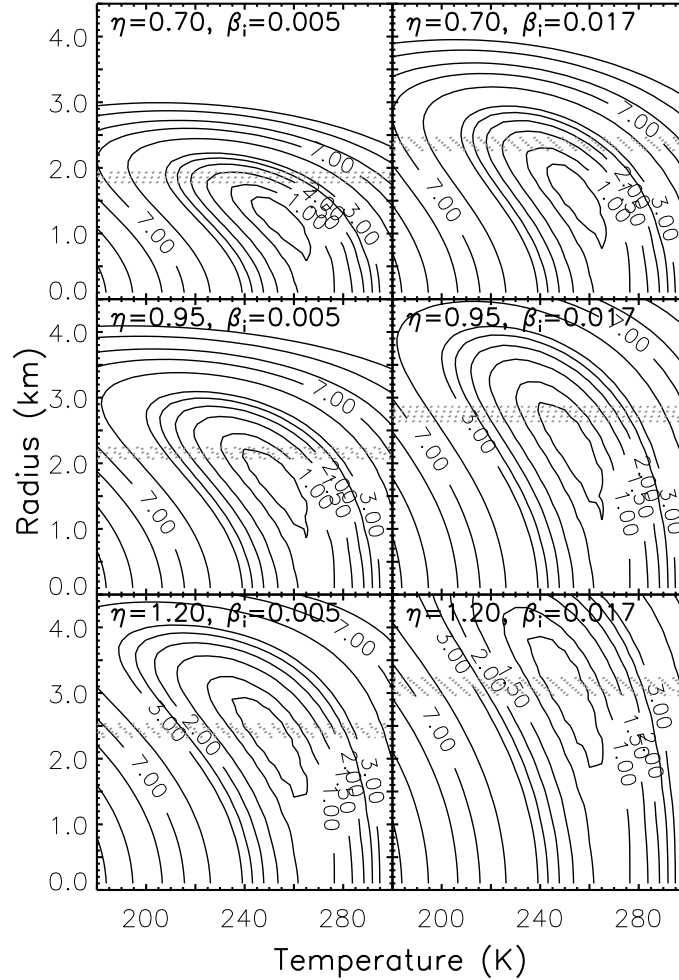


Figure 5.7: χ^2 plots of Encke dust temperature and nucleus size. Here are contour plots of χ^2_{ν} showing that the simple model described in the text – dust black body spectrum plus nucleus STM spectrum – adequately fits the *ISO* spectrum and is consistent with the ground-based results. Shaded rectangles indicate the $1\text{-}\sigma$ range of nuclear radii implied by our ESO data. Contour levels are 0.75, 1.0, 1.5, 2.0, 2.5, 3.0, 5.0, 7.0, 9.0, 12.0, and 15.0. Each panel represents one value of β_i and one value of η , leaving the other two parameters of the model – dust temperature and nuclear radius – to be plotted.

the radar cross section divided by πR_N^2 , is 0.061 ± 0.041 , a value comparable to the one at optical wavelengths and to that found for other comets (Harmon *et al.* 1989, Campbell *et al.* 1989). Following the argument and assumptions made by Harmon *et al.* (1989) in their treatment of Comet *IRAS-Araki-Alcock* (C/1983 H1), the dielectric constant of the Encke nucleus' surface layer is 2.3 ± 0.7 , corresponding to (not surprisingly) a mixture of dust and snow.

5.6 Summary of Encke Results

We have discussed the properties of the nucleus of Comet 2P/Encke as derived from data obtained during its close approach to Earth in July 1997. The *CONTOUR* spacecraft is scheduled to encounter comet Encke in 2003 and this information can aid in the mission planning and design. We measured the thermal continuum of the comet in the 8 to 12 μm range with the TIMMI instrument at the ESO 3.6-m telescope and in the 3.6 to 100 μm range with the ISOPHOT photometer on the *ISO* spacecraft. We also used the STIS CCD aboard *HST* to measure the optical (5500-11000 Å) scattered continuum of the comet. We find the following:

- 1. Assuming the nucleus' thermal behavior can be described using the Standard Thermal Model (STM; Lebofsky and Spencer 1989), the effective nuclear radius is $2.4 \text{ km} \pm 0.3 \text{ km}$ and the subsolar temperature at a distance of 1.2 AU from the Sun is $365 \pm 14 \text{ K}$. The effective radius is smaller than the upper limits found by other researchers using thermal continuum observations (Ney 1974, Campins 1988, and Gehrz *et al.* 1989), and within the range found via the radar experiment in 1980 (Kamoun *et al.* 1982). The applicability of the STM could be questioned since the thermal inertia is unknown, but the effective radius is probably at most only a few tenths of a kilometer larger than the value given above.

- 2. Using our *HST* data and other datasets (JM87, LJ90, Garradd 1997) along with various photographic data from previous apparitions, we find the optical phase law of Encke's nucleus out to 106° can be well fit with a Lumme-Bowell phase law (Lumme and Bowell 1981) with absolute R_C band magnitude 15.2 ± 0.5 and $Q = -0.09$. The equivalent linear slope is 0.06 mag/degree, which is one of the steepest slopes known for any small body of the Solar System. The negative value of Q and the steep slope imply that the nucleus' surface is rougher than the typical asteroid used to create the Lumme-Bowell law. The absolute magnitude yields a visual geometric albedo for the nucleus of 0.05 ± 0.02 . Use of this absolute magnitude does mean that bright ($\sim 1 \text{ mag}$) but spatially-unresolved outbursts were observed at several separate aphelia (4 AU) by many observers.

- 3. The nucleus' rotation period is likely $15.2 \text{ hr} \pm 0.3 \text{ hr}$, but our data cannot rule out some harmonics of this value, as they also show or imply a double-peaked light curve (i.e., as if we had observed a rotating nucleus). Optical measurements give $15.08 \pm 0.08 \text{ hr}$ (LJ90), so our data are consistent with this value.

- 4. We measured a peak-to-peak amplitude (p.t.p.a.) of the light curve of $0.7 \pm 0.1 \text{ mag}$, though it may be larger since we could not sample the entire rotational phase. With a model that assumes the nucleus is a triaxial ellipsoid with an angular momentum vector (a) initially pointing in the direction found by Sekanina (1988a) and (b) "precessing" in a circle due to a torque from the outgassing vents on the surface, we combined our dataset and the p.t.p.a. reported by JM87 and LJ90 to

find that the precession period is less than 81 years, one axial ratio a/c is at least 2.6, and the other one b/c satisfies $1.0 \leq b/c \leq 0.5 \times a/c - 0.3$. The precession circle's axis must be at least 14° from the angular momentum vector. We surmise that a significant mass ejection event could have occurred in the mid-1980s to start the angular momentum vector moving again, since, according to Sekanina (1988a), on average it was in the same place for much of the 20th century.

- 5. The nucleus' radius is toward the low end of known radii of nuclei, while the axial ratio is toward the high end (Meech 1999). The albedo is comparable to Halley's and not unlike the other few comets for which it has been measured (Chapter 9). Among known near-Earth asteroid properties, the radius is in the middle, and the albedo is on the low end. However the samples of comets and NEAs both suffer from incompleteness and observational bias.

- 6. Under the STM formalism, we can constrain neither the beaming parameter η nor the infrared phase coefficient β_i other than to say Encke's thermal behavior is consistent with the values found for these parameters from asteroids and icy satellites. Future studies of comet Encke's nucleus should try to employ a wide range of phase angles and a wider range of wavelengths to better understand its thermal phase behavior and improve the interpretation of radiometry.

Chapter 6

The Nucleus of Comet Hyakutake C/1996 B2

6.1 Background

Six months after the discovery of Hale-Bopp, a Japanese amateur astronomer discovered his second long-period comet in a seven-week period, an 11th magnitude smudge (Nakamura and Nakano 1996). Four days later it was realized that this comet would make a very close approach to Earth in late March and probably be an easy naked-eye object (Marsden 1996). The rest of the story is well known: comet Hyakutake blazed through the Northern Hemisphere sky at a visual magnitude of about 0 and sported a tail extending many tens of degrees. The photograph in Fig. 6.1 shows how the comet looked to my camera on 25 Mar 1996; the field of view is about 40 degrees wide. In contrast to Hale-Bopp later on, Hyakutake flashed in and out of our skies in a week. The short lead time necessitated a scramble for requesting access to telescopes; fortunately many observatory directors recognized the special significance of this comet – the closest one to Earth since 1983 and the brightest one since 1976 – for which comet scientists were exceedingly grateful.

6.2 Thermal Measurements

A track of observations was done at the Very Large Array (VLA), two days after the March 25th close approach of the comet. I have described that experiment elsewhere (Fernández *et al.* 1997a) and I reproduce much of the text here. Our infrared thermal data were obtained around the time of the comet's close approach, and have been described in detail by Lisse *et al.* (1999b). Since most of the work in that wavelength regime for this comet was done by Lisse, I will give space to those results only as they relate to my data.

6.2.1 Details of Observations

Our VLA observations consisted of one twelve-hour track from 0700 UT to 1900 UT on 27 March, 1996. The flux calibrator was 3C 286 (QSO J1331+3030, flux of about 5.2 Jy), and our phase calibrator was 4C 76.03 (a radio galaxy having a flux of about 2.2 Jy) (Perley and Taylor 1996). Individual integrations were ten seconds long; the total amount of time spent integrating on the comet was about ten hours. Phase stability during the track was good.

During the observation, the comet itself was between 0.121 and 0.131 AU from Earth, 1.00 and 0.989 AU from the Sun, and the phase angle was between 85.7° and 90.2° . The ephemeris that was used at the time of the observation was provided by D. K. Yeomans (private communication), but, owing to the proximity of the comet, had formal positional uncertainties of 8 arcsec in right ascension and 2 arcsec in



Figure 6.1: Comet Hyakutake in a 40° -wide field of view. This is a photograph of the comet taken by me near the time of closest approach on 25 Mar 1997. The field of view on the long dimension is about 40 degrees; the tail is clearly visible over most of that arc.

declination ($1\text{-}\sigma$). The proper motion of the comet ranged from 4.7 to 5.5 arcsec per integration-time, and decreased by about 0.065 arcsec per integration-time per hour.

The VLA telescopes can only track the linear proper motion of a source. But, due to the rapid motion of the comet, we had to take into account the second order motion. We updated the linear tracking rates every 3 to $3\frac{1}{2}$ minutes so that the array was always pointed within one synthesized beam (3.5 arcsec) of the most accurate formal position of the comet available at the time.

6.2.2 Data Reduction and Correction

The standard data reduction yielded no significant signal from the comet. One problem we considered was that, due to the positional uncertainty of the comet, the signal might have been smeared during the course of our observation. A more accurate ephemeris of the comet, produced by D. K. Yeomans a few weeks after perigee, revealed that our tracking rates were not significantly in error (off by ≤ 0.01 arcsec per integration time), but the center of pointing was indeed offset from the true position of the comet by up to 6.6 arcsec at times during our observing run. It should be pointed out here that the half-power bandwidth (HPBW) of the VLA telescopes at our observing frequency is 5.3 arcmin and primary beam attenuation is negligible for these offsets. In essence, the amplitude and phase of the complex integration data points were correct, but the projected baselines (or uv -spacings) of the telescopes were slightly offset, because of the difference in the observed and actual position of the comet. We recalculated the correct uv -spacings for each baseline for every ten-second integration, and inserted these corrected spacings into the dataset. After the correction, we obtained a more robust map.

This problem is important to consider for any interferometric observation of a fast-moving object, because of the inherent uncertainty in the ephemeris and in the way the data are taken at the observatory. To stress this latter point, it was important that, in order to correctly reduce our data, we understand intimately where the telescopes point at a given time, and what information pertaining to that are stored as “data.” In this case the “data” were not correct, and we were forced to alter them by hand. Since the VLA (or any radio interferometric array) typically does not perform observations of this sort, we emphasize the special requirements of the data analyst in this situation. A description of some of the problems with interferometric observations of close, fast objects is given by de Pater *et al.* (1994).

Our CLEAN map, with 2- and 3- σ contours, is shown in Fig. 6.2. Since we had directly manipulated the data (via the corrections), we would expect the signature from the comet to appear in the middle of the map. The synthesized beam – 3.5 arcsec wide – is shown in the lower left. The field of view in this map is 4.2 arcmin by 4.2 arcmin, slightly smaller than the HPBW of the telescopes’ primary beam. With such a synthesized-beam size, the nucleus would have appeared as a point source. The r.m.s. noise in our map is $7.6 \mu\text{Jy}/\text{beam}$.

There appear to be some linear structures or streaks running generally north-east to southwest in the map. These may be extended background sources passing through the field of view as the array tracked the comet, or indicative of a few

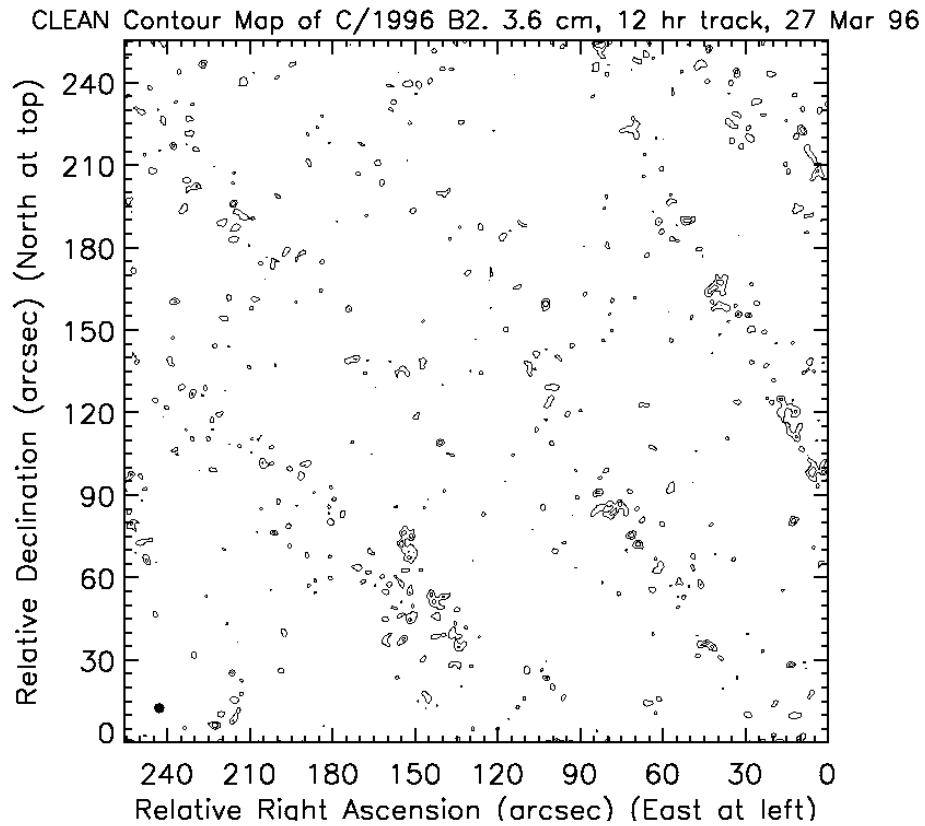


Figure 6.2: CLEAN contour map of C/1996 B2. This is actually the CLEAN contour map of the field of view containing the comet, since we did not detect the object at the $3\text{-}\sigma$ level. We used the VLA on 27 Mar 1996 to generate this image, and the synthesized beam is the black dot at lower left.

anomalous visibility-data points. It is important to stress, however, that the structures appear only on the 1- and 2- σ level, and as such are not statistically significant. A histogram of pixel values is well-described by a Gaussian of $\sigma = 7.6 \mu\text{Jy}$ and shows no excess of pixels 1- or 2- σ from the mean. In addition, the structures have a low intensity. Integrating over the roughly $\sim 10^{2.5}$ synthesized-beams that they cover, the flux density is about 1 to 10 mJy. Had the hypothetical structures been tracked, they would have covered around 30 to 100 synthesized beams, based on the thickness of the streak. This implies their surface brightness was only ~ 10 to 100 $\mu\text{Jy}/\text{beam}$.

6.2.3 Implications for the Nucleus

Our measurement of the r.m.s. flux in the synthesized beam from the comet allows us to place a 3- σ upper limit on the thermal microwave continuum flux of 22.8 μJy at 3.55 cm. Of the six interferometric observations of a comet's microwave continuum, five (including Hyakutake) are upper limits. Our Hale-Bopp observations (Chapter 4) resulted in the only detection. Our Hyakutake upper limit is smaller than the other four: comet Austin (C/1982 M1 = 1982g = 1982 VI) was observed at 6 cm (Snyder *et al.* 1983) with an upper limit of 140 μJy ; comet IRAS-Araki-Alcock (C/1983 H1 = 1983d = 1983 VII) was observed at 2 and 6 cm (de Pater *et al.* 1985) with upper limits of 750 and 90 μJy , respectively; comet Crommelin (27P = 1983n = 1984 IV) was observed at 2 cm (Schenewerk *et al.* 1986) with an upper limit of 136 μJy ; and comet Halley (1P/1982 U1 = 1982i = 1986 III) was observed at 2 cm (Hoban and Baum 1987) with an upper limit of 100 μJy .

As mentioned in Chapter 3, it is not obvious which thermal model is the most applicable. The rotation period is about 6.3 hr (see next section), which would put the thermophysical parameter Θ close to unity for lunar-like thermal inertia. However, since the microwave data sample colder, subsurface layers, the ILM or even an isothermal model is probably more applicable. Also the high activity of the nucleus – approximately 50% of the surface is active (Lisse *et al.* 1999b) – probably helps to keep the insolation energy from penetrating deep below the surface, since much of it is being used to sublimate ice. Since we do not have information on the shape of the nucleus and since there does not yet seem to be a comprehensive model of the nucleus' rotation state, we will simplify matters by calculating an upper limit to the nucleus' radius by assuming the subsurface layer that we have sampled is isothermal.

To obtain an estimate of the nuclear size, we use

$$S_\lambda = \frac{2\pi kT}{\lambda^2} \epsilon_\lambda \frac{R^2}{\Delta^2}, \quad (6.1)$$

where S_λ is the measured flux density from the nucleus ($\leq 22.8 \mu\text{Jy}$), λ is the wavelength (3.55 cm), Δ is the geocentric distance (averaging 0.126 AU during the observation), k is the Boltzmann constant, T is the nuclear temperature, ϵ_λ is the emissivity at 3.55 cm, and R is the nucleus' effective radius.

Radar measurements of cometary nuclei have indicated that the microwave albedo is quite low, a few percent (Campbell *et al.* 1989). Thus, the emissivity of the nuclei is probably around 0.95, assuming that the emissivity is close to one

minus the albedo. For comparison, the emissivity of NEAs is roughly as high, 0.8 to 0.9 (Goldstein *et al.* 1984). The temperature is more problematical, but based on our efforts for Hale-Bopp (in Chapter 4), a temperature of 150 K for the sampled layer in Hyakutake's nucleus is not unreasonable. The extreme limits to the temperature range from about 300 or 350 K (for a very conductive nucleus) down to roughly 50 K (roughly the temperature of formation in the Kuiper Belt [Rickman 1991]).

We have combined all of this information into Fig. 6.3. Effective radius is plotted vs. temperature, with the solid curves representing four possible emissivities. The dotted line marks the temperature of an isothermal blackbody at the heliocentric distance, and the dashed line marks the approximate sublimation temperature for water ice. For the true emissivity and observed temperature of the nucleus, the radius could lie anywhere to the left of the appropriate point. For $\epsilon = 0.9$ and $T = 150$ K, the $3\text{-}\sigma$ upper limit to the radius is 3.0 km. This is consistent with our result obtained from the thermal-IR imaging (Lisse *et al.* 1999b), 2.4 ± 0.5 km, as well as the radar results by Harmon *et al.* (1997), 1.5 ± 0.5 km. Our estimate of the radius is not very sensitive to the temperature when $T \sim 200$ to 300 K, but it becomes 5 km for the 50 K limit.

6.2.4 The X-ray Connection

Our observations were simultaneous with many of the *ROSAT* observations of Hyakutake that occurred a few days after perigee (Lisse *et al.* 1996). Since non-thermal radio emission is frequently coincident with X-ray emission from other astrophysical sources, we were motivated to place an upper limit on the microwave emission from the location of the X-rays in Hyakutake's coma; the VLA field of view overlaps a portion of the X-ray emitting region reported by Lisse *et al.* (1996). The center of brightness of the X-ray emission with respect to the nucleus is about $2'$ north and $2\frac{1}{2}'$ east of the nuclear position (on 27.7 March UT), whereas our map extends only $2.1'$ from the nucleus. If we approximate the size of the X-ray emitting region as a $4'$ -by- $8'$ oval, with the short axis on the Sun-comet line, then the overlap between the VLA field of view and the X-ray emitting region is a wedge that contains about 9% of the total X-ray flux, and about 13% of the total VLA field of view. Assuming the microwave flux from the coma follows the same spatial distribution as the X-ray flux, we calculate that the $3\text{-}\sigma$ upper limit to the microwave flux from the X-ray emitting region is 223 mJy. This value is more than a factor of two lower than that reported by Minter and Langston (1996), using the same-size X-ray emitting region of the coma. This result indicates that the mechanism responsible for the production of X-rays is not able to produce much microwave radiation. Lisse *et al.* (1996) found an X-ray luminosity of 4×10^{15} erg/s from the coma as measured by the *ROSAT* HRI, which is sensitive to 0.1- to 2.0-keV photons. Assuming a power law spectrum, where the intensity is proportional to $\nu^{-\alpha}$ (where ν is the frequency and α is the spectral index), and using the largest possible effective bandpass (1.9 keV) and our microwave upper limit, we find that α must be less (i.e., flatter) than 0.59, fairly flat. Some of the mechanisms postulated by Lisse *et al.* (1996) to explain the X-ray emission (e.g., magnetic field-line reconnection and magnetospheric

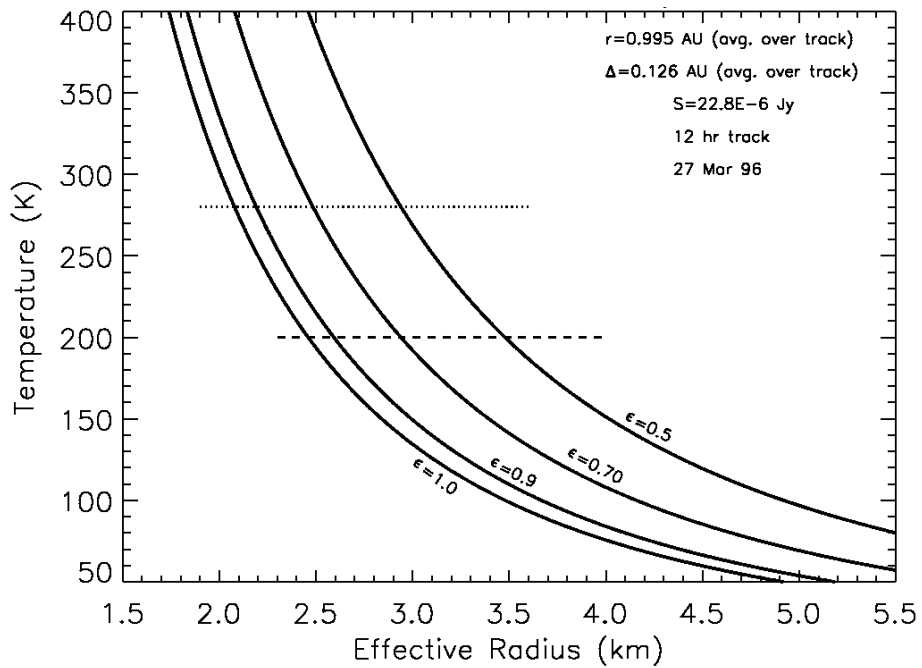


Figure 6.3: Size and temperature of C/1996 B2 nucleus. Here, the loci of points on the temperature-radius parameter plane that can satisfy the upper limit to the microwave flux are displayed. The different curves represent different microwave emissivities.

disruption) would necessarily produce some microwave radiation, but these theories are not yet developed enough to provide a prediction of the microwave flux to compare with our results. However, the derived flatness of the spectrum does rule out synchrotron emission (which typically has a spectral index of 1 to 2) as the source of the X-rays, as would be expected from the typically low strength of the interplanetary magnetic field.

6.3 Optical Measurements

I have described much of this information in a paper first-authored by my colleague (Lisse *et al.* 1999b), and I reproduce much of the text here.

6.3.1 Coma-to-Nucleus Contrast in the Images

The optical data are four nights worth of imaging during 19 to 23 March, 1996, at the KPNO 0.9-m telescope. The sky during three of the nights was photometric or nearly photometric. I used a 2048-by-2048 pixel CCD with a field of view of over 20 arcmin, so I have good maps of the inner coma immediately before the large outburst of activity that coincided with the widely-reported fragmentation of the nucleus (Lecacheux *et al.* 1996, Weaver 1996). The wavelengths I will concentrate on here are at 4845 Å and 6840 Å, the wavelengths of the narrowband continuum in the International Halley Watch filter set. The image scale was 0.68'' per pixel side. During the run the comet was 0.23 to 0.12 AU from Earth, 1.17 to 1.08 AU from the Sun, and 37° to 42° in phase angle. Typical FWHM of the seeing disk during the photometric and partially photometric time averaged 1.8''.

Considering the size of the nucleus, the gas and dust output of the comet was extremely prodigious. Whereas most comets have up to just 1% of their nuclear surface area active, Hyakutake seems to be more in the vicinity of 50%, possibly 100% (Lisse *et al.* 1999b). This high fraction is strong evidence for an icy grain halo contributing to the output of water; the total surface area of cometary solids available to release gas is not just the $4\pi R^2$ of the nucleus, but all of the icy grains as well. Moreover the radar experiment (Harmon *et al.* 1997) clearly shows that some of the echo power came from grains moving a few meters per second near the nucleus.

The repercussion of this phenomenon is that our optical images of the comet do not have sufficient spatial resolution to photometrically extract the nucleus. Our coma-fitting technique fails to find a central point-source; the coma is swamping all of the nuclear flux. Not only is this a problem in our KPNO data, where the pixels subtend 0.68'' on a side, but also in *HST* WFPC2 data, where the pixels subtend only 0.045'' on a side – or just 3.3 km at the comet during closest approach (Weaver *et al.* 1996).

Shown in Fig. 6.4 is an example of the coma-fitting technique applied to one of our KPNO images. The figure is taken from Lisse *et al.* 1999b and is their Fig. 1. There is clearly a point-source residual, but it is far too bright to be just reflected light from the nucleus, unless, as we mention in the paper, the nucleus has an absurd geometric albedo of about 0.5. It only takes a small amount of dark absorbing material mixed with the ice to reduce the albedo below this value.

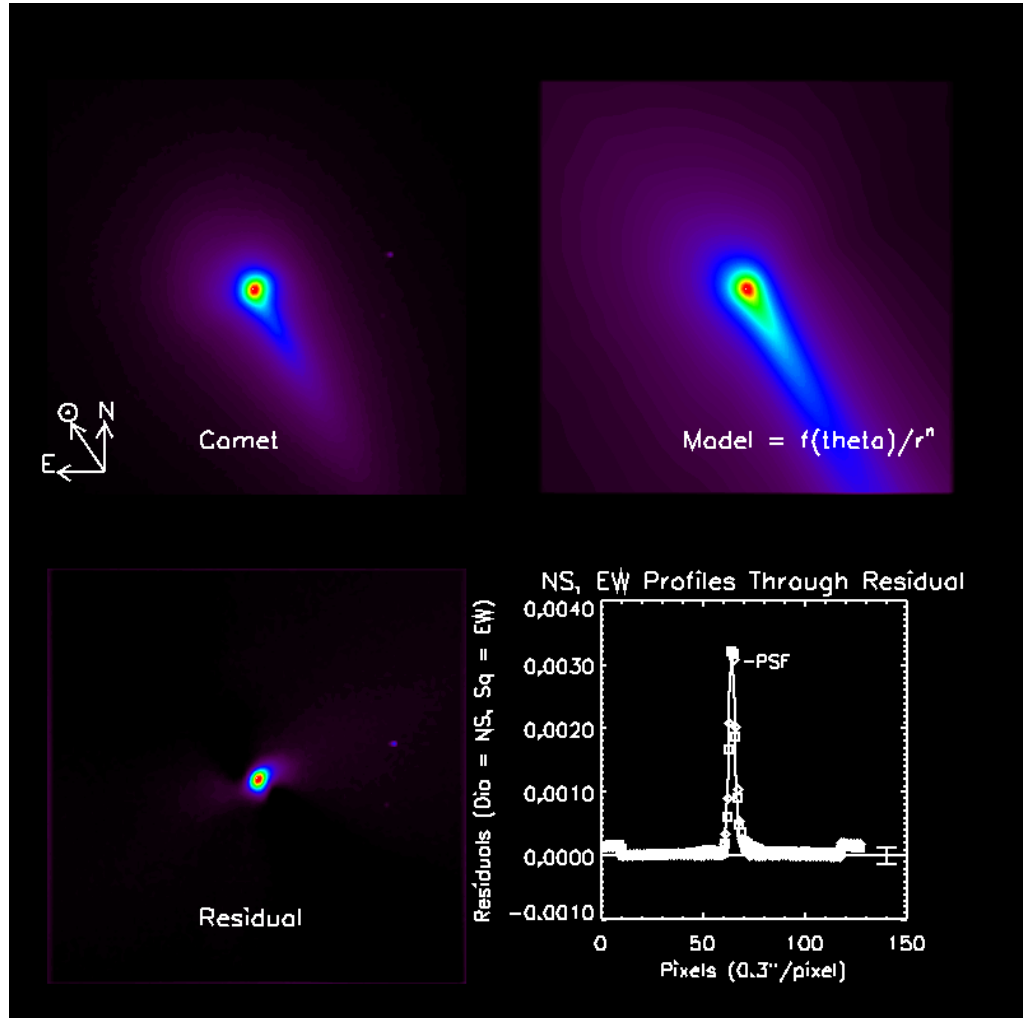


Figure 6.4: Coma-fitting method applied to optical image of Hyakutake. Here I show the results of this image processing technique for Hyakutake. The upper left panel is the original image, the upper right panel is the model, the lower left panel is the difference, and the lower right panel compares the profiles of the residual and the PSF. The residual is point-like but far too bright to be just scattered light from the nucleus. Apparently there was a halo of sublimating icy grains around the nucleus contributing to the optical flux, and the grains were too close to be accounted for in our image processing technique.

6.3.2 Rotation Period

One physical property that we had more success on is the rotation period. Two different methods were used, both the photometric and the morphological methods described in Chapter 3.

Figure 6.5 shows a sequence of narrowband continuum images of the comet over a period of several hours. The overall trend of the coma's brightness – a reciprocal dependence on the cometocentric distance (“ $1/\rho$ ”) – has been removed to bring out some of the detail in the coma. Thus it is easier to see when a feature in the coma returns to the same azimuth after one rotation period. The period can be clearly measured as approximately 6 hours, with the caveats mentioned regarding this method in Chapter 3.

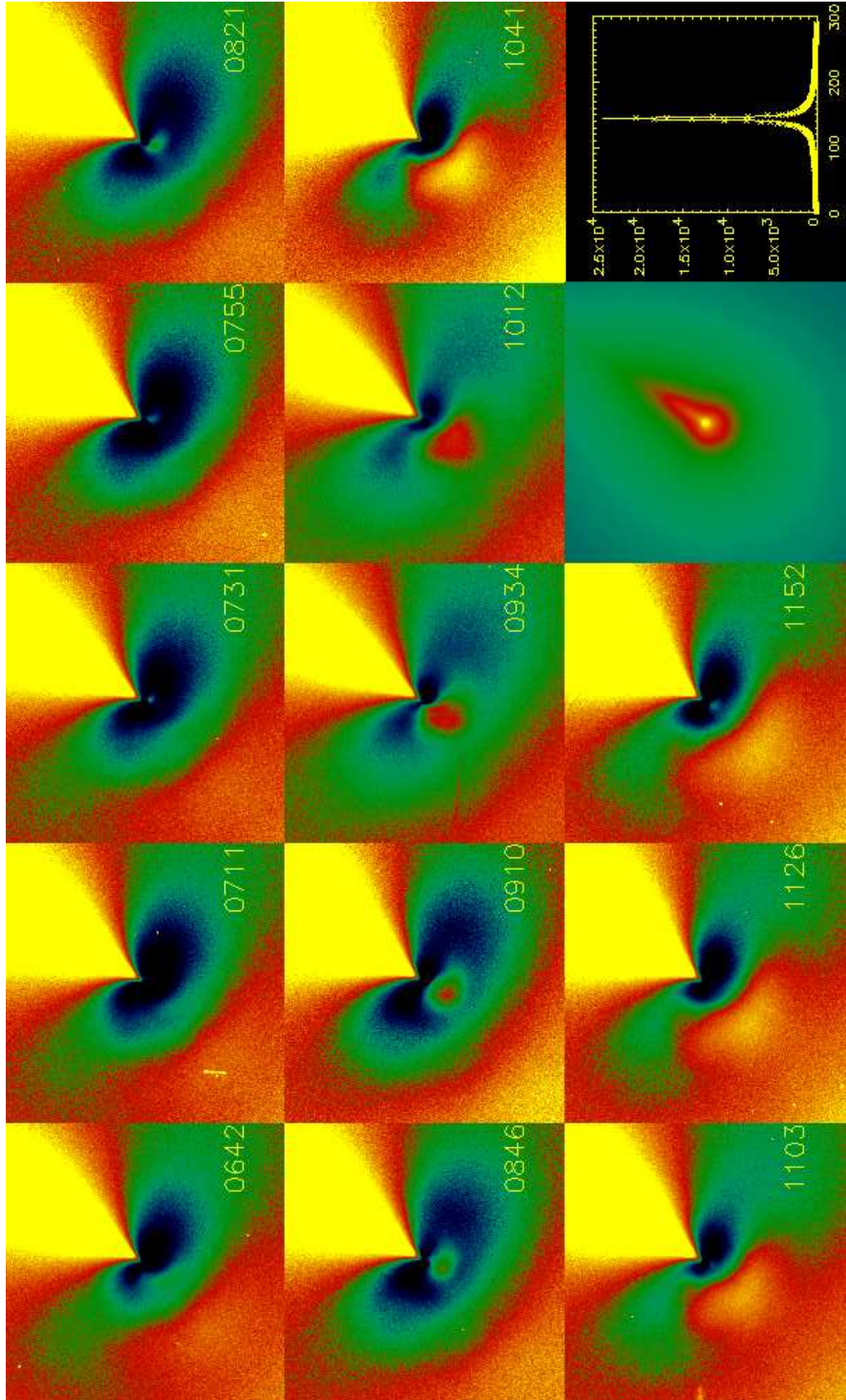
A tighter constraint on the period is derived from the photometric data. Figure 6.6 shows the photometry of the comet (nucleus and coma) over 3 nights. The top panel is the absolute flux, the bottom panel has the linear trend removed from the data and an arbitrary sine wave plotted through the points. The data have been scaled in the lower panel to simplify the plotting of this sine wave. The asterisks give the 6840Å flux and the crosses give the 4845Å flux. The circular aperture used for this photometry was 1000 km wide at the comet. The period is quite easily distinguished as 6.3 ± 0.03 hr just by varying the frequency of the sine wave. While this analysis cannot rule out a 12.6-hr period, which would yield a classic double-peaked curve, the coincidence of this period with the morphological evidence in Fig. 6.5 indicates that 6.3 hr and not 12.6 hr is the more tenable choice. The morphological changes and the periodicity are consistent with that found for Hyakutake by Schleicher *et al.* (1998c).

6.4 Summary of Hyakutake Results

The thermal microwave data places a constraint on the nucleus' effective radius of about 3 km. This is consistent with the radar results (Harmon *et al.* 1997) and the mid-IR imaging results (Lisse *et al.* 1999b). Unfortunately, the comet was too active to let us use the coma-fitting method on the optical data to derive the nucleus' optical cross section; this problem even existed for the extreme high resolution *HST* images (Weaver *et al.* 1996). Our only constraint is the geometric albedo of the nucleus is less than 50%.

The rotation period, however, was extractable from the optical data, and combining the photometric and morphological methods, I find a period of 6.3 ± 0.03 hr. The variation in flux within a 1000-km wide aperture was very drastic and mostly due to coma features sweeping in and out of view, not the variation of the nucleus' cross section. The advantage to this is that the period determination became fairly easy. The quoted rotation period has also been widely discovered independently (e.g., Schleicher *et al.* 1998c). The rotation period is toward the low end of known periods, implying that the comet does not have much tensile strength (Lisse *et al.* 1999b).

Figure 6.5: Rotation sequence of comet Hyakutake. This is a sequence of processed optical images of the comet showing the jets sweeping in and out of view over the course of a rotation period. From this it is possible to constrain the rotation period to about 6 hours. The last 2 panels (right side of bottom row) show an original, unprocessed image and the profile of the comet's photocenter, respectively. In the other thirteen panels, the general $1/\rho$ trend of the coma has been removed to help bring out the jet features.



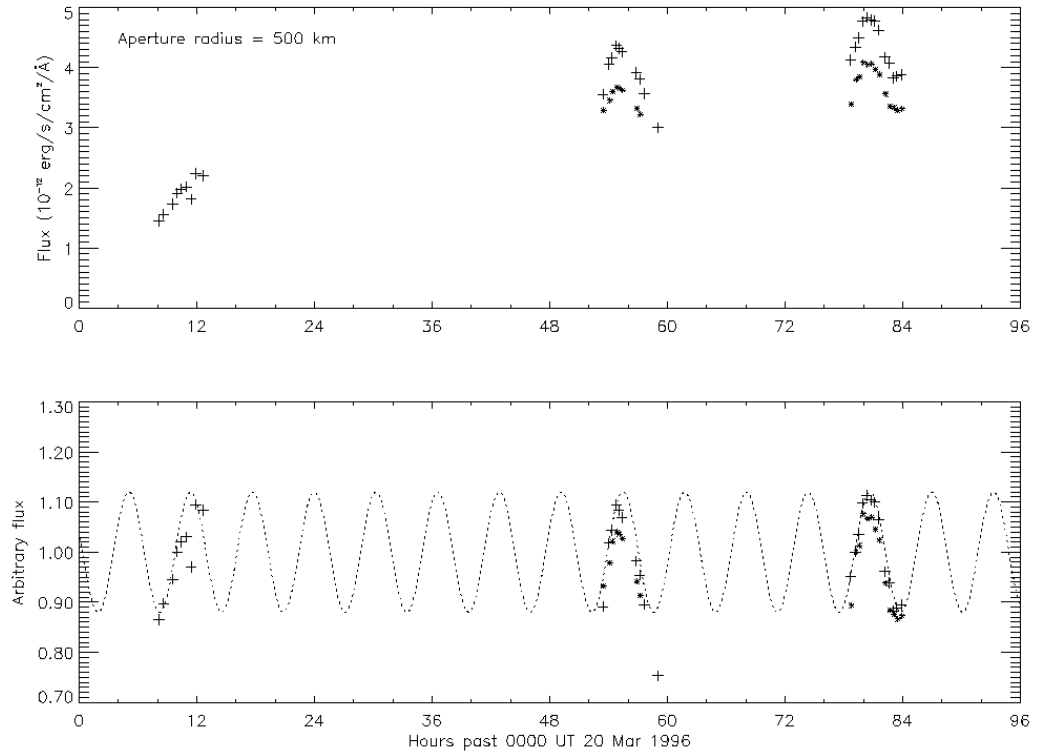


Figure 6.6: Photometry light curve of comet Hyakutake's photocenter. The top panel shows the absolutely calibrated light curve of the comet at two optical wavelengths, over the course of several days. Data from two continuum narrowband filters (4845 Å and 6840 Å) were used. In the bottom panel, a linear trend has been removed, so we can place a sinusoid on top of the light curve to derive a period of about 6.3 hr \pm 0.05 hr.

Chapter 7

The Nucleus of Comet Tempel-Tuttle

7.1 Background

Comet 55P/Tempel-Tuttle currently is the third-longest known periodic comet. Chinese records indicate it was observed in October 1366; only P/Swift-Tuttle and P/Halley have been observed longer than that. The more tactile claim to fame, however, is the comet's parentage of the Leonid meteor stream. The November meteor shower associated with it becomes a veritable storm for a few lucky locations on Earth roughly every 33 years, that is, around the time of perihelion of this 33-year period comet. In addition to all the other reasons for studying nuclei, models of the meteor stream grain population depend on the parameters of the nucleus and the dust production rate.

I have described much of this work elsewhere (Fernández *et al.* 1999a) and will reproduce some of the text here.

7.2 Thermal Measurements

We observed this comet on 21 Jan 1998 at NASA/IRTF with the MIRLIN mid-IR imager, and on 22 to 24 Jan 1998 with a CCD on the UH 2.2-m telescope on Mauna Kea. The comet's heliocentric distance (r) was 1.15 to 1.13 AU, the geocentric distance (Δ) was 0.39 to 0.43 AU, and the phase angle was between 55.0° and 59.3° .

Our mid-IR dataset is shown in Fig. 7.1 (in logarithmic intensity scale); each frame shows a separate filter, and the filter's wavelength and bandpass of the are written in white (in μm). There are two images of the comet (and two negatives) in each frame because our chop and nod throws were smaller than the field of view of the instrument. An M band ($4.7 \mu\text{m}$) observation is not shown since only upper limits could be had from that wavelength. There is some coma visible in the images, and we performed the coma-fitting method to extract the nucleus. At each wavelength, about 50 to 60% of the flux is due to coma. We performed photometry on the residuals and the result is shown as a broad-band spectrum in Fig. 7.2. The S/N is low but we find a consistent flux of about 1 Jy in the 10-micron range. This is one of the few mid-IR broadband spectra of a cometary nucleus in existence (cf. e.g. Hanner *et al.* 1985).

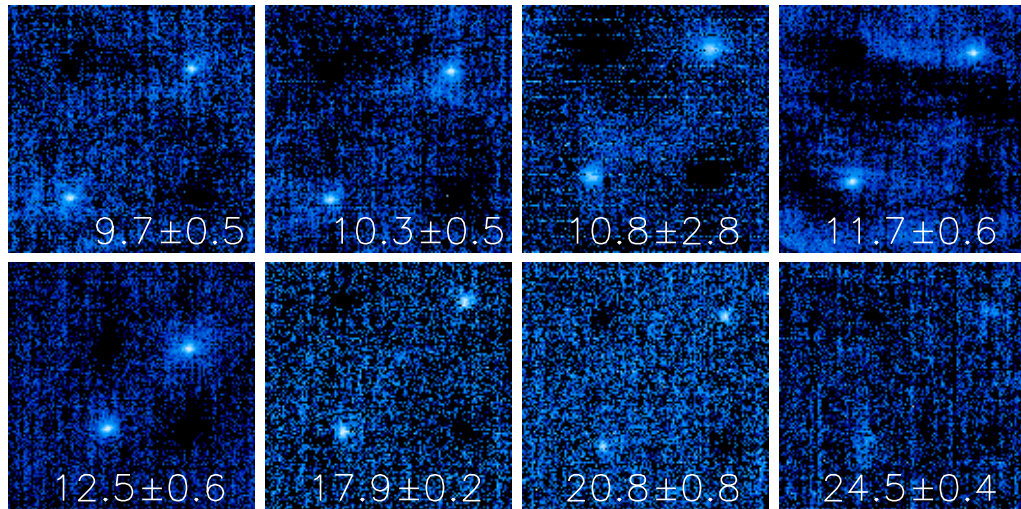


Figure 7.1: Mid-infrared images of comet Tempel-Tuttle. The two positive and two negative comets in each image are caused by the chop and nod throws being smaller than the field of view of the detector. The wavelength and bandpass are written in each frame.

The current best estimate of the rotation period is about 15 hr (Jorda *et al.*, reported by Green 1998). For a lunar-like thermal inertia, the nucleus of Tempel-Tuttle is reasonably modeled with the STM, and plotted on the spectrum in Fig. 7.2 are model spectra based on the STM. The usual plausible input parameters – mentioned in previous chapters – yield an effective radius of 1.75 ± 0.4 km, a subsolar temperature (T_{SS}) of 380 to 410 K, and a brightness temperature (T_B) of about 280 to 350 K.

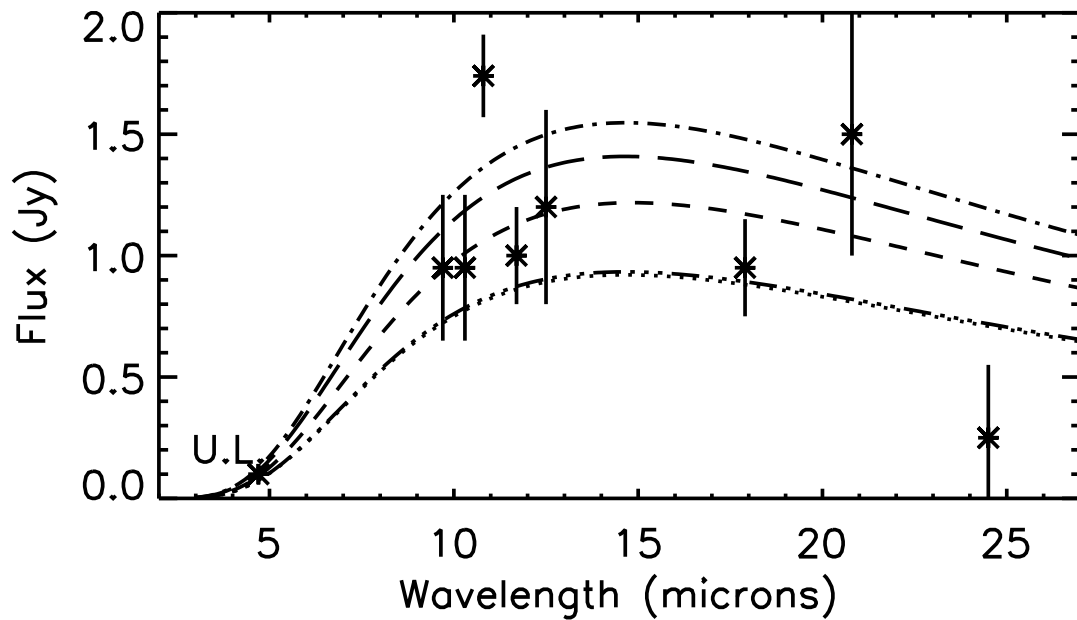


Figure 7.2: Mid-infrared spectrophotometry of comet Tempel-Tuttle's nucleus. The model spectra drawn through the data are based on the STM and varying all of the STM's parameters indicate that the effective nuclear radius is 1.75 ± 0.4 km. The plotted example models assume a beaming parameter of 0.8, an emissivity of 0.9, an infrared phase coefficient ranging between 0.005 and 0.015 mag/degree, and an effective radius ranging between 1.35 and 2.15 km. "U.L." indicates the $3\text{-}\sigma$ upper limit to the flux at that wavelength.

7.3 Optical Measurements

A typical R -band optical image and its analysis products are shown in Fig. 7.3 (in logarithmic intensity scale). The left panel is an original (reduced) image, the middle panel is the model of the coma from the coma-fitting method, and the right panel is the residual from the subtraction of the two. Clearly good removal of the coma was apparently achieved, as can be seen from a comparison of the PSF, the residual's profile, and the original comet profile (plot in Fig. 7.3). The residual is a point-source, and we ascribe its flux as reflected light from the nucleus. The photometry of the residual has magnitude $R_C = 16.8 \pm 0.2$. This magnitude does not have rotational context but the uncertainty from removing the coma ameliorates this somewhat. An independent analysis of this optical dataset has not revealed any clear rotational signature in the comet's photocenter (J. M. Bauer, private communication), so the nucleus may happen to be not very elongated.

We now characterize the optical phase effect, ϕ , of the nucleus by combining our data with the magnitudes reported by Lamy (1998) and Hainaut *et al.* (1998) in Fig. 7.4. The asterisk is from this work, the triangle is from Lamy, the rhombuses are photometric points from Hainaut *et al.*, and the crosses are possibly photometric points from Hainaut *et al.* A straight line gives a satisfactory fit with $\beta = 0.041$ mag/deg, a not atypical value for nuclei (Jewitt and Meech 1988). We have also fit the data according to the pan-asteroidal phase law of Lumme and Bowell (1981), as we did in Chapter 5 with comet Encke. Though the two models yield equally good fits, we prefer the latter since it has a physical basis. The parameter Q , which attempts to account for multiple scattering of light on the surface, is around -0.037 , implying that here, just as with comet Encke, the surface of the cometary nucleus is rougher than for the typical asteroid. The zero-phase absolute magnitude is 15.6 ± 0.2 ; note the 0.4-mag difference in absolute magnitudes between the two models.

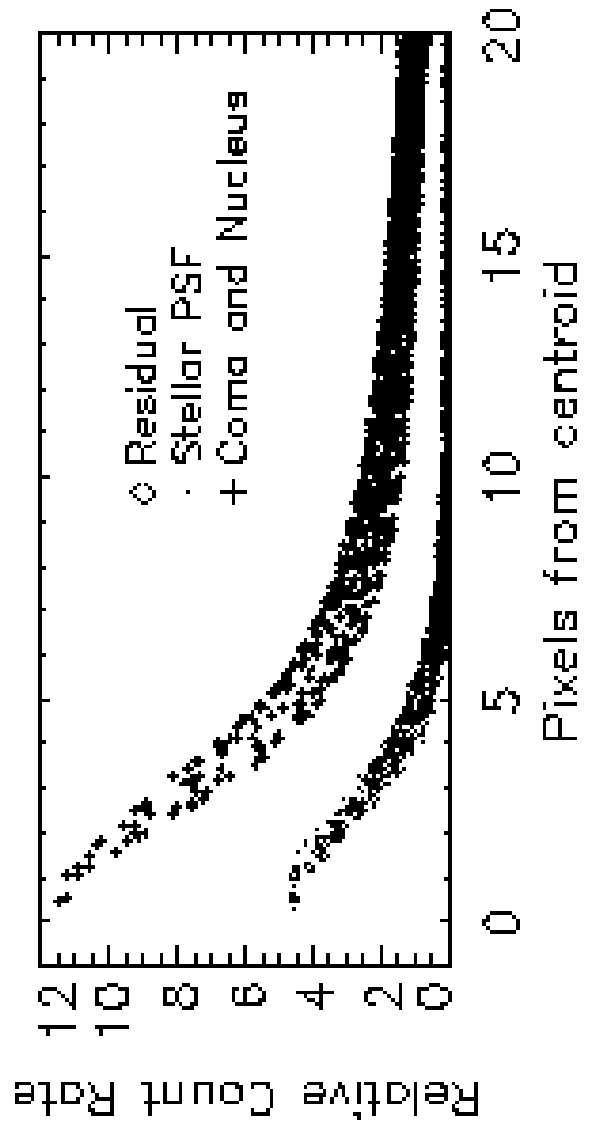
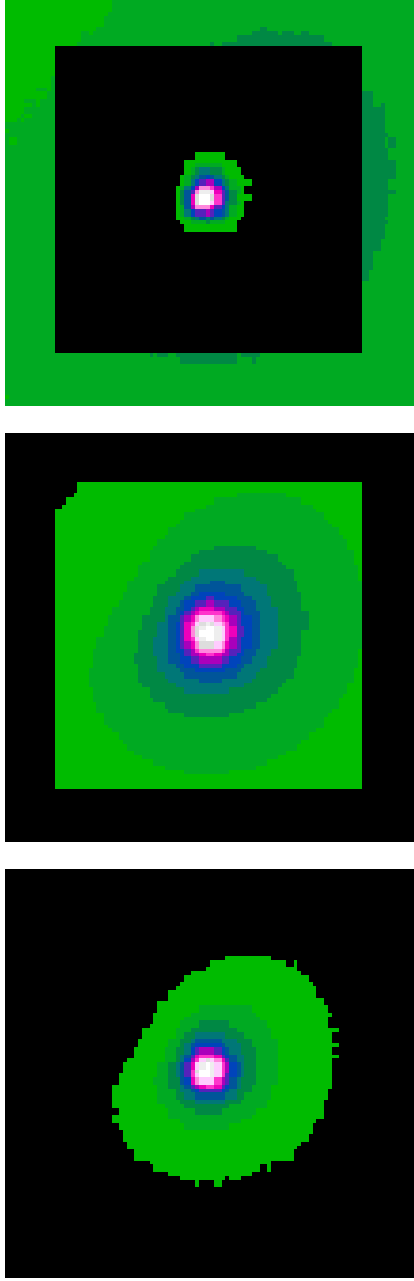
Using this phase-law and the absolute magnitude, our derived radius implies that the geometric albedo p is 0.06 ± 0.025 , higher than the canonical value but not out of the range. (Assuming the β -formalism for ϕ would have yielded $p = 0.04 \pm 0.01$.)

7.4 Summary of Tempel-Tuttle Results

Our observations of Tempel-Tuttle resulted in several unique data products. First we have one of the few mid-IR spectra of a cometary nucleus in existence. This allowed us to derive the radius (1.75 ± 0.4 km) based on the STM, although the low S/N does not allow us to derive beaming parameters (Harris *et al.* 1998).

Second we have constrained the optical phase law, although the rotational context of all the optical data is unknown. With that caveat, the phase law is equivalent to a linear coefficient of 0.04 mag/degree, or, in the Lumme and Bowell (1981) formalism, $Q = -0.04$, implying a surface rougher than the typical asteroid. The albedo of the nucleus based on our determination of the absolute magnitude is $6 \pm 2.5\%$.

Figure 7.3: Coma-fitting method applied to optical image of Tempel-Tuttle. On the left is an R band image of comet Tempel-Tuttle, in the middle is a model of the coma from the coma-fitting method, and on the right is the difference between the two. The plot compares the residual's profile with the PSF and the original comet profile; it is clear that we have found a point source nucleus after subtracting the coma.



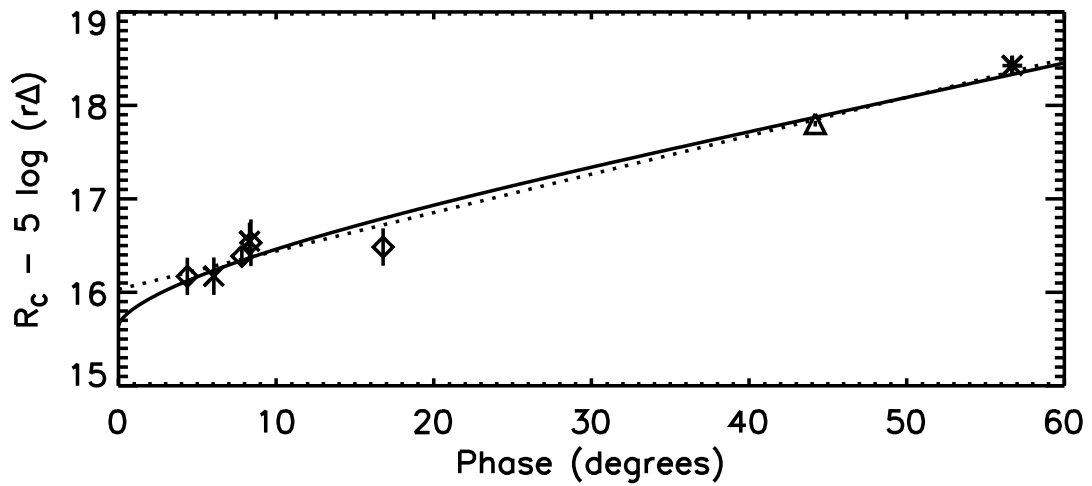


Figure 7.4: Optical phase behavior of comet Tempel-Tuttle's nucleus. The data include the measurement in this Chapter and other magnitudes culled from the literature. The straight line fits well, but since a physically-based phase law (Lumme and Bowell 1981) does also, we use the latter to derive the absolute magnitude.

Chapter 8

The Nuclei of Comets Wild 2 and Utsunomiya

8.1 Background

These are the two comets for which I have the least amount of data, so I will discuss both in one chapter. Much of the text I have already presented elsewhere (Fernández *et al.* 1999a).

81P/Wild 2 is the target of the *Stardust* mission, which is currently en route. If successful, the spacecraft will collect grains from the comet's dust coma by trapping them with an aerogel, and return them to Earth. An interesting factoid about the comet itself is that it was perturbed into its present orbit only in 1974, when it passed less than 12 Jovian-radii – within Ganymede's orbit – from the gas giant's cloud tops. Before that, the comet lived almost totally in the outer planetary region, with a perihelion slightly within Jupiter's orbit and aphelion around Uranus' orbit and beyond. Thus, among the short-period population, this is likely one of the least processed objects, having spent so little time within 5 AU of the Sun.

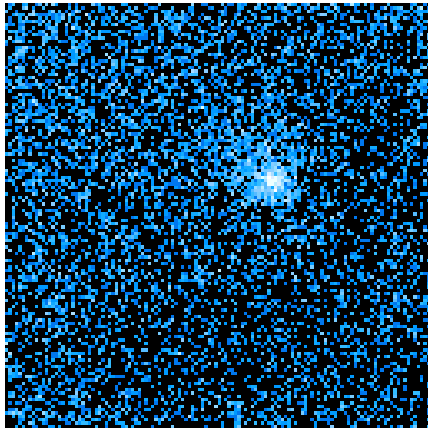
Comet Utsunomiya 1997 T1 was discovered at 11th magnitude by an amateur. This comet is old in the Oort sense, having an original semimajor axis of 862 AU (Marsden and Williams 1999). It is one of many run-of-the-mill long period comets that we must eventually sample in great numbers.

8.2 Utsunomiya

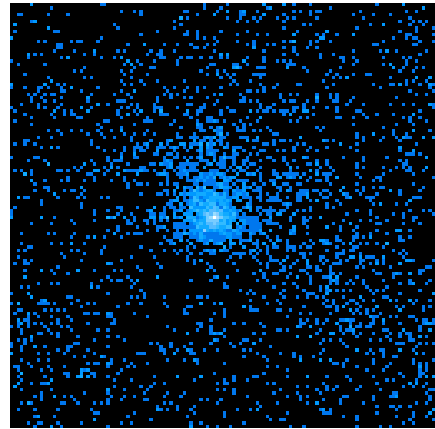
On 23.9 Nov 1997 we imaged Utsunomiya at NASA/IRTF with the MIRAC infrared camera. At the time, $r = 1.38$ AU, $\Delta = 1.65$ AU, and $\alpha = 36.6^\circ$.

The comet had a flux of 0.6 ± 0.1 Jy at $10.6 \mu\text{m}$ and is shown in Fig. 8.1a as the median of 13 images. It was slightly extended, apparently not a point-source. In Fig. 8.2 I show a model coma which, when subtracted from the image, leaves hardly any point-source remaining: about 10% of the flux. However this does *not* mean the dust coma dominated the signal, since the centroiding and adding of the 13 images together was tricky due to the low S/N per pixel. It is entirely possible that the “dust coma” is spurious because of incorrect registering of the image centroids.

Strictly speaking, we can only calculate an upper limit to the effective radius. Assuming all of the flux is nuclear, I assign the usual ranges for the parameters of the STM and find an effective radius $R_N = 5.8 \pm 2.0$ km, $T_{SS} = 350$ to 370 K, and $T_B = 275$ to 315 K. To our knowledge this is the only infrared data on this comet and



a



b

Figure 8.1: Mid-infrared images of comets Utsumomiya and Wild 2. On the left (a) is an image of comet Utsumomiya at a wavelength of $10.6 \mu\text{m}$, and on the right (b) is comet P/Wild 2 at $11.7 \mu\text{m}$. The comets are extended sources but it is unclear whether this is due to real dust comae or just a consequence of the tricky registering of multiple images of a faint comet.

the only estimate of its nuclear size. Unfortunately we have access to neither nuclear magnitudes of this comet nor deep images, so we cannot yet estimate p . Also, the rotation period is unknown, so there is no rotational context for this measurement. If the nucleus were a rapid rotator and if the rotation axis were perpendicular to the Sun-comet-Earth plane at the time of observation, the effective radius would be higher, about 9 ± 2 km.

8.3 P/Wild 2

On 29.3 Jan 1997 we imaged Wild 2 at NASA/IRTF with the MIRAC infrared camera. At the time, $r = 1.85$ AU, $\Delta = 0.87$ AU, and $\alpha = 5.9^\circ$.

The comet had a flux of 0.5 ± 0.1 Jy at $11.7 \mu\text{m}$ and is shown in Fig. 8.1b as the median of 53 images. It too was slightly extended, apparently not a point-source, however the S/N per pixel was even lower than for Utsunomiya. In Fig. 8.3 I show a model coma which, when subtracted from the image, leaves hardly any point-source remaining: less than 10% of the flux. I am less confident of the reality of the “dust coma” for this comet than for Utsunomiya.

Hence again we can only calculate an upper limit to the effective radius. Assuming all of the flux is nuclear, and again assuming the usual range of parameters for the STM, I find $R_N = 3.0 \pm 0.6$ km, $T_{SS} = 300$ to 320 K, and $T_B = 265$ to 285 K. We were unable to acquire any rotational information, so we cannot tell how much variation there is in the cross section. However Meech and Newburn (1999) report that time series of optical flux while the comet was at high heliocentric distances do not show much rotational signature at all; i.e., there is a good chance that the comet is close to spherical. So the lack of rotational context for our mid-IR measurement may not be a problem.

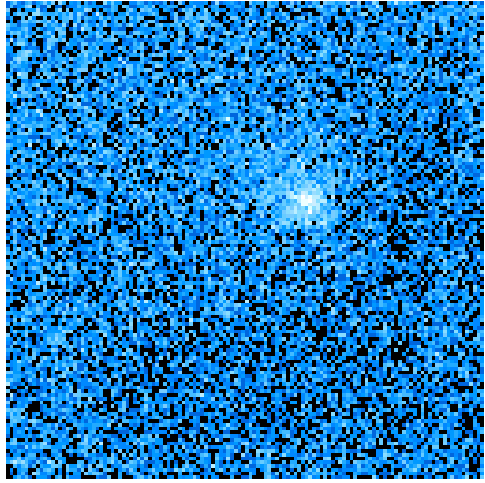
Meech and Newburn (1999) have also derived the nucleus’ optical cross section: $pR_N^2 = 0.165 \pm 0.014$ km². With our derived value of R_N , we calculate p to be 0.018 ± 0.005 (formal error), lower than the canonical value. An overestimation of the nuclear IR flux due to coma contamination might explain the low albedo. However there are comets with comparably low values (see Chapter 9).

If the nucleus were a rapid rotator, it would have to be close to spherical and the radius based on my mid-IR data would be about 6.5 ± 1 km. Moreover the albedo would then be even lower than quoted above.

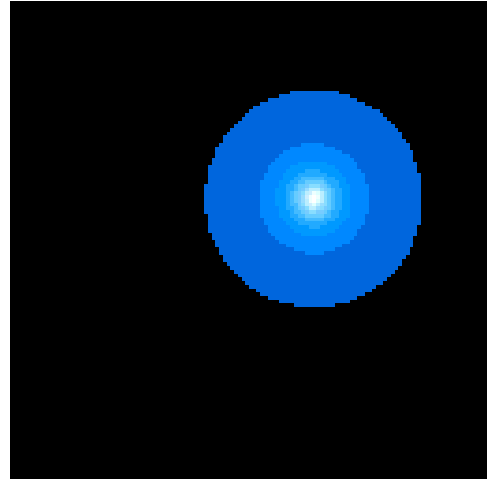
8.4 Summary of This Chapter

Comets Utsunomiya and P/Wild 2 were briefly imaged in the mid-IR from the Infrared Telescope Facility in Hawaii. The former comet has a maximum effective radius of 5.8 ± 2.0 km if the STM is valid, or about 10 km if it is instead a rapid rotator. No companion optical data are available, and the rotation state is unknown.

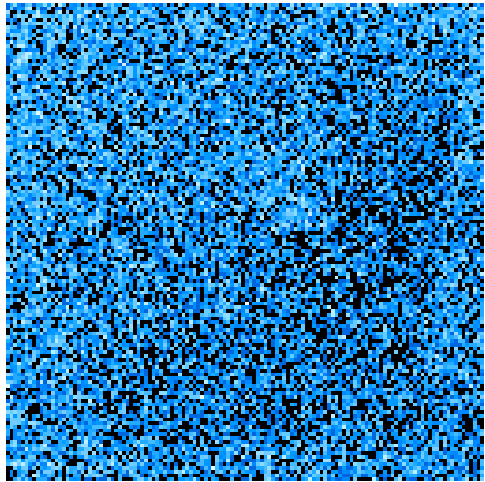
The latter comet is the target of a spacecraft and thus is a more popular object for study. Our mid-IR data imply a radius of 3.0 ± 0.6 km if the STM is valid. Optical data (Meech and Newburn 1999) imply that the nucleus is either spherical or has a very long (on order of days) rotation period. The albedo is apparently very low, about 2%, but it is possible that there is some coma contamination in the thermal data.



Image

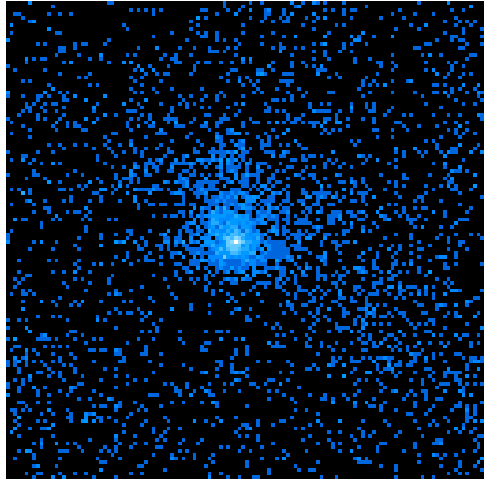


Model Coma

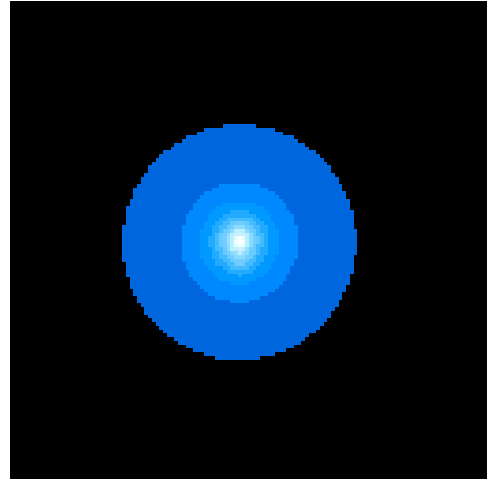


Difference

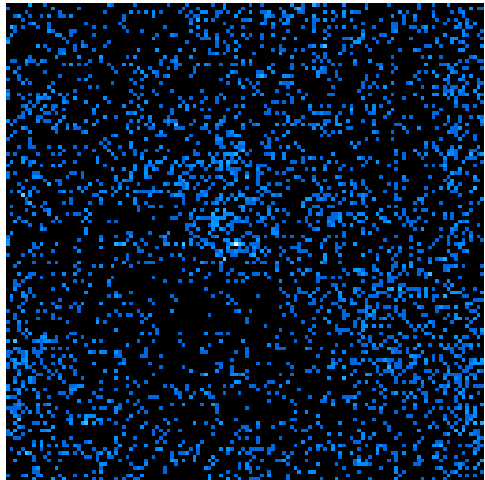
Figure 8.2: Coma-fitting method applied to comet Utsunomiya. Here I show the results of the coma-fitting method after application to comet Utsunomiya's mid-IR image. Virtually all of the flux can be modeled as comatic, since there is very little flux left in the difference image, but since the individual images of the comet were difficult to centroid properly, this may be just an error in pixel registering.



Image



Model Coma



Difference

Figure 8.3: Coma-fitting method applied to comet P/Wild 2. Here I show the results of the coma-fitting method after application to the mid-IR image of comet P/Wild 2. Virtually all of the flux can be modeled as comatic, since there is very little flux left in the difference image, but since the individual images of the comet were difficult to centroid properly, this may be just an error in pixel registering.

Chapter 9

Conclusions and The Future

In this chapter I will specify some conclusions that can be drawn by combining the results presented in this thesis with earlier studies of cometary nuclei. Of course my work has not made the sample of nuclei complete, and a few dozen more objects with well-determined physical properties would be helpful before any analysis becomes statistically defensible. However it is interesting to collate the current information and see what trends may be appearing, and what observational biases are dominating the study of comets.

9.1 Comets and Their Disguised Relations

Figure 9.1 shows a plot of the effective diameters and geometric albedos for several cometary nuclei, including the ones I have discussed in this thesis. Also plotted are nuclei studied by others, and several NEAs and Centaurs. The data are listed in Table 9.1, with the information from this thesis having an arrow in the “Ref.” column. Not all data in Table 9.1 are plotted on Fig. 9.1. Here are some caveats about this table:

- Most of the entries are from reports of a nuclear size measurement made using thermal infrared techniques. In a few cases, radar or optical observations that have spatially-resolved images of the object were used. Observations in those wavelength regimes that just have cross section-integrated photometry were not used.
- The vast majority of the radii and albedos were derived using the Standard Thermal Model. A few used the Rapid Rotator Model, and one was even derived from the Isothermal Model. I have not made an attempt to reanalyze these data, I simply have quoted the values and errors that the authors themselves state, even though there are very clearly cases where the error bars are underestimated. Considering the uncertainties in some of the parameters that go into the thermal models (such as the beaming factor and the phase behavior; Chapter 3), the systematic error of the absolute flux calibration (about 5%, Tokunaga 1984, Rieke *et al.* 1985), and the experience of the several comets presented in this thesis, it seems that some of the diameters’ error bars could be closer to 20%, and the albedos’ error bars closer to 40%. This is especially true where the thermal data is of low S/N , and this does not even include any systematic error with using an idealized model. Exceptions to this include but are not limited to: Comet Halley and Asteroid (433) Eros, which have been optically imaged with sub-km spatial resolution; Asteroid (4179) Toutatis, which has been the subject of multiple extensive radar experiments; and Comet *IRAS-Araki-Alcock*, which passed so close to Earth and resulted in a multiwavelength data cache so large that it was probably only a matter of time before someone collated everything into a coherent picture (Sekanina 1988c).

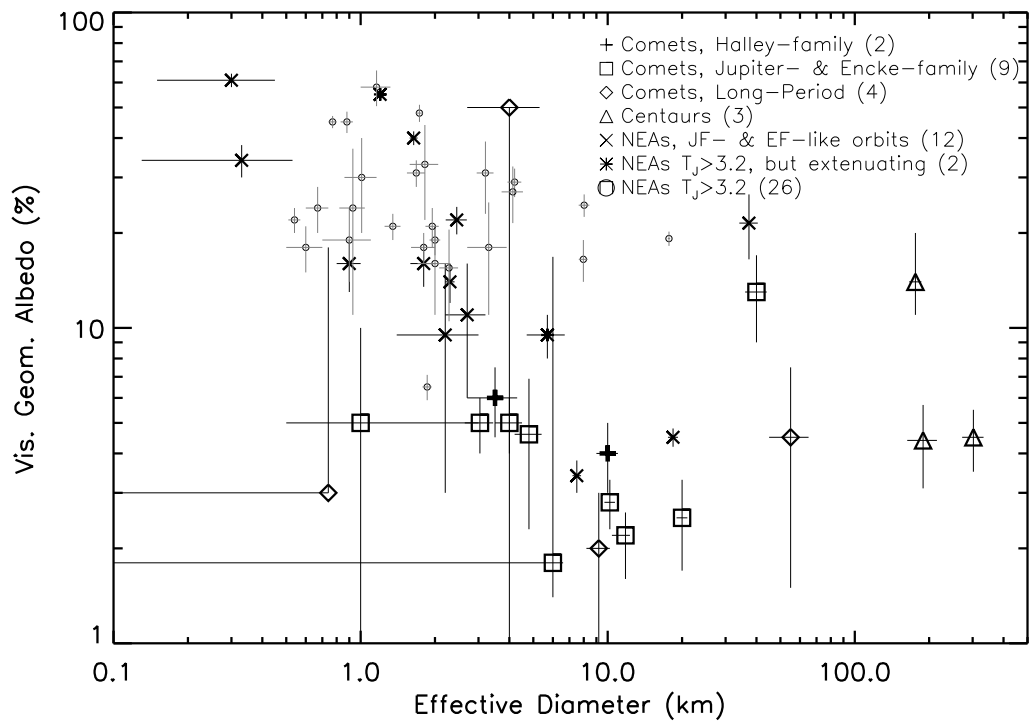


Figure 9.1: The sizes and albedos of active cometary nuclei, some near-Earth asteroids, and Centaurs. The “cometary” region is now starting to fill out, thanks to many thermal studies done since the mid-1990s.

- One notices that some cometary diameters have no attendant albedos. Ironically it is often the case that reliable optical cross sections do not exist for the comets that have been observed in the mid-IR. In the future, more coordination between observations in the multiple wavelength regimes is needed. In Chapter 1 I discussed some of the problems of nucleus observation that contribute to this lack of optical cross sections.

- The “Rotation?” column shows many more entries with “N” than with “Y,” i.e. for most of the listed objects, the rotational context is unknown. This has not been reflected in the error bars of the diameters and albedos, so the true error bars are even higher for many objects. For some objects this is not a problem because the observations took so long that the rotational variation has probably been averaged out, and so is incorporated into the error estimate already. For example, the multiple mid-IR exposures of Hyakutake cover several hours of time, and hence a large fraction of the rotation period.

- Note that the “Cometary Nuclei” in the title is in quotation marks. I have included many asteroids in the table, some fraction of which are extinct comets. I will now discuss this point in more detail.

The Tisserand parameter, T_J , is a constant of motion in a restricted three-body problem. Considering the Sun, Jupiter, and a small body as the three members of a system, as long as the body is not having a close encounter with Jupiter at the time of the observation, the value of T_J is constant. In practice the value fluctuates by a few percent due to perturbations by other planets. The definition is (Danby 1962, p.189):

$$T_J = \frac{a_J}{a} + 2 \cos i \sqrt{\frac{1 - e^2}{a_J/a}}, \quad (9.1)$$

where a_J is the semimajor axis of Jupiter, 5.2 AU, a is the object’s semimajor axis, e is the object’s eccentricity, and i is the object’s orbital inclination. Tisserand himself recognized in the late 19th century that this constant of motion could be used to identify two comets observed far apart in time as the same object, if the comet had had a close encounter with Jupiter in the interval and thus had its orbital elements drastically changed.

The value of the parameter indicates the strength of the dynamical coupling of the object’s orbit to Jupiter. Most asteroids have $T_J > 3$, while the short-period comets mostly have $T_J < 3$; i.e., $T_J = 3$ is the boundary between the coupling – almost all short-period comets are dynamically coupled to Jupiter, while most asteroids are not. An indication of this can be seen in the q_{ap} column in Table 9.1; for objects with $2 < T_J < 3$, the aphelion is close to Jupiter.

Of course the $T_J = 3$ border is not perfect. There are asteroids that have $T_J < 3$ – these are usually NEAs with a sufficiently large aphelion distance – and there are comets that have $T_J > 3$ – the so-called “Encke” Family (Levison 1996), which so far only has two known members, both of which are in Table 9.1. These are comets in more classic NEA orbits, i.e. the aphelion distance is never high enough to bring them close to Jupiter.

The explanation for the asteroids in cometary orbits follows from the supposed typical life cycle of a short-period Jupiter Family comet. After being perturbed

out of the Kuiper Belt and into the outer planetary region, the nucleus is at the mercy of the gas giants. Approximately thirty percent of these comets that leave the Kuiper Belt become part of the Jupiter Family (Levison and Duncan 1997); the rest are either ejected or sent farther out in the Solar System. Centaurs are thought to be Kuiper Belt objects currently in transition, since their dynamical lifetimes is roughly only 10^6 year (Dones *et al.* 1996).

Once an object is in the Jupiter Family, its dynamical lifetime there is about 10^5 years (Wetherill 1991), after which the comet collides with a planet or the Sun, or is sent into a classic NEA orbit, decoupled from Jupiter. Of course during those 10^5 years the comet is outgassing, since it passes close enough to the Sun, but the store of volatile material in the comet will only last about 10^4 years – either the comet will disintegrate by then or the mantled surface will be too thick, choking off the available ice (Levison and Duncan 1997). Hence on average a comet will become dormant while still coupled to Jupiter. Observationally, one would discover an asteroid in a comet-like orbit ($T_J < 3$), a few of which are noted in Table 9.1. However it is possible that a comet will be quickly sent into an NEA orbit and decoupled from Jupiter before all available ice is gone, and we will see active comets in NEA ($T_J > 3$) orbits, which we do see most famously as comet Encke. The existence of this comet and comet Wilson-Harrington guarantee that, despite the fact that the Main Belt can potentially provide a large fraction of the kilometer-size and larger NEAs (Rabinowitz 1997), some fraction of the NEAs must be dead cometary nuclei. The trick, which we have not yet solved, is to find some diagnostic that indicates which of the NEAs are cometary and which are asteroidal (McFadden 1994). Future studies of NEAs and nuclei may shed light on this problem.

In Table 9.1 I have made an arbitrary separation at $T_J = 3.2$ to mark which asteroids might dynamically have a higher probability of being dead comets. However, there are two intriguing asteroids that have high T_J and yet could very well be cometary. Asteroid (3200) Phaethon is the parent to the Geminid meteor stream (Whipple 1983), which is strong evidence for a cometary origin, despite the fact that its aphelion distance is almost 2 full AU smaller than the next smallest cometary one (Encke). Asteroid (2201) Oljato was observed to have a transient blue excess by McFadden *et al.* (1993), which they argued was caused by a cometary outburst. One problem with Oljato is its high albedo, much higher than all of the known cometary nuclei. Nevertheless, I have separated these objects from the other high T_J crowd to emphasize that these objects have additional extenuating circumstances.

Immediately one notices that there are some very black asteroids in both the low- T_J and high- T_J sections. In my opinion these objects are the prime candidates for being extinct nuclei and further study is needed to find out if there is any distinguishing characteristic observable from Earth that separates them from the other, Main Belt-derived NEAs.

Furthermore, there are many asteroids, such as (944) Hidalgo, (5335) Damocles, and 1984 BC that have low T_J – 2.07, 1.15, and 2.78 respectively – but that simply have not yet had their thermal flux measured. Presumably, when that happens, they will take their place alongside the other low-albedo objects.

Table 9.1: Sizes and Albedos of “Cometary Nuclei”

Object	Diameter	Albedo	T_J	q_{ap}	Rotation?	Ref.	In Fig.
	(km)	(%)		(AU) ^a	^b	^c	9.4?
<i><u>Halley Family Comets</u></i>							
1P/Halley	10 ± 1	4 ± 1	-0.61	35.3	NA	2	Y
55P/Tempel-Tuttle	3.5 ± 0.8	6 ± 1.5	-0.64	19.7	N	1 ←	Y
“	3.3 ± 0.3	4.5 ± 1	-0.64	19.7	N	3	N
109P/Swift-Tuttle	15 ± 3	^d	-0.28	51.7	N	35	N
126P/ <i>IRAS</i>	$< 2.86 \pm 0.16$	^d	1.96	9.5	N	3	N
<i><u>“Encke” Family Comets</u></i>							
2P/Encke	4.8 ± 0.6	4.6 ± 2.3	3.03	4.1	Y	1 ←	Y
107P/(4015) Wilson-Harrington	4.0 ± 0.5	5 ± 1	3.08	4.3	N	4	Y
<i><u>Jupiter Family Comets</u></i>							
6P/d’Arrest	~ 3.5	^d	2.71	5.6	N	34	N
10P/Tempel 2	$11.8^{+0.5}_{-1.4}$	$2.2^{+0.4}_{-0.6}$	2.96	4.7	Y	5	Y
21P/Giacobini-Zinner	~ 2	~ 5	2.47	6.0	N	31	Y

Table 9.1 – cont'd

Object	Diameter	Albedo	T_J	q_{ap}	Rotation?	Ref.	In Fig.
	(km)	(%)		(AU) ^a	<i>b</i>	<i>c</i>	9.4?
<i>Jupiter Family Comets (cont'd)</i>							
22P/Kopff	3.04 ± 0.4	5 ± 1	2.87	5.3	N	3	Y
24P/Schaumasse	< 6.6	<i>d</i>	2.51	6.9	N	36	N
28P/Neujmin 1	20 ± 1	2.5 ± 0.8	2.16	12.3	Y	6	Y
29P/Schwassmann-Wachmann 1	40 ± 4	13 ± 4	2.99	6.3	N	7	Y
49P/Arend-Rigaux	10.2 ± 0.5	2.8 ± 0.5	2.71	5.7	Y	8	Y
81P/Wild 2	$< 6.0 \pm 1.2$	$> 1.8 \pm 0.4$	2.88	5.3	N	1 ←	Y
103P/Hartley 2	$< 1.16 \pm 0.24$	<i>d</i>	2.64	5.85	N	3	N
<i>Oort-sense Old Long-Period Comets</i>							
C/1983 H1 IRAS-Araki-Alcock	9.2 ± 1	2 ± 1	<i>e</i>	<i>e</i>	Y	32	Y
C/1983 J1 Sugano-Saigusa-Fujikawa	$\lesssim 0.74$	$\gtrsim 3$	<i>e</i>	<i>e</i>	N	33	N
C/1995 O1 Hale-Bopp	50 ± 10	4.5 ± 3	<i>e</i>	<i>e</i>	N	1 ←	Y
C/1996 B2 Hyakutake	4 ± 1.3	< 50	<i>e</i>	<i>e</i>	N	29,30, 9 ←	Y

Table 9.1 – cont'd

Object	Diameter	Albedo	T_J	q_{ap}	Rotation?	Ref.	In Fig.
	(km)	(%)		(AU) ^a	<i>b</i>	<i>c</i>	9.4?
<u>Oort-sense Old Long-Period Comets (cont'd)</u>							
C/1997 T1 Utsumomiya	$< 11.6 \pm 4.0$	<i>d</i>	<i>e</i>	<i>e</i>	N	1 ←	N
C/1998 U5 LINEAR	~ 2	<i>d</i>	<i>e</i>	<i>e</i>	N	31	N
<u>Oort-sense New Long-Period Comets</u>							
None							
<u>Centaur</u>							
95P/(2060) Chiron	$176 \pm 10.$	14_{-3}^{+6}	3.36	18.95	N	10	N
(5145) Pholus	$189 \pm 26.$	4.4 ± 1.3	3.20	31.8	N	11	N
(10199) 1997 CU ₂₆	$302 \pm 30.$	4.5 ± 1.0	3.48	18.4	N	12	N
<u>NEAs with Low T_J</u>							
(1036) Ganymed	37.3 ± 3.2	21.5 ± 5	3.03	4.1	N	13	N
(1580) Betulia	7.5 ± 0.3	3.4 ± 0.4	3.07	3.3	N	14	Y
(1915) Quetzalcoatl	0.33 ± 0.2	34 ± 4	3.12	4.0	N	13	N

Table 9.1 – cont’d

Object	Diameter	Albedo	T_J	q_{ap}	Rotation?	Ref.	In Fig.
	(km)	(%)		(AU) ^a	^b	^c	9.4?
<u>NEAs with Low T_J (cont’d)</u>							
(2608) Seneca	0.9 ± 0.1	16 ± 3	3.17	3.95	N	15	Y
(3360) 1981 VA	1.80 ± 0.21	16 ± 2.5	2.97	4.3	N	13	Y
(4179) Toutatis	2.8 ± 0.1	17.5 ± 1.5	3.15	4.1	Y	16 ^f	Y
(4197) 1982 TA	1.64 ± 0.06	$40 \pm 2.$	3.09	4.1	N	13	N
(3552) Don Quixote	18.39 ± 0.85	4.5 ± 0.3	2.31	7.3	N	13	Y
(6063) Jason	1.4 ± 0.1	16 ± 2	3.19	3.9	N	17	Y
(6178) 1986 DA	2.3 ± 0.1	14 ± 2	3.04	4.5	N	18	Y
(6489) Golevka	0.30 ± 0.01	61 ± 3	3.18	4.0	Y	19	N
1983 VA	2.7 ± 0.1	7 ± 1	2.97	4.4	N	20	Y
<u>NEAs with High T_J but Extenuating Circumstances</u>							
(2201) Oljato	1.20 ± 0.05	55 ± 2	3.30	3.7	N	13	N
(3200) Phaethon	4.7 ± 0.5	14 ± 3	4.51	2.4	N	21,22	Y

Table 9.1 – cont’d

Object	Diameter	Albedo	T_J	q_{ap}	Rotation?	Ref.	In Fig.
	(km)	(%)		(AU) ^a	^b	^c	9.4?
<u>NEAs with High T_J</u>							
(433) Eros	18 ± 1	19 ± 3	4.58	1.8	NA	28 ^f	N
(887) Alinda	4.13 ± 0.41	27 ± 5.5	3.22	3.9	N	13	N
(1566) Icarus	0.88 ± 0.04	45 ± 3.5	5.30	2.0	N	13	N
(1620) Geographos	1.95 ± 0.12	21 ± 3	5.07	1.7	N	13	N
(1627) Ivar	7.97 ± 0.33	16.5 ± 2.5	3.88	2.6	N	13	N
(1685) Toro	3.20 ± 0.25	31 ± 8	4.72	2.0	N	13	N
(1862) Apollo	1.35 ± 0.1	21 ± 2	4.41	2.3	N	27	N
(1863) Antinous	$1.8 \pm ?$	$18 \pm ?$	3.30	3.6	N	18 ^g	N
(1865) Cerberus	0.93 ± 0.11	24 ± 13	5.59	1.6	N	13	N
(1866) Sisyphus	8.03 ± 0.4	24.5 ± 2	3.51	2.9	N	13	N
(1943) Anteros	1.68 ± 0.14	31 ± 3	4.64	1.8	N	13	N
(1980) Tezcatlipoca	4.20 ± 0.27	29 ± 3	4.00	2.3	N	13	N

Table 9.1 – cont’d

Object	Diameter	Albedo	T_J	q_{ap}	Rotation?	Ref.	In Fig.
	(km)	(%)		(AU) ^a	^b	^c	9.4?
<i>NEAs with High T_J (cont’d)</i>							
(2062) Aten	0.9 ± 0.2	19 ± 5	6.18	1.1	N	25,26	N
(2100) Ra-Shalom	2.48 ± 0.35	13 ± 4	6.94	1.2	N ^h	23	N
“	2.04 ± 0.1	11.5 ± 1	6.94	1.2	N	15	Y
“	1.67 ± 0.1	21 ± 3	6.94	1.2	N	13	N
(2368) Beltrovata	2.28 ± 0.2	15.5 ± 5	3.63	3.0	N	13	N
(3103) Eger	1.16 ± 0.16	58 ± 7.5	4.61	1.9	N	13	N
(3199) Nefertiti	1.73 ± 0.06	48 ± 3	4.19	2.0	N	13	N
(3288) Seleucus	1.82 ± 0.24	33 ± 11	3.67	3.0	N	13	N
(3362) Khufu	0.67 ± 0.07	24 ± 4	6.02	1.45	N	13	N
(3551) Verenia	0.77 ± 0.03	45 ± 2	3.58	3.1	N	13	N
(3554) Amun	2.0 ± 0.1	19 ± 2	6.11	1.25	N	18	N
(3757) 1982 XB	0.54 ± 0.03	22 ± 2	3.90	2.65	N	13	N

Table 9.1 – cont’d

Object	Diameter	Albedo	T_J	q_{ap}	Rotation?	Ref.	In Fig.
	(km)	(%)		(AU) ^a	^b	^c	9.4?
<i>NEAs with High T_J (cont’d)</i>							
(4688) 1980 WF	0.6±?	18±?	3.45	3.4	N	18 ^g	N
(6053) 1993 BW3	3.3 ± 0.6	18 ± 7	3.44	3.3	Y	24	N
(9856) 1991 EE	1.01 ± 0.15	30 ± 10	3.33	3.65	N ⁱ	23	N
1978 CA	1.86 ± 0.08	6.5 ± 0.6	5.44	1.4	N	15	Y

^a Object’s aphelion distance.

^b Has the object’s rotation been explicitly taken into account in the quoted values’

errors? Note that in some cases the integration times or the error bars themselves

may be so large as to obviate this point. Also, sometimes partial coverage of the rotational

variation was obtained.

Table 9.1 – cont'd

-
- ^c References. 1 This Thesis. 2 Keller *et al.* 1986. 3 Jorda *et al.* 1999.
4 Campins *et al.* 1995. 5 A'Hearn *et al.* 1989. 6 Campins *et al.* 1987.
7 Cruikshank and Brown 1983. 8 Millis *et al.* 1988. 9 Lisse *et al.* 1999b.
10 Campins *et al.* 1994. 11 Davies *et al.* 1993. 12 Jewitt and Kalas 1998.
13 Veeder *et al.* 1989. 14 Lebofsky *et al.* 1978. 15 Lebofsky *et al.* 1979.
16 Hudson and Ostro 1995. 17 Bell *et al.* 1988. 18 Tedesco and Gradie 1987.
19 Mottola *et al.* 1997. 20 Tedesco 1992. 21 Veeder *et al.* 1984.
22 Green *et al.* 1985. 23 Harris *et al.* 1998. 24 Pravec *et al.* 1997.
25 Cruikshank and Jones 1977. 26 Morrison *et al.* 1976. 27 Lebofsky *et al.* 1981.
28 Murchie *et al.* 1999. 29 Harmon *et al.* 1997. 30 Sar meanic *et al.* 1997.
31 Fernández *et al.* in preparation. 32 Sekanina 1988c. 33 Hanner *et al.* 1987.
34 Campins and Schleicher 1995. 35 Fomenkova *et al.* 1995. 36 Hanner *et al.* 1996.
-

Table 9.1 – cont’d

^d Reference only gives radius; no reliable optical cross section measurement yet exists to be able to calculate the albedo.

^e T_J and q_{ap} are not really practical quantities for long-period comets.

^f Reference only gives radius; albedo calculated using the known absolute magnitude.

^g Unpublished, albedo mentioned in this reference without error bars; radius calculated using the known absolute magnitude.

^h Explicitly mentions that these values are for the lightcurve maximum.

ⁱ Explicitly mentions that these values are for the lightcurve mid-brightness.

9.2 Comparing Radii and Albedos of “Cometary Nuclei”

We turn our attention to Fig. 9.1, a comparison of the albedos and diameters. The addition of several points to that graph with this thesis and by other workers in the last few years has started to fill out the “cometary” region on the graph. In the figure I have only used objects from Table 9.1 that have both a known diameter and an albedo, or at least claimed limits. There are two points that I want to make about the plot.

- Clearly there is some overlap between the NEAs and the cometary nuclei. The nuclei all have a geometric albedo p less than 14%, and several asteroids reside in this region as well, including some with high T_J . The overlap can be used to estimate the fraction of NEAs that are cometary nuclei. If we use $p = 14\%$ as the boundary, seven of the forty asteroids are on the cometary side: 18%. Since not all of those seven need be dead comets, this could be interpreted as an upper limit. However there is an observational bias to discovering bright, shiny asteroids over dark ones, and hence thermal studies of NEAs will preferentially measure more of the high albedo objects, simply because we know more of them. This effect means that we may be underestimating the fraction of cometary NEAs – there are more (dark, carbonaceous) C- and D-type NEAs out there waiting to be discovered.

Of course, if one discovers asteroids through their thermal emission, the bias flows the other way, since then a lower albedo object would be easier to see (all else being equal). However currently the vast majority of NEAs are discovered optically.

Numerical integrations have been done showing that the NEA population’s source can be the Main Belt, via three main mechanisms (Greenberg and Nolan 1989, Migliorini *et al.* 1998): the 3:1 resonance with Jupiter, the ν_6 resonance with Saturn, and perturbations by Mars. However the existence of active comets in NEA orbits implies a non-negligible fraction of old cometary nuclei are there, and this ought to be taken into account when attempting to model the NEA taxonomic distribution. A more complete database of the taxonomic types of NEAs would in itself be valuable, if for example there are more C- and D-type NEAs (i.e., those with low albedo) than one would expect from the Main Belt delivery mechanisms, which predominately operate on the inner Main Belt where there are a higher fraction of S-type objects (Gradie *et al.* 1989). Recent estimates of the cometary contribution to the NEA population have been low, even approaching zero (e.g. Rabinowitz 1997), although others (e.g. Wetherill 1988) have suggested fractions higher than the 18% value I give above.

- There is no apparent constraint on the size of the nuclei; there are objects occupying every size scale from sub-kilometer to hundreds of kilometers. It is worthwhile to note that there are several more comets that are not listed in Table 9.1 that probably have sizes in the sub-kilometer range, and a few unlisted Kuiper Belt objects are probably larger than the plotted Centaurs. No thermal studies have been done of these objects, so the albedos are unknown; this is only based on optical studies and the range of possible albedos. For example, comet 45P/Honda-Mrkos-Pajdušakova has a diameter of less than 1 km even if the albedo is as low as 2% (Lamy *et al.* 1997). On the other extreme, Kuiper Belt object 1996 TO₆₆ is at least 450 km wide, using its absolute magnitude (Marsden 1997) and $p \leq 14\%$. The only

asteroids larger than this size are (1) Ceres, (2) Pallas, and (4) Vesta.

The KBOs and many of the objects in Fig. 9.1 have a common origin, and the question of the distribution of these original objects or their collisional fragments, will require many more hours at the telescope to build up a statistically significant sample. However it is gratifying that we have sampled almost three orders of magnitude of cometary sizes. There seems to be no doubt as to the existence of small comets, and interpreting that population in a size distribution of nuclei will likely shed light on the aging and active lifetime of these bodies.

9.3 Albedo and Orbital Parameters

A'Hearn *et al.* (1995), after analyzing the molecular abundances and dust production rates in the comae of about seven dozen comets, found a correlation between a comet's dust-to-gas mass ratio and its perihelion distance. They concluded that this was due to the effect of the solar heating cycle on the mantle of the nucleus – the mantle is presumably thicker for smaller perihelia, making it harder for grains to be entrained in the escaping gas, leading to a lower dust-to-gas ratio. In Fig. 9.2 I have plotted the cometary albedos versus perihelion distance, but there does not yet seem to be any clear trend. Thus, while there is some thermal processing of the surface layers of a comet, this does not appear to influence the albedo. This may argue against the existence of near-surface ice on cometary nuclei, since in that case one might expect the objects with larger perihelia – e.g., the Centaurs – to be more reflective. This would corroborate the findings from simultaneous IR and optical observations of nuclei that indicate cross section, and not emissivity or albedo, cause the brightness variations (e.g., A'Hearn *et al.* 1989). The cometary ice appears to be in a matrix with the rock in a porous subsurface layer. However adding several more objects to Fig 9.2 would strengthen (or refute) this conclusion.

Figure 9.3 compares the albedo and the Tisserand invariant. The dashed line marks the nominal traditional separation between asteroids and comets. There is no apparent trend with this parameter either, reiterating that the albedos are seemingly not tied to the orbital characteristics of the objects, at least with the sample we currently have. Had the aging of a comet affected the albedo, one might have expected that a comparison of Halley Family with long-period comets and Centaurs with short-period comets would have shown different clustering. No such trend is evident with the current sample.

9.4 A Motivator for the Future

In Fig. 9.4 I have shown a current estimate of the size distribution of cometary nuclei. In this case I have defined cometary nuclei very liberally, including many of the asteroids that I mentioned in the previous subsection. The 25 objects that were used to make this graph are noted in Table 9.1; note that I have not included the three Centaurs. Also plotted are three possible size distribution power laws.

The value of the power law exponent in a system of colliding particles that have some self-gravity has been the target of various numerical models over the years. Davis *et al.* (1985) find that the cumulative power law goes as $D^{-2.5}$ for objects smaller than 20 km wide and flattens out for larger objects. A cometary distribution

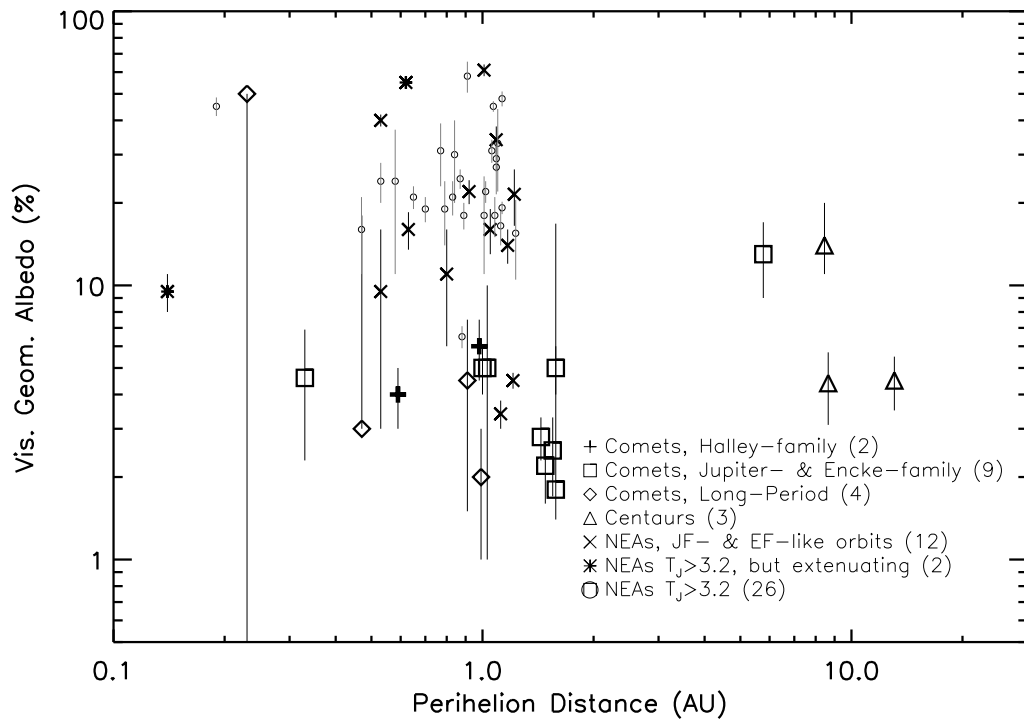


Figure 9.2: A comparison of the albedos of cometary nuclei and related objects to their perihelion distance. No trend is apparent, although A'Hearn *et al.* (1995) find that the Sun thermally processes the mantle and affects the size distribution of the dust entrained with the gas. This affect does not seem to manifest itself in albedo, however.

that approaches this would indicate a high frequency of collisions among the comets; conversely, a different size distribution shape would contradict this idea. Clearly the current distribution is nowhere near this power law, being more proportional to D^{-1} , but the sampling is of course not complete and it remains to be seen how this law will change in the coming years as more thermal studies are done of comets and NEAs.

Connected to this issue are the separate size distributions of the Oort Cloud comets – today’s Halley Family and long period objects – and the Kuiper Belt comets – today’s current KB residents and the Jupiter Family objects. The collision histories of the two sets of objects differ (Stern 1988, Stern 1995), and presumably once a large number of cometary nuclei are sampled the evidence will be there.

In an ideal situation, we could sample many long-period comets that are new in the Oort sense and see what the current distribution of sizes is *today* in the Oort Cloud. Information on the rotational state of these bodies would also determine just how pristine the objects are – are they rotating faster or slower than the current inner Solar System population? Since splittings and non-gravitational forces act on the active comets and affect the rotation rate, in addition to any repercussions of the comet’s most recent collision, it would be interesting to see what the relatively pristine OC comets were originally like. One ought to note that there are precisely zero Oort-sense new long-period comets listed in Table 9.1. This is mainly because there are simply fewer “new” Oort Cloud comets discovered compared to “old” ones.

The cometary connection with the asteroids needs to be solidified with more observational data. There seems to have been a deceleration in the number of thermal studies of NEAs in the past decade; one hopes that this trend will be reversed since there are about 800 NEAs currently known, with new discoveries being made at an increasing rate due to the fecundity of asteroid search programs. Even optical information, to obtain a complete census of the representation of the taxonomic classes among the NEAs, would be useful, since that can be correlated with the taxonomic gradient in the other source region, the Main Belt.

Another, more direct approach is to look for faint gas emission around near-Earth asteroids. Comet Wilson-Harrington is the most successful example of this phenomenon: the comet was discovered in 1949, then re-discovered in its asteroidal incarnation in 1979, and the two apparitions were linked in 1992 (Bowell and Skiff, reported by Marsden 1992). I discussed the cometary nature of the 1949 data in a separate work (Fernández *et al.* 1997). A deep search for any OH signature around several NEAs would provide strong, direct (and modern) evidence for the evolutionary connection between the asteroids and comets.

9.5 Future Data Rates

The future of thermal observations of comets is bright. *SIRTf* will be available in a few years to give us unprecedented sensitivity in the thermal regime. In principle, since the lifetime of the satellite is expected to be three to five years, a systematic survey of all of the Jupiter Family comets could be done. Furthermore, the size distribution of the Kuiper Belt objects could be measured, since the sensitivity will finally allow us to measure the trickle of blackbody radiation coming from those objects. This is all contingent on the allocation of sufficient observing time.

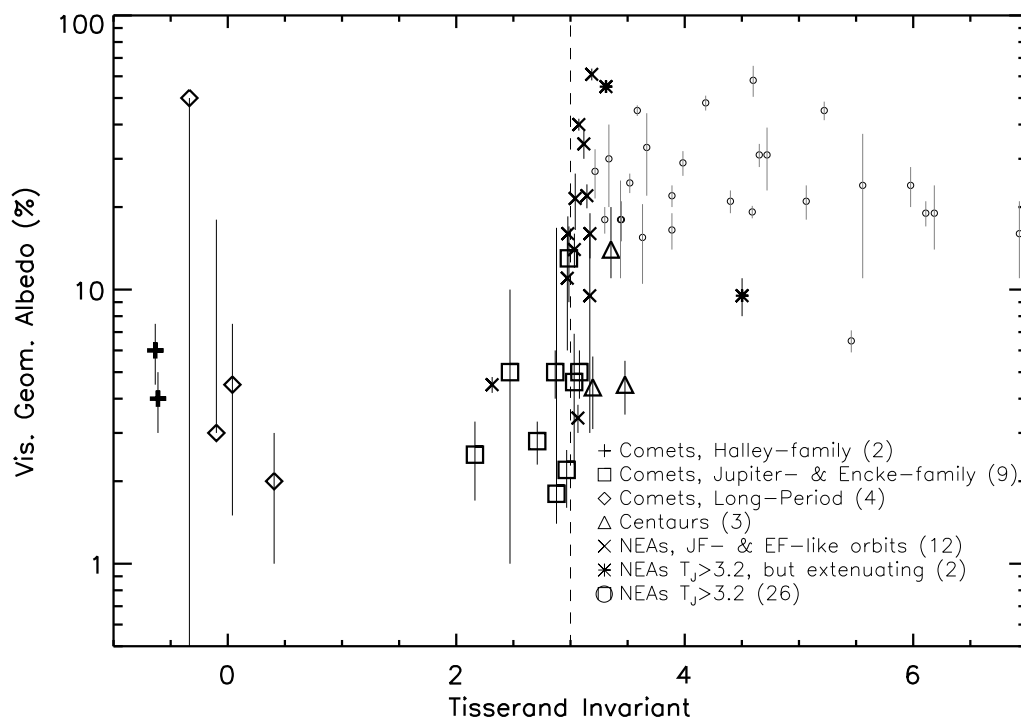


Figure 9.3: The Tisserand invariant is compared to the albedos. An aging affect might have manifested itself in albedo differences between long-period and Halley family comets, and Jupiter family and Centaurs, but no such trend is yet in evidence.

It should be clear from this thesis that the advent of large arrays of 10 and 20 μm detectors was critical for the success of this work, and that the continued increase in size and sensitivity will make it easier to sample more comets from the ground in the coming years. Based on our experience, one detailed study of a short-period comet and quick looks at two other comets (short- or long-period) can be done per mid-IR observing run. An obvious benefit of having frequent observing runs for scheduled short-period comets is the increased probability of being at a telescope when a newly discovered long-period comet (unknown at the time of the telescope's proposal deadline) is available. There are approximately 3 short-period comets worthy of intense study per year, and if a few fortuitous comets are also observable, then optimistically, we could have some physical information about a dozen cometary nuclei every two to three years or so. The observing efficiency is even better for NEAs, since there are more of them. By the time the *Rosetta* spacecraft encounters comet 46P/Wirtanen in 2012, we may start to have a handle on the ensemble properties of the nuclei.

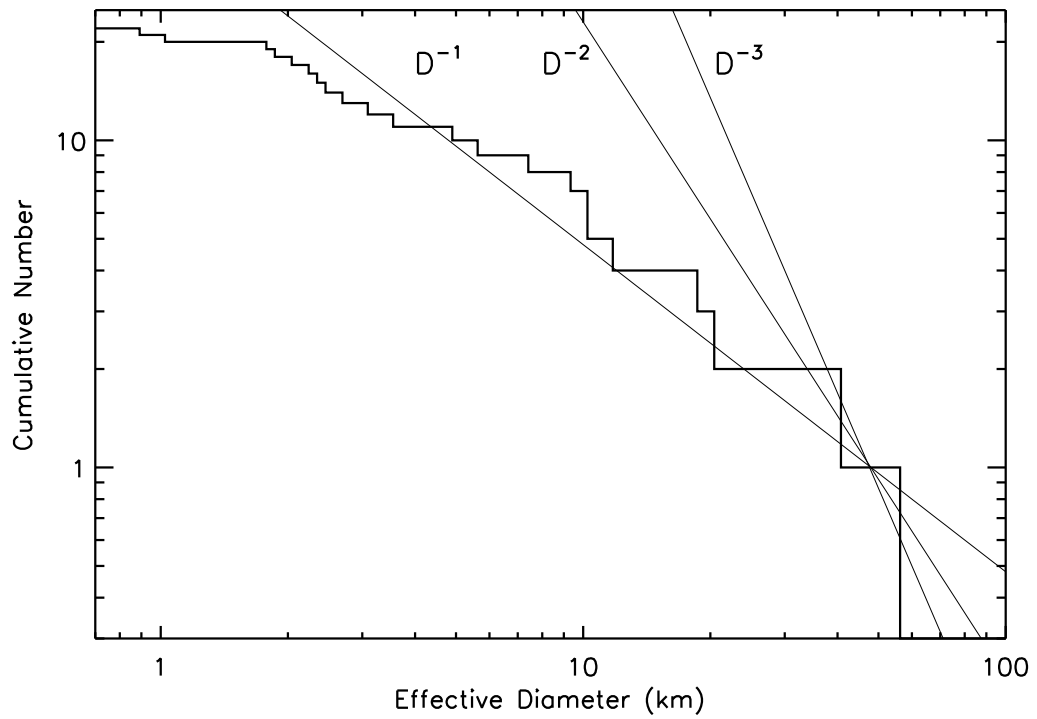


Figure 9.4.: The current size distribution of cometary nuclei and related objects that may be nuclei. This is not to claim that the sample of objects is complete on any size scale. The eventual slope of the real distribution function will give clues to the collisional history of the cometary population.

REFERENCES

- A'Hearn, M. F., 1991. Photometry and polarimetry network. In *The Comet Halley Archive Summary Volume* (Z. Sekanina and L. Fry, Eds.), pp. 193-235. Jet Propulsion Laboratory, Pasadena.
- A'Hearn, M. F., H. Campins, D. G. Schleicher, and R. L. Millis 1989. The nucleus of comet P/Tempel 2. *Astroph. J.* **347**, 1155-1166.
- A'Hearn, M. F., R. L. Millis, D. G. Schleicher, D. J. Osip, and P. V. Birch 1995. The ensemble properties of comets: Results from narrow band photometry of 85 comets, 1976-1992. *Icarus* **118**, 223-270.
- A'Hearn, M. F., D. G. Schleicher, P. D. Feldman, R. L. Millis, and D. T. Thompson 1984. Comet Bowell 1980b. *A. J.* **89**, 579-591.
- Allen, C. W. 1973. *Astrophysical Quantities*, 3d ed., Athlone Press, London.
- Altenhoff, W. J., and 20 colleagues 1999. Coordinated radio continuum observations of comets Hyakutake and Hale-Bopp from 22 to 860 GHz. *Astron. & Astrophys.* **348**, 1020-1034.
- Altenhoff, W. J., W. K. Batrla, W. K. Huchtmeier, J. Schmidt, P. Stumpff, and M. Walmsley 1983. Radio observations of comet 1983d. *Astron. & Astrophys.* **125**, L19-L22.
- Barker, E. S., A. L. Cochran, and P. M. Rybski 1981. Observations of faint comets at McDonald Observatory: 1978-1980. In *Modern Observational Techniques for Comets* (J. Brandt, J. M. Greenberg, B. Donn, and J. Rahe, Eds.), pp. 150-155. NASA Jet Propulsion Laboratory, Pasadena.
- Bell, J. F., B. R. Hawke, and R. H. Brown 1988. Composition and size of Apollo asteroid 1984 KB. *Icarus* **73**, 482-486.
- Belton, M. J. S., 1991. Characterization of the rotation of cometary nuclei. In *Comets in the Post-Halley Era* (R. L. Newburn, Jr., M. Neugebauer, and J. Rahe, Eds.), pp. 691-721. Kluwer Academic Publishers, Boston.
- Bessel, M. S., 1979. *UBVRI* photometry II: the Cousins *VRI* system, its temperature and absolute flux calibration, and relevance for two-dimensional photometry. *Publ. Astron. Soc. Pacific* **91**, 589-607.
- Bessel, M. S., 1990. *UBVRI* passbands. *Publ. Astron. Soc. Pacific* **102**, 1181-1199.
- Biermann, L., 1951. Kometschwerfe und solare Korpuskularstrahlung. *Z. Astrophys.* **29**, 274-286.
- Biver, N., and 22 colleagues 1999. Long term evolution of the outgassing of comet Hale-Bopp from radio observations. *Earth Moon & Plan.*, accepted.
- Bobrovnikoff, N. T., 1931. Halley's comet in its apparition of 1909-1911. *Publ. of Lick Obs.* **17**, 309-482.
- Boss, A. P., 1998. Evolution of the solar nebula. IV. Giant gaseous protoplanet formation. *Astrophys. J.* **503**, 923-937.
- Brown, R. H., 1985. Ellipsoidal geometry in asteroid thermal models – the standard radiometric model. *Icarus* **64**, 53-63.
- Bus, S. J., and 20 colleagues 1996. Stellar occultation by 2060 Chiron. *Icarus* **123**, 478-490.
- Campbell, D. B., J. K. Harmon, and I. I. Shapiro 1989. Radar observations of comet Halley, *Astrophys. J.* **338**, 1049-1105.
- Campins, H., 1988. The anomalous dust production in periodic comet Encke. *Icarus* **73**, 508-515.
- Campins, H., M. F. A'Hearn, and L. A. McFadden 1987. The bare nucleus of comet Neujmin 1. *Astroph. J.* **316**, 847-857.
- Campins, H., D. J. Osip, G. H. Rieke, and M. J. Rieke 1995. Estimates of the radius and albedo of comet-asteroid transition object 4015 Wilson-Harrington based on infrared observations. *Plan. & Sp. Sci.* **43**, 733-736.
- Campins, H., and D. G. Schleicher 1995. Comet d'Arrest: a small and rapidly rotating nucleus? [abstract]. *Bull. Amer. Astron. Soc.* **27**, 1113.
- Campins, H., C. M. Telesco, D. J. Osip, G. H. Rieke, M. J. Rieke, and B. Schulz 1994. The color temperature of (2060) Chiron: A warm and small nucleus. *Astron. J.* **108**, 2318-2322.
- Chambers, G. F., 1909. *The Story of the Comets*, Clarendon Press, London.

- Combes, M., J. Lecacheux, Th. Encrenaz, B. Sicardy, Y. Zeau, and D. Malaise 1983. On stellar occultations by comets. *Icarus* **56**, 229-232.
- Cruikshank, D. P., and R. H. Brown. The nucleus of comet P/Schwassmann-Wachmann 1. *Icarus* **56**, 377-380.
- Cruikshank, D. P., and T. J. Jones. The diameter and albedo of asteroid 1976 AA. *Icarus* **31**, 427-429.
- Danby, J. M. A., 1962. *Fundamentals of Celestial Mechanics*. The MacMillan Co., New York.
- Davies, J., J. Spencer, M. Sykes, D. Tholen, and S. Green 1993. (5145) Pholus. *Int'l Astron. Union Circ.* **5698**.
- Davis, D. R., C. R. Chapman, S. J. Weidenschilling, and R. Greenberg 1985. Collision history of asteroids: evidence from Vesta and the Hirayama families. *Icarus* **62**, 30-53.
- de Pater, I., P. Palmer, D. L. Mitchell, S. J. Ostro, D. K. Yeomans, and L. E. Snyder 1994. Radar aperture synthesis observations of asteroids. *Icarus* **111**, 489-502.
- de Pater, I., C. M. Wade, H. L. F. Houppis, and P. Palmer 1985. The nondetection of continuum radiation from comet IRAS-Araki-Alcock (1983d) at 2- to 6-cm wavelengths and its implication on the icy-grain halo theory. *Icarus* **62**, 349-359.
- Divine, N. 1981. Numerical models for Halley dust environments. In *The Comet Halley Dust & Gas Environment* (B. Battrock and E. Swallow, Eds.), pp. 25-30. European Space Agency Scientific and Technical Publications Branch, Noordwijk, The Netherlands.
- Divine, N. and 10 colleagues 1986. The Comet Halley dust and gas environment. *Sp. Sci. Rev.* **43**, 1-104.
- Dones, L., H. F. Levison, and M. Duncan 1996. On the dynamical lifetimes of planet-crossing objects. In *Completing the Inventory of the Solar System* (T. W. Rettig, J. M. Hahn, Eds.), pp.233-244. Astronomical Society of the Pacific, San Francisco.
- Donn, B. D., 1990. The formation and structure of fluffy cometary nuclei from random accumulation of grains. *Astron. & Astrophys.* **235**, 441-446.
- Donn, B., 1991. The accumulation and structure of comets. In *Comets in the Post-Halley Era* (R. L. Newburn, Jr., M. Neugebauer, and J. Rahe, Eds.), pp. 335-339. Kluwer Academic Publishers, Boston.
- Duncan, M., T. Quinn, and S. Tremaine 1987. The formation and extent of the solar system comet cloud. *Astron. J.* **94**, 1330-1338.
- Dworetsky, M. M., 1983. A period-finding method for sparse randomly spaced observations or "How long is a piece of string?" *Mon. Not. Royal Astron. Soc.* **203**, 917-924.
- Edgeworth, K. E. 1949. The origin and evolution of the Solar System. *Mon. Not. Royal Astron. Soc.* **109**, 600-609.
- Farinella, P., and D. R. Davis 1996. Short-period comets: primordial bodies or collisional fragments?. *Science* **273**, 938-941.
- Farnham, T. L., D. G. Schleicher, and M. F. A'Hearn 1999. The HB narrowband comet filters: standard stars and calibrations. *Icarus*, submitted.
- Fernández, J. A., 1980. On the existence of a comet belt beyond Neptune. *Mon. Not. Roy. Astron. Soc.* **192**, 481-491.
- Fernández, Y. R., and 11 colleagues 1999a. Survey of the physical properties of cometary nuclei: Recent progress. In *Cometary Nuclei in Space and Time, A.S.P. Conference Series* (M. F. A'Hearn, Ed.), accepted. Astronomical Society of the Pacific, San Francisco.
- Fernández, Y. R., and 14 colleagues 1999b. The inner coma and nucleus of comet Hale-Bopp: results from a stellar occultation. *Icarus* **140**, 205-220.
- Fernández, Y. R., C. M. Lisse, H. U. Käuff, S. B. Peschke, H. A. Weaver, M. F. A'Hearn, P. L. Lamy, T. A. Livengood, and T. Kostiuik 1999c. Physical properties of the nucleus of comet 2P/Encke. *Icarus*, submitted.
- Fernández, Y. R., A. Kundu, C. M. Lisse, and M. F. A'Hearn 1997a. X-Band VLA observations of comet Hyakutake (C/1996 B2) and implications for nuclear properties. *Planetary & Space Science* **45**, 735-739.
- Fernández, Y. R., L. A. McFadden, C. M. Lisse, E. F. Helin, and A. B. Chamberlin 1997b. Analysis of POSS images of comet-asteroid transition object 107P/1949 W1 (Wilson-Harrington).

Icarus **128**, 114-126.

- Fernie, J. D. 1983. Relationships between the Johnson and Kron-Cousins VRI photometric systems. *Publ. Astron. Soc. Pacific* **95**, 782-785.
- Finlay, W. H., and W. L. Elkin 1882. *Mon. Not. Roy. Astron. Soc.* **43**.
- Fomenkova, M. N. B. Jones, R. Piña, R. Puetter, J. Sarmecanic, R. Gehrz, and T. Jones 1995. Mid-infrared observations of the nucleus and dust of comet P/Swift-Tuttle. *Astron. J.* **110**, 1866-1874.
- Gabriel, C., J. Acosta-Pulido, I. Heinrichsen, H. Morris, and W. M. Tai 1997. The ISOPHOT interactive analysis PIA, a calibration and scientific analysis tool. In *Astronomical Data Analysis Software and Systems VI: A.S.P. Conference Series Vol. 125* (G. Hunt and H. E. Payne, Eds.), pp. 108-111. Astronomical Society of the Pacific, San Francisco.
- Garradd, G. J. 1997. Comet 2P/Encke. *Int'l Astron. Union Circ.* **6717**.
- Gehrz, R. D., E. P. Ney, J. Piscitelli, E. Rosenthal, and A. T. Tokunaga 1989. Infrared photometry and spectroscopy of comet P/Encke 1987. *Icarus* **80**, 280-288.
- Gilmore, A. C., and P. M. Kilmartin 1978. Periodic comet Encke. *Int'l Astron. Union Circ.* **3210**.
- Goldstein, R. M., R. F. Jurgens, and Z. Sekanina 1984. A radar study of comet IRAS-Araki-Alcock 1983d. *Astron. J.* **89**, 1745-1754.
- Gombosi, T. I., T. E. Cravens, and A. F. Nagy 1985. Time-dependent dusty gasdynamical flow near cometary nuclei. *Astrophys. J.* **293**, 328-341.
- Gombosi, T. I. and H. L. F. Houppis 1986. An icy-glue model of cometary nuclei. *Nature* **324**, 43-44.
- Gombosi, T. I., A. F. Nagy, and T. E. Cravens 1986. Dust and neutral gas modeling of the inner atmosphere of comets. *Rev. Geophys.* **24**, 667-700.
- Gombosi, T. I., K. Szegő, B. E. Gribov, R. Z. Sagdeev, V. D. Shapiro, V. I. Shevchenko, and T. E. Cravens 1983. Gas dynamic calculations of dust terminal velocities with realistic dust size distributions. In *Cometary Exploration* (T. I. Gombosi, Ed.), vol. 2, pp. 99-111. Central Research Institute for Physics, Hungarian Academy of Sciences, Budapest.
- Gradie, J. C., C. R. Chapman, and E. F. Tedesco 1989. Distribution of taxonomic classes and the compositional structure of the asteroid belt. In *Asteroids II* (R. P. Binzel, T. Gehrels, M. S. Matthews, Eds.), pp. 316-335. Univ. of Arizona Press, Tucson.
- Green, D. W. E. 1998. Comet 55P/Tempel-Tuttle. *Int'l Astron. Union Circ* **6816**.
- Green, S. F., A. J. Meadows, and J. K. Davies 1985. Infrared observations of the extinct cometary candidate minor planet (3200) 1983 TB. *Mon. Not. Roy. Astron. Soc.* **214**, 29p-36p.
- Greenberg, R., and M. C. Nolan 1989. Delivery of asteroids and meteorites to the inner Solar System. In *Asteroids II* (R. P. Binzel, T. Gehrels, M. S. Matthews, Eds.), pp. 778-804. Univ. of Arizona Press, Tucson.
- Hainaut, O. R., K. J. Meech, H. Boehnhardt, and R. M. West 1998. Early recovery of comet 55P/Tempel-Tuttle. *Astron. & Astrophys.* **333**, 746-752.
- Hanner, M. S., D. K. Aitken, R. Knacke, S. McCorkle, P. F. Roche, A. T. Tokunaga 1985. Infrared spectrophotometry of comet IRAS-Araki-Alcock (1983d) - A bare nucleus revealed? *Icarus* **62**, 97-109.
- Hanner, M. S., R. H. Giese, K. Weiss, and R. Zerull 1981. On the definition of albedo and application to irregular particles. *Astron. & Astrophys.* **104**, 42-46.
- Hanner, M. S., D. K. Lynch, R. W. Russell, J. A. Hackwell, R. Kellogg, D. Blaney 1996. Mid-infrared spectra of comets P/Borrelly, P/Faye, and P/Schaumasse. *Icarus* **124**, 344-351.
- Hanner, M. S., R. L. Newburn, H. Spinrad, and G. J. Veeder 1987. Comet Sugano-Saigusa-Fujikawa (1983V) - a small, puzzling comet. *Astron. J.* **94**, 1081-1087.
- Harmon, J. K., and 15 colleagues 1997. Radar detection of the nucleus and coma of comet Hyakutake (C/1996 B2). *Science* **278**, 1921-1924.
- Harmon, J. K., D. B. Campbell, A. A. Hine, I. I. Shapiro, and B. G. Marsden 1989. Radar observations of comet IRAS-Araki-Alcock. *Astrophys. J.* **338**, 1071-1093.
- Harris, A. W. 1998. A thermal model for near-Earth asteroids. *Icarus* **131**, 291-301.
- Harris, A. W., J. K. Davies, and S. F. Green 1998. Thermal infrared spectrophotometry of the near-Earth asteroids 2100 Ra-Shalom and 1991 EE. *Icarus* **135**, 441-450.

- Helin, E., E. Ney, and B. Hatfield 1980. Periodic comet Encke. *Int'l Astron. Union Circ.* **3501**.
- Hellmich, R., 1981. The influence of the radiation transfer in cometary dust halos on the production rates of gas and dust. *Astron. & Astrophys.* **93**, 341-346.
- Henyey, L. G., and J. L. Greenstein 1941. Diffuse radiation in the galaxy. *Astrophys. J.* **93**, 70-83.
- Hoban, S., and S. Baum 1987. A VLA search for 2-cm continuum radiation from comet Halley. *Icarus* **70**, 264-268.
- Hobbs, R. W., J. C. Brandt, S. P. Maran, W. J. Webster, Jr., and K. S. Krishna Swamy 1975. Microwave continuum radiation from comet Kohoutek 1973f: emission from the icy-grain halo? *Astrophys. J.* **201**, 749-755.
- Hobbs, R. W., S. P. Maran, and J. C. Brandt 1977. Microwave continuum radiation from comet West 1975n. *Astrophys. J.* **218**, 573-578.
- Högbom, J. A., 1974. Aperture synthesis with a non-regular distribution of interferometer baselines. *Astron. & Astrophys. Suppl.* **15**, 417-426.
- Hudson, R. S., and S. J. Ostro 1995. Shape and non-principal axis spin state of asteroid 4179 Toutatis. *Science* **270**, 84-86.
- Jacoby, G. H., D. A. Hunter, and C. A. Christian 1984. A library of stellar spectra. *Astrophys. J. Suppl. Ser.* **56**, 257-281.
- Jewitt, D., 1991. Cometary photometry. In *Comets in the Post-Halley Era* (R. L. Newburn, Jr., M. Neugebauer, and J. Rahe, Eds.), pp. 19-65. Kluwer Academic Publishers, Boston.
- Jewitt, D., and P. Kalas 1998. Thermal observations of Centaur 1997 CU₂₆. *Astroph. J.* **499**, L103-L106.
- Jewitt, D., and K. Meech 1987 [JM87]. CCD photometry of comet P/Encke. *Astron. J.* **93**, 1542-1548.
- Jewitt, D. C., and K. J. Meech 1988. Optical properties of cometary nuclei and a preliminary comparison with asteroids. *Astroph. J.* **328**, 974-986.
- Jorda, L., *et al.* 1999. The rotation period of comet Hale-Bopp from observations of the dust jets at Pic du Midi Observatory. *Earth, Moon, & Planets*, accepted.
- Jorda, L., P. L. Lamy, I. Toth, and M. F. A'Hearn 1999. Properties of the nucleus of short-period comets from ISO observations [abstract]. In *Abstracts: Asteroids, Comets, Meteors, Cornell University, July 26-30, 1999*, p. 75. Cornell University, Ithaca, NY.
- Kamoun, P. G., D. B. Campbell, S. J. Ostro, G. H. Pettengill, and I. I. Shapiro 1982. Comet Encke: radar detection of nucleus. *Science* **216**, 293-295.
- Käuff, H. U. 1997. *TIMMI filter wheel configuration*, World Wide Web URL <http://www.eso.org/lasilla/Telescopes/360cat/timmi/timmi-filters.html>, 26 February 1997.
- Käuff, H. U., R. Jouan, P. O. Lagage, P. Masse, P. Mestreau, and A. Tarrus 1994. TIMMI, ESO's new 10 μ m camera/spectrometer. *Infrared Phys. Technol.* **35**, 203-210.
- Kazarovets, A. V., N. N. Samus, O. V. Durlevich, M. S. Frolov, S. V. Antipin, N. N. Kireeva, and E. N. Pastukhova 1999. The 74th special name-list of variable stars. *Info. Bull. on Var. Stars* **4659**.
- Keller, H. U., 1990. The nucleus. In *Physics and Chemistry of Comets* (W. F. Huebner, Ed.), pp. 13-68. Springer-Verlag, Berlin.
- Keller, H. U., and 17 colleagues 1986. First Halley multicolour camera imaging results from Giotto. *Nature* **321**, 320-326.
- Keller, H. U., and 21 colleagues 1987. Comet P/Halley's nucleus and its activity. *Astron. & Astrophys.* **187**, 807-823.
- Kharitonov, A. V., V. M. Tereshchenko, and L. N. Knyazeva 1988. *Spectrophotometric catalogue of stars*, Izdatel'stvo Nauka Kazakhskoi SSR, Alma-Ata, Kazakh SSR.
- Klaas, U., H. Krüger, I. Heinrichson, A. Heske, and R. Laureijs 1994. *ISOPHOT observer's manual*, World Wide Web URL http://isowww.estec.esa.nl/manuals/iso_pht/om311.html, 9 May 1994.
- Kuiper, G. P., 1951. Origin of the solar system. In *Astrophysics: A Topical Symposium* (J. A. Hynek, Ed.), pp. 357-424. McGraw-Hill, New York.

- Labs, D., H. Neckel, P. C. Simon, and G. Thuiller 1987. Ultraviolet solar irradiance measurement from 200 to 358 nm during Spacelab 1 mission. *Sol. Phys.* **107**, 203-219.
- Lamy, P., 1998. Comet 55P/Tempel-Tuttle. *Int'l Astron. Union Circ.* **6851**.
- Lamy, P. L., and I. Toth 1995. Direct detection of a cometary nucleus with the Hubble Space Telescope. *Astron. & Astrophys.* **293**, L43-L45.
- Lamy, P. L., I. Toth, M. F. A'Hearn, H. A. Weaver 1997. The nucleus of comet 45P/Honda-Mrkos-Pajdušakova [abstract]. *Bull. Amer. Astron. Soc.* **29**, 1029.
- Lamy, P. L., I. Toth, L. Jorda, H. A. Weaver, and M. A'Hearn 1998a. The nucleus and inner coma of comet 46P/Wirtanen. *Astron. & Astrophys.* **335**, L25-L29.
- Lamy, P. L., I. Toth, H. A. Weaver 1998b. Hubble Space Telescope observations of the nucleus and inner coma of comet 19P/1904 Y2 (Borrelly). *Astron. & Astrophys.* **337**, 945-954.
- Larson, S. M. and M. F. A'Hearn 1984. Comet Bowell (1980b) - measurement of the optical thickness of the coma and particle albedo from a stellar occultation. *Icarus* **58**, 446-450.
- Laureijs, R. J., U. Klaas, P. J. Richards, and B. Schulz 1998. *ISOPHOT data users manual*, World Wide Web URL http://isowww.estec.esa.nl/manuals/pht_idum4/, October 1998.
- Lebofsky, L. A., M. J. Lebofsky, and G. H. Rieke 1979. Radiometry and surface properties of Apollo, Amor, and Aten asteroids. *Astron. J.* **84**, 885-888.
- Lebofsky, L. A. and J. R. Spencer 1989. Radiometry and thermal modeling of asteroids. In *Asteroids II* (R. P. Binzel, T. Gehrels, M. S. Matthews, Eds.), pp. 128-147. Univ. of Arizona Press, Tucson.
- Lebofsky, L. A., M. V. Sykes, E. F. Tedesco, G. J. Veeder, D. L. Matson, R. H. Brown, J. C. Gradie, M. A. Feierberg, R. J. Rudy 1986. A refined "standard" thermal model for asteroids based on observations of 1 Ceres and 2 Pallas. *Icarus* **68**, 239-251.
- Lebofsky, L. A., G. J. Veeder, M. J. Lebofsky, and D. L. Matson 1978. Visual and radiometric photometry of 1580 Betulia. *Icarus* **35**, 336-343.
- Lebofsky, L. A., G. J. Veeder, G. H. Rieke, M. J. Lebofsky, D. L. Matson, C. Kowal, C. G. Wynn-Williams, and E. E. Becklin 1981. The albedo and diameter of 1862 Apollo. *Icarus* **48**, 335-338.
- Lecacheux, J., L. Jorda, A. Enzian, J. Klinger, F. Colas, E. Frappa, and P. Laques 1996. Comet C/1996 B2 (Hyakutake). *Int'l Astron. Union Circ.* **6354**.
- Lecacheux, J., W. Thuillot, Th. Encrenaz, P. Laques, D. Rouan, and R. Despiou 1984. Stellar occultations by two comets: IRAS-Araki-Alcock (1983d) and P/IRAS (1983j). *Icarus* **60**, 386-390.
- Lemke, D., and 48 colleagues. ISOPHOT – capabilities and performance. *Astron. & Astroph.* **315**, L64-L70.
- Levison, H., 1996. Comet taxonomy. In *Completing the Inventory of the Solar System* (T. Rettig and J. M. Hahn, Eds.), pp. 173-191. Astronomical Society of the Pacific, San Francisco.
- Levison, H. F., and M. J. Duncan 1997. From the Kuiper Belt to Jupiter family comets: the spatial distribution of ecliptic comets. *Icarus* **127**, 13-32.
- Licandro, J., *et al.* 1999. The spin axis of comet 1995 O1 (Hale-Bopp). *Earth, Moon, & Planets*, accepted.
- Lien, D. J., 1998. Asteroid debris trails: evidence for recent collisions in the asteroid belt [abstract]. *Bull. Amer. Astron. Soc.* **30**, 1207.
- Lisse, C. M., and 11 colleagues 1996. Discovery of X-ray and EUV emission from comet Hyakutake C/1996 B2. *Science* **274**, 205-209.
- Lisse, C. M., and 14 colleagues 1999a. Infrared observations of the dust emitted by comet Hale-Bopp. *Earth, Moon & Plan.*, accepted.
- Lisse, C. M., M. F. A'Hearn, Y. R. Fernández, E. Grün, H. U. Käuffl, T. Kostiuk, D. J. Lien, T. A. Livengood, D. J. Osip, and S. B. Peschke 2000. ISOPHOT measurements of dust emitted from periodic comets 126P/IRAS (1996) and 2P/Encke (1997). *Icarus*, submitted.
- Lisse, C. M., M. F. A'Hearn, M. G. Hauser, T. Kelsall, D. J. Lien, S. H. Moseley, W. T. Reach, and R. F. Silverberg 1998. Infrared observations of comets by COBE. *Astroph. J.* **496**, 971-991.

- Lisse, C. M., Y. R. Fernández, A. Kundu, M. F. A'Hearn, A. Dayal, L. K. Deutsch, G. G. Fazio, J. L. Hora, and W. F. Hoffmann 1999b. The nucleus of comet C/1996 B2 (Hyakutake). *Icarus* **140**, 189-204.
- Lumme, K., and E. Bowell 1981. Radiative transfer in the surfaces of atmosphereless bodies. II. Interpretation of phase curves. *Astron. J.* **86**, 1705-1721.
- Lumme, K., E. Bowell, and A. W. Harris 1984. An empirical phase relation for atmosphereless bodies [abstract]. *Bull. Amer. Astron. Soc.* **16**, 684.
- Luu, J., and D. Jewitt 1990 [LJ90]. The nucleus of comet P/Encke. *Icarus* **86**, 69-81.
- Lyttleton, R. A., 1953. *The Comets and Their Origin*. University Press, Cambridge.
- Lyttleton, R. A., 1963. Introduction. In *The Nature of Comets* (N. B. Richter; A. Beer, trans.), pp. xvii-xxxviii. Methuen & Co. Ltd., London.
- Marconi, M. L. and D. A. Mendis 1983. The atmosphere of a dirty-clathrate cometary nucleus: a two-phase, multifluid model. *Astrophys. J.* **273**, 381-396.
- Marconi, M. L., and D. A. Mendis 1984. The effects of the diffuse radiation fields due to multiple scattering and thermal reradiation by dust on the dynamics and thermodynamics of a dusty cometary atmosphere. *Astrophys. J.* **287**, 445-454.
- Marsden, B. G., 1971. Comets in 1970. *Quart. J. Roy. Astron. Soc.* **12**, 244-273.
- Marsden, B. G., 1972. Comets in 1971. *Quart. J. Roy. Astron. Soc.* **13**, 415-435.
- Marsden, B. G., 1973. Comets in 1972. *Quart. J. Roy. Astron. Soc.* **14**, 389-406.
- Marsden, B. G., 1974. Comets in 1973. *Quart. J. Roy. Astron. Soc.* **15**, 433-460.
- Marsden, B. G., 1985a. Comets in 1980. *Quart. J. Roy. Astron. Soc.* **26**, 156-167.
- Marsden, B. G., 1985b. Comets in 1982. *Quart. J. Roy. Astron. Soc.* **26**, 530-540.
- Marsden, B. G., 1992. (4015) 1979 VA = Comet Wilson-Harrington (1949 III). *Int'l Astron. Union Circ.* **5585**.
- Marsden, B. G., 1996a. Comet C/1996 B2 (Hyakutake). *Int'l Astron. Union Circ.* **6304**.
- Marsden, B. G., 1996b. Come P/1996 N2 (Else-Pizarro). *Int'l Astron. Union Circ.* **6457**.
- Marsden, B. G., 1997. 1996 TO₆₆. *Minor Plan. Elec. Circ.* **1997-M05**.
- Marsden, B. G., and E. Roemer 1978a. Comets in 1974. *Quart. J. Roy. Astron. Soc.* **19**, 38-58.
- Marsden, B. G., and E. Roemer 1978b. Comets in 1975. *Quart. J. Roy. Astron. Soc.* **19**, 59-89.
- Marsden, B. G. and G. V. Williams 1999. *Catalogue of Cometary Orbits*, 13th ed. International Astronomical Union, Cambridge, Mass.
- Matson, D. L. 1972. Ph.D. Thesis, California Institute of Technology.
- McFadden, L. A. 1994. The comet-asteroid transition: recent telescopic observations. In *Asteroids Comets Meteors 1993* (A. Milani, M. Di Martino, A. Cellino, Eds.), pp. 95-120. Kluwer Academic Publ., Dordrecht.
- McFadden, L. A., A. L. Cochran, E. S. Braker, D. P. Cruikshank, and W. K. Hartmann 1993. The enigmatic object 2201 Oljato - Is it an asteroid or an evolved comet? *J. Geophys. Res.* **98**, 3031-3041.
- Meech, K. J., 1991. Physical aging in comets. In *Comets in the Post-Halley Era* (R. L. Newburn, Jr., M. Neugebauer, and J. Rahe, Eds.), pp. 629-669. Kluwer Academic Publishers, Boston.
- Meech, K. J., 1999. Physical properties of comets. In *Asteroids, Comets, Meteors '96: Proceedings of the 10th COSPAR Colloquium* (A.-C. Levasseur-Regourd and M. Fulchignoni, Eds.), in press. Pergamon-Elsevier, Oxford.
- Meech, K. J. and D. C. Jewitt 1987. Observations of comet P/Halley at minimum phase angle. *Astron. & Astrophys.* **187** 585-593.
- Meech, K. J., and R. L. Newburn 1999. Comet 81P/Wild 2, inn preparation.
- Meier, R., T. C. Owen, D. C. Jewitt, H. E. Matthews, M. Senay, N. Biver, D. Bockelée-Morvan, J. Crovisier, and D. Gautier 1998a. Deuterium in comet C/1995 O1 (Hale-Bopp): detection of DCN. *Science* **279**, 1707-1710.
- Meier, R., T.C. Owen, H. E. Matthews, D. C. Jewitt, D. Bockelée-Morvan, N. Biver, J. Crovisier, and D. Gautier 1998b. A determination of the HDO/H₂O ratio in comet C/1995 O1 (Hale-Bopp). *Science* **279**, 842-844.
- Migliorini, F., P. Michel, A. Morbidelli, D. Nesvorny, and V. Zappalà 1998. Origin of Earth-crossing asteroids: a quantitative simulation. *Science* **281**, 2022-2024.

- Millis, R. L., M. F. A'Hearn, and H. Campins 1988. An investigation of the nucleus and coma of comet P/Arend-Rigaux. *Astroph. J.* **324**, 1194-1209.
- Minter, A. H. and G. Langston 1996. 8.35 and 14.35 GHz continuum observations of comet Hyakutake C/1996 B2. *Astrophys. J. Lett.* **467**, 37-40.
- Monet, D. G., C. C. Dahn, F. J. Vrba, H. C. Harris, J. R. Pier, C. B. Luginbuhl, and H. D. Ables 1992. U.S. Naval Observatory CCD parallaxes of faint stars. I. Program description and first results. *Astron. J.* **103**, 638-665.
- Morrison, D., J. C. Gradie, and G. H. Rieke 1976. Radiometric diameter and albedo of the remarkable asteroid 1976 AA. *Nature* **260**, 691.
- Mottola, S., and 28 colleagues 1997. Physical model of near-Earth asteroid 6489 Golevka (1991 JX) from optical and infrared observations. *Astron. J.* **114**, 1234-1245.
- Mumma, M. J., M. A. DiSanti, N. Dello Russo, M. Fomenkova, K. Magee-Sauer, C. D. Kaminski, and D. X. Xie 1996. Detection of abundant ethane and methane, along with carbon monoxide and water, in Comet C/1996 B2 Hyakutake: evidence for interstellar origin. *Science* **272**, 1310-1314.
- Murchie, S., and 15 colleagues. Imaging results from NEAR's flyby of 433 Eros [abstract]. In *Abstracts: Asteroids, Comets, Meteors, Cornell University, July 26-30, 1999*, p. 13. Cornell University, Ithaca, NY.
- Nakamura, T., and S. Nakano 1996. Comet 1996 B2. *Int'l Astron. Union Circ.* **6299**.
- National Radio Astronomy Observatory, The, 1997. *The AIPS Cookbook*, version 15-APR-1998, NRAO, Charlottesville, Virginia.
- Neckel, H. and D. Labs 1984. The solar radiation between 3300 and 12500 Å. *Sol. Phys.* **90**, 205-258.
- Ney, E. P., 1974. Multiband photometry of comets Kohoutek, Bennett, Bradfield, and Encke. *Icarus* **23**, 551-560.
- Oort, J. H., 1950. The structure of the cloud of comets surrounding the Solar System and a hypothesis concerning its origin. *Bull. Astron. Inst. Neth.* **11**, 91-110.
- Osborn, W. H., M. F. A'Hearn, U. Carsenty, R. L. Millis, D. G. Schleicher, P. V. Birch, H. Moreno, and A. Gutierrez-Moreno 1991. Standard stars for photometry of comets. *Icarus* **88**, 228-245.
- Perley, R. A., and G. B. Taylor 1996. *The VLA calibrator manual*, National Radio Astronomy Observatory, Socorro, New Mexico.
- Perryman, M. A. C., 1997. *The Hipparcos and Tycho Catalogues: Astrometric and Photometric Star Catalogues Derived from the ESA Hipparcos Space Astrometry Mission*, ESA Publications Division, Noordwijk, Netherlands.
- Perryman, M. A. C., and 18 colleagues 1997. The Hipparcos catalogue. *Astron. & Astroph.* **323**, L49-L52.
- Pollack, J.B., O. Hubickyj, P. Bodenheimer, J. J. Lissauer, M. Podolak, and Y. Greenzweig 1996. Formation of the giant planets by concurrent accretion of solids and gas. *Icarus* **124**, 62-85.
- Pravec, P., M. Wolf, L. Sarounova, A. W. Harris, and J. K. Davies 1997. Spin vector, shape, and size of the Amor asteroid (6053) 1993 BW₃. *Icarus* **127**, 441-451.
- Qi, C., G. A. Blake, D. O. Muhleman, and M. A. Gurwell 1998. Interferometric imaging of comet Hale-Bopp with the Owens Valley Millimeter Array [abstract]. *Bull. Amer. Astron. Soc.* **30**, 1453.
- Rabinowitz, D. L., 1997. Are main-belt asteroids a sufficient source for the earth-approaching asteroids?. *Icarus* **127**, 33-54.
- Reach, W. T., M. V. Sykes, D. Lien, and J. K. Davies 1999. The dust trail of comet Encke. In preparation.
- Reitsema, H. J., W. A. Delamere, A. R. Williams, D. C. Boice, W. F. Huebner, and F. L. Whipple 1989. Dust distribution in the inner coma of comet Halley: comparison with models. *Icarus* **81**, 31-40.
- Richter, N. B., 1963. *The Nature of Comets*, English rev. ed. (A. Beer, trans.), Methuen & Co. Ltd., London.

- Rickman, H., 1991. The thermal history and structure of cometary nuclei. In *Comets in the Post-Halley Era* (R. L. Newburn, Jr., M. Neugebauer, and J. Rahe, Eds.), pp. 733-760. Kluwer Academic Publishers, Boston.
- Rickman, H., 2000. To appear in *Cometary Nuclei in Space and Time* (M. F. A'Hearn, Ed.), Astronomical Society of the Pacific, San Francisco.
- Rieke, G. H., M. J. Lebofsky, and F. J. Low 1985. An absolute photometric system at 10 and 20 microns. *Astron. J.* **90**, 900-906.
- Roemer, E., 1965. Observations of comets and minor planets. *Astron. J.* **70**, 397-402.
- Roemer, E., and R. E. Lloyd 1966. Observations of comets, minor planets, and satellites. *Astron. J.* **71**, 443-457.
- Röser, S. and U. Bastian 1991. *PPM Star Catalogue*. Astronomisches Rechen-Institut Heidelberg and Spektrum Akademischer Verlag, Heidelberg.
- Salo, H., 1988. Monte Carlo modeling of the net effects of coma scattering and thermal reradiation on the energy input to cometary nucleus [sic]. *Icarus* **76**, 253-269.
- Samarasinha, N. H., 1997. Preferred orientations for the rotational angular momentum vector of periodic comets [abstract]. *Bull. Amer. Astron. Soc.* **29**, 743.
- Samarasinha, N. H., and M. J. S. Belton 1995. Long-term evolution of rotational stress and nongravitational effects for Halley-like cometary nuclei. *Icarus* **116**, 340-358.
- Sarmecanic, J., M. Fomenkova, B. Jones, and T. Lavezzi 1997. Constraints on the nucleus and dust properties from mid-infrared imaging of comet Hyakutake. *Astrophys. J. Lett.* **483**, L69-L72.
- Schenewerk, M. S., P. Palmer, L. E. Snyder, and I. de Pater 1986. VLA limits for comets Austin (1982 VI) and P/Crommelin (1983n) - evidence for a diffuse OH halo. *Astron. J.* **92**, 166-170.
- Schleicher, D. G., T. L. Farnham, B. R. Smith, E. A. Blount, E. Nielsen, and S. M. Lederer 1998a. Nucleus properties of comet Hale-Bopp (1995 O1) based on narrowband imaging [abstract]. *Bull. Amer. Astron. Soc.* **30**, 1063-1064.
- Schleicher, D. G., R. L. Millis, and P. V. Birch 1998b. Narrowband photometry of comet P/Halley: Variation with heliocentric distance, season, and solar phase angle. *Icarus* **132**, 397-417.
- Schleicher, D. G., R. L. Millis, D. J. Osip, and S. M. Lederer 1998c. Activity and the rotation period of comet Hyakutake (1996 B2). *Icarus* **131**, 233-244.
- Sekanina, Z., 1982. Split comets. In *Comets* (L. L. Wilkening, Ed.), pp. 251-287. University of Arizona Press, Tucson.
- Sekanina, Z., 1988a. Outgassing asymmetry of periodic comet Encke. I. Apparitions 1924-1984. *Astron. J.* **95**, 911-924.
- Sekanina, Z., 1988b. Outgassing asymmetry of periodic comet Encke. II. Apparitions 1868-1918 and a study of the nucleus evolution. *Astron. J.* **96**, 1455-1475.
- Sekanina, Z., 1988c. Nucleus of comet IRAS-Araki-Alcock (1983 VII). *Astron. J.* **95**, 1876-1894.
- Sekanina, Z., 1997. The problem of split comets revisited. *Astron. & Astrophys.* **318**, L5-L8.
- Sekanina, Z., 1999. A determination of the nuclear size of comet Hale-Bopp (C/1995 O1). *Earth, Moon, & Plan.*, accepted.
- Shao, C.-Y., 1973. Periodic comet Encke. *Int'l Astron. Union Circ.* **2591**.
- Shao, C.-Y., and G. Schwartz 1980. Periodic comet Encke. *Int'l Astron. Union Circ.* **3526**.
- Silva, D. R., and M. E. Cornell 1992. A new library of optical spectra. *Astrophys. J. Suppl. Ser.* **81**, 865-881.
- Smithsonian Astrophysical Observatory 1966. *Smithsonian Astrophysical Observatory Star Catalog*. Smithsonian Institution, Washington.
- Snyder, L. E., P. Palmer, and C. M. Wade 1983. An upper limit to the microwave continuum radiation from comet Austin (1982g). *Astrophys. J. Lett.* **269**, 21-23.
- Space Telescope Science Institute 1998. *Space Telescope Imaging Spectrograph instrument handbook*, World Wide Web URL <http://www.stsci.edu/cgi-bin/stis?cat=documents&subcat=ihb>, 1 June 1998.
- Spencer, J. R., 1990. A rough-surface thermophysical model for airless planets. *Icarus* **83**, 27-38.

- Spencer, J. R., L. A. Lebofsky, and M. V. Sykes 1989. Systematic biases in radiometric diameter determinations. *Icarus* **78**, 337-354.
- Stellingwerf, R. F., 1978. Period determination using phase dispersion minimization. *Astrophys. J.* **224**, 953-960.
- Stern, S. A., 1988. Collisions in the Oort Cloud. *Icarus* **73**, 499-507.
- Stern, S. A., 1995. Collisional time scales in the Kuiper Disk and their implications. *Astron. J.* **110**, 856-868.
- Stern, S. A., and J. M. Shull 1988. The influence of supernovae and passing stars on comets in the Oort cloud. *Nature* **332**, 407-411.
- Swings, J.-P. 1985. *Transactions of the International Astronomical Union: Volume XIXB: Proceedings of the Nineteenth General Assembly*, Reidel Publishing Co., Dordrecht.
- Sykes, M. V., and R. G. Walker 1992. Cometary dust trails. I. Survey. *Icarus* **95**, 180-210.
- Tedesco, E. F., 1992. The IRAS minor planet survey. Technical Report PL-TR-92-2049. Phillips Laboratory, Hanscom Air Force Base, MA.
- Tedesco, E. F., and J. Gradie 1987. Discovery of M class objects among the near-Earth asteroid population. *Astron. J.* **93**, 738-746.
- Thomas, N., and H. U. Keller 1987. Comet P/Halley's near-nucleus jet activity. In *Symposium on the Diversity and Similarity of Comets* (E. J. Rolfe and B. Battrock, Eds.), pp. 337-342. European Space Agency Publications Division, Noordwijk, The Netherlands.
- Thomas, N., and H. U. Keller 1990. Interpretation of the inner coma observations of comet P/Halley by the Halley Multicolour Camera. *Ann. Geophys.* **8**, 147-166.
- Tokunaga, A., 1984. A reevaluation of the 20-micron magnitude system. *Astron. J.* **89**, 172-175.
- van Biesbroeck, G., 1962. Comet observations. *Astron. J.* **67**, 422-428.
- van der Blik, N. S., J. Manfroid, and P. Bouchet 1997. Infrared aperture photometry at ESO (1983-1994) and its future use. *Astron. & Astroph. Supp.* **119**, 547-557.
- Vanýsek, V., 1984. Photometric system for the International Halley Watch. In *Asteroids Comets Meteors* (C.-I. Lagerkvist and H. Rickman, Eds.), pp. 355-358. Astronomiska Observatoriet, Uppsala, Sweden.
- Veeder, G. J., M. S. Hanner, D. L. Matson, E. F. Tedesco, L. A. Lebofsky, and A. T. Tokunaga 1989. Radiometry of near-earth asteroids. *Astron. J.* **97**, 1211-1219.
- Veeder, G. J., C. Kowal, and D. L. Matson 1984. The Earth-crossing asteroid 1983 TB. In *Lunar and Planetary Science XV: Abstracts of Papers Submitted to the Fifteenth Lunar and Planetary Science Conference*, pp. 878-879. Lunar and Planetary Institute, Houston, TX.
- Vorontsov-Velyaminov, B., 1946. Structure and mass of cometary nuclei. *Astrophys. J.* **104**, 226-233.
- Weaver, H. A., 1996. Comet C/1996 B2 (Hyakutake). *Int'l Astron. Union Circ.* **6363**.
- Weaver, H. A., P. D. Feldman, M. F. A'Hearn, C. Arpigny, J. C. Brandt, M. C. Festou, M. Haken, J. B. McPhate, S. A. Stern, and G. P. Tozzi 1997. The activity and size of the nucleus of comet Hale-Bopp (C/1995 O1). *Science* **275**, 1900-1904.
- Weaver, H. A., P. D. Feldman, M. F. A'Hearn, C. Arpigny, J. C. Brandt, and C. E. Randall 1996. An HST spectroscopic and imaging investigation of comet Hyakutake (C/1996 B2) [abstract]. *Bull. Amer. Astron. Soc.* **28**, 925.
- Weaver, H. A., and P. L. Lamy 1999. Estimating the size of Hale-Bopp's nucleus. *Earth, Moon, & Plan.*, accepted.
- Weissman, P. R., 1986. Are cometary nuclei primordial rubble piles?. *Nature* **320**, 242-244.
- Weissman, P. R., 1991. Dynamical history of the Oort Cloud. In *Comets in the Post-Halley Era* (R. L. Newburn, Jr., M. Neugebauer, and J. Rahe, Eds.), pp. 463-486. Kluwer Academic Publishers, Boston.
- Wetherill, G. W., 1988. Where do the Apollo objects come from?. *Icarus* **76**, 1-18.
- Wetherill, G. W., 1991. End products of cometary evolution - Cometary origin of earth-crossing bodies of asteroidal appearance. In *Comets in the Post-Halley Era* (Newburn, R. L., M. Neugebauer, J. Rahe, eds.). Kluwer Academic Publishers, Dordrecht, pp. 537-556.

- Whipple, F. L., 1950. A comet model. I. The acceleration of comet Encke. *Astrophys. J.* **111**, 375-394.
- Whipple, F. L., 1982. The rotation of cometary nuclei. In *Comets* (L. L. Wilkening, Ed.), pp. 227-250. University of Arizona Press, Tucson.
- Whipple, F. L., 1983. 1983 TB and the Geminid meteors. *Int'l Astron. Union Circ.* **3881**.
- Whipple, F. L., and S. Zekanina 1979. Comet Encke: precession of the spin axis, nongravitational motion, and sublimation. *Astron. J.* **84**, 1894-1909.
- Williams, D. M., C. G. Mason, R. D. Gehrz, T. J. Jones, C. E. Woodward, D. E. Harker, M. S. Hanner, D. H. Wooden, F. C. Witteborn, and H. M. Butner 1997. Measurement of submicron grains in the coma of comet Hale-Bopp C/1995 01 during 1997 February 15-20 UT. *Astrophys. J.* **489**, L91-L194.
- Winter, D. F., and J. M. Saari 1969. A particulate thermophysical model of the lunar soil. *Astrophys. J.* **156**, 1135-1151.
- Woodgate, B. E., and 43 colleagues 1998. The Space Telescope Imaging Spectrograph design. *Publ. Astron. Soc. Pacific* **110**, 1183-1204.
- Wurm, K., 1939. On the interpretation of the spectra of comets and their forms. *Astrophys. J.* **89**, 312-319.
- Zombeck, M. V., 1990. *Handbook of Space Astronomy and Astrophysics*, 2nd ed., University Press, Cambridge.

